UNIVERSITÀ DEGLI STUDI DI PADOVA

Sede Amministrativa: Università degli Studi di Padova

Dipartimento di GEOSCIENZE

SCUOLA DI DOTTORATO DI RICERCA IN SCIENZE DELLA TERRA

CICLO: XXII

ANALYSIS OF A TRAMPLED FORMATION: THE BROWN LEUCITIC TUFF (Roccamonfina volcano, Southern Italy)

Direttore della Scuola: Ch.mo Prof. Gilberto Artioli
Supervisore: Ch.mo Prof. Paolo Mietto
Co-Supervisore: Ch.mo Hans-Ulrich Schmincke

Dottorando:Lisa Santello

Analysis of a trampled formation: the Brown Leucitic Tuff (Roccamonfina volcano, Southern Italy)

Lisa Santello

2010

We keep moving forward, opening up new doors and
doing new things, because we're curious,
and curiosity keeps leading us down new paths...

Walter Elias Disney

To my parents and Ale

Acknowledgement

I have to thank many people for their help during these three years.

First of all, I thank my supervisor, Prof. Paolo Mietto, another father for me, for the opportunity to carry out this PhD project, with fruitful discussions and always supporting me. His guidance and experience, as well as the constant encouraging during the last three years allowed me to complete the thesis in this short period.

Thanks to Prof. H.U. Schmincke and Dr. M. Sumita for their help and advises and their ability to inject the passion for volcanology into me.

A very sincere thank to Prof. Steve Sparks for hosting me 7 months in Bristol and for his precious suggestions.

Many thanks also to Stuart Kearns for his help with SEM analyses.

A friendly thanks to Alison Rust who gave me a roof and a warm bed during the time spent in Bristol, and above all their special friendship; Angela and Manabu for the discussions about the English customs; Jenny for the last month in Bristol.

I express my gratitude to Dr. Lucia Gurioli and Prof. Joan Martì for the precious succestion on my thesis.

These wonderful PhD three years in Padova wouldn't have been so nice and gorgeous without the friendships of the other PhD students and researchers who shared not only the working life, but especially enjoyed the social life outside the university: Ale, Annuccia, Chiaretta, Guido, Jacopo, Manuel, Matteo, Marco, Nereo, Pier and Giovanni: it was wonderful, guys! I thank them again for the time

spent in the discussion on my problematic project.

Sincere thanks to all the group of Roccamonfina:
Adolfo for the passion for his territory, his incomparable help and generosity;
Marco and Carmen for their help in the mapping and their kindness;
Angelo and his family for the practical and physical support and their "giulietto";
Vittorio and Rino for their availability;
the group of archeologists (Alessandra, Rossella, Claudia, Maria Teresa, Pietro, Simona, Fabiola, Isabella) for their help for cleaning of the surface;
the "I vigliucci" country house for the endless lunches, dinners and liquors and their hospitality;
the authorities of Tora e Piccilli and Marzano Appio municipal districts, the "Comunità Montana Monte S. Croce Roccamonfina", the "Parco Regionale Roccamonfina – Foce del Garigliano" and the "Soprintendenza dei beni culturali di Salerno, Avellino, Benevento e Caserta" for the help in the logistic organization of the field trips and archaeological campaigns.
A thank to all the technicians of the Dipartimento di Geoscienze, Università degli studi di Padova, for the help during these three years: Stefano Castelli, Maria Luisa Perissinotto (Maui), Micola Michelon, Luca Peruzzo, Leonardo Tauro and Federico Zorzi; I express my gratitude also to Sara and Angela (Secretary Office) for their availability.

Many thanks go to Mara and Matteo for the proof-reading of this thesis.

A special thanks to MyMax Edutainment, especially Massimo My, Vanni Gandolfo, Marco Leopardi, Marco Salustro and Maria Teresa Tringali, for the wonderful experience of being part of a documentary.
Thanks to "Voyager" television programme, (Rai 2), with the hope that it will not modify the interviews in order to put in the words "Maya", "2012", "UFO" and "knight templars" in the documentary.

Thanks to the IAS for partially supporting the field activity and the Ing. "Aldo Gini" foundation for the opportunity to spend 7 month in Bristol (U.K.).

Finally, I wish to thank my wonderful parents for the constant support, and physical help as well, during all the period of my PhD.

My last thanks go to Ale, for his love, the endless patience during the hard times and for his help in writing this thesis.

Thank you all!

Contents

Extended Abstracts

ENGLISH

Introduction and Problems

Several human footprints were discovered few years ago in the Roccamonfina volcanic complex (Southern Italy, Foresta locality, Mietto et al., 2003). The trails were impressed over the surface of one of the numerous pyroclastic flow deposits of the volcano. $^{40}Ar/^{39}Ar$ analyses dated the unit at 345 ± 6 ka (Scaillet et al., 2008). Therefore, the trails represent the oldest *Homo* tracks ever found in Europe. The importance of the discovery has pointed out the need of a study to understand: 1) the origin of these deposits; 2) when the footprints were impressed; 3) what kind of mechanisms permitted the impression and the conservation of the footprints. No data from literature could answer to these questions, since the detailed volcano-sedimentologic characteristics of the trampled deposits, called Brown Leucitic Tuff (BLT) were rarely examined. An in-depth volcanological study of the deposits is the base to understand the features of the deposition phenomenon. Geochemical and petrographical analyses, on their part, permit to make out the connection between the post-depositional events and the impression-conservation of the traces.

Stratigraphy: The Brown Leucitic Tuff (BLT)

A detailed survey of the Foresta locality and of the north-eastern area of the volcanic district allows the identification in the BLT sediments of a succession of different pyroclastic deposits. This formation is composed on the whole by eight pyroclastic units. The trampled surface is represented by one of these units. Thus, they have been all carefully analyzed. Some of them, including the trampled one, are early lithified.

Sedimentologic and granulometric analyses, followed by a statistical data processing, permitted to characterize the particular eruptive style and to unequivocally subdivide

the units.

The BLT is the result of a Plinian to Sub-Plinian eruption characterized by the deposition of a series of pyroclastic flows. Granulometric data and thickness analyses support this conclusion. The stratigraphy of the BLT reflects the evolution of pyroclastic currents originated by collapses of eruptive columns. This eruptive phase marked the Roccamonfina volcano's explosive cycle.

Geochemical and Petrographical characteristics of the BLT

Roccamonfina volcanic rocks are generally subdivided into two geochemical series: high K (HK) and low K (K). Appleton (1972) defined the HK series to encompass ne- and lc-normative leucite-bearing lavas, and the K series to include Qz-normative olivine basalts, trachybasalts, and biotite augite latites. Analyses were made on the whole rocks samples of the pyroclastic flow units and they testify that BLT rocks mainly belong to HK series. So the BLT eruption took place before the geochemical change in the magma chamber.

Post-depositional processes: the lithification

The lithification process occurred very shortly after the emplacement of the pyroclastic flow unit. In this kind of deposits the zeolitization is the lithifying process. But when and how does this process occur?

The $^{40}Ar/^{39}Ar$ dating of the trampled and of the overlaying units suggest a timing range between the two explosive events less than 4 ka. So the zeolitization process lasted at most 4000 years, because only the trampled deposits and the four below it, not the overlaying ones, are lithified. During this time interval meteoric water permeated the incoherent volcanic deposits. The surface became thus plastic and cold, allowing the passage of the hominids. Later, zeolitization occurred: this is a chemical process of alteration of volcanic instable glass by means of fluids. Such fluids dissolved the unstable parts and precipitated zeolite minerals, which are generally stable at low temperature (about 60-40°C). The zeolites cemented the ground mass creating a rigid framework among the components of the rock (minerals, lithic fragments…). The deposit was thus lithified, permitting the conservation of the human footprints, even after following pyroclastic events.

Dating of the surface

Two aspects concern the dating: they aim to understand 1) when the footprints were impressed and 2) why it is possible to observe the footprints now.

The answer to the first question is given by the dating of the eruptive event. Several samples collected along the stratigraphic log were analyzed in the Berkeley Geochronology Center, with the collaboration of Prof. Paul Renne. The results show that the age of the trampled pyroclastic flow unit is comparable with the overlaying unit (trampled deposit 349 ± 3 ka, overlaying deposits 350 ± 3 ka). Thus the trampling event and the lithification process occurred in a time span of about 4000 years.

The second aspect concerns the timing of the exposure of the surface. It was permitted by historical archives research and lichenometric data. Historical researches are based on the study of the origin of the "Ciampate del Diavolo" (Devil's trails) place

name. Thus, it is possible to establish how long the site is known. Aboundant precipitation and landslides occurred around 1807-1816 in Foresta area. These landslides involved the not lithified parts over the trampled surface, permitting the exposure of the latter one.

Lichenometric analyses use the growing rate of *Aspicilia cinerea* lichen to know the time exposure of the ichnological site. By this calculation it was possible to deduce that the exposure was since the early 19th century.

Both the methodologies thus confirm that before the beginning of the 19th century the surface was covered by other deposits.

Conclusions

Summarizing: BLT is constituted by a series of pyroclastic units. All these units belongs to the same volcanic series. the time interval between each unit is about 3-4 ka. During these non-deposition intervals, meteoric precipitations occurred, saturating the surface. Afterwards several hominids walked over the plastic and relatively cold surface, leaving the traces of their passage. Because of the presence of meteoric fluids, the zeolitization process developed, permitting the lithification and then the conservation of the footprints. Later the eruptive activity started again with the same characteristics, but the lithification process did not occur again. During the 19th century anomalous documented precipitations eroded the overlaying not lithified units, permitting the exposure of the trampled surface.

ITALIANO

Introduzione e problematiche

Qualche anno fa sono state scoperte numerose impronte umane in depositi appartenenti al vulcano di Roccamonfina (Italia meridionale, località Foresta, Mietto et al., 2003). Le piste sono state impresse sulla superficie di uno dei suoi numerosi flussi piroclastici. Attraverso il metodo $^{40}Ar/^{39}Ar$ l'unità con le impronte è stata datata a 345 ± 6 ka (Scaillet et al., 2008). Pertanto, queste impronte risultano essere le più antiche appartenenti al genere *Homo* mai trovate in Europa.

Data l'importanza della scoperta, si è deciso di portare avanti uno studio che permettesse di capire: 1) quale sia stata l'origine del deposito; 2) quando le impronte siano state impresse; 3) che tipo di meccanismo abbia permesso l'impressione e la conservazione delle impronte. Le risposte a queste domande non sono supportate da dati di bibliografia: le caratteristiche di dettaglio sia vulcanologiche che sedimentologiche raramente sono state affrontate nei lavori passati. Uno studio di dettaglio sulla sedimentologia dei depositi, chiamati Brown Leucitic Tuff (BLT), rappresenta dunque il punto di partenza per meglio comprenderne le caratteristiche deposizionali. Analisi geochimiche e petrografiche permettono invece di capire il legame tra gli eventi post-deposizionali e la conservazione delle impronte.

Stratigrafia: il Brown Leucitic Tuff (BLT)

Un rilevamento di dettaglio in località Foresta e nella porzione nord-orientale del distretto vulcanico ha permesso l'identificazione nel Brown Leucitic Tuff (BLT) di una successione di differenti depositi piroclastici. Questa formazione è composta da otto unità piroclastiche che sono state analizzate molto attentamente. Su una di queste unità sono state infatti impresse le impronte umane. Parte dei depositi, inclusi quelli contenenti le impronte, risultano litificati.

Analisi sedimentologiche e granulometriche, accompagnate da un'analisi statistica dei dati, hanno permesso di caratterizzare lo stile eruttivo che ha portato alla deposizione del BLT e di suddividere le unità in sub-unità.

Il BLT è il risultato di un'eruzione di tipo Pliniano-SubPliniano caratterizzato dalla deposizione di una serie di flussi piroclastici, come supportato da dati granulometrici e dallo studio degli spessori delle unità stesse. La stratigrafia del BLT riflette l'evoluzione di correnti piroclastiche originate da collassi di colonne eruttive. Questo ciclo eruttivo marca l'inizio della fase esplosiva della storia del vulcano di Roccamonfina.

Caratteristiche petrografiche e geochimiche del BLT

In letteratura i depositi del vulcano di Roccamonfina vengono suddivisi in due serie magmatiche: alte in potassio (HK) e basse in potassio (K). Appleton (1972) ha definito come serie HK quelle comprendenti lave ne e lc- normative ricche in leucite, e come serie K quelle che includono basalti olivinici qz-normativi, trachibasalti e latiti ricche in biotite ed augiti. Le analisi sono state compiute su campioni di roccia totale presi dalle unità piroclastiche. Queste analisi testimoniano che le rocce del BLT

appartengono principalmente alle serie HK. Questo dato permette di affermare che il ciclo eruttivo che ha generato il BLT si è verificato prima del cambiamento geochimico avvenuto nella camera magmatica.

Processi post-deposizionali: la litificazione

Il processo di litificazione è avvenuto poco tempo dopo la messa in posto del flusso piroclastico su cui sono state trovate le impronte. In questo tipo di depositi la litificazione avviene tramite il processo di zeolitizzazione. Ma quando e come questo processo si è verificato?

Le datazioni $^{40}Ar/^{39}Ar$ dell'unità con le impronte e di quella immediatamente superiore suggeriscono che il tempo intercorso tra i due eventi esplosivi sia inferiore ai 4 ka. Di conseguenza il processo di zeolitizzazione è durato al massimo 4000 anni, in quanto solamente l'unità con le impronte e le quattro sottostanti sono litificate e non quelle sovrastanti. Durante questo intervallo temporale l'acqua meteorica ha permeato i depositi vulcanici incorenti. L'acqua ha raffreddato e reso plastico il deposito, permettendo così il passaggio degli ominidi. In seguito ha avuto inizio il processo di zeolitizzazione. Questo è un processo di alterazione del vetro vulcanico instabile tramite la circolazione di fluidi nel deposito. I fluidi dissolvono le parti termodinamicamente instabili e precipitano zeoliti, stabili a bassa temperatura (circa 60-40°C). Le zeoliti possono così cementare la massa di fondo creando un reticolo rigido tra i componenti del deposito (minerali, frammenti litici …). Il deposito è stato dunque litificato permettendo la conservazione delle impronte umane anche dopo la deposizione del flusso piroclastico successivo.

Datazioni della superficie

Due sono le domande alle quali le datazioni cercano di dare una risposta: 1) quando sono state impresse le impronte; 2) perchè esse sono oggi visibili?

Alla prima domanda si risponde datando gli eventi eruttivi. Diversi campioni sono stati raccolti e analizzati al Berkeley Geochronology Center con la collaborazione del Prof. Paul Renne. I risultati mostrano che l'età dell'unità con le impronte è comparabile all'età del flusso successivo (flusso improntato 349 ± 3 ka, flusso sovrastante 350 ± 3 ka). Il passaggio degli ominidi e il processo di litificazione si sono verificati dunque al massimo entro un intervallo di 4000 anni.

Da quanto tempo però questa superficie è esposta? Per rispondere a questa domanda sono stati effettuate ricerche d'archivio ed effettuate analisi lichenometriche. Le ricerche d'archivio si basano sull'origine del toponimo "Ciampate del Diavolo". In questo modo è possibile stabilire da quanto tempo il sito è conosciuto. Tra il 1807 e il 1816 l'area di Foresta è stata interessata da precipitazioni straordinarie e numerose frane. Queste hanno coinvolto la parte non litificata del BLT al di sopra delle impronte portando così alla luce la superficie.

Le analisi lichenometriche si basano sul tasso di crescita di un particolare tipo di licheni (*Aspicilia cinerea*) e sono state utilizzate per capire da quanto tempo la superficie è in esposizione. Secondo questo dato la superficie risulta esposta dagli inizi del 1800.

Entrambe le metodologie quindi confermano l'esposizione della superficie

dall'inizio del XIX secolo.

Conclusioni

L'attività eruttiva del Roccamonfina ha dato luogo alla deposizione di una serie di unità piroclastiche. Durante il periodo di quiescenza tra un evento eruttivo e il successivo, durato al massimo 3000-4000 anni, le precipitazioni meteoriche hanno saturato il deposito. In seguito gli ominidi hanno camminato al di sopra di questa superficie plastica e fredda, lasciando le tracce del loro passaggio.

A causa del fluidi circolanti legati alle precipitazioni, si è sviluppato il processo di zeolitizzazione che ha permesso la litificazione e quindi la conservazione delle impronte. Successivamente il complesso vulcanico ha ripreso la sua attività, ma nessuno dei flussi successivi ha subito litificazione. Durante il XIX secolo abbondanti precipitazioni hanno eroso le parti non litificate del BLT permettendo così l'esposizione della superficie e quindi la venuta a giorno delle impronte così come le vediamo oggi.

Chapter 1

Introduction

1.1 The "Ciampate del Diavolo" site

The "Ciampate del Diavolo" site is an important ichnological site worldwide, characterized by the preservation of several human footprints impressed over a volcanic surface (Fig. 1.1). The site was known by the inhabitants as "Ciampate del Diavolo" (which means "Devil's trails"): they knew the volcanic origin of the site. Only a supernatural being could walk over a surface when this was not yet lithified.

Up to now these researches have been focused on the ichnological aspect. The study of the characteristics of the footprints, aimed to know who made the traces. Our ancestors but...how old?

The site has never been studied from the viewpoint of the characteristics of the trampled deposits. They belong to Brown Leucitic Tuff complex (BLT) and they are dated at 385-325 ka (Luhr & Giannetti, 1987), Middle Pleistocene. This dating fixes

Fig. 1.1 - Panorama of the "Ciampate del Diavolo" site, Foresta locality (Roccamonfina volcano)

the "Ciampate del Diavolo" site as the oldest site in Europe and one of the oldest in the world, giving a great value to the finding. Few years ago Mietto et al. (2003) established the importance of the site and the researches in the Foresta locality and in other similar areas began.

During the researches of the last 6 years numerous archeological campaigns were carried out to clear the primary surface. This permitted the discovery of new footprints. Besides a new ichnological site, Carangi, was discovered during the survey of BLT deposits in the surrondings of the "Ciampate del Diavolo" site. The two sites have similar patterns: the formation where the footprints were impressed and the characteristics of the footprints are the same, even if the preservation in the second site is not so good. Why is this formation so suitable for the conservation of the footprints? A detailed analysis of depositional and post-depositional events is therefore developed in this PhD thesis, supplementing the ichnological researchers on the site.

The "Ciampate del Diavolo site" has an extension of about 2000 m^2 and it is characterized by an original sloping surface (from 45° to 70°). The direction of the three main trails is similar, outward the caldera center, but they have different characteristics.

All the tracks are characterized by a pace of about 60 cm and a stride of about 120 cm. The pace angle is around 160° in trackways C and B and arrives to 90° at the end of the trackways A (Fig. 1.2).

The **trackway A** is 13.4 cm long and it is composed of 27 footprints impressed over a sloping surface 4.5 m high (Fig. 1.3). This trackway has a Z-shape with two sharp angulations. This choice of the individual to go through the slope in this way is really peculiar because the track covers the less sloping part of the surface. In some cases it is possible to see a double impression of the footprints, probably because during the touchdown phase of the walk, the surface suffered a break-up of a superficial crust and the trackmaker sank and slipped.

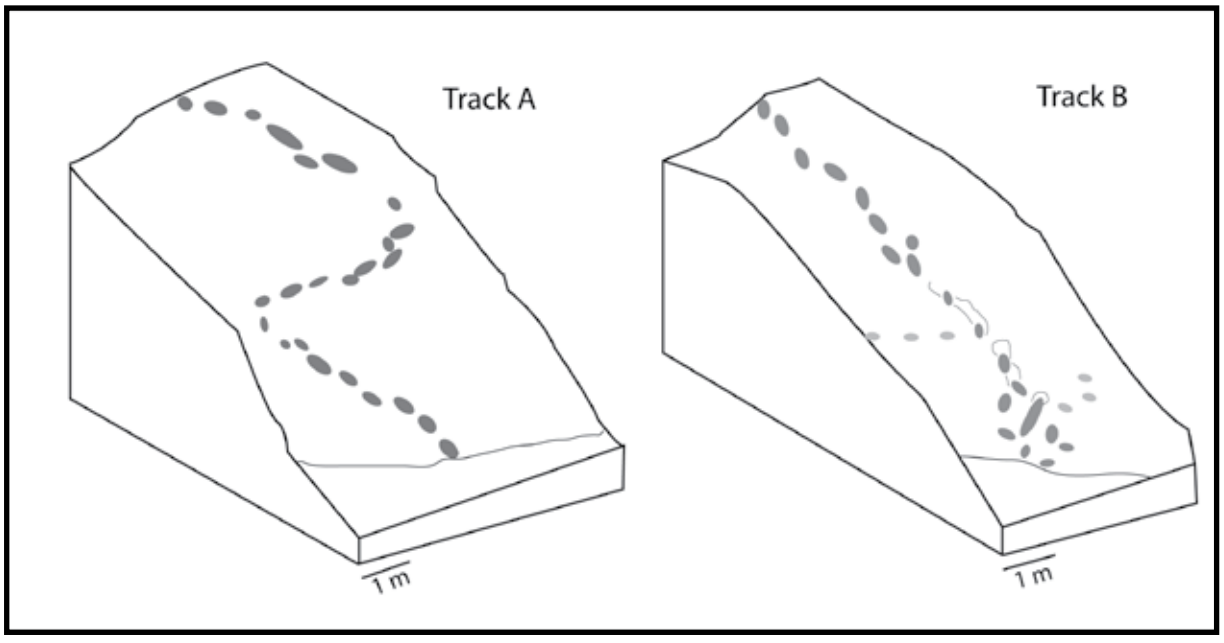

Fig. 1.2 - Diagrams of the trackways A and B (modified from Mietto et al., 2003)

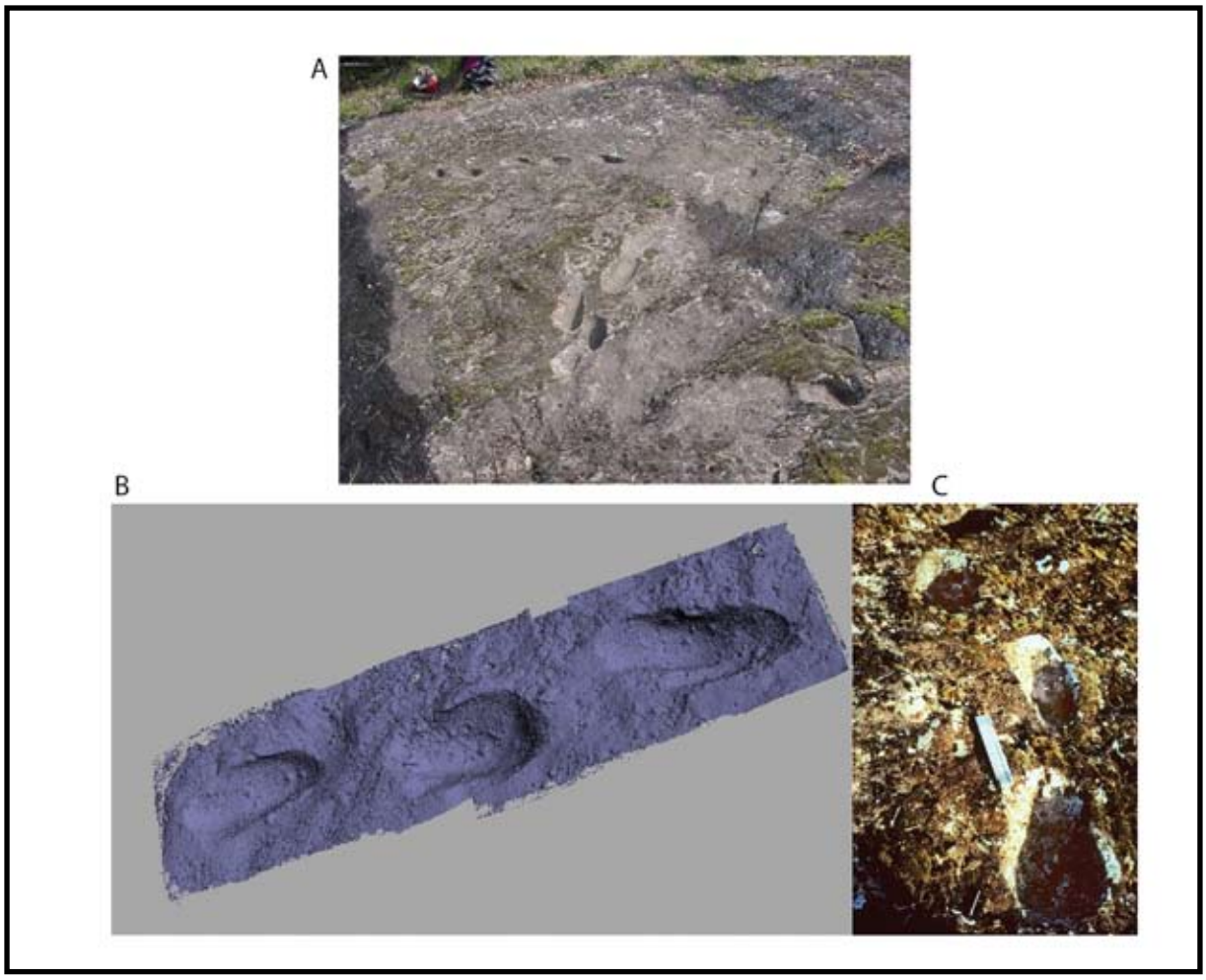

Fig. 1.3 - Trackway A. A) General view of the trackway; B) Laser-scanner image of part of the trackway; C) Picture of the scanned segment of the trackway A.

The **trackway B** (Fig. 1.4) is instead about 9 m long and consists of 19 footprints with an elevation of the surface of 3 m. This trackway has irregular footprints, cutting the surface along the maximum slope. It can be subdivided into three sections in relation to the changes in the sloping surface. The first segment is regular because of the flat surface, and the footprints reflect this regularity. Instead, in the following part the footprints are very close to each other, because of the high slope.

Finally, in the last sector, the slope is interrupted by a second and higher step. The trackmaker stood on the right foot and put the left behind for a better equilibrium. Then the left foot was lifted and moved forward in the proximity of the edge of the step. Here the individual lost the balance because the substrate subsided and the footprint began a long slide continuing also during the following step. There are also the impressions of the hands of the individual because they helped in the equilibrium. The balance was re-established with the following step. At this point the incline of the slope increased and the heel dug deeply into the substrate. When the slope became excessive (70-80°), the trackmaker stopped again and moved on the left, where the slope was less steep. In this last section the depth of heel prints is over 40 cm, it is probable that the hands were used again, placed with an open palm at the side of the trunk.

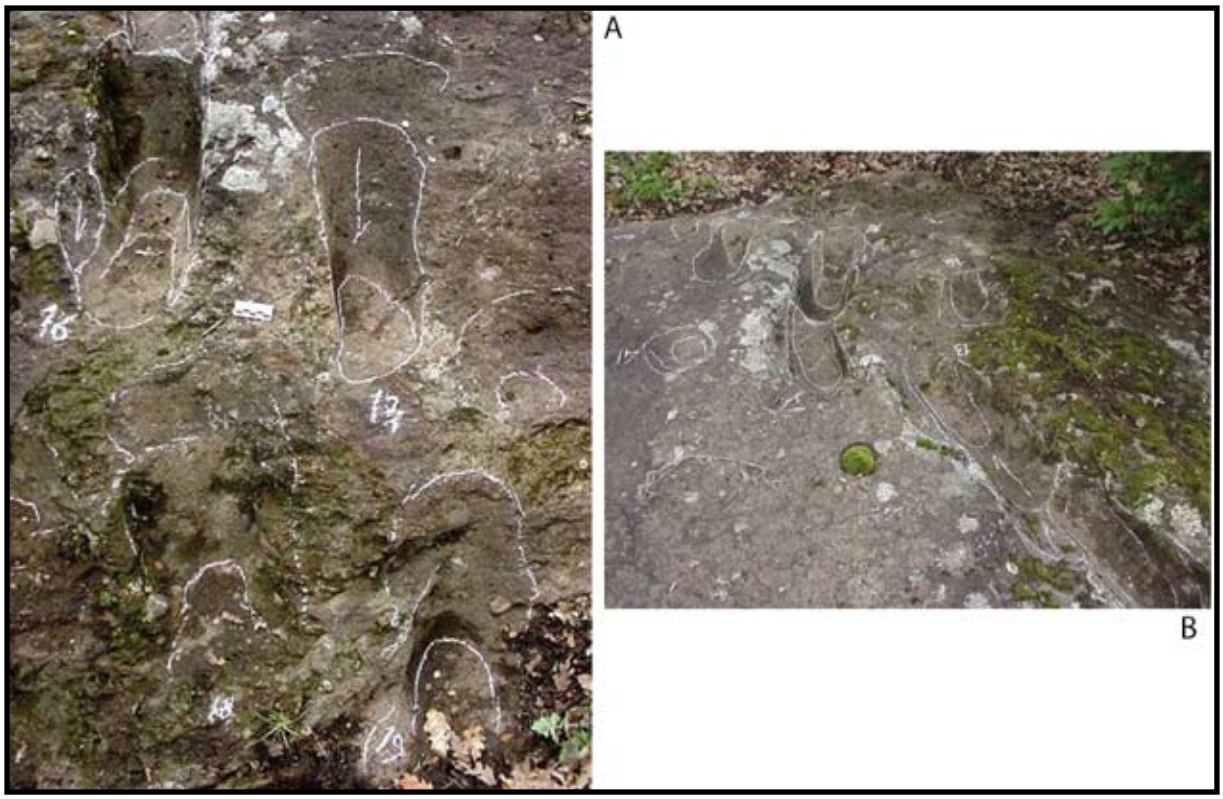

Fig. 1.4 - Trackway B. A) Picture of the end of the trackway; B) General view of the trackway B.

In the **trackway C** the footprints are organized in a straight line with a total length of 10 m, 6 m of it covered by detritus. It consists of 10 footprints with a difference in elevation of the track-bearing surface of 2.5 m. This track cuts across a slope that has a slight incline and with its straight-line direction and modest signs of sliding represents the most regular trackway in the site, which is related to a slow and constant pace.

The Roccamonfina footprints are the oldest known in Europe and a rare example of Paleolithic tracks not preserved in a cave environment. These tracks were made by a *presapiens* species of Homo. No previous records of pre-late Pleistocene hominid tracks were left in descending a slope and show associations with hand-prints (Garcia, 1999; Lockley & Meyer, 2000). Whereas tracks from Late Pleistocene cave habitats are quite well-known, the Roccamonfina discovery suggests that other hominid and vertebrate tracks in older, subaerial paleo-environments can be found.

The locomotor pattern displayed by the trails of hominid footprints is still under study, but it is clear that the Middle Pleistocene hominids at Roccamonfina had a fully bipedal and free-standing gait with the use of arms only for supporting or regaining balance in very steep passages. These prints have different parameters and morphological characteristics depending on the direction of the trackway in respect to the line of maximum inclination of the slope. According to bibliography formulae (Grieve & Gear, 1966; White, 1980; Charteris et al., 1982), and using the average ratio foot length/height = 15.5%, all the trackways indicate adult individuals who were no taller than 1.56 m. The value is compatible with about 1.60 m plotted on the diagram

used by Tuttle et al. (1990) to understand the nature of the famous Laetoli footprints. The speed of the trackmakers calculated by the method of Alexander (1984) is 1.09 m/s. Normally humans adapt their walking speeds to their purposes and the conditions of the environment with relative speed in the range from 0.8 to 1.7 m/s for modern adults and 0.86 m/s for normal younger adults (Bornstein & Bornstein, 1976; Charteris et al., 1982).

The Roccamonfina trails were left while the individuals were descending a slope with a slippery surface; the speed was therefore higher than those of previously known human trackways. The dating of the trackways to the Middle Pleistocene, also emphasized in this thesis, suggests they are the only available documentation of human tracks from this period.

1.2 HUMAN FOOTPRINTS SITES IN THE WORLD

In the world, several ichnological sites with hominids footprints were known (Fig. 1.5). Most sites are characterized by the presence of a volcanic substratum. Few cases exist of human footprints preserved in sedimentary (s.s.) environment, such as in caves, lakes and fossils dunes. The oldest hominid tracksites reported are in Africa and they have been interpreted as representing the footprints of extinct species.

Only one hominid tracksite outside the African continent site appears to represent a non-*sapiens* species. This is the case of the Roccamonfina site (Mietto et al., 2003; Avanzini et al., 2008). It is adjacent to Africa, and its date (385–325 ka, Luhr & Gianneti, 1987) is consistent with the timing of hominid colonization of Europe (Palombo & Mussi, 2006). The discovery of these footprints sites, although they are not numerous, is a good representation of the evolution of the human species.

Pliocene Footprints from Laetoli, Tanzania

Hominid footprints from Laetoli site (Tanzania) are certainly the most famous and oldest hominid footprints known nowadays (Fig. 1.6. Leakey & Hay, 1979; Hay & Leakey, 1982; Leakey & Harris, 1987). They have been dated at about 3.7 Ma. Basing on this age, many authors deduce that the trackmaker was probably a gracile australopithecine, possibly like the famous Lucy: that is, *Australopithecus*

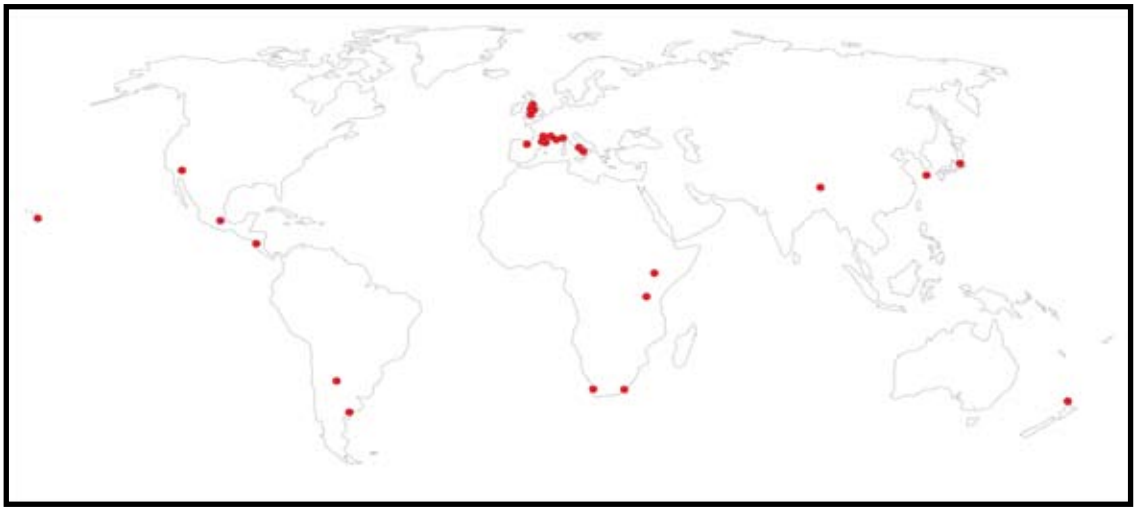

Fig. 1.5 - Distribution of the human footprints sites in the world

Fig. 1.6 - Human footprints of Laetoli site (Tanzania, the original exposure, modified after photograph by John Reader, courtesy of Getty Foundation)

afarensis (Suwa, 1984; Lockley 1999). The three trackways recorded belonged to small individuals with a height ranging from about 1.10-1.15 m to about 1.32-1.52 m (White & Suwa, 1987). This estimated adult size is slightly larger than "Lucy's", whose foot is too small to fit in the largest tracks but too large for the small tracks. Although the hominid tracks at Laetoli are the most famous, the hominid tracksite is only one of the 18 that were recorded. Recognizable prints were recorded and counted at about half these sites (Leakey & Harris, 1987), leading to a cumulative count of more than 9500 tracks at nine sites.

Early Pleistocene of Lake Turkana

The post Pliocene hominid track record in East Africa continues, albeit with a huge temporal gap of about 2 million years, with the Early Pleistocene report of the world's second oldest hominid tracksite (Fig. 1.7). This 1.5–1.6 million-year-old hominid tracksite was recorded in the Koobi Fora Formation on the shores of Lake Turkana. Here, at least 7 trackways are visible and it is possible that they have been made by *Homo erectus*. The

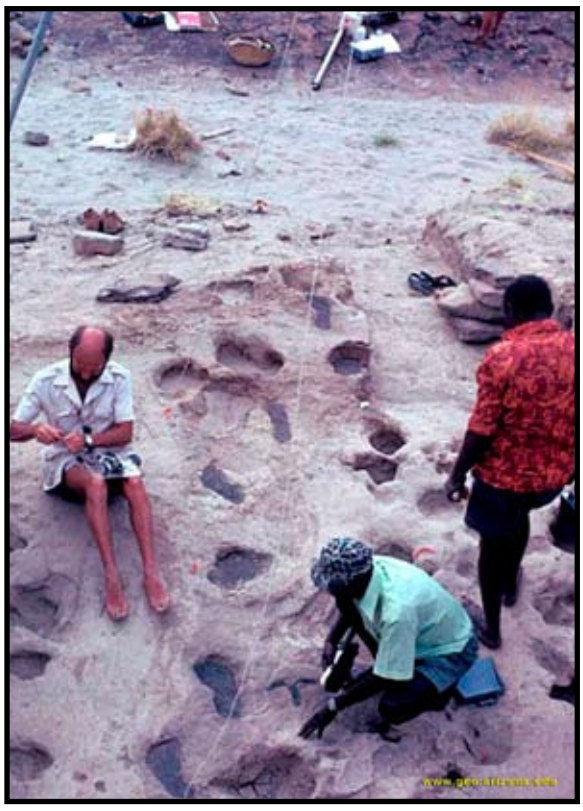

Fig. 1.7 - Human footprints on the Koobi Fora Formation on the shore of Lake Turkana (Mountain, 1996)

tracks range in length from 25–32 cm, and the mean foot size dimensions are estimated at 26 cm long and 10 cm wide, suggesting an individual 1.6–1.8 m in height.

Mid Pleistocene of Europe and the Middle East

Then there is the mid Pleistocene Roccamonfina Volcano site (Mietto et al., 2003; Avanzini et al., 2004, 2008). The tracks occur in a volcanic ash substrate dated at 345 ± 6 ka by Scaillet et al. (2008). Basing on these dating, they are likely to have been made by a pre-*sapiens* or pre-*neanderthalensis* species such as the Neanderthal ancestor *H. heidelbergensis*.

Another Mid Pleistocene European site is the Terra Amata site, near Nice (France). Here a single footprint is present impressed in a cave over a planar surface (Fig. 1.8. De Lumley, 1967; Miskovski, 1967; Meldrum, 2006).

Fig. 1.8 - Human footprints of Terra Amata site (France, courtesy of Dott. Marco Avanzini)

Middle-Late Pleistocene Transitions in Southern Africa

Two hominid footprint discoveries from South Africa (Roberts, 2008) fill an important chronological gap between Middle Pleistocene and much younger late Pleistocene "human" track sites. The two sites are at Nahoon Point, near East London (Deacon, 1966; Mountain, 1966) and in the Langebaan Lagoon area in the West Coast National Park (Fig. 1.9). The Nahoon Point tracks were originally dated at about 29 ka (Deacon, 1966), but this age has recently been revised to about 127 ± 8 ka (Roberts, 2008). The Langebaan tracks were dated to about 117 ka (Gore, 1997; Roberts & Berger, 1997; Roberts, 2008). Tracks at both sites are poorly preserved on the sloping surface of calcareous dunes. The Nahoon Point tracks include small human footprints, about 19 cm long, with one showing moderately well-preserved toe impressions and associated bird and mammal tracks on the same surface. The Langebaan lagoon tracks are larger (about 23 cm long) but less well-defined.

Fig. 1.9 - Human footprints of Langebaan lagoon (West Coast National Park, Southern Africa; Roberts, 2008)

All other Late Pleistocene hominid tracksites dated with confidence are no more than half this age (about 60-65 ka). So the trackmakers were modern humans (*H. sapiens sapiens*)

or a closely related species (*H. sapiens neanderthalensis*; Avanzini et al., 2008).

Late Pleistocene of France, Spain and Italy

Fossil footprints have been found at a number of subterranean cave sites in southern France and Italy. Some of these sites are as famous for their cave art as they are for tracks or other evidence of Late Paleolithic culture. Among the better known sites are the Niaux cave system (Fig. 1.10. Pales, 1976). These include groupings of footprints that may represent children at play (Lockley & Meyer, 2000). In Fontanet Cave there is evidence that suggests a child following a puppy or fox into a cave, and at Arìege three trackways of

Fig. 1.10 - Human footprints of Niaux cave system (France; after Pales, 1976, Lockley & Meyer, 2000)

children are recorded (Bahn & Vertut, 1988). Thus, the footprints of children seem to be an important component of the track record of Paleolithic caves. For example, Chauvet Cave near Vallon-Pont-d'Arc in southern France, which has yielded what are claimed to be the oldest footprints of *Homo sapiens*, reveals a trail of footprints of a young boy (estimated at about 8 years old) about 1.5 m tall. The footprints extend for about 50 m across the cave floor and may be between 20 and 30 ka (Harrington, 1999; Garcia, 2001).

The cave known as Tana della Basura near Toirano, Northern Italy, is characterized by numerous footprints. The tracks were discovered in 1950 (Chiapella, 1952) and are attributable to Neanderthal Man (Pales, 1954, 1960) at about 12 ka. Hundreds of human footprints were also discovered in an inaccessible part of Ojo Guareña, a cave near Burgos, Spain. Basing on previous ^{14}C dates of 15600 obtained from carbonized wood at the site and the "light patina of carbonate" covering the tracks, which gives them "a very ancient appearance", an age of Late Pleistocene is implied (Lockley et al., 2008).

Late Pleistocene of Tibet

Zhang & Li (2002) and Zhang et al. (2003) reported a series of hand and footprints associated with calcareous tufa deposits at a height of 4200 meters on the Tibetan Plateau, about 85 km from Lhasa. The tufa was optically dated at about 20 ka. This find is one of the few in which hand and footprints are associated (compare with the Roccamonfina Volcano site in Italy). This unusual combination is attributed to the fact that hot springs are present in the site. Thus, it was used as a campsite, as it is shown by the presence of a hearth. Previous to the fortuitous discovery of the footprints, there had been no archaeological evidence of human habitation on the Tibetan Plateau before 4 ka.

Late Pleistocene of Korea

Hominid tracks were recently reported from the Late Pleistocene of a coastal site on Jeju (Cheju) Island, South Korea (Fig. 1.11. Kim et al., 2008). These tracks, which include several trackway sequences, are associated with tuffaceous sediments that also contain a variety of bird and mammal tracks, as well as invertebrate body and trace fossils and plant remains. More than 20 stratigraphic horizons with tracks are recorded in a section only 2 m thick. Hominid tracks occur at only one horizon (Kim et al., 2004). The track-bearing layer has been dated at about 15 ka (Kim et al., 2008).

Fig. 1.11 - Human footprints of Jeju Island (Cheju, South Korea; after Kim et al., 2004)

Mesolithic-Neolithic of the United Kingdom

Like in the Korean site, there are two significant coastal hominid tracksites in Britain: one in the Severn Estuary, near Uskmouth (Aldhouse Green et al., 1995), and another at Formby, near Liverpool (Fig. 1.12. Cowell et al., 1993; Roberts et al., 1996). The former site is dated between about 5720 and 6250 years BP and has yielded four hominid trackways, including one of an individual who was about 2.00 m tall. The hominid tracks occur in association with the tracks of deer and birds. On the contrary, the latter site, dated at about 5500 years BP, has yielded more than 180 human trackways in association with the footprints of aurochs, red deer, roe deer, unshod horses, cranes and oystercatchers (Roberts et al., 1996; Lockley & Meyer, 2000).

Fig. 1.12 - Human footprints of Formby, Liverpool (U.K.; after Roberts et al., 1996)

New World Track sites

Hominid track sites have been reported from various sites in Argentina, Chile, Mexico and Nicaragua. It appears that at least one track has been reported from the Chilean site of Monte Verde, which may be as old as 11.5–12.5 ka (Dillehay, 1999).

Some tracksites have been reported from Mexico (Ordõnez, 1945; Aveleyra Arroyo de Anda, 1950; Rodriguez de la Rosa et al., 2004), though few have been dated with accuracy, and in many cases specimens recorded by photographs are lost. The most controversial of these is an important Late Pleistocene tracksite from Valsequillo (near Puebla Mexico) dated at about 40 ka (Fig.

1.13. Gonzalez et al., 2006; Huddart et al., 2008). This date is much older than any accepted date for occupation of the new

Fig. 1.13 - Human footprints of Valsequillo, Puebla Mexico (Huddard et al., 2008)

world by *Homo sapiens*. Consequently, the authenticity of the "alleged" footprints (*sensu* Renne et al., 2005) has been questioned, and it has been suggested that the marks may be artifacts produced recently by quarrying operations. These same authors (Renne et al., 2005) suggested dates of 1.3 Ma, supported significantly by paleomagnetic studies. However, Gonzalez et al. (2006) argue that the dating of Renne et al. (2005) is incorrect.

At present, hominid tracksites from Argentina are better documented than those from Mexico. They include two sites from La Olla and a site at Monte Hermoso that have yielded hundreds of hominid trackways in association with mammal and bird footprints, stone tools and skeletal remains of sea lions and guanaco, which were probably hunted in a coastal lagoon setting. The age of the tracks is about 7000 years BP (Bayon & Politis, 1998). In one region of the Monte Hermoso site more than 400 human footprints, along with footprints of birds and artiodactyls, have been recorded in an area of 420 m^2.

Hominid tracks from Acahualinca, near Managua the capital of Nicaragua have been known since the late 19th century (Fig. 1.14. Flint, 1883; Brinton, 1887). The tracks are associated with the shores of Lake Xolotlan (Lake Managua) and have been ^{14}C dated at 5945 ± 145 BP (Bryan, 1973) and at 6500 by Bice (1979). Tracks are well preserved in long parallel trackways in a mudstone covered by black volcanic ash (Schmincke et al., 2008). Surprisingly, despite the presence of a museum (Huellas de Acahualinca) at the

Fig. 1.14 - Hominid tracks of Acahualinca, Managua (Nicaragua; Lockley et al., 2007)

site since the 1950s, the tracks have never been described in any detail. Early in 2006, Lockley made a map of the site recording the trackways of at least 15 individuals, an ungulate, an opossum and a bird (Lockley et al., 2008). In addition to the main museum site, an additional site known as El Recreo was also reported from the Managua area (Williams, 1952) that yielded bison and tapir tracks.

The oldest North American human footprints locality is the Oro Grande Site near Victorville, southern California. Radiocarbon age determination was given as 5070 ± 120 years (Rector, 1983), based on a charcoal

lens found just above the silty clay containing a total of at least 54 footprints. According to Rector (1979, 1983, 1999), at least four, possibly five trackmakers, including three immature and two adult individuals, may have been foraging for sheltered zone with dense vegetation.

An Important Bronze Age Site

Human and other animal footprints were recently reported from Nola, a Bronze Age village near Naples, Italy, destroyed by an ash fall (Fig. 1.15). According to Mastrolorenzo et al. (2006) and Di Vito et al. (2009), the 3780-yr-BP eruption of Vesuvius, known as the Avellino Plinian eruption, caused the fallout of lapilli and ash to the north-northeast and a final pyroclastic surge to the north-northwest. The lapilli and ash accumulated to more than a meter in depth as far as 35 km east of the source, burying houses and individuals. As indicated by footprints pressed into all horizons in the ash bed, the evacuation occurred during the settling of the surge cloud. Flood and lahar deposits overlying the surge bed also include footprints and local raindrop imprints as well, thus testifying that the ongoing exodus occurred during both the ash fall and the post-eruption rainstorms and floods (Mastrolorenzo et al., 2006).

Fig. 1.15 - The ichnological site of Nola, Naples (Italy; Mastrolorenzo et al., 2006)

Other Sites

Iron Age footprints have been reported from beneath a Roman Amphitheatre in Chester, England. According to Edwards (2006) several human and animal tracks were revealed in a hollow which appears to have been wet and muddy shortly before it was covered by the first amphitheatre. Radiocarbon dates obtained from postholes in the surface that immediately preceded amphitheatre construction date to the middle of the Iron Age.

Two footprints reported from Rawthey Cave, Cumbria, England (Chamberlain et al., 1997), with length measurements of 17.9 and 20.4 cm, have been attributed to children aged 5-6 and 8-9, respectively. The date of these tracks is uncertain but could be as recent as the 14th century AD.

Human tracks have been reported from various agricultural sites in Gunma Prefecture, Japan (Harada & Noto, 1984) that date from about 400 to 1280 AD (about 720–1600 BP). At both these sites volcanic ash fall evidently smothered a number of rice fields that had been heavily trampled, leaving large samples of footprints. Human tracks have been reported from at least four stratigraphic levels in a volcanic ash sequence from the Sunde

Site, Motutapu Island, New Zealand (Nichol, 1982). The site has been dated at about 1400 AD and reveals evidence of many individuals apparently not deterred by the continuing activity of ash falling over the area (Nichol, 1982). Indeed, Nichol (1982) also suggests that "a juvenile's rather peculiar print, with a very narrow heel appears on both the first and the second shower, so people do seem to have been able to survive the ash".

One of the youngest but most interesting fossil footprint sites is that reported from the footprint reserve at Hawaii Volcanoes National Park site (Jaggar, 1921; Swanson & Christiansen, 1973; Swanson & Rausch, 2008). Although dated to a Kilauea eruption and ashfall in 1790, the site can technically be considered prehistoric, as all reports of the influence of the ashfall on indigenous people are oral. The eruption is considered, in some interpretations, to have induced the local people to flee and perhaps perish as a direct result of a hot and relatively ash-free base surge; the footprints are purported to record the drama. Such a scenario is reminiscent of the well-documented drama reconstructed for the 3780-year-old Avellino site in Italy.

Chapter 2

The Roccamonfina Volcanic Complex

2.1 Geographical setting

The Roccamonfina volcano is a Quaternary volcano of Center-Southern Italy, between the Roman and the Campanian Regions. The volcanic complex borders on the Mesozoic-Cenozoic calcareous sediments of the Aurunci Mountains to the NW, Mount Massico to the SW, Mount Maggiore to the SE, and Mounts Cesima and Camino to the N (Fig. 2.1).

The volcanic deposits spread on the plain between Garigliano and Volturno rivers for about 450 km^2 and lies under Quaternary fluvial and lacustrine sediments (Bergomi et al., 1969). The surrounding carbonate and

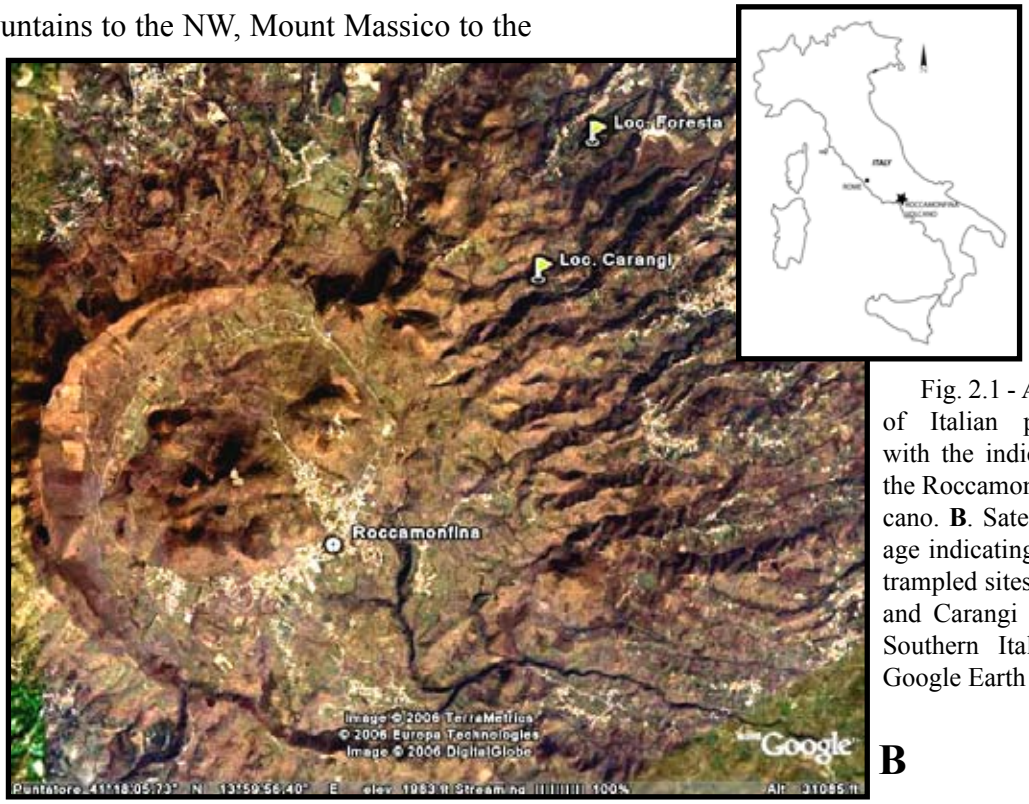

Fig. 2.1 - **A**. Sketch of Italian peninsula with the indication of the Roccamonfina volcano. **B**. Satellitar image indicating the two trampled sites: Foresta and Carangi (Caserta, Southern Italy; from Google Earth 2006)

marls horsts of Cretaceous age form the lateral margins of the basin in which Roccamonfina developed.

In origin it was a stratovolcano of about 1700-1800 m high, now mainly preserved in the western and southern sectors of the area. The preserved caldera is elliptic in shape, with the main axis 6 km long in NW-SE direction, and 600 m high. There is another caldera (named Northern caldera), close to the main one in the northern sector. In the center of the main caldera there are two lava domes, Mt. S. Croce and Mt. Lattani, 1006 and 810 m high respectively. In the outer parts there are many outlying vents such as Colle Friello, Mt. Tuororame and Mt. Atano.

2.2 GEOLOGICAL SETTING

The Roccamonfina volcano belongs to the volcanic belt of the Tyrrhenian margin (Fig. 2.2). From Upper Pleistocene intense volcanism took place along this margin, with the formation of several volcanic centers. Two big magmatic provinces bound the Roccamonfina volcano: the Roman and Campanian provinces. These provinces occupy a great area and include, besides Roccamonfina, also other important Italian volcanic centers such as Alban Hills and Mt.s Sabatini for the Roman region and Campi Flegrei and Somma-Vesuvio for the Campanian region. The origin of this magmatic activity is related to the eastern extensional structures of the Tyrrhenian basin, between the orogenic belt of the Apennines and the slow spreading center of the Tyrrhenian Sea. To the East of the Apennines, the Apulian micro-plate is subducted beneath the European plate, a convergent margin which is believed to be responsible for a classical arc-tectonic association of collision and extension, and onset of calc-alkaline to ultra-potassic volcanism typical of the

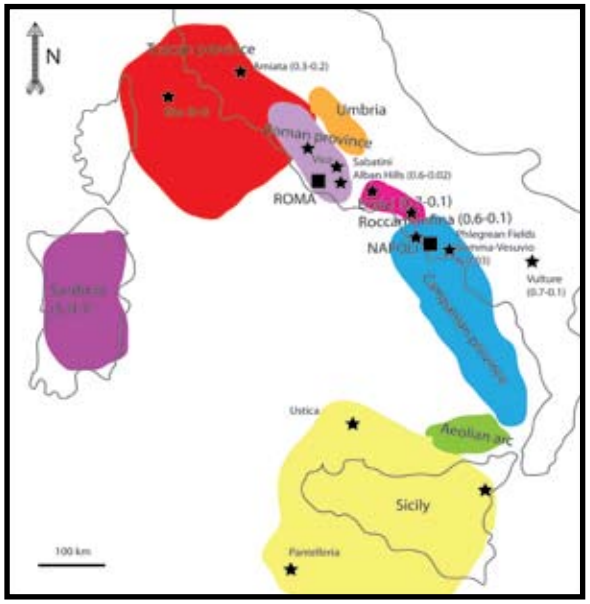

Fig. 2.2 - Distribution of recent magmatism in Italy. Different colour indicate various magmatic province (modified from Peccerillo, 2003)

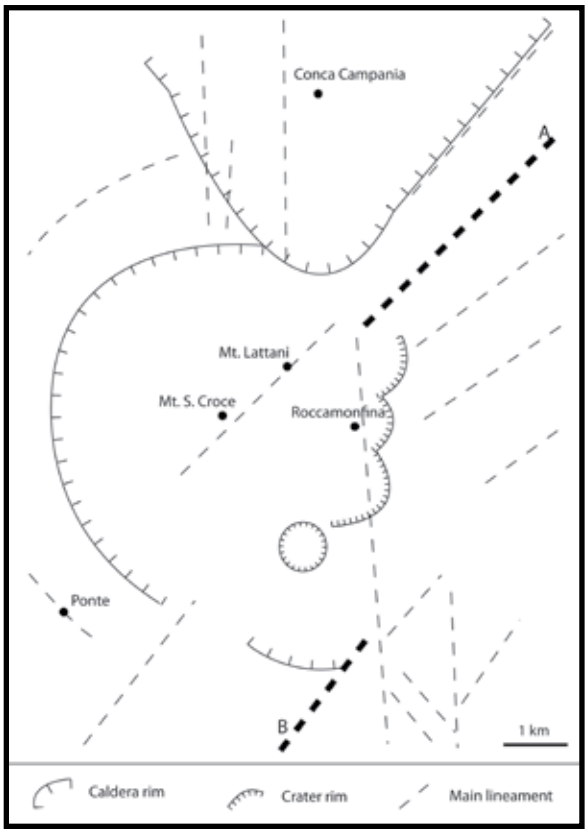

Fig. 2.3 - Simplified tectonic sketch of the Roccamonfina volcanic area (modified from de Rita & Giordano, 1996). A: extension of the lineament bordering Mt. Cesima; B: extension of the Mt. Massico fault

central-southern Italy (Peccerillo, 2005).

In fact, the Roccamonfina edifice lies in a tectonic depression between the NW-trending regional faults and the NE-trending faults related with Garigliano graben and the extensional structures (Fig. 2.3). The movements created a series of horst and graben, favoring the magma discharge. The whole Central-Southern Italian volcanism is the expression of this extensional regime.

2.3 THE EVOLUTION OF THE ROCCAMONFINA VOLCANIC COMPLEX

The activity of the Roccamonfina stratovolcano began about 630 ka and ended around 53 ka (De Rita & Giordano, 1996). Its activity is subdivided into three main epochs, corresponding to three different supersynthems (Fig. 2.4. De Rita et al., 1997). The first one (630-385 ka) is characterized by the growing of the stratovolcano and of several small volcanic centers. This edifice collapsed at the end of this phase. The second activity epoch (385-230 ka) is characterized by a succession of explosive eruptions cycles of mean intensity (Ballini et al., 1989; Ballini et al., 1990). The last phase instead lasted until 53 ka. During this period minor freatomagmatic activity and lava domes (Mt. Santa Croce and Mt. Lattani) occurred (Giannetti, 1970; Giannetti, 1974; Ghiara et al., 1977).

The geochemical evolution of this volcano is historically subdivided into two stages (Fig. 2.5. Appleton, 1972). They correspond to two different magmatic series: the high-K

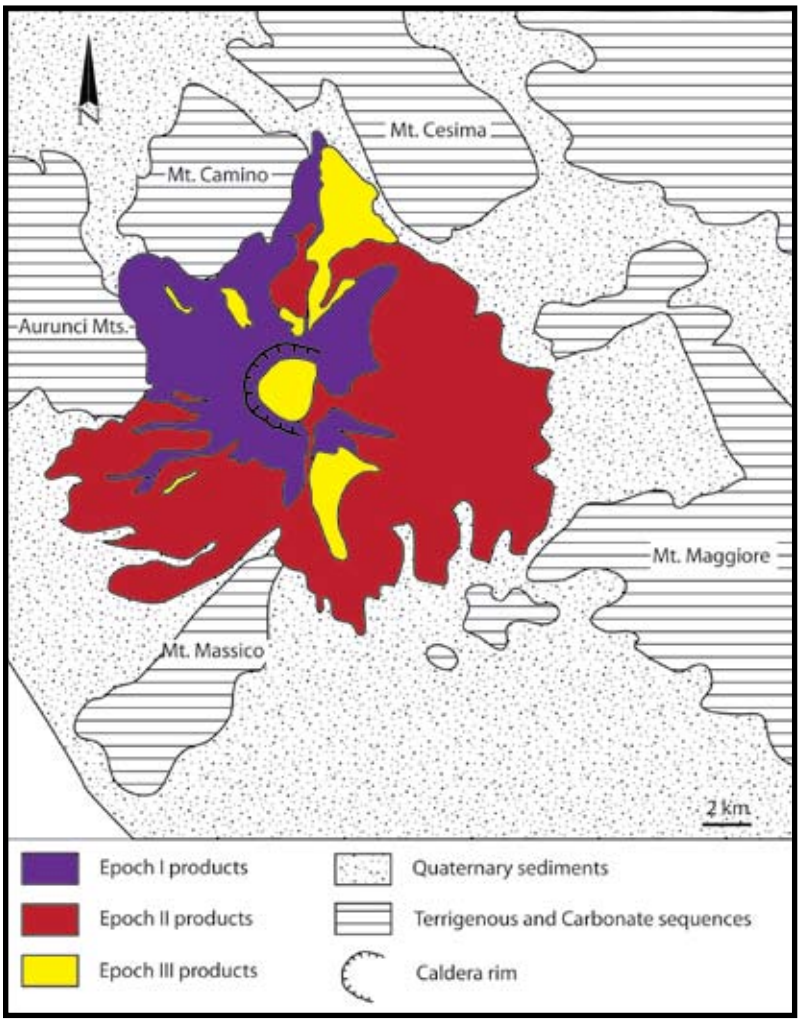

Fig. 2.4 - Sketch o fthe distribution of the three different activity epochs products (modified from De Rita & Giordano, 1996)

series, rich in leucite (HK or stage I), and the low-K series, poor in leucite (K or stage II). The activity of the stage I characterized mostly the volcanic history of Roccamonfina, from 630 to 340 ka (Giannetti et al. 1979; De Rita & Giordano, 1996). During this period the main cone was built by lava flows, minor pyroclastic falls and flows, and mudflows. Deposits cover the compositional interval from leucitic-tephrite to phonolite. At the end of the stage I the pyroclastic activity was dominant. A big explosive eruptive cycle occurred at the end of this stage, around 385 ka: the Brown Leucitic Tuff (BLT).

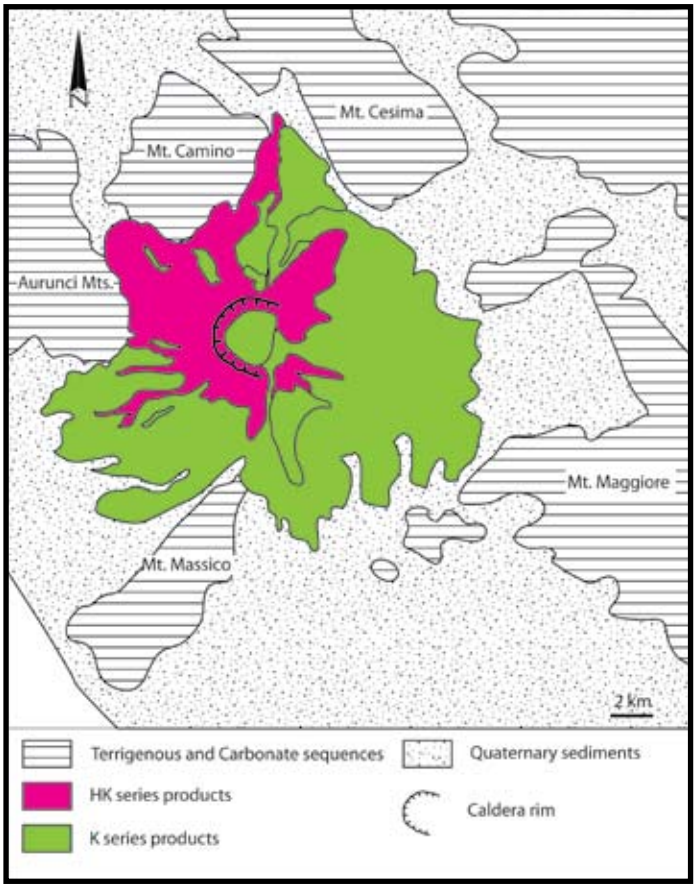

Fig. 2.5 - The subdivision of the Roccamonfina volcanic products in HK and K magmatic series (modified from De Rita & Giordano, 1996)

The beginning of the stage II (K series) is marked by the deposition of the White Trachytic Tuff (WTT) eruptions cycle, from 325-230 ka (Giannetti & Luhr, 1983; Ballini et al., 1989; Giannetti & Francaviglia, 1992; Giannetti & De Casa, 2000). Then a complex series of eruptive events occurred, forming Gli Stagli caldera, intracaldera lava domes and intracaldera phreatomagmatic eruptions. The Yellow Trachytic Tuff (YTT) eruptive cycle (Giannetti, 1996) and the mudflows of Conca Campania and Vezzara represent the moment of major activity of this phase. All the products of K series are significantly poor in K and in incompatible elements in relation to the HK series; HK series (Appleton, 1972) has low $^{87}Sr/^{86}Sr$ ratio and high $^{143}Nd/^{144}Nd$ and $^{206}Pb/^{204}Pb$ ratio (Cox et al., 1976; Hawkesworth & Vollmer 1979; Vollmer & Hawkesworth 1980) showing a progressively weakening of the influence of continental sources.

The most recent events in the Roccamonfina volcanic area enclose the deposition of distal flow units, in relation with Ignimbrite Campana, erupted by Campi Flegrei system about 40 ka.

The First Epoch

The first phase in the building of the stratovolcano belongs to Stage I. It is mainly characterized by effusive activity with the emission of sub-saturated lava flows. A dating on lava deposits on the western flank of the volcano gave an age of about 630 ka (Giannetti, 1979), so the activity probably began before this data. The original slope of the strato-volcano is still preserved in the western flanks of the edifice. Several parasitic centers were emplaced, such as Tuoro Piccolo and Mt. Capitolo (Cole et al., 1992; Rouchon et al., 2008). According to geochemical data of Appleton (1972), this epoch was characterized by the eruption of HK series magma having various parental melt compositions, differentiated dominantly at deep crustal levels. The onset of BLT (385-325 ka) and Rio Rava (440 ka) eruptions are marked by the upwelling of magmas derived from higher degrees of partial fusion, and less contaminated by subduction than the rest of HK series products. This may confirm the idea of Marra et al. (2004) about the existence of melt production cycles in the underlying lithosferic mantle.

The Second Epoch

At the end of Stage I a series of explosive eruptions emplaced a group of medium-small pyroclastic deposits. Luhr & Giannetti (1987) called this pyroclastic complex Brown Leucitic Tuff (BLT). Giannetti et al. (1979) supposed that BLT deposits were related to the formation of the main caldera. The main caldera had an elliptic shape with the main axis 6.5 km long and a NW-SE direction and the shorter axis 5 km long. The margins are well preserved in southern and western margins where the walls are 290 m high. The northern and eastern margins are worse preserved. The chronological collocation of the formation of the caldera is still debated.

The BLT places itself between HK and K series products. Thus, it postdated the last HK series lavas, while the early K series lavas were erupted after the BLT. The BLT resulted from the emptying of a zoned HK magma chamber (Luhr & Giannetti, 1987) during the K series magma recharge. The sharp geochemical shift at about 355 kys observed by Rouchon et al. (2008) is correlated with the evolution of the BLT pumices throughout their eruption in a single crisis. The evidences give a little support to the existence of a HK-K series concurrent stage (Giannetti et al., 2001) as the BLT marked the purge of all HK series magma.

The younger of BLT pyroclastic deposits is the Campagnola Tuff, mainly emplaced in the eastern sectors of the volcanic area. So at least this unit must to be a post main caldera event. Pumices in these deposits were almost always altered and the leucite crystals were changed into analcime, so the original composition does not often reflect the erupted magma composition.

Actually the relationship between BLT and the main caldera has been highly debated during decades (Capuano et al., 1992; Cole et al., 1992; Chiesa et al., 1995; De Rita & Giordano, 1996; Giannetti, 2001). The formation of this crater by a caldera-forming event (e.g. deep reservoir collapse) was rejected by Watts (1987) and De Rita & Giordano (1996) after deep borehole investigation of the main crater, which did not indicate the presence of a disrupted or subsided basement. Alternatively, it has been

suggested that the main caldera resulted from a lateral sector collapse linked to the eruption of the BLT (Chiesa et al., 1985; Watts, 1987; Chiesa et al., 1995), or to the instability of the eastern flank as a result of its continuous down throwing by the Mt. Massico fault (De Rita & Giordano, 1996). My survey appears to support this last theory. The BLT was very likely produced for tectonic reasons. Morphostructural observations, however, reveal that the western and southern sectors are two distinct structures. The crater rim of the southern sector is capped by the pre-Rio Rava center near Tuoro Piccolo (about 470 ka, Rouchon et al., 2008), while the post-Rio Rava-pre-BLT Mt. Capitolo (about 390 ka, Rouchon et al., 2008) stands inside the main crater at its eastern border (De Rita & Giordano, 1996). Both evidences imply that the southern rim of the main crater was formed between these two events, while only the rim of the western sector is linked to the eruption of the BLT. The northward opening of the southern sector and the time range for its formation are consistent with the age and northwards location of the Rio Rava deposits. The higher degree of erosion of the southern sector compared to the western sector is a direct consequence of their about 100 ka difference of exposure, and the elliptical shape of the main crater is a consequence of its incremental formation during the HK stage (Rouchon et al., 2008) rather than produced by the synchronous development of two overlapping main cones, as it was proposed by Cole et al. (1992)

The K stage started at about 340 ka, which corresponds to the final activity of the BLT eruption. The following cycle activity occurred at around 320 ka with the deposition of the White Trachytic Tuff (WTT, Giannetti & De Casa, 2000). The lower part of these deposits (LWTT), which represent about 80% vol of the whole WTT succession, was emplaced. Pyroclastic flow deposits of the LWTT contain frequent lithic accumulation zones of clasts derived from the demolition of the main cone, and dominantly from trachyandesite units in the main crater (Giannetti & De Casa, 2000). Although the volume of the outcropping effusive products of the K stage

Fig 2.6 - Lava domes: Mt. S. Croce and Mt. Lattani, in the central part of the central caldera

is rather small in comparison with those of the HK stages, it can't be excluded that small central volcanoes were built-up between BLT and WTT eruptions. They could be cyclically destroyed by WTT Plinian activity throughout WTT period. After LWTT activity, a number of trachybasaltic and shoshonitic parasitic centres erupted, including Colle Friello (270 ka; Rouchon et al., 2008). The main crater activity was also characterized by the emplacement of the shoshonitic basalts in the western part of the crater floor (245 ka) and by strombolian activity in the main crater, testified by the presence of latitic proximal ejecta (Fontanafredda deposits) dated 232 ka (Rouchon et al., 2008). Upper-WTT units represent limited erupted volumes related to localized explosions, emplaced 230 ka (Giannetti & De Casa, 2000).

The Third Epoch

The end of the K series corresponds to the third and last supersynthem of the Roccamonfina volcano history (De Rita & Giordano, 1996). It includes the building of lava domes (Fig. 2.6. Mt. S. Croce and Mt. Lattani) in the main caldera and minor explosive eruption. The domes are about 400 m high on the floor of the caldera and the materials volume is about $900x10^6$ m^3. Mt S. Croce was dated at about 150 ka and Mt. Lattani at about 170 ka with $^{40}Ar/^{39}Ar$ methodology (Radicati di Bronzolo et al., 1988). They represent the most recent activity inside the caldera (Giannetti, 1964).

An important sequence of deposits crops out near the locality Fontanafredda. This sequence is characterized by the presence of volcanic deposits re-elaborated as fluvial sediments and by the deposition of a scoriae-rich pyroclastic deposit with abundant lapilli levels (Giannetti, 1998). A lot of basaltic-trachy-andesitic scoriae and numerous degassing pipes characterize the deposits, especially in the upper part of the unit flow. It is very difficult to correlate these deposits and the other material filling the caldera, but it is clear that this unit is related to an explosive phase during the domes growing.

The northern caldera was built by intense volcanic activity in the last part of Roccamonfina history. This activity created a circular depression cutting the main caldera.

It is likely to have been created by Yellow Trachytic Tuff eruption (YTT; Giannetti, 1996). It was formed by a single maar-forming event associated with the emplacement of the YTT at 227 ka (Giannetti, 1996) and Conca Ignimbrite (Cole et al., 1992) by magma-water interaction. These deposits are present only in the northern caldera and they spread to 5 km from the vent, forming a sort of plain northward of Monte Friello. In the surroundings the YTT is covered by airfall and phreatomagmatic surge, representing the end of the activity of the caldera.

During the last phase activity of the Roccamonfina volcanic complex, the main caldera activity was more localized and gave more basic products. The northern caldera instead, was characterized by more explosive activity, involving the emission of trachytic magma.

Chapter 3

The Stratigraphy of BLT formation

3.1 Introduction

The Brown Leucitic Tuff (BLT) is the result of an explosive eruption with the deposition of several units (Luhr & Giannetti, 1987). Pyroclastic flow, pyroclastic surge and tephra fall units were deposited in short time interval (325-385 ka, Luhr & Giannetti, 1987). This is testified by the lack of paleosoils among the units. Under BLT formation scarce pyroclastic flow and mudflow deposits are locally present but they are mainly related to the stratovolcano construction epoch since their stratigraphical position below the BLT early deposits.

In the early works on Roccamonfina volcanic deposits, BLT and WTT were grouped in a single formation, called "chaotic fragmental volcanic deposits" (Tedesco, 1964; Bergomi et al., 1969). They are described as chaotic fragmental deposits that show evidences of emplacement by flowing. Afterwards, BLT became a unique formation characterized by consolidation and by crystallization of secondary minerals (Di Girolamo, 1968). Later, Luhr & Giannetti (1987) studied its mineralogy and compositional characteristics, concluding that BLT derived from a progressive emptying of a compositionally stratified magma chamber.

The eruption cycle began about 385 ka, near the end of Stage I and finished about 325 ka (Luhr & Giannetti, 1987; Ballini et al., 1990). Cole et al. (1993) considered the BLT the last events of a complex sequence of pyroclastic flow units.

It corresponds to the beginning of the second synthems of the activity of this volcanic complex (De Rita & Giordano, 1996). The few trachytic parts show that the BLT formation, especially at the end, also spreads into the Stage II of the geochemical history of the Roccamonfina volcano, with K series products.

A controversial aspect concerning BLT is its relation with the main caldera formation.

During the decades BLT was periodically related or not with the building of the main caldera (Capuano et al., 1992; Cole et al., 1992; Chiesa et al., 1995; De Rita & Giordano, 1996; Giannetti, 2001). Finally, De Rita & Giordano (1996) observed instead the lack of disrupted or subsided basement, establishing that the crater was not formed by a caldera-forming event. Giannetti (2001) pointed out that the walls of the central caldera are better preserved in its western half rather than in the eastern. These two portions are separated by a SW-NE fault (Giannetti, 1979) or by two distinct tectonic faults trending SW and NE (Luhr & Giannetti, 1987; De Rita & Giordano, 1996). The faults intersect eccentric tephritic scoria cones at the base of Mt. Cesima. So these faults truncated the central caldera and lowered the eastern sector of the volcano. The rim of the central caldera is so punctuated by the parasitic centers. Few of them lie at the intersection of the caldera ring fault with the SW and NE trending faults. Thus Giannetti (2001) affirmed that: there is a relationship between the parasitic centers and the ring faulting; some of these centers rest on the dissected central caldera wall; the BLT also rests or drapes either the dissected remnants of the caldera wall or the ring vent (Giannetti, 1979; Luhr & Giannetti, 1987; De Rita & Giordano, 1996), implying that BLT deposits were erupted after the collapse and the ring vent centers.

Recently Rouchon et al. (2008) affirm that there is a relationship between the explosive structures and the BLT eruption. So according to these authors the BLT is the cause of a lateral sector collapse of the edifice.

3.2 DISTRIBUTION AND CHARACTERISTICS

The formation occupies a wide area around the Roccamonfina volcanic complex. It is deposited predominantly in its north-eastern and southern sectors. In the western part instead there are very few outcrops, probably because of the presence of caldera rims and because of the presence of the faults systems. It created a structural high, which exposed BLT to erosion. So here the deposits of the BLT eruption are thinner than in other sectors.

From careful analyses of the deposits it appears that the BLT is not related with the central caldera formation. During the survey the attention was focused on the boundaries among the BLT, the caldera zone and the deposits below. The BLT was mainly deposited from the northern to the south-western sectors, and was completely lacking in the north-western sector. It was supposed that the reason of this particular distribution is that NE to SW sectors were already depressed at the moment of the eruption. Following the boundary, the observation of De Rita & Giordano (1996) and Giannetti (2001). it was observed that Mount Atano, Mount Tuororame and Mount Capitolo were formed after the caldera collapse near the caldera rims. BLT formation lies over the deposit of these small edifices, so the BLT eruption took place after the caldera collapse. In each part of this formation no debris avalanche or rock fall at the base of the BLT formation were found. The model of the eruption caused by sector collapse of the edifice proposed by Chiesa et al. (1985) and Watts (1987) is thus no supported by field data. Also the data of the bore-hole, drilled on the western edge of the Mt. Santa Croce latite dome (Watts,

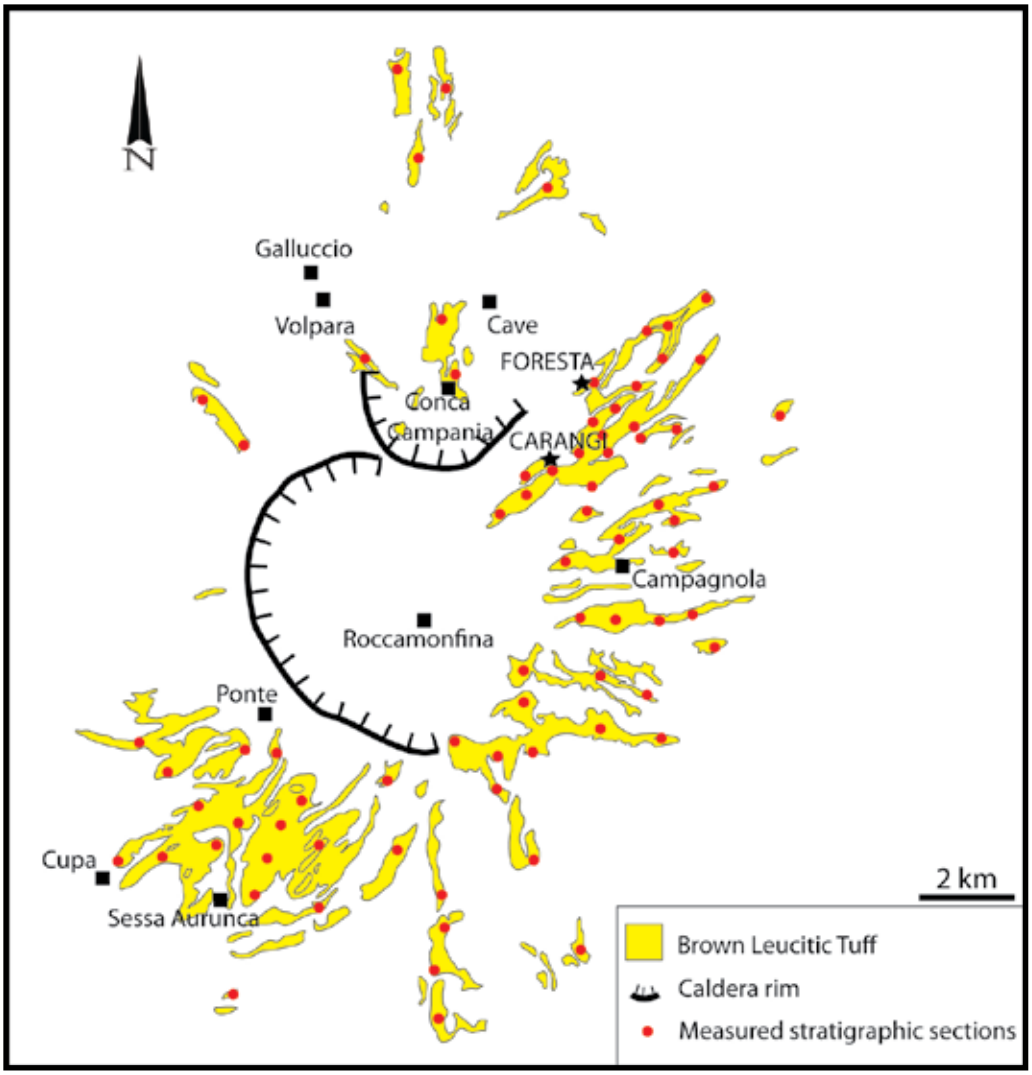

Fig. 3.1 - Distribution of BLT outcrops. The red dots represent the measured stratigraphic sections (76)

1987), show only sedimentary reworked explosive deposits interbedded with tephra layer and mudflow layers. Probably only the early phase of this eruption is related to the formation of the caldera, and a change in the chemistry seems to cause the end of this explosive phase.

The collapse of the composite volcano had already happened at the time of BLT eruption.

3.3 METHODOLOGY

The work consists in a detailed analysis of the stratigraphy of the BLT in order to understand and describe the eruption dynamics of the trampled formation. During the survey of the BLT deposits, 76 stratigraphic sections were measured (Fig. 3.1). Afterwards, all the 76 stratigraphies were connected in a single stratigraphic log involving BLT deposits on the whole. This permitted to understand in detail each phase of the development of the eruption, in order to have the possibility to locate the trampling event in a precise time window.

Sedimentological analyses were carried out with a careful subdivision of the deposits in facies, units and subunits. Isopachs maps for each pyroclastic flow sub-unit follow these data.

The extension and the mean thickness of the formation have been considered to calculate the volume of the deposits. I took into account the limits of this calculation due to the difficulty of the estimation of the ash dispersal and the eroded material from Pleistocene to our days.

The granulometric analyses were made using thin sections (20-25 thin sections for each unit) and counting manually the diameter of each particle using the optical microscope, because the lithification of part of the samples does not permit the use of sieves. No image analysis software was used because of the difficulty in discerning lithic fragments contours. Most of the lithic fragments in fact are lava fragments belonging to the stratovolcano and have a porphyric structure. Therefore the software recognized as particles also the phenocrystals inside the fragments. All these data were later elaborated using statistical parameters methods (Inman, 1952; Folk, 1966). The statistical parameters used for the description and the characterization of the deposits are:

Φ	Granulometric glass
Md_{Φ}	Median
M_{Φ}	Mean
σ_{Φ}	Sorting
σ_I	Inclusive graphic standard deviation
a_{Φ}	Skewness
Sk_I	Inclusive graphic skewness
KG	Graphic Kurtosis

3.4 FACIES

In the outcrops of the BLT different patterns permitting an empiric subdivision of this formation are recognizable. The color is one of the most evident characteristics but the relative percentage of pumices and lithics, the alteration and the lithification rate were considered, too. They altogether permit the subdivision of the facies into three parts: the white, the brown and the ochre one (sensu Luhr & Giannetti, 1987).

The white facies

Deposits of the white facies crop out in the south-western part of the volcanic area, and they are about the 20% vol of the whole surveyed BLT (Fig. 3.2). They are the expression of the more recent emission of the BLT eruptive cycle. Thus they occupy highest stratigraphic position.

The great abundance of white pumices and ash and the low lithic fragments content (<10% vol) determine the white color of the facies. The dimension of the clasts goes from 20 cm to 1 cm for the pumices and from 5 cm to less than 1 cm for the lithic fragments.

The layers are thicker than the immediately following flow units of the WTT which are similar in the aspect. The thickness varies

Fig. 3.2 - White facies outcrop, near Ponte locality

from 1 m to 2.5 m. It is characterized by the scarcity of pumices-fall layers at the base of the units, which is typical of the HK units.

Low-angle cross bedding are not as abundant as those that characterize the basal WTT units (Giannetti & Luhr, 1983).

The brown facies

This facies are about 40% of the BLT deposits and it is manly located in the southern flanks of the central caldera. They are the oldest deposits of the BLT eruptive cycle, so they are at the base of the overall stratigraphy.

The features of this facies are the brownish color of the outcrops, the poor lithification and the large abundance of lithic fragments, sometimes also metric with respect to the content of pumices and ash.

The lithics amount varies from 20% vol to 80% vol, in few lenses at the base of the pyroclastic flow units. The dimensions of the lithics vary from 1 m to few cm. The pumices are dark grey when fresh, but they usually show bleaching at the margins. In many outcrops, only the cores of the bigger pumices are not altered, instead the smaller ones are completely bleached.

The ochre facies

The ochre facies crops out in the northeastern part of the volcanic area and it forms the remnant 40% of the BLT rocks (Fig. 3.3).

The matrix is characterized by a strong lithification and by a low content in lithic fragments (10-30% vol) that are usually less than 5 cm in size. Large lithic fragments are absent.

The alteration of matrix glass and pumices determined the ochre color of the outcrops. It is so strongly that the pumices are often completely weathered out leaving holes.

The partial alteration of the pumices in brown facies units is probably a precursor of the complete alteration in ochre facies units.

The large distribution of the lithification in the ochre facies outcrops is linked to the formation of the chabazite and phillipsite in the deposits.

Fig. 3.3 - Ochre facies outcrop, near Foresta locality

3.5 STRATIGRAPHY

The "Ciampate del Diavolo" site is mainly characterized by the outcropping of BLT deposits. A detailed analysis of the deposits is necessary to understand the eruption dynamics influencing the trampling and post-trampling phenomena.

BLT outcrops can be subdivided into 8 units. Each unit represents a phase activity of the eruption and expresses its evolution (Fig. 3.4).

The BLT formation lies above the deposits of the stratovolcano, separated by an erosive surface, which is clearly visible close to Carangi locality (Fig. 3.5). These deposits are mainly tephrites and phonolites rich in

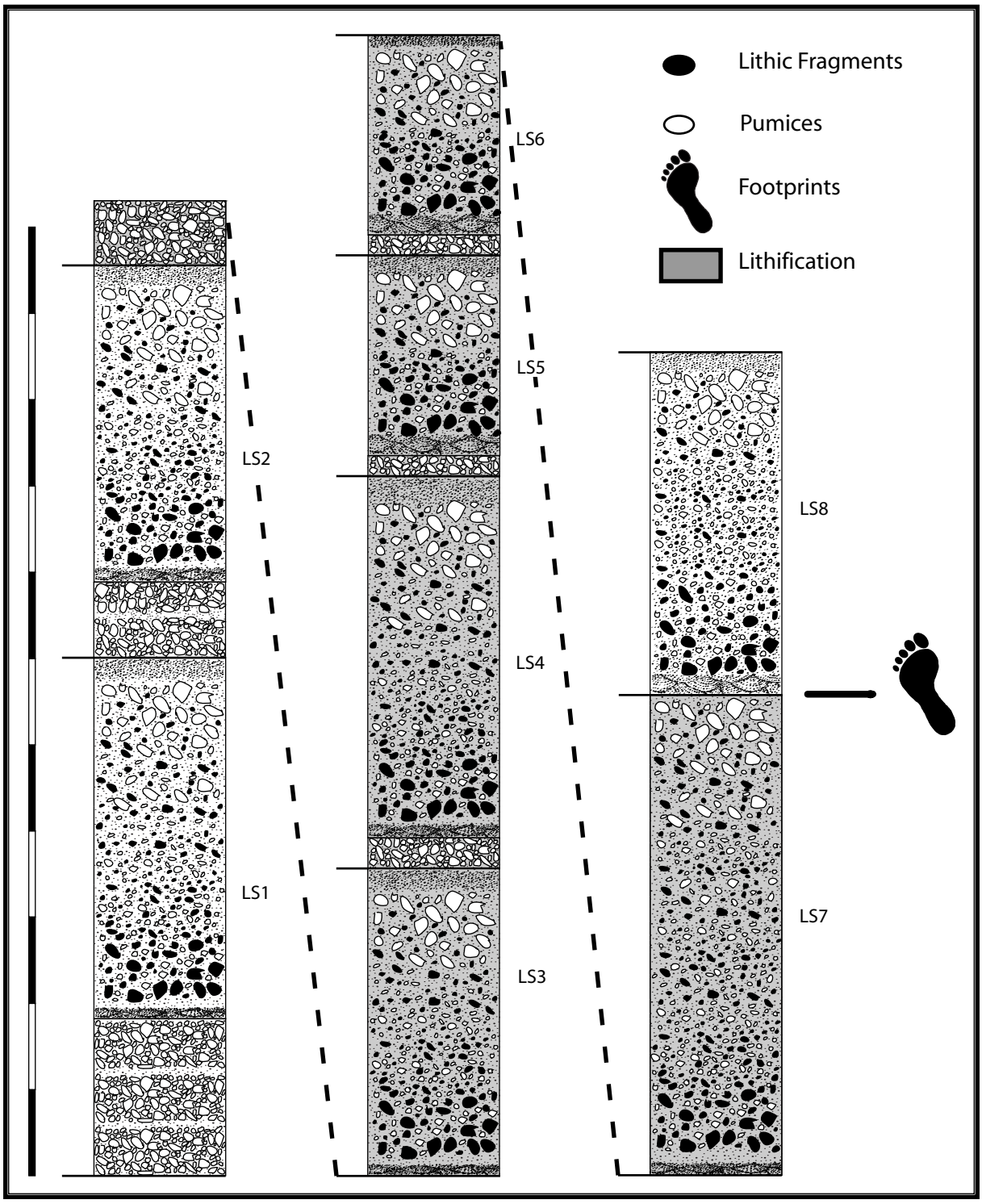

Fig. 3.4 - Stratigraphy of the whole BLT deposits with the indication of the units

leucites (Tedesco, 1964; Giannetti, 1979). The discontinuity marks the end of the building of the stratovolcano and expresses a different time interval depending on the erosion rate.

Near the vent and under the discontinuity there is a paleosoil, partially eroded both for the erosion during the quiescence time between the stratovolcano phase and the following activity represented by BLT deposits.

Here the hydrographical reticule is highly developed and the outcrops are characterized by the presence of the WTT filling the gorges of BLT formation or by the presence of a

Fig. 3.5 - Picture at the boundary startovolcano lavas - BLT (Carangi locality)

thin paleosoil between the BLT and the more recent WTT deposits. Among BLT units no paleosoil can be observed, suggesting that the whole eruption took place in a relatively short time interval, or at least not long time interval passed among the deposition of the units.

In the Foresta site only six of the total units are present (Fig. 3.6), probably because of the lack of deposition of these units or the complete erosion of two units. They belong to the ochre facies because of the color of the rocks and the widespread lithification.

The 8 units are similar and they are constituted by different sub-units, marking distinct eruptive phase during the eruption.

I am going to describe each part for only the first unit **LS1**. The others are similar to this one and differ only for the thickness.

The lowermost unit of the BLT formation is the **LS1** unit and lies on the stratovolcano lavas. Its basal part (**LS1'**) is a very thick layer mainly constituted by pumices (80%) and few scoriae and lithic fragments (20%). Thin beds of fine ash are present within it and their are at most 10 cm thick. The whole thickness of **LS1'** sub-unit goes from 2 m to 1. The coarser beds are about 20-30 cm thick. The pumices diameter ranges from 15 to less than 1 cm. They are white or light gray. Most of them are highly altered and the survived ones have highly irregular shapes and fluidal structures. Lithic fragments are smaller than pumices. Their sizes range from 5 cm to less than 1 cm. The alternation between pumice-rich beds with ash-rich beds is an evidence

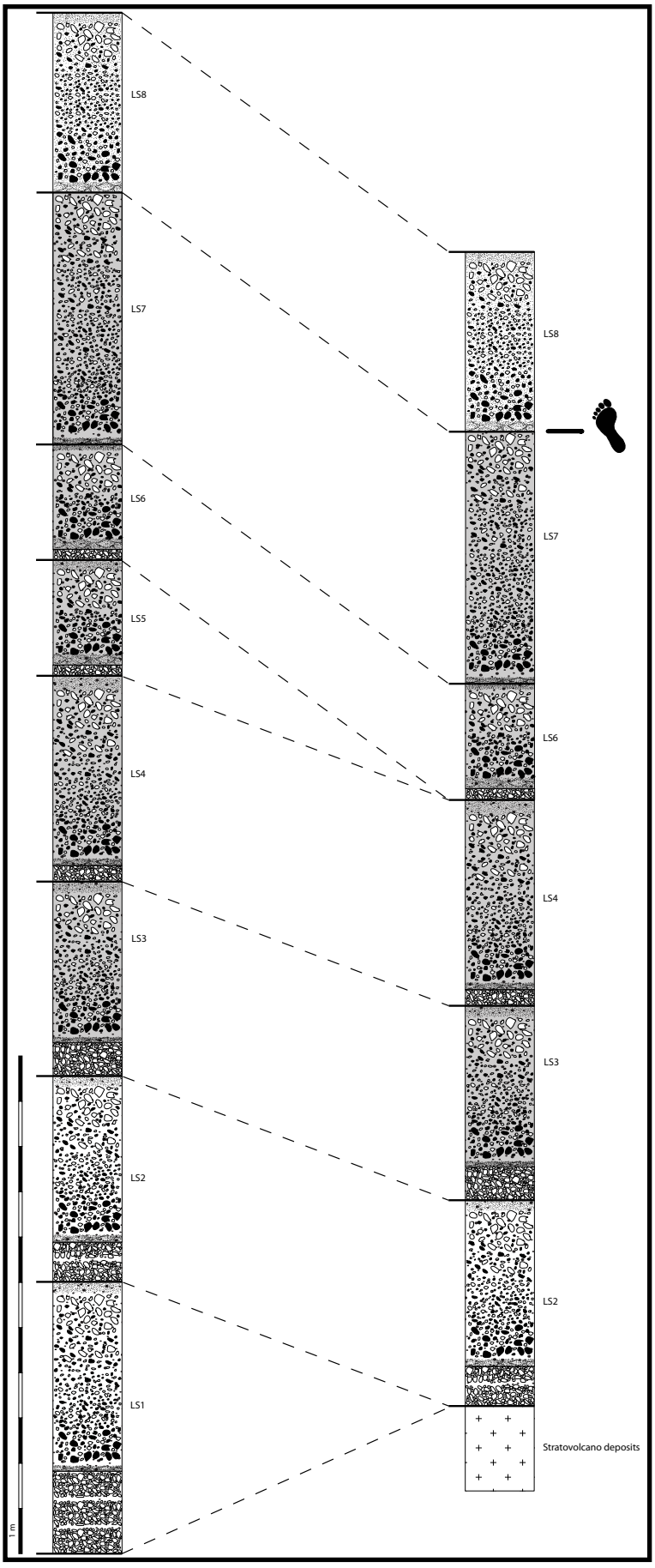

Fig. 3.6 - Stratigraphy of the BLT deposits at Foresta locality

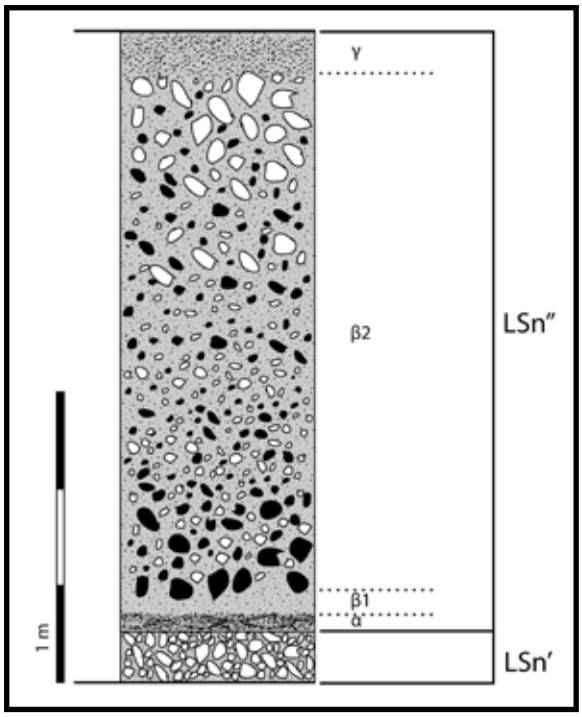

Fig. 3.7 - The subdivision in sub-units and levels of each unit

of an instable sustained eruptive column. The pumice-rich part formed during the sustained column phase, and the ash-rich bed represent stasis interval permitting the deposition of the finest parts, in suspension in the atmosphere. Its high thickness is probably due to the proximity of the original volcano flanks and decreases toward the outer parts. The pumices present a slight bedding, mainly visible near the vent. Probably it is linked to the slope of the volcano flanks. The sorting value of **LS1'** sub-unit is relatively low (σ_Φ = 1.7), indicating a homogeneity in the clasts' dimensions.

Over **LS1'** sub-unit there is a very thick layer (**LS1"**), expression of a pyroclastic flow event. It is mainly constituted by ash, pumices, scoriae, lithic fragments and crystals. Inside this layer four different members can be recognized, labeled **α**, **β1**, **β2** and **γ** (Fig. 3.7). The sub-unit does not present particular sedimentary structures on the whole. The color of **LS1"** is brown-orange and presents wide lithification, not observed in the former sub-unit (**LS1'**).

α bed is a thin level of a few centimeters average thickness (11 - 2 cm). It is rich in crystals (K-feldspars, augites, biotites, etc) and small lithic fragments. Generally the lithic fragments are about the 65% of the level and the crystals the remaning 35%. The particles are less than 1 cm in size. The crystals are on average smaller than lithic fragments. No kind of stratification can be observed because of its thickness. This level is present in most of the BLT units, with various thicknesses.

Over this level a thin part (level **β1**) is always visible. It is a light gray to orange and its thickness varies from 1 cm to less than 10 cm. It corresponds to layer 2a of Sparks et al. (1973) and it is the fine-grained basal part of a pyroclastic flow unit. Normal gradation of the particles can be observed, but not other sedimentary structures are visible. The composition of this level is mainly fine ash and crystals such as augite, anorthite, sanidine, Ti-biotite and minor zeolites. The crystals form the 20% of the bed. The particles mean sizes goes from 3 mm to less than 1 mm.

Over **β1** there is a massive and thicker layer (level **β2**), corresponding to the layer 2b of Sparks et al. (1973). Its thickness ranges from 6 m to 1 m. The boundary with the layer below is not sharp, but it is gradual. It is possible to draw a limit because of the difference of fragments abundance, not present in the layer below. It is homogeneous and not particular sedimentary structures are present. Even so, an iso-orientation of the more elongate fragments is locally visible, expression of the flowage of the pyroclastic flow. A slight normal gradation for the lithic fragments is visible, ranging from few

centimeters at the base to few millimeters at the top. The relative dimensions of the fragments differ in relation with the distance from the vent. In these portions the lithic fragments are bigger that those of Foresta site (5 km of distance). Fragments are irregular or slightly rounded. Compositionally, they are mainly tephritic, phono-tephritic, similar to those of the stratocone.

The pumices in this layer present an inverse gradation. The largest pumices are on the top of the layer and the smallest are on the bottom. They are irregular, with fluidal structures and strongly altered. The ground mass is mainly fine ash and small crystals, mainly augite and sanidine with minor biotite, and it is partially cemented by zeolite aggregates.

The last part of the sub-unit **LS1"** is a very fine and granulometrically homogeneous ash bed (level **γ**). It is a discontinuous level, not always visible. Where it is not present it was probably eroded by the deposition of the subsequent unit or not sedimented.

This particular succession of sub-units is repeated also in the following units. In fact the BLT deposits are composed by several eruptive pulses with similar characteristics. They have the tephra layer at the base, similar to **LS1'**, and they are called **LS2'-LS8'**, and similar to **LS1"** massive sub-unit (**LS2"-LS8"**), that progressively decrease in thickness outward the vent.

In the "Ciampate del Diavolo" site, the lower layer recognizable is the tephra fall layer named **LS2'**. It is a clasts-supported medium-thick layer of predominantly large altered irregular pumices and lithic fragments enclosed by ash. They are angular, suggesting little transport. The dimensions of the lithics range from few centimeters to millimeters. This layer is pseudo-horizontal like the other layers above. It has not any particular structures like gradation or stratification, but it is visible an alternation between lithic-rich and pumices-rich beds is visible. The thickness of this layer increases towards the vent, where it is about 10 cm thick, instead towards the Foresta site it is only 1-3 cm thick.

Over this layer there is the sub-unit **LS2"**. It is similar to the layer **LS1"** but it has a lower juvenile clasts and lithic fragments percentage. The other units **(LS3-LS8**) progressively increase in thickness, reaching in Foresta site less than 1 m for the units **LS7** and **LS8**. The content in lithic fragments instead decreases gradually. It ranges from 10% for the **LS1** to 3-4% for the **LS7** and **LS8** units.

Some of these units are strongly lithified by zeolitization process. Aggregates of zeolite minerals (chabazites and phillipsites) cemented the matrix and transformed glass shards and part of the pumices and scoriae. The units involved in this process are **LS3-LS7**. The human footprints were impressed over the last lithified unit (**LS7**) and they were covered by **LS8** not lithified unit, which was eroded in historical period. This unit was covered by deposits of the following eruptive cycle (WTT).

3.6 GRAIN-SIZE ANALYSES

Grain-size analyses were made to better understand each phase of the activity originating the BLT. They are useful also to discover the presence of sudden changes or stasis in the emplacement mechanism. The results depend on the original composition of the erupted material and also on the eruptive

processes such as fragmentation, transport and deposition.

Aperture (mm)	Φ
> 256	-8
256-181	-7,5
181-128	-7
128-90.5	-6,5
90.5-64	-6
64-45.3	-5,5
45.3-32	-5
32-22.6	-4,5
22.6-16	-4
16-11.3	-3,5
11.3-8	-3
8-5.66	-2,5
5.66-4	-2
4-2.8	-1,5
2.8-2	-1
2-1.4	-0,5
1.4-1	0
1-0.710	0,5
0.710-0.5	1
0.5-0.355	1,5
0.355-0.250	2
0.250-0.180	2,5
0.180-0.125	3
0.125-0.090	3,5
0.090-0.063	4
0.063-0.045	4,5
0.045-0.031	5
<0.031	5,5

Tab. 3.1 - Discrete dimensional classes in which the samples are subdivided

The granulometric analyses use different discrete dimensional classes, in which the samples are subdivided. In each class there are fragments with dimensions within a precise interval. This interval (Φ) is defined as $\Phi = -\log_2(d)$, where d is the diameter in mm (Wentworth, 1922; Krumbein, 1938). Thus this is a dimensionless value directly related to the diameter of the particle (Tab. 3.1).

Most of the samples were lithified so the sieves were not used for granulometric analyses to avoid breackage of the clasts. In this case I used the thin-sections and high-resolution pictures of the thin sections; grains were counted manually using a grid of 0,01 mm, chosen corresponding to the least dimension of the grains. The samples were also collected from different parts of the same unit, in order to understand the evolution of a single eruptive event. Particles bigger than 2 cm were counted directly in the outcrops, using a grid of 1 m x 1 m.

An important aspect of the granulometric analyses is the choice of the granulometric

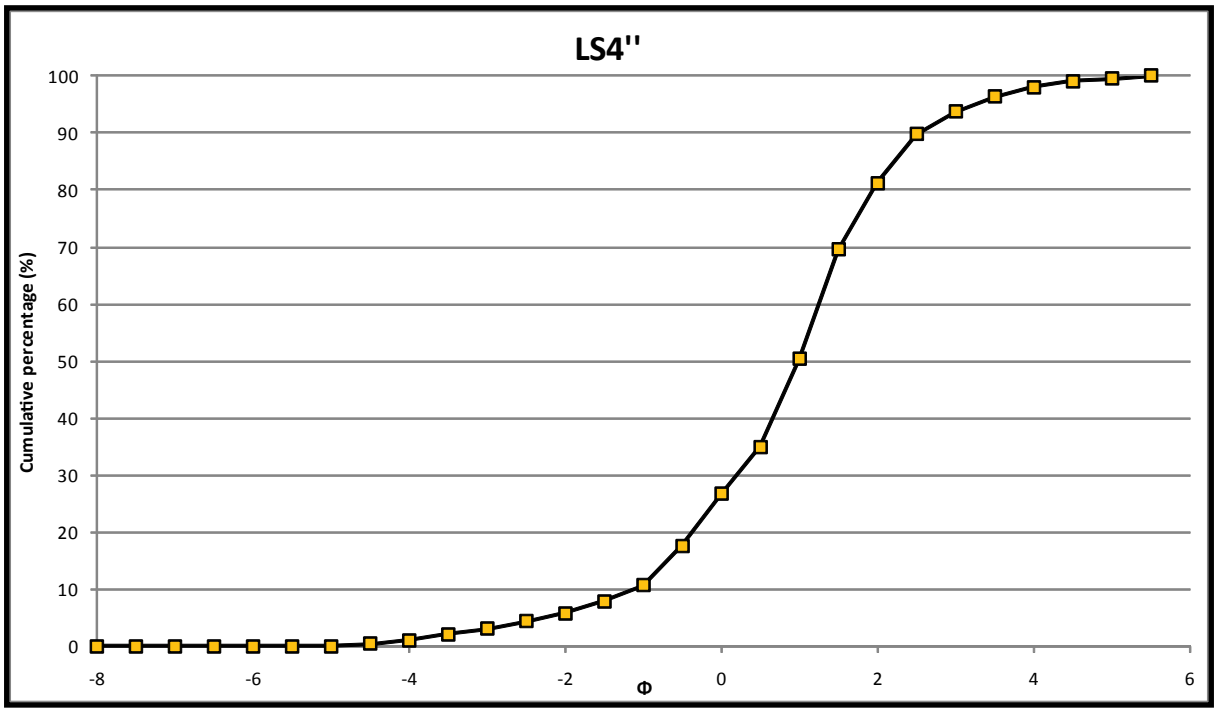

Fig. 3.8 - Exemple of one of the calculated granulometric curves (LS4'' sub-unit)

interval between the classes. Here 0.5 value was chosen as difference between Φ, suitable to characterize possible subpopulations or polymodalities in the grain-size distribution. The obtained values were converted in percentage of the corresponding granulometric class considering the total of the measured fragments in each thin section. In this study 27 granulometric classes were considered, from -8 Φ (>256 mm) to 5 Φ (0.045-0.031 mm). Particles smaller than 0.031 mm were all grouped in class 5.5 Φ. The grain size distributions of all the analyzed samples are unimodal.

For the statistical analyses of the different units, the most widespread statistical parameters were used. Using the percentage of each dimensional class the cumulative percentage curve was drawn for each unit (Fig. 3.8). With this distribution it is possible to establish the Φ values in relation to particular cumulative percentage values, called percentile (5, 16, 50, 84, 95), useful for statistical analyses.

One of the principal statistical parameter used is the *median* (Md_{Φ}) that is the diameter corresponding to the 50% of the cumulative curve (Φ_{50}). This parameter is a good representation of the total size distribution of the stratigraphical unit (Tab. 3.2).

Another important parameter is the *mean* (M_{Φ}), a statistical parameter depending upon the total distribution of the grain size of a deposit.

Mean diameter:
$M_{\Phi} = (\Phi_{16}+\Phi_{84}) / 2$ (Inman, 1952).

Another essential parameter is the *Sorting* (σ_{Φ}), a way to represent the grade of selection of a deposit. It corresponds to the graphical standard deviation (Tab. 3.2).

Unit	Md_{Φ}	σ_{Φ}
LS1'	-2,25	1,75
LS1''	0,42	2,66
LS2'	-1,09	2,50
LS2''	0,85	1,45
LS3'	0,08	2,25
LS3''	0,76	1,80
LS4'	0,77	1,46
LS4''	0,99	1,39
LS5'	0,74	1,47
LS5''	0,98	1,36
LS6'	0,85	1,89
LS6''	0,31	2,68
LS7''	0,31	2,50
LS8''	0,69	2,19

Tab. 3.2 - Md_{Φ} e σ_{Φ} calculated for each sub-unit

Sorting:
$\sigma_{\Phi} = (\Phi_{84} - \Phi_{16}) / 2$ (Inman, 1953)

where

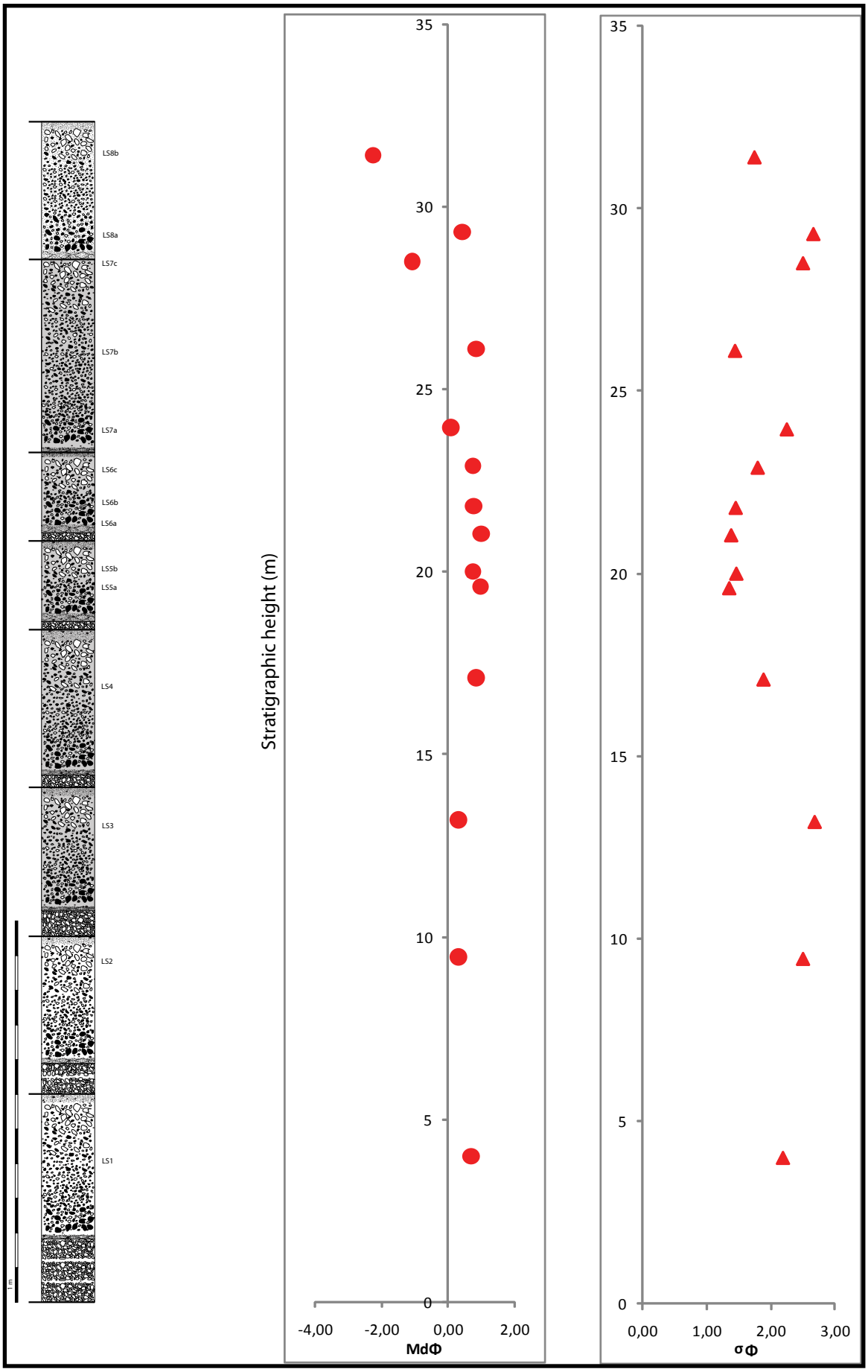

Fig. 3.9 - Md_{Φ} e σ_{Φ} in relation to a schematic stratigraphy of BLT deposits

$\sigma_\Phi < 1\Phi$	very well sorted
$1\Phi < \sigma_\Phi < 2\Phi$	moderately sorted
$2\Phi < \sigma_\Phi < 4\Phi$	poorly sorted
$\sigma_\Phi > 4\Phi$	very poorly sorted

In Fig. 3.9 the Md_Φ and σ_Φ are represented along the stratigraphy. The variation of both the parameters are quite wide, because of the nature of the deposits.

Also the Inclusive Graphic Standard Deviation is important, because it is also influenced by 5 and 95 percentile, thus it is more representative of the complexity of the whole granulometric distribution.

Inclusive Graphic Standard Deviation:

$\sigma I = \{(\Phi_{84}-\Phi_{16})/4\}+(\Phi_{95}+\Phi_5) / 6.6$ (Folk, 1966)

where:

$\sigma I < 0.35$	very well sorted
$0.35 < \sigma I < 0.5$	well sorted
$0.5 < \sigma I < 1$	moderately well sorted
$1 < \sigma I < 2$	poorly sorted
$2 < \sigma I < 4$	very poorly sorted
$\sigma I > 4$	extremely poorly sorted

For the characterization of the distribution of the grain-size there exist some parameters that are a measure of the asymmetry of the distribution curve. Very rarely a granulometric curve presents the classic Gaussian distribution. The *Skewness parameter* (a_Φ) describes this asymmetry. In particular the skewness is a measure of the deviation of the curve from the symmetry and it is influenced by the presence or absence of the fine or coarse fraction in excess in the granulometric distribution (Fig. 3.10).

Skewness:

$a_\Phi = (M_\Phi - Md_\Phi)/ \sigma_\Phi$ (Inman, 1953)

The Inclusive Graphic Skewness is a good representation of the symmetry of the granulometric distribution curve.

Inclusive Graphic Skewness:

$SkI = \{(\Phi_{16}+\Phi_{84}-2\Phi_{50}) / 2 (\Phi_{84}-2\Phi_{16})\} + (\Phi_5+\Phi_{95}-2\Phi_{50}) / 2 (\Phi_{95}-\Phi_5)$ (Folk, 1966)

where:

$-1 < SkI < -0.31$	very negative skewed
$-0.31 < SkI < -0.11$	negative skewed
$-0.11 < SkI < 0.09$	nearly symmetrical
$0.09 < SkI < 0.29$	positive skewed
$0.29 < SkI < 1$	very positive skewed

Thus positive values reflect an excess of fine fraction, whereas negative values reflect an excess of coarse fraction.

Another important parameter is the measure of *kurtosis* (KG). This parameter describes in particular the shape of the granulometric distribution. Considering a granulometric histogram, the kurtosis represents how much the mode rises over the rest of the distribution.

In particular, the kurtosis is the measure of the ratio between the sorting in the outer part of the distribution and the sorting in the central part of the distribution. If the central part is more selected than the outer part, the granulometric curve will have a central peak (leptokurtica). On the contrary, if the outer part is more selected that the central part, the curve will have a flat and large peak (platikurtica, Fig. 3.11).

Graphic Kurtosis:

$KG = (\Phi_{95}+ \Phi_5) / 2.44 (\Phi_{75}- \Phi_{25})$

Φ	JUVENILE (%)	CRYSTALS (%)	LITHIC FRAGMENTS (%)
-8	0	0	0
-7,5	0	0	0
-7	0	0	0
-6,5	0	0	0
-6	0	0	0
-5,5	0	0	0
-5	1,8	0	0
-4,5	1,5	0	0,7
-4	3,2	0	1,1
-3,5	8,7	0	1,8
-3	13,4	0	2,3
-2,5	16,1	0,2	2,5
-2	17,3	0,3	1,7
-1,5	13,7	2,1	1,1
-1	8,2	2,2	1,2
-0,5	7,4	3,1	4,5
0	5,2	2,5	8,3
0,5	3,2	12,7	5,4
1	0,3	13,9	6,7
1,5	0	14,2	12,6
2	0	14,8	4,2
2,5	0	14,2	8,2
3	0	12,3	13,3
3,5	0	5,4	14,5
4	0	2,1	6,1
4,5	0	0	2,6
5	0	0	1,2
5,5	0	0	0
	100	100	100

	Φ5	Φ16	Φ25	Φ50	Φ75	Φ84	Φ95
Juveniles	-4,23438	-3,47015	-3,13433	-2,34682	-1,52555	-0,99324	-0,14423
Crystals	-0,96774	0,220472	0,568345	1,457746	2,316901	2,654472	3,231481
Lithic fragments	-3,19565	-0,6	-0,01205	1,511905	2,977444	3,289655	3,901639

Skewness
0,057869828
-0,0867634
-0,200503028

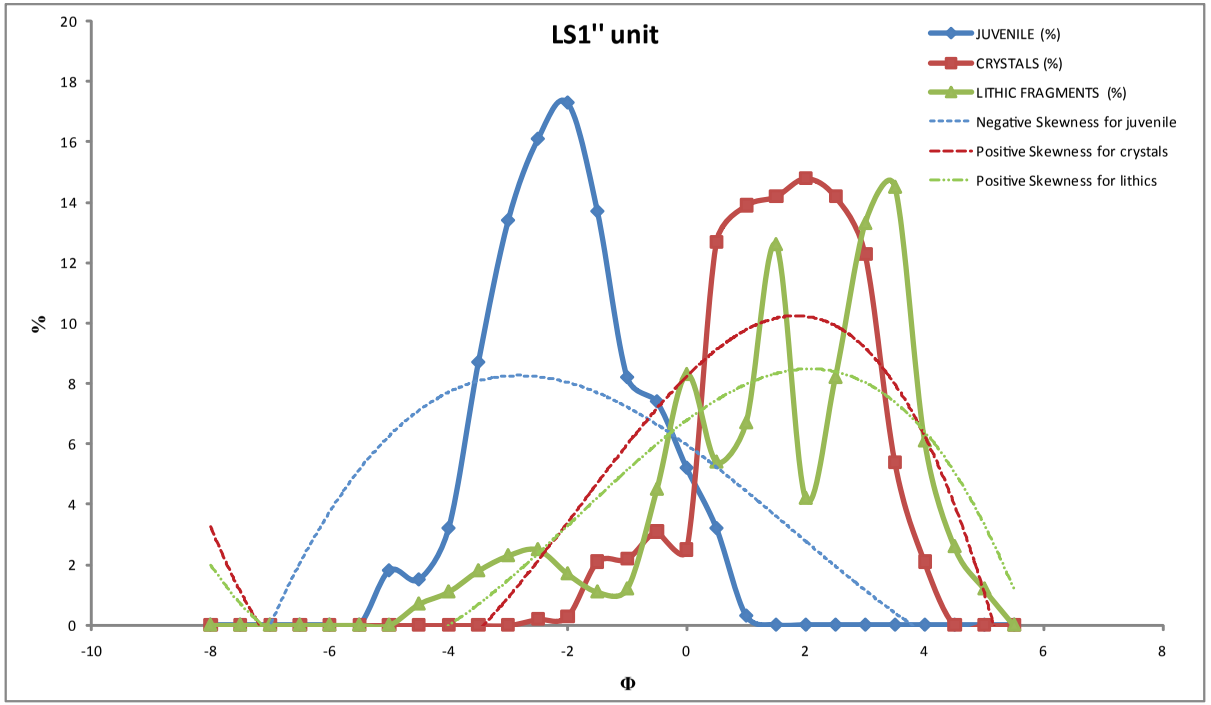

Fig. 3.10 - Graphic vision of the skewness for the calculated granulometric curves of LS1" sub-unit

Φ	JUVENILE (%)	CRYSTALS (%)	LITHIC FRAGMENTS (%)
-8	0	0	0
-7,5	0	0	0
-7	0	0	0
-6,5	0	0	0
-6	0	0	0
-5,5	0	0	0
-5	1,8	0	0
-4,5	1,5	0	0,7
-4	3,2	0	1,1
-3,5	8,7	0	1,8
-3	13,4	0	2,3
-2,5	16,1	0,2	2,5
-2	17,3	0,3	1,7
-1,5	13,7	2,1	1,1
-1	8,2	2,2	1,2
-0,5	7,4	3,1	4,5
0	5,2	2,5	8,3
0,5	3,2	12,7	5,4
1	0,3	13,9	6,7
1,5	0	14,2	12,6
2	0	14,8	4,2
2,5	0	14,2	8,2
3	0	12,3	13,3
3,5	0	5,4	14,5
4	0	2,1	6,1
4,5	0	0	2,6
5	0	0	1,2
5,5	0	0	0
	100	100	100

	Φ5	Φ16	Φ25	Φ50	Φ75	Φ84	Φ95
Juveniles	-4,23438	-3,47015	-3,13433	-2,34682	-1,52555	-0,99324	-0,14423
Crystals	-0,96774	0,220472	0,568345	1,457746	2,316901	2,654472	3,231481
Lithic fragments	-3,19565	-0,6	-0,01205	1,511905	2,977444	3,289655	3,901639

Graphic Kurtosis
1,041962026
0,984236776
0,972983445

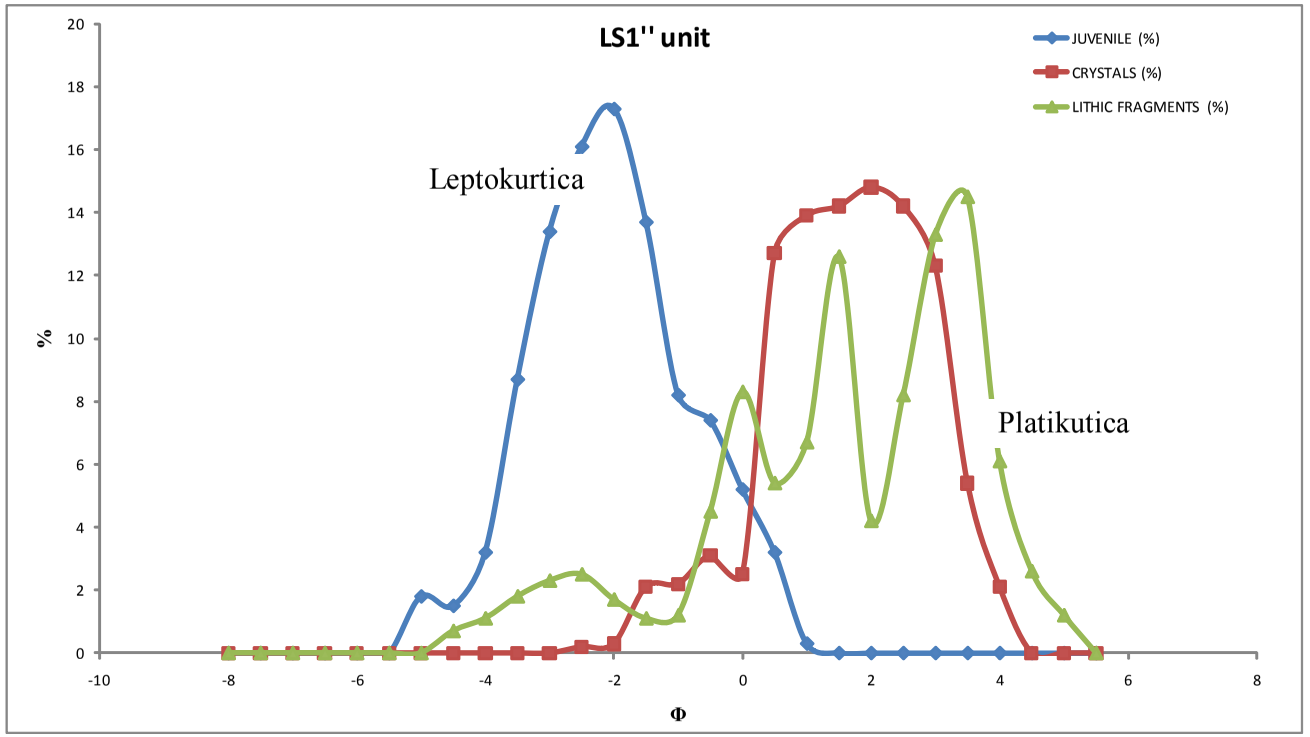

Fig. 3.11 - Graphic vision of the Kurtosis for the calculated granulometric curves of LS1'' sub-unit

	Skewness			Graphic Kurtosis		
	Juveniles	Crystals	Lithics	Juveniles	Crystals	Lithics
LS1'	-0,092	-0,087	0,077	1,202	0,957	0,936
LS1"	0,058	-0,087	-0,201	1,042	0,984	0,973
LS2'	-0,035	-0,101	-0,251	0,970	1,231	1,058
LS2"	-0,208	0,011	-0,210	0,989	1,342	1,123
LS3'	-0,022	-0,157	-0,310	1,069	0,986	1,058
LS3"	-0,139	0,130	-0,080	1,144	0,744	1,227
LS4'	-0,210	-0,037	-0,095	1,176	1,484	1,157
LS4"	-0,241	0,198	-0,045	1,246	1,352	1,346
LS5'	-0,123	0,018	-0,156	1,147	1,224	1,411
LS5"	-0,177	0,253	-0,117	1,163	1,555	1,627
LS6'	-0,245	-0,116	-0,250	0,920	0,960	1,039
LS6"	0,031	-0,140	-0,235	0,884	1,052	0,996
LS7"	0,066	-0,021	-0,249	0,834	1,002	1,075
LS8"	0,010	-0,127	-0,201	0,847	0,927	0,973

Tab. 3.3 - Skewness and Graphic Kurtosis calculated for each sub-unit

(Folk, 1966)
where:

KG < 0.67	very platykurtic
0.67 < KG < 0.90	platykurtic
0.90 < KG < 1.11	mesokurtic
1.11 < KG < 1.50	leptokurtic
1.50 < KG < 3.00	very leptokurtic
KG > 3.00	extremely leptokurtic

Walker (1971) introduced a diagram for the classification of pyroclastic deposits. Using Md_Φ and σ_Φ parameters it is thus possible to delineate fields of existence for different kind of pyroclastic deposits: fall, flow and surge (Fig. 3.12). Thus, t is possible to discriminate two sub-population in the analyzed deposits. These two groups correspond to the two sub-units recognizable in each unit: fall and flow deposits.

In sum, the statistical parameter used for the description of the BLT deposits and their formulae are listed below:

Φ	
Md_Φ	Φ_{50}
M_Φ	$M_\Phi = (\Phi_{16}+\Phi_{84}) / 2$
σ_Φ	$\sigma_\Phi = (\Phi_{84} - \Phi_{16}) / 2$
σ_I	$\sigma I = \{(\Phi_{84}-\Phi_{16})/4\}+(\Phi_{95}+\Phi_5) / 6.6$
a_Φ	$a_\Phi = (M_\Phi-Md_\Phi)/ \sigma_\Phi$
Sk_I	$SkI = \{(\Phi_{16}+\Phi_{84}-2\Phi_{50}) / 2 (\Phi_{84}-2\Phi_{16})\} + (\Phi_5+\Phi_{95}-2\Phi_{50}) / 2 (\Phi_{95}-\Phi_5)$
KG	$KG = (\Phi_{95}+ \Phi_5) / 2.44 (\Phi_{75}- \Phi_{25})$

Unit	Md_Φ	σ_Φ
LS1'	-2,25	1,75
LS1''	0,42	2,66
LS2'	-1,09	2,50
LS2''	0,85	1,45
LS3'	0,08	2,25
LS3''	0,76	1,80
LS4'	0,77	1,46
LS4''	0,99	1,39
LS5'	0,74	1,47
LS5''	0,98	1,36
LS6'	0,85	1,89
LS6''	0,31	2,68
LS7''	0,31	2,50
LS8''	0,69	2,19

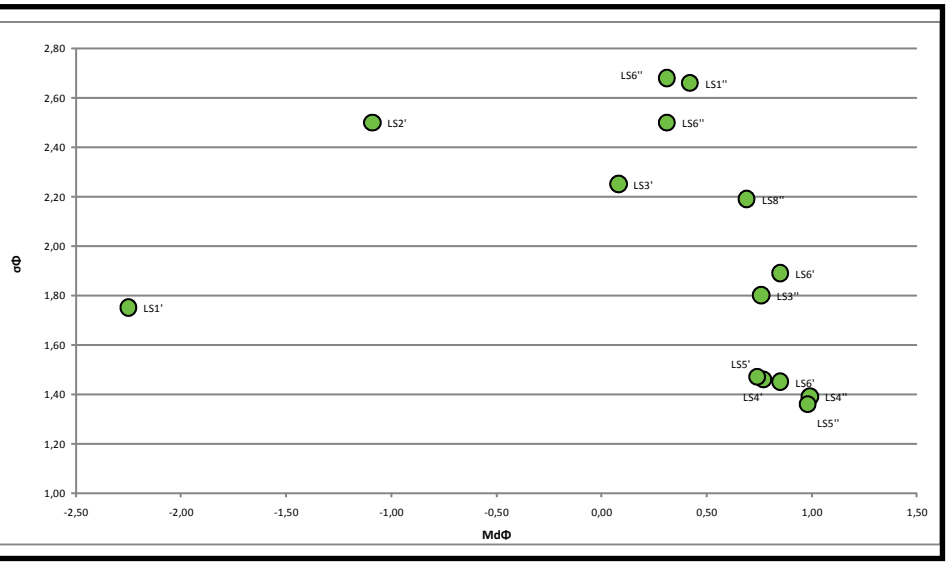

Fig. 3.12 - Distinction between pyroclastic flow deposits and tephra deposits in the BLT units

Results

From the study of the different statistical parameters it can be deduced that the different units LS1-LS8 have similar granulometric distribution. This could mean that each unit is the result of eruptive events with similar characteristics.

Inside each unit it is possible to discriminate five different portions, not always visible with the naked eye in the outcrops. These different parts are the expression of the sub-units LSn' and LSn'' with its α, β1, β2 and γ.

As the diagrams confirm, the unit LSn' corresponds to a tephra fall layer, but considering its sorting value and Md_Φ, a slight deviation is observed. The cause of this deviation could be due to local features of the topography, especially near the caldera rim.

Instead the other LSn'' samples are compatible with a pyroclastic flow deposits, since their sorting is relatively high, and the median varies widely.

Observing the distribution curves of juvenile clast with respect to the other curves it is possible to observe that the distribution of the fragments, direct products of the explosivity of the eruption, are slightly shifted to the left. This fact is the expression of the presence in the deposits of a high percentage of coarse juvenile particles. This means that the fragmentation in the BLT eruptive columns was not so highly energetic.

Valuating the ratio between the outer parts and the central parts of granulometric distributions of the juvenile particles, it is possible to deduce that there is not a wide distribution, since the central parts are more frequent than the outer parts.

3.7 COMPONENTS ANALYSES

The different granulometric classes were not only used for a quantitative analysis but also for the qualitative analyses of the different components of the rocks. These components are mainly subdivided in juvenile and lithic components. The juvenile components include pumices and scoriae, whereas the lithic fragments include lavas stratovolcano fragments.

The lithic fragments are tephritic lavas fragments of the stratovolcano. Their shape is

generally slightly rounded but they are mainly sharp fragments. They present a bimodal distribution and they are mainly concentrated in the classes > 0 - 0.5. This distribution can be related to the fragmentation process during the explosion. The shape of these particles was however maintained and it was predominantly slightly elongate and rounded. For each component of each unit was calculated the %wt distribution also in relation to the granulometric class. The ratio between juvenile and lithic fragments is about 1:1.

The considered juvenile fraction is mainly characterized by pumices and scoriae fragments. These parts are highly altered in lithified units LS3-LS7. The volcanic glass is so replaced by zeolite group minerals (K-chabazite and phillipsite). In particular in the lithic fragments phillipsite aggregates are more frequent, whereas in the juvenile fragments K-chabazite is present, because of the different heat capacity (see Chapter 5).

3.8 ISOPACH MAPS

The isopach maps for the BLT flow sub-units (LSn'') show that during the eruptive cycle the principal dispersion occurred mainly in the north-east sector (Fig. 3.13). However each sub-unit shows slightly different distribution pattern. They are probably expression of a slight variation in the topography during the emplacement of BLT deposits. Thus, the main direction of the isopach is in relation with the shape of the caldera rims at the moment of the BLT eruptive cycle. This also is confirmed by other following eruptive cycles that do not seem to be influenced by the wind. In fact the following WTT deposits are homogeneous in all the volcanic area, because BLT sediments

As introduced by De Rita & Giordano (1996), the BLT eruption occurred when the caldera was already formed. The isopachs of the pyroclastic LSn'' flow units testify these observations: they localize the center of the distribution in the eastern area of the caldera depression and the deposits mainly in the eastern sectors. Very few deposits are present in the western parts. Considering the vent position in all the flow sub-units it can be supposed that it moved as the eruption evolved.

3.9 ERUPTIVE VOLUME

It is very difficult to establish the eruptive volume of BLT on the whole. The irregular topography of the area and the lack of information about the ash fall dispersion and the wide erosion processes do not allow a precise estimate. Recently Brauer et al. (2007) testified the presence of a tephra layer comparable to BLT in composition. It is documented in varved interglacial lake deposits from Pianico-Sellere (Southern Alps). This confirms how the correct estimation of the whole BLT deposits is difficult. The differential fillings of the valleys have to be considered, too. The deposits near the vent are thick about 150 - 170 m, whereas in the distal parts they are few decimeters thick. It follows that the mean BLT thickness is about 40 - 50 m. If the deposits areal dispersion is about 160 km^2, the calculate overall volume of the BLT deposits is about 6.4 - 8 km^3.

Walker (1973, 1980) introduced two indexes related to the dispersion and the fractionation of the erupted fall deposits.

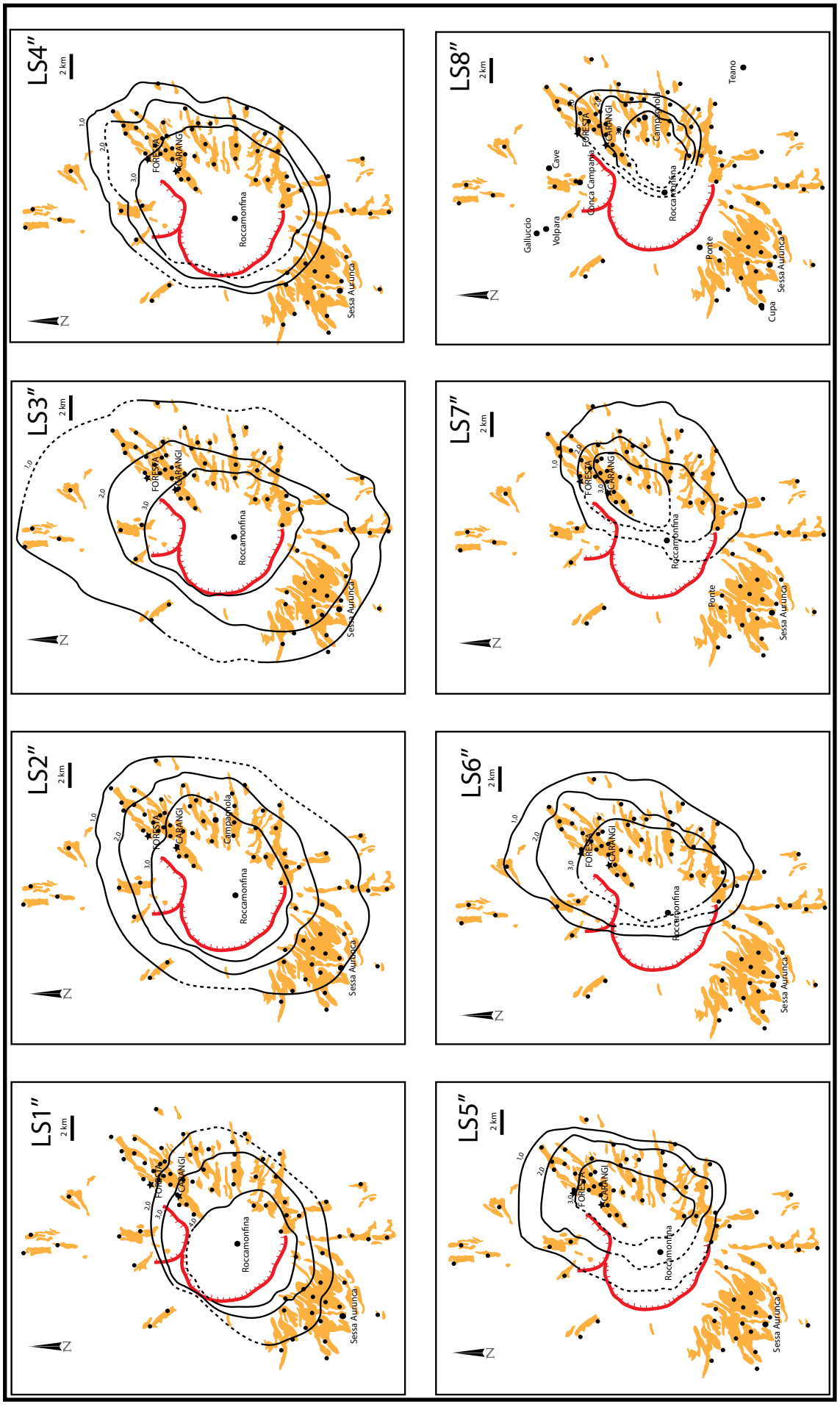

Fig. 3.13 - Isopach maps of the units composing the BLT. Isopach contours are in m, insteads the dashed contours represent the estimated thickness

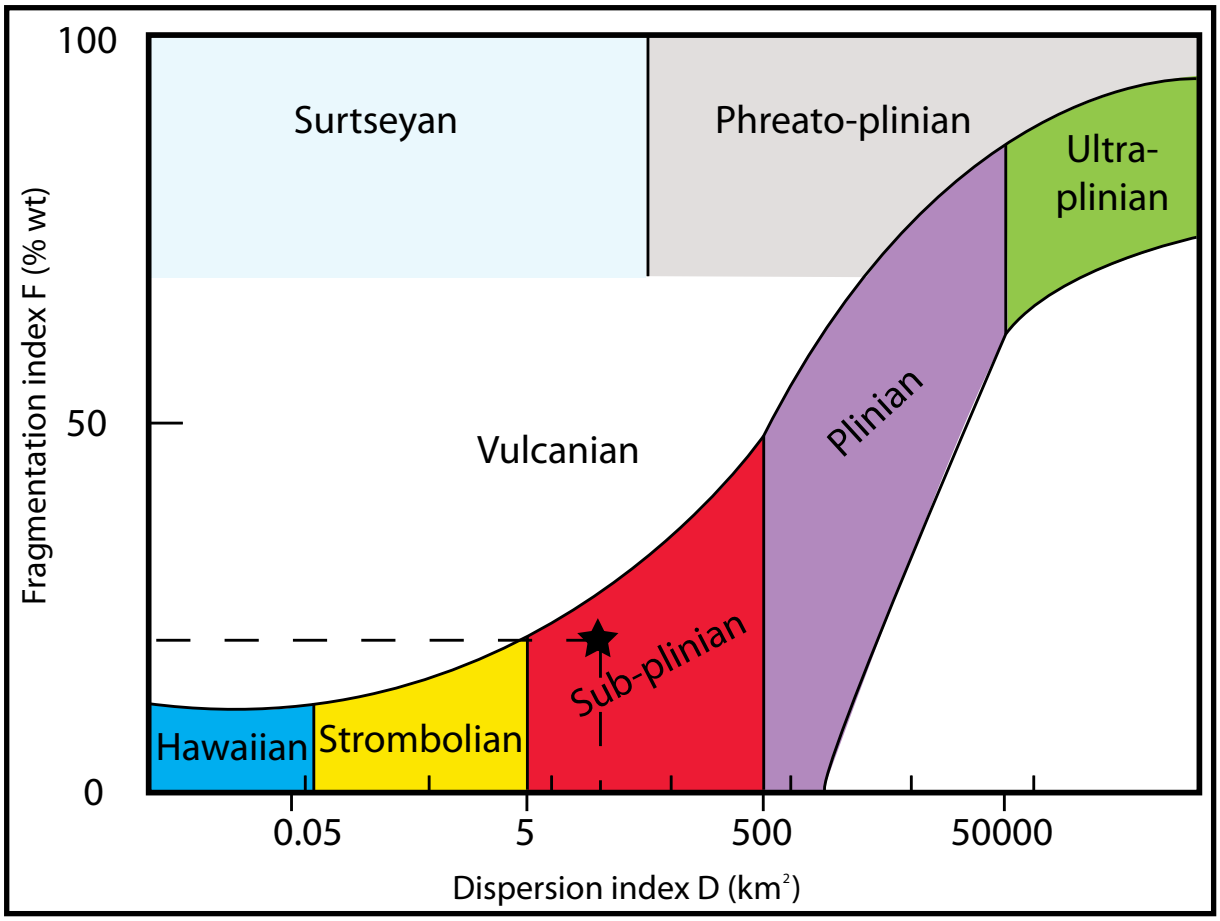

Fig. 3.14 - Classification of BLT eruptive cycle using Walker diagram (Walker 1973, 1980)

Thus, it is possible to establish the kind of eruptive event deposited BLT. The F index is the percentage (%wt) of the tephra products lower than 1 mm, of a sample collected where the dispersion axis intersects the isopach of 1/10 of the maximum thickness. The D index corresponds to the area defined by the isopach with the value of 1/100 of the maximum thickness measured near the vent. On the basis of these indexes it is possible to classify the eruption of BLT as a Sub-Plinian eruption (sensu Walker, 1973). The F index for BLT fall deposits is about 19% and the D index is about 40 km^2 (Fig. 3.14).

3.10 CONCLUSIONS: ERUPTIVE DYNAMICS

Sub-Plinian phase

The BLT eruption cycle is interpreted as a complete succession of sub-Plinian events. It was characterized by several pulses, with the collapses of each eruptive columns. It gives rise to the multiplicity of the units with the same characteristics in the stratigraphic section. Each single eruption phase represents a sub-Plinian event because of the ratio of the valued volume of erupted product and the level of fragmentation of the products on the basis of the Walker classification (1973, 1980). The characteristics of the grain-size distribution of juvenile clasts confirm this hypothesis. The phenomenology is similar to Plinian eruption but the deposits cover minor area and are less intense. Between one phase and the following stasis periods occurred. These periods appear to be not long time intervals because no soils were formed.

Each eruptive phase began with the throw of pumice fragments and lithics from the conduit of the stratovolcano, which brought to the deposition of the LSn' sub-unit. This is the early phase of each impulse, followed by the deposition of pyroclastic flow sub-units (LSn''). At the base of each sub-unit there is a fine ash-bed, expression of the expulsion of coarse fragments for the dispersion forces among the particles. Then the basal fine part of the pyroclastic flow deposits occurs, followed by the thick and massive portion. At the end a fine ash bed is the result of the deposition of the ash cloud remained in the atmosphere. The human footprints were found on the top of one of these units (LS7). As a consequence it can be suppose that between this flow unit and the following a brief time interval passed, permitting the trampling over a cold surface and the quick lithification of the deposits.

Footprint overview

The trampling event must have taken place during the lull period between the deposition of a unit and the following one. Immediately after the end of LS7 unit deposition abundant meteoric precipitation occurred. An active erosion of the deposits, with the setting of a hydrographic pattern took place. Because of the wide circulation of water the surface was soaked in fluids. It permitted the trampling of humans over the surface, and the subsequent impression of the traces. Then a lithification process (zeolitization) cemented the LS7 unit and the ones below (LS3-LS7). It permitted the conservation of the footprints also after the deposition of the following LS8 not lithified unit.

Chapter 4

The petrography and geochemistry of BLT

4.1 Introduction

The composition and the geochemical characteristics of the BLT were both widely studied in the past and recently (Appleton, 1972; Luhr & Giannetti, 1987; Rouchon et al., 2008; Conticelli et al., 2009). These works were mainly focused on the collocation of the BLT eruptive cycle in the history of the Roccamonfina volcano. In particular they aim to put the BLT in relation with the formation of the central caldera.

The geochemical and petrographical analyses of the units of the BLT complex were useful to have a complete picture of the deposits after the stratigraphical description. These data are going to be used also to understand the post-depositional processes involving the deposits and their importance in relation with the conservation of the human footprints.

4.2 Methodology: sampling and analyses

The samples were collected in the whole areas where the BLT crops out. The attention was mainly focused in the area close to the "Ciampate del Diavolo" site, at the Foresta locality. For each unit about 10 kg of rocks were sampled (Fig. 4.1).

The samples were washed with deionized water to avoid possible reactions and afterwards were sent to Acme analytical laboratories ltd. (Canada) for the analyses. Here the samples were dried at 60°C and then crushed and pulverized to 85% passing 200 mesh, to produce homogeneous sub-samples representative of the rocks.

The total abundances of the major oxides and minor elements were reported on a 0.1 g sample analyzed by ICP-emission spectrometry following a Lithium metaborate/ tetrabortate fusion and dilute nitric digestion. Loss on ignition (LOI) is by weigh difference after ignition at 1000°C.

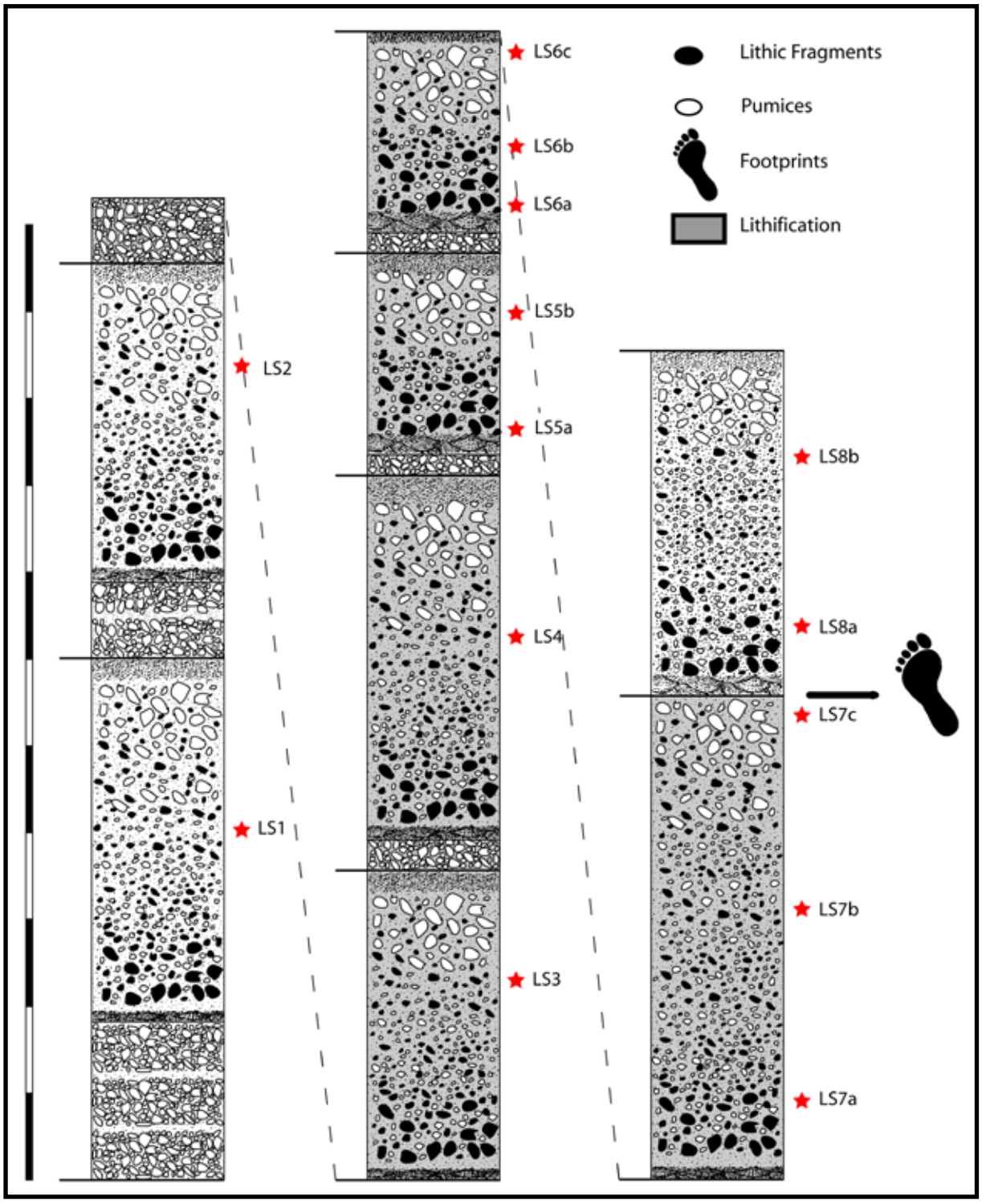

Fig. 4.1 - Stratigraphy of the BLT deposits with the collocation of the analyzed samples

For the rare earth and refractory elements the same procedure was carried out. In addition a separate 0.5 g split is digested in "Aqua Regia" and analyzed by ICP Mass Spectrometry to report the precious and base metals.

4.3 DATA

The whole-rock compositions on the basis of the major and minor elements are reported in Tab. 4.1 and 4.2, for all the 14 samples.

From these analyses it is possible to observe that alkali elements vary from 1.20 to 2.36 for Na_2O and 3.47 to 5.35 for K_2O.

4.4 RESULTS

TAS diagram

On the basis of TAS classificative diagram (Les Bas et al., 1986), BLT rocks range from phonolitic leucite-tephrite to tephritic leucite-phonolite. As a consequence of the alteration of primary leucite, analcime-rich BLT rocks are displaced from the primary trend to the fields for basalt to latite. In these rocks CaO decreases smoothly from 7.41 to 4.46 wt%. Besides, part of the samples show a relative low content in alkali. They correspond to the units presenting an extensive lithification (Fig. 4.2).

Geochemical diagrams

For a complete description of the BLT rocks a geochemical characterization of the deposits was also necessary. This permits to ascribe the BLT deposits to one of the two magmatic series in which the rocks of the Roccamonfina volcano is subdivided (HK or K).

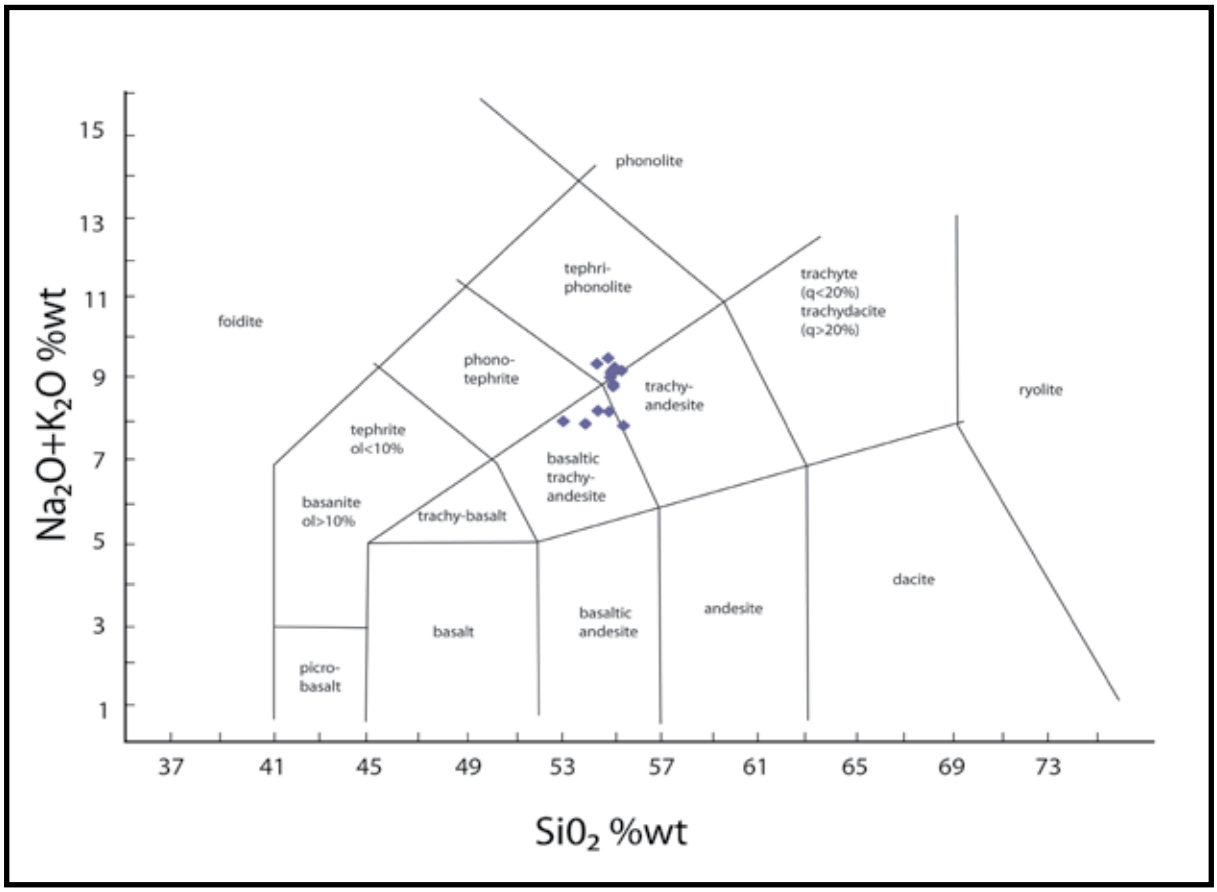

Fig. 4.2 - TAS diagram with the collcation of the BLT samples (the silica and alkali percentages were normalized)

	SiO2	Al2O3	Fe2O3	MgO	Cao	Na2O	K2O	TiO2	P2O5	MnO	Cr2O3	Ni (ppm)	Sc (ppm)	LOI (%)
LS1	49,31	17,88	5,90	2,43	7,03	2,04	3,47	0,60	0,22	0,15	0,006	<20	11,00	10,40
LS2	49,49	17,80	5,33	2,60	7,41	1,36	5,31	0,62	0,23	0,10	0,007	<20	13,00	9,30
LS3	47,91	22,04	7,78	1,87	4,31	1,20	4,51	0,67	0,21	0,12	0,016	<20	9,00	8,80
LS4	50,55	20,12	5,96	2,01	4,94	2,36	4,55	0,60	0,20	0,11	0,006	<20	9,00	8,20
LS5a	49,34	19,04	6,89	2,24	5,62	1,46	4,43	0,61	0,23	0,21	0,006	<20	10,00	9,20
LS6a	49,75	18,30	5,75	2,28	6,75	1,90	5,25	0,57	0,20	0,13	0,004	<20	10,00	8,70
LS6b	49,73	18,07	5,68	2,35	6,74	1,55	5,35	0,58	0,21	0,13	0,006	<20	10,00	9,10
LS7a	50,38	18,99	5,90	2,18	6,56	1,93	4,96	0,61	0,22	0,11	0,004	<20	9,00	7,70
LS8a	50,40	18,84	5,85	2,21	6,60	1,93	5,01	0,62	0,22	0,11	0,007	<20	10,00	7,70
LS5b	50,83	19,09	6,12	2,42	6,40	2,04	4,64	0,64	0,22	0,10	0,005	<20	11,00	6,90
LS7b	50,64	18,80	6,04	2,43	6,69	2,06	4,54	0,63	0,22	0,10	0,005	<20	11,00	7,30
LS6c	50,00	20,64	6,63	2,45	5,24	1,95	4,09	0,67	0,27	0,12	0,005	<20	12,00	7,50
LS7c	48,82	20,57	8,14	2,09	4,46	1,63	4,03	0,65	0,25	0,11	0,006	<20	11,00	8,80
LS8b	49,30	18,48	5,89	2,35	6,79	1,60	5,42	0,60	0,22	0,19	0,005	<20	10,00	8,70

Tab. 4.1 - Geochemical composition of the BLT deposits. Major elements

MgO	Ba (ppm)	Co (ppm)	Sc (ppm)	Al_2O_3	Zr (ppm)	Nb (ppm)	La (ppm)	Ce (ppm)
2,43	761,00	14,20	11,00	17,88	278,00	20,70	89,70	179,20
2,60	766,00	15,60	13,00	17,80	245,10	19,00	84,10	170,50
1,87	1183,00	12,50	9,00	22,04	343,70	28,30	120,40	212,20
2,01	806,00	10,80	9,00	20,12	297,20	24,40	96,30	192,10
2,24	1019,00	14,80	10,00	19,04	299,50	22,30	167,90	182,80
2,28	731,00	12,60	10,00	18,30	284,20	21,20	91,10	173,90
2,35	767,00	13,50	10,00	18,07	280,90	21,20	92,90	176,70
2,18	812,00	13,40	9,00	18,99	282,50	21,00	92,80	181,40
2,21	835,00	13,50	10,00	18,84	286,60	21,00	91,20	178,50
2,42	865,00	13,70	11,00	19,09	297,30	21,00	99,00	180,80
2,43	847,00	14,40	11,00	18,80	298,70	20,70	98,70	181,50
2,45	863,00	14,00	12,00	20,64	334,60	23,20	98,70	198,20
2,09	737,00	12,70	11,00	20,57	340,20	23,80	98,70	188,60
2,35	707,00	13,50	10,00	18,48	297,20	20,50	87,10	167,50

Tab. 4.2 - Geochemical composition of the BLT deposits. Principal minor elements (see appendix for the other elements)

Major and rare elements were plotted against CaO (Fig. 4.3, 4.4 and 4.5), to compare the samples with the other analyses of Luhr & Giannetti (1987) and Conticelli et al. (2009). CaO was also used as principal compositional index because it shows a wide variation in the BLT suite (4.46-7.41 %). It correlates strongly with most of the other elements: CaO has traditionally been chosen as an index variable for Italy's potassic igneous rocks (Appleton, 1972; Giannetti, 1982).

The elements can be divided into three groups on the basis of their behavior with respect to CaO:

Group 1 (Positively correlated with CaO): TiO_2, FeO^T, MgO, P_2O_5, V, Cu, Sr, Ba, Sc, Cr, Co, Nd, Sm, Eu, and Tb;

Group 2 (Negatively correlated with CaO): SiO_2, Al_2O_3, K_20, Zr, Nb, La, Ce, Yb, Lu, Pb, Th, Sb, Hf, and U;

Group 3 (Constant or irregular behavior with CaO): Na_20, Mn, Zn, Ga, Y, Cs, Ta, and Rb.

Representative elements from Groups 1, 2 and 3 are plotted on CaO-variation diagrams.

4.5 DISCUSSION

The rocks of the sampled units of BLT are comparable with bibliographical data (Luhr & Giannetti, 1987) and approximately cover the range of the entire HKS magma spectrum. For many elements (e.g. Mg and Ti), BLT trends reflect those of HK lavas (Appleton, 1972; Luhr & Giannetti, 1987). Important deviations are shown by the alkalies. These deviations are clearly related to widespread analcimization of abundant small leucite in these deposits and by the zeolitization that affected part of the pyroclastic unit. Also analcimization of leucite probably modified concentrations of Rb and Cs. These two elements are concentrated in leucite

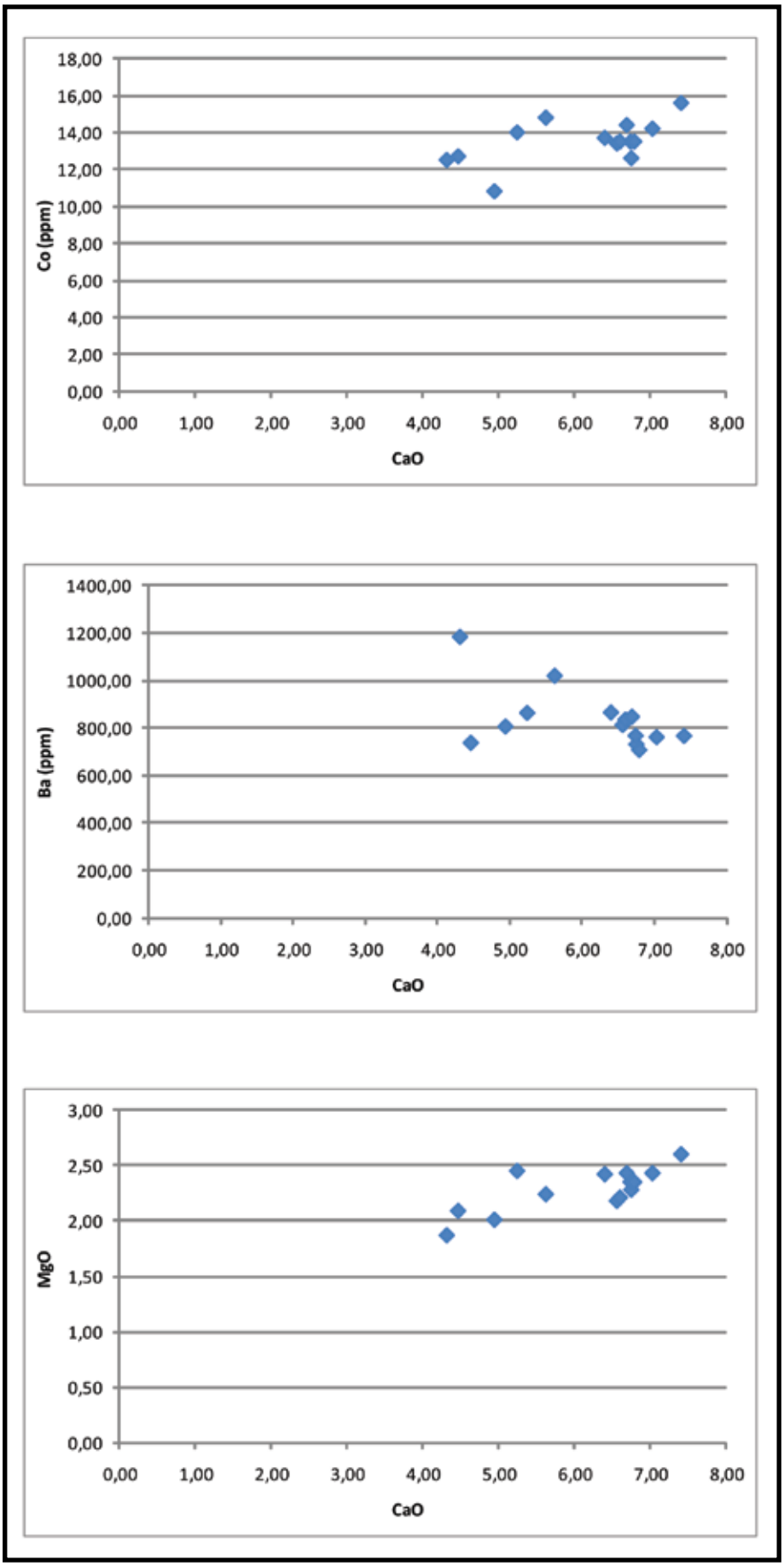

Fig. 4.3 - CaO variation diagrams for BLT samples

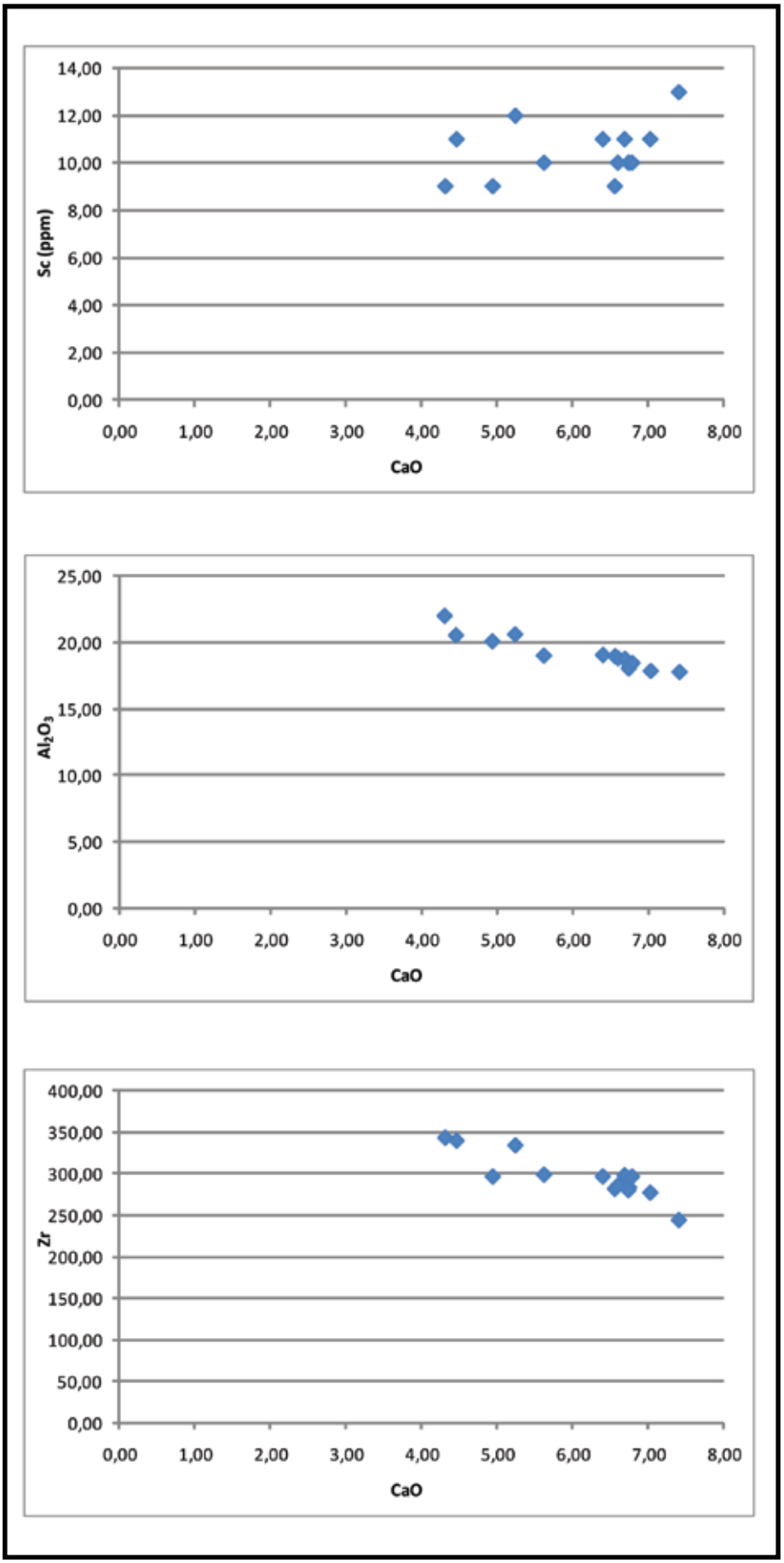

Fig. 4.4 - CaO variation diagrams for BLT samples

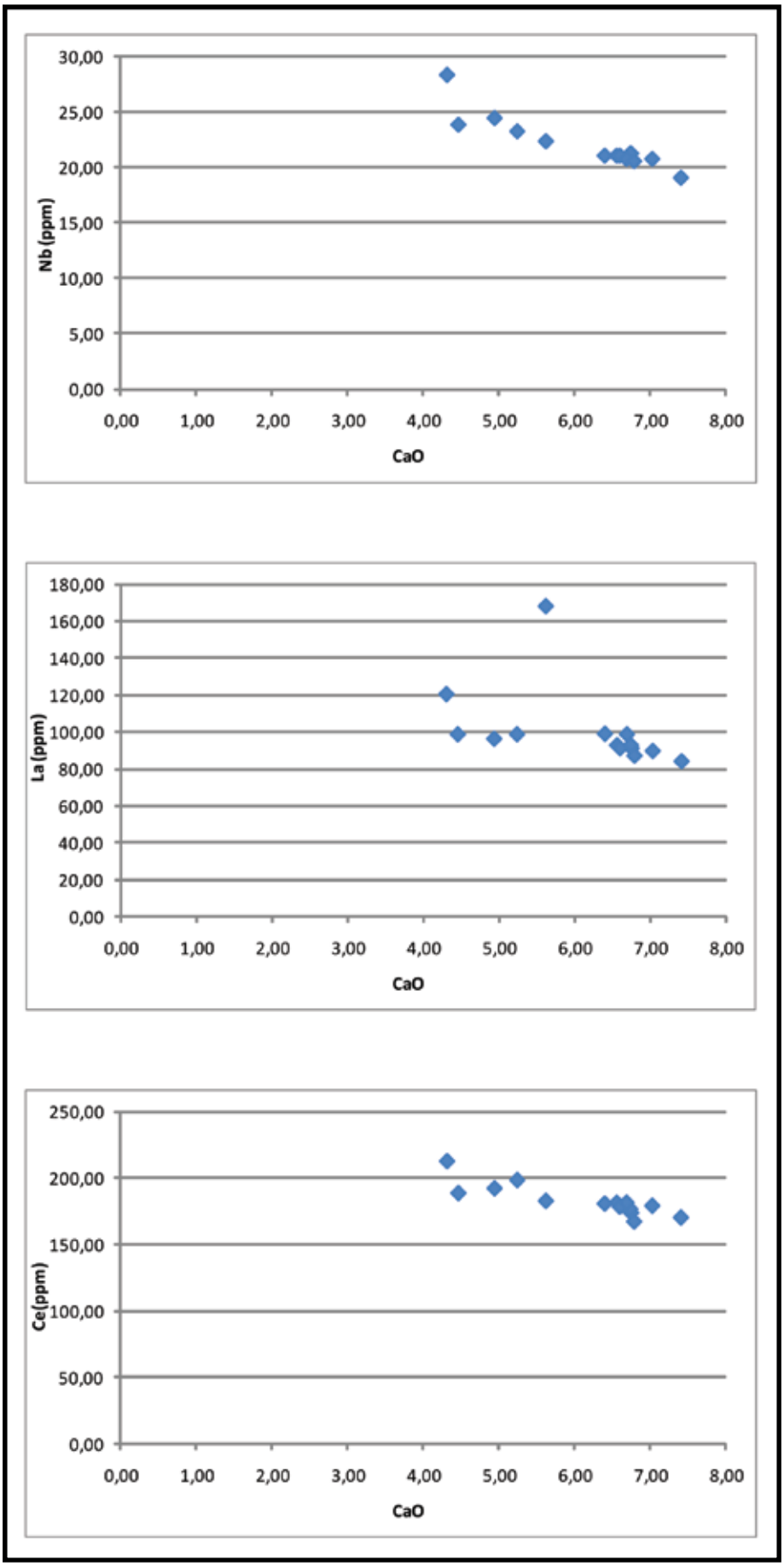

Fig. 4.5 - CaO variation diagrams for BLT samples

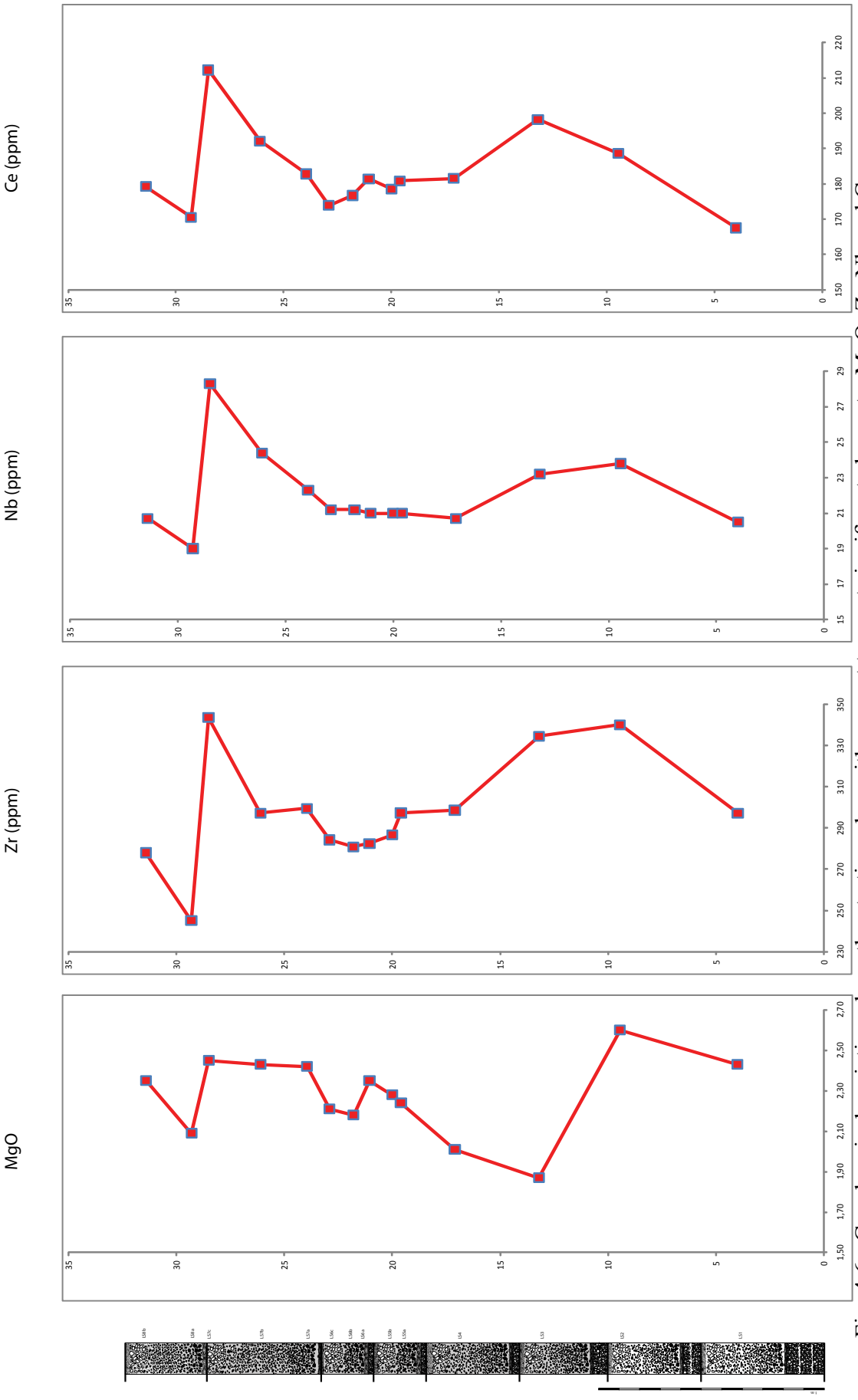

Fig. 4.6 - Geochemical variation along the stratigraphy, with respect to most significant elements: MgO, Zr, Nb and Ce

(Peccerillo et al., 1984) and increase strongly during analcimization of leucite (Fornaseri & Penta 1960). These elements show a wide scatter on CaO-variation diagrams for BLT samples.

From the diagrams it is possible to observe that the BLT can be modeled as an inverted compositionally zoned magma chamber. Magma compositions becomes progressively more basic as the eruption evolved (Hildreth 1981; Giannetti & Luhr 1983; Luhr & Giannetti, 1987). In detail, however, the pattern is more complex, as evidenced by interbedded brown, ochre, and white units in some upper sections.

In bibliography it is well established that with time most major pyroclastic eruptions display systematic changes from acid toward more basic magma compositions and mineralogies (Smith & Bailey 1965; Smith 1979; Hildreth 1979, 1981, and 1983). These systematic zonations are generally interpreted as the progressive emptying of a compositionally stratified magma chamber. So it is possible to argue that the BLT eruptive cycle is the result of the emptying of a magma chamber occurred by steps, from a less to a more basic composition.

However the interpretation of BLT petrogenesis is more complicated by the almost complete analcimization of leucite that has affected all pumices. In particular the more basic samples (> 5.6 wt% CaO), which contain a large number of secondary analcime crystals in their matrices. A further problem came from the widespread zeolitization of the deposits, which completely alters the ground mass and the pumices.

Chapter 5

The lithification process

5.1 Introduction

An important process occurring in the trampled deposits of the "Ciampate del Diavolo" and Carangi sites is the rapid lithification of the sediments. This phenomenon is the key process for the preservation of the footprints. After the deposition of the unit LS7 something should occurr to cold the surface permitting the passage of the hominids. Secondly the surface should be rapid cemented; this must have happened before the emplacement of the following unit (LS8) that covered the surface preventing its erosion. The lithification process was complete or almost complete when LS8 was deposited, otherwise the weight of the sediments could have flattened the detailes of the "Ciampate del Diavolo" footprints, clearly visible until now.

The process of lithification involved the formation of particular secondary minerals, the zeolites. They form aggregates in the ash matrix, substituting the volcanic glass shards and creating a rigid framework among the particles. Moreover this process did not only involve the glass shards but also the fragments themselves, with the formation of zeolites also inside the lithic fragments (Fig. 5.1).

XRF analyses show that BLT units are mainly characterized by K-feldspar, plagioclase (30-38% wt), augite (7-9% wt) and biotite (6-8% wt). Frequently, biotite is a Ti-

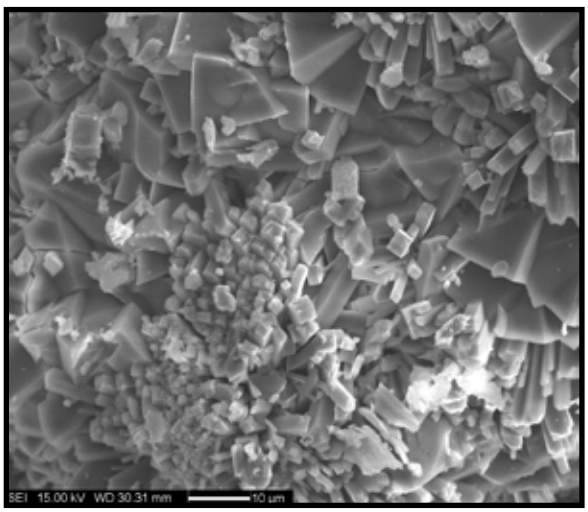

Fig. 5.1 - SEM pictures of chabazites and phillipsites aggregate in a lithified sample

rich biotite. The secondary phases are mainly chabazite (43-48%wt) with minor phillipsite (6-10%wt) and scarce smectite. Moreover large parts of ground mass glass are not altered (15-22% wt). The lithic fragments of BLT are mainly tephritic while the leucite phenocrystals are almost completely replaced by analcime.

Thermal analyses performed on chabazite crystals allowed to specify the cationic composition of the zeolitic phase (Fig. 5.2).

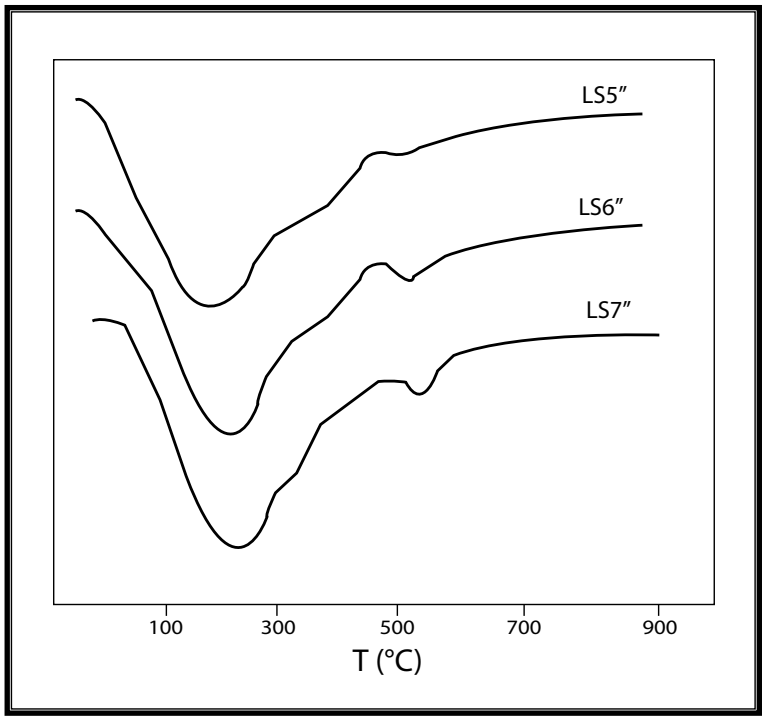

Fig. 5.2 - Thermal curves (DTA) from samples collected in the "Ciampate del Diavolo" site

At about 200°C a wide endothermic effect is present, but each curve show also a characteristics "shoulder" around 300°. This is related to K-rich chabazites (de' Gennaro & Franco, 1976). Another weak endothermic effect is also present at about 500°C and could be ascribed to the presence of small quantity of halloysite.

SEM analyses permit to observe the K-chabazite crystals with rhomboedral habit and the prismatic habit of phillipsite, as well as where the aggregates formed. In particular, aggregates of K-chabazites formed substituting glass shards and inside the pumices, whereas phillipsite crystals mainly formed near lithic fragments. So the formation of zeolites is the key process for the lithification and for the subsequent conservation of the footprints (Cappelletti et al., 2006).

Hence the necessity to understand and to evaluate what the zeolite existence field are. Five parameters were studies: temperature, water content, glass chemistry, timing and deposit characteristics. These data are then completed with dating, in order to define a time window for the trampling event itself (see Chapter 6).

5.2 CONSTRAINTS FOR ZEOLITIZATION

The volcanic glass represents an instable component of the pyroclastic deposits. Its al-

teration is a very common process. The dissolution of volcanic shards creates a solution oversaturated with respect to many minerals (Chipera & Apps, 2001). The most characteristic minerals forming in this kind of deposits are the zeolites, because of the slower kinetics involved in forming the more stable assemblage.

The parameters influencing the formation of one particular zeolite are various and are widely studied by numerous authors (Chipera & Apps, 2001; de' Gennaro et al., 2000; Passaglia & Vezzalini, 1985). Aqueous silica activity, cations concentration and pH are important aspect of the fluids from which zeolite aggregates precipitate. The characteristics of the deposits include their temperature, the composition of the volcanic glass, the composition and the content of water of the rocks. These factors are related to the formation environment of the zeolites. There are essentially two of them (Gottardi et al., 1989). The first one is the diagenesis at a very low grade metamorphism, and the other is the hydrothermal genesis. The former consist in the formation of the zeolites by transformation of primary component of the sediments, such as in soils, in hydrologically open and closed systems, in geoautoclave system and in marine sediments. The latter consists in the formation of zeolites in geothermal fields, in ore deposit, in pegmatites and in veins or geodes.

In the world, there are numerous cases of zeolite crystallization in pyroclastic deposits, such as Thrace (Greece; Marantos et al., 2007), Bulgaria (Aleksiev et al., 1997), Gran Canaria (Canary Island, Garcia Hernandez et al., 1993; Perez Torrado et al., 1995), Oregon (USA; Altaner & Grim, 1990), Idaho (USA; Sheppard, 1991) and Olduvai Gorge (Tanzania; Hay, 1963). Important zeolitized deposits can also be found in central and southern Italy: they are related with explosive eruptions and with the deposition of pyroclastic flow units (e.g. Tufo Rosso a Scorie Nere, Vico Caldera, Bear et al., 2009; Tufo Lionato, Colli Albani volcanic complex, Giampaolo et al., 2006; Neapolitan yellow tuff, Campi Flegrei, de' Gennaro et al., 2000, Giordano et al. 2006). The origin of the zeolitization process in these volcanic complex deposits could be related either to percolating meteoric water or to a geoautoclave system (a close hydrologically system), where the zeolite species depend on eruptive and depositional mechanisms.

Several works proved that temperatures, glass chemistry and water content are funda-

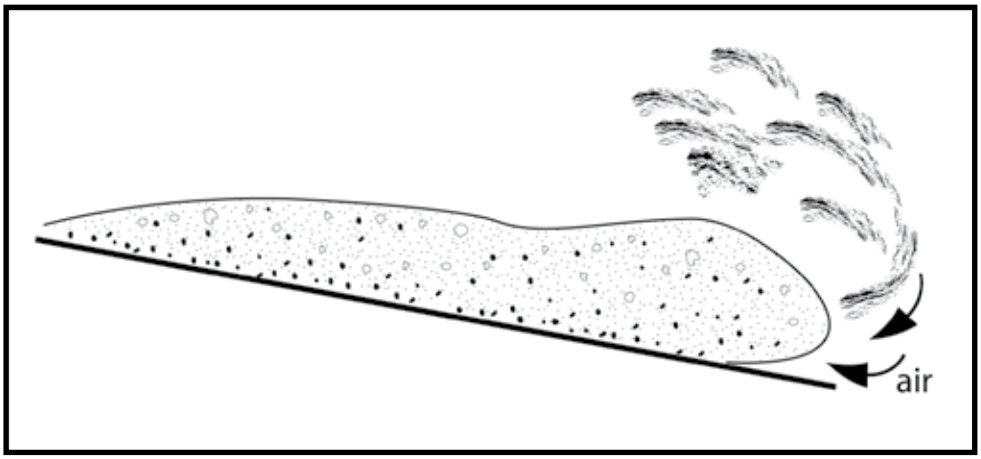

Fig. 5.3 - Air ingestion of a pyroclastic flow

mental factors for zeolite precipitation (Chipera & Apps, 2001; de' Gennaro et al., 2000; Hall, 1998; Passaglia & Vezzalini, 1985), because they directly influence the environment where the zeolite aggregates form. The timing of the process, the characteristics of the deposits and the dynamics of the deposition and therefore the kind of eruption, are other important factors to be considered.

Temperature

One of the main factors that influenced the formation of different kind of zeolites is the temperature (Chipera & Apps, 2001). Several aspects of the thermal evolution of the deposits have to be considered. The most important are the emplacement temperature of the pyroclastic flow deposit and therefore the cooling evolution of the unit (Fig. 5.4. Hall, 1998).

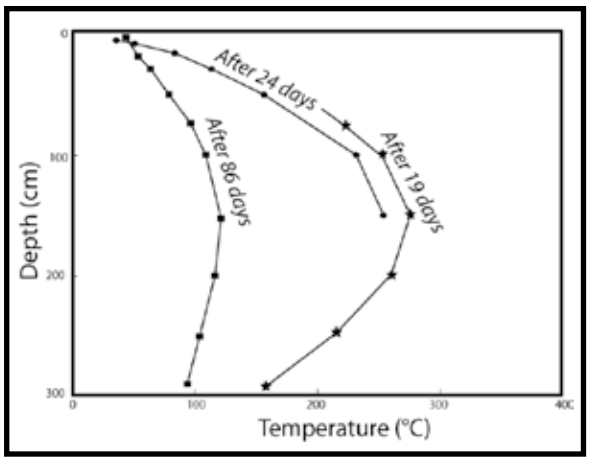

Fig. 5.4 - Thermal evolution of a pyroclastic deposit of the 1980 eruption of Mount St. Helens at various time after the eruption (modified from Hall, 1998)

Several studies about the temperature measurements were made on pumiceous clasts of the pyroclastic deposits of the 1980 eruption of Mount St. Helens (Banks & Hoblitt, 1981). These studies prove that the temperature of the pumices of pyroclastic flows decrease rapidly between leaving the vent and coming to rest. The reduction of the temperature is due to adiabatic expansion and the mixing with air during the flowage of the pyroclastic flow (Fig. 5.3).

The cooling rate of the volcanic ash is the other important aspect concerning the temperature. In fact it influences the timing of suitable condition for zeolitization process. It can be determined by water and by what kind of pyroclastic deposit involves. In pumice-flow the temperature at around 40 cm of depth fell from 500°C to less than 100°C within two years (Hall, 1998) or less than 50°C with fumarolic activity. Instead pumice-fall deposits reach the ambient temperature at around 50 days from the eruption, because they favor the dispersion of the heat. This is very important for the formation of zeolites aggregates. The crystallization of zeolites range goes from 15 to 300°C. For each zeolite there is a particular window of formation, in relation with the thermal evolution of the pyroclastic flow (de' Gennaro & Colella, 1991; Hall, 1998). The initial temperature of a pyroclastic deposit is around 500°C and the zeolites formed when the temperature lowered enough to reach their formation range.

The period of zeolites formation is very important, because it must have particular stable temperature of formation of K-chabazite and phillipsite (the two phases present in the lithified units). The K-chabazite has a temperature interval of formation from 15°C to about 70-80°C, whereas the phillipsite forms at about 70-100°C (Fig. 5.5. Chipera & Apps, 2001). Most of ash deposits reach the temperature of about 100°C after a decade from the eruption, without considering a re-heating due to hydrothermal fluids, which was not observed during the field survey.

Since the stability temperature of the for-

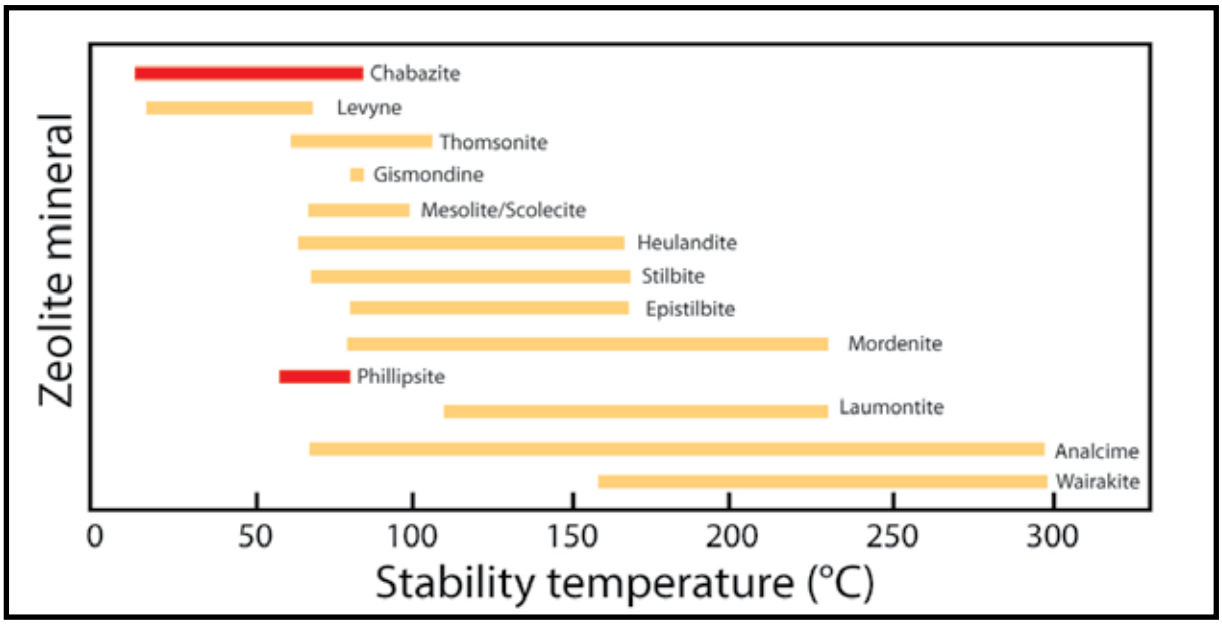

Fig. 5.5 - Temperature stability fields of the most common zeolites (modified from Chipera & Apps, 2001)

mation of chabazite and phillipsite is around 100°C, the temperature of the deposit during the cooling and at the trampling instant was at most that value.

The relative low temperature of the deposit as indicated by the stability fields for K-chabazite and phillipsite is also supported by the presence of the footprints itself: human feet cannot tolerate such high temperature. Besides, by analyzing the trails it can be deduced that the trackmakers were walking and not running, like they would have done on such a hot surface (Mietto et al., 2003).

Water content

Water is essential to permit the hydration-dissolution of volcanic glass; 10% of the mass of a pumice clast is required to convert it into zeolites or zeolites aggregate (Hall, 1998).

The presence of water also has a strong influence on the cooling rate (Riehle et al., 1995). The difference in the cooling rate of an ash flow deposited was calculated without water influence, in a layer of water, and under rainfall (Fig. 5.6).

The presence of a normal amount of rainfall can lower the temperature by about 200°C. However the circulation of water inside the deposit can also redistribute the heat inside it, so hotter parts can occur. Generally it can be affirmed that the major part of ash deposits reaches the temperature of about 100°C after about two years from the eruption. The reheating of the deposits for circulation of hot water or for magmatic activity is nonetheless to be considered as well.

The origin of the water can be various. It can have an internal origin, as it is the case with magmatic water or the pyroclastic as volatiles: nonetheless an external source for water is very frequent, especially for the eruptions involving groundwater or lake water. These are the preferred case for the main examples of zeolitized ignimbrites (de' Gennaro et al., 1995; de' Gennaro & Langella 1996; de' Gennaro et al., 2000). The percolating water from meteoric precipitation is an easier but not frequent cause for the formation of zeolites in pyroclastic deposits. Other environments suitable for the formation of

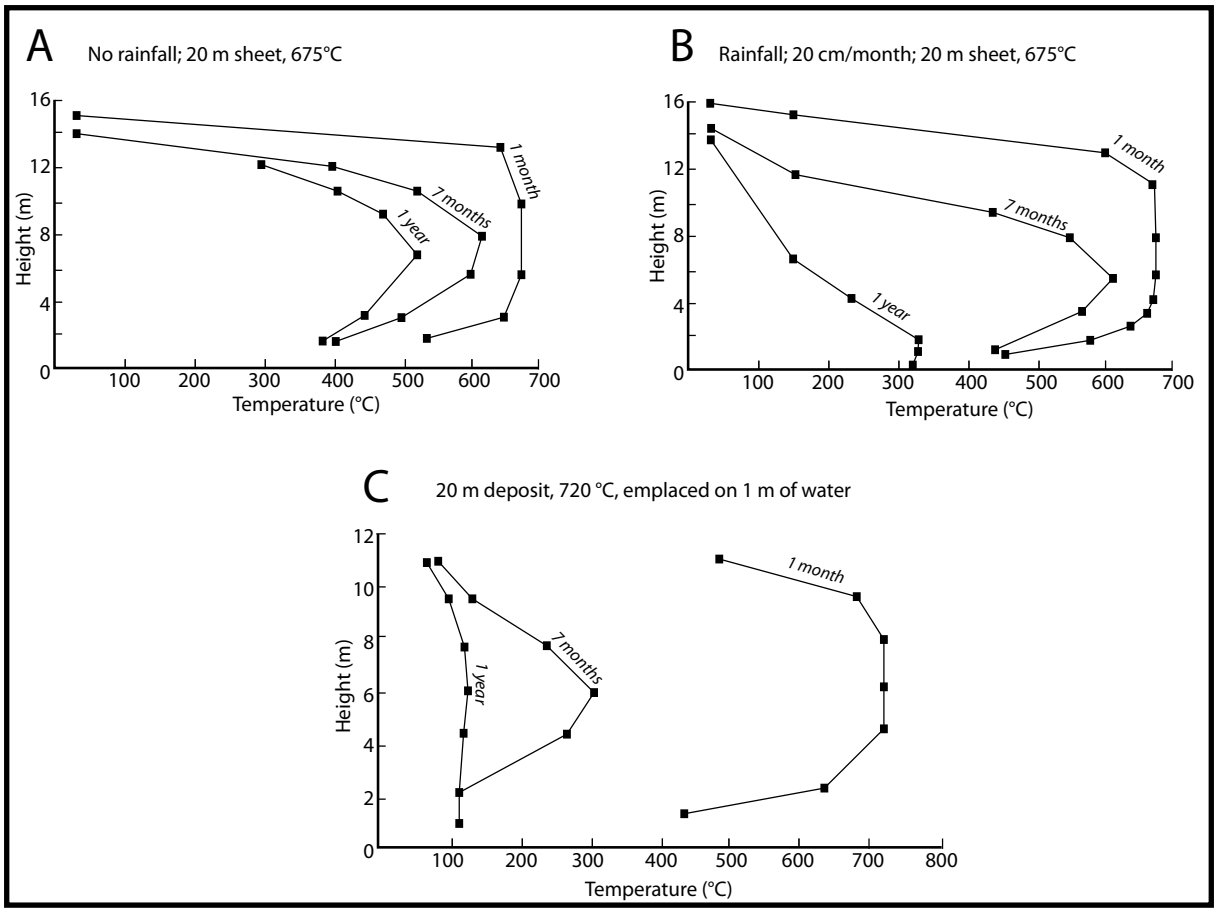

Fig. 5.6 - Thermal evolution of an ash deposit at various times after the deposition. **A**, no rainfall; **B**, heavy rainfall (20 cm/month); **C**, ash deposited in 1 m of water (modified from Hall, 1998)

these groups of minerals are the subaqueous environments, because of the large amount of water available (Passaglia & Vezzalini, 1985; Hall, 1998; de' Gennaro et al., 2000).

The BLT lithified units (LS3-LS7) present an extensive and inhomogeneous distribution of zeolitization (Fig. 5.7). The content in zeolites changes vertically along the stratigraphy. In fact, at the base of the pyroclastic flows the concentration of phillipsite is higher than the concentration of K-chabazite minerals. Instead at the top of the flow the content of phillipsite decreases relatively and the K-chabazite aggregates are pervasive. The origin of this differentiation can be ascribed to the fact that in the bottom the lithic fragments are more abundant. The phillipsite crystals preferentially formed near lithic fragments: there the temperature was higher because lithics more slowly dispersed heat. The zeolitization process involved on the whole five of the eight pyroclastic flows units; the amount of zeolites decreased towards the bottom of the lithified deposits. This is the index of a process having its maximum action at the top of the pyroclastic units and gradually reducing its action toward the bottom. Also laterally the zeolitization process is not homogeneous, so it is possible to recognize the lateral boundary of its action, despite its large development.

The presence of water during BLT eruptive cycle was not observed in its deposits. In the outcrops analyzed for this work no accretional lapilli were recognized, and the granulometric data show that the amount of ash in the ground mass is not substantial. In thin sections no blocky shapes, hydration

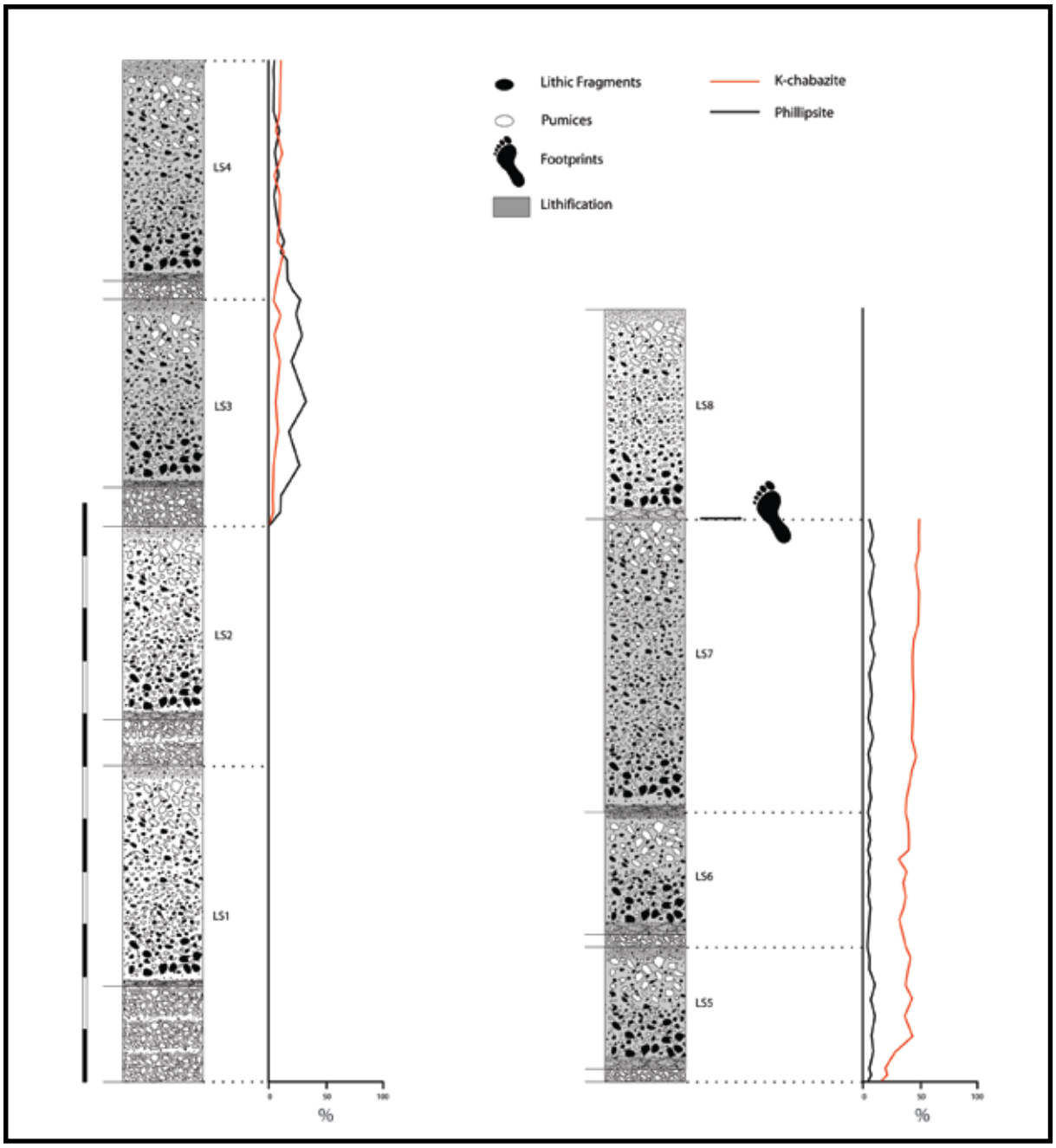

Fig. 5.7 - Distribution of K-chabazite and phillipsite in the BLT deposits

cracks or highly vesciculation structures are observed. The original temperature of the pyroclastic flow seems not high, but surely higher than in phreato-magmatic eruption.

The composition of the meteoric water is an important factor too. It is supposed to be acid, in relation with the acid gases emitted during an eruption and returned by rainfall. The acidity of the pore water in the deposits must be removed before the beginning of zeolitization process, because this process is favored in alkaline environment (Hall, 1998). The solution is the removal of Cl and F, main components of acid gases. However, a certain amount of Cl and F remains in the glasses. Experimental analyses (Ghiara et al., 1991) during the production of alkaline solution from volcanic glass, proved that HF and HCl are not formed (Hall, 1998). Cl and F are released into the solution as chloride and fluo-

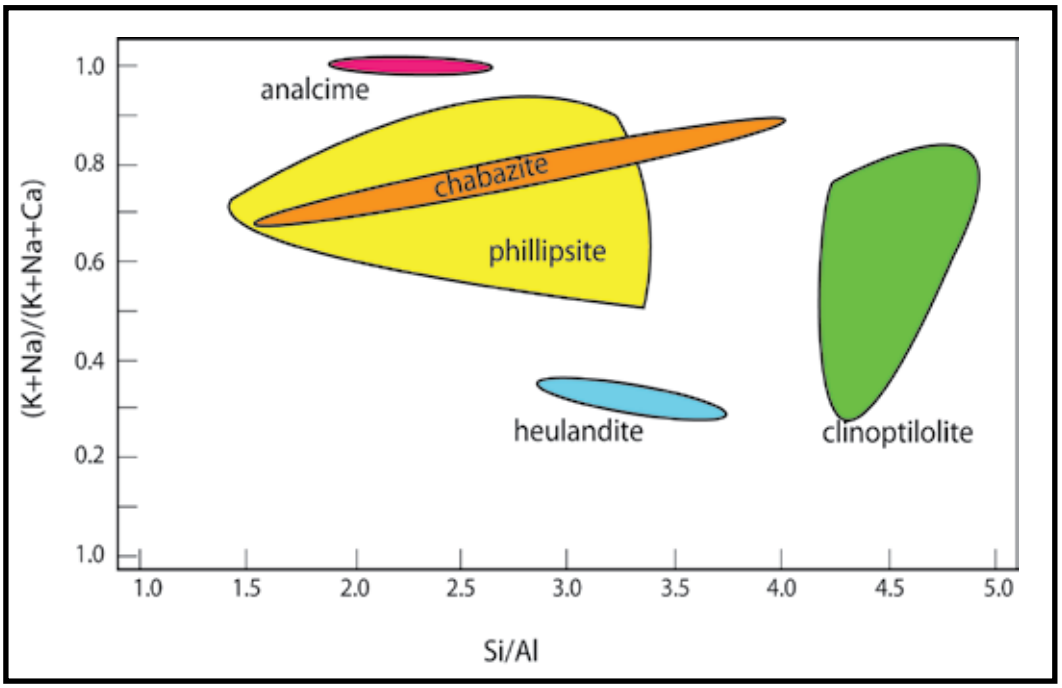

Fig. 5.8 - Chemical compositions of different zeolites. The same zeolites formed in different geologic enviroments often show a wide variation in chemical composition (modified from Chipera & Apps, 2001)

ride ions accompanying alkali cations during the zeolitization process, so that the acidity of the deposits is neutralized.

The presence of the footprints is an important factor to verify the water content after the emplacement of the pyroclastic flows. In fact all the characteristics of the footprints, such as the expulsion rims and the depth, the morphology of the inclined surface with soil creep, and the presence of mud-cracks on the surface are index of the plasticity of the deposits due to water content.

Glass chemistry

Zeolite minerals are the result of an alteration of volcanic glasses through hydratation and dissolution processes. This phenomenon is influenced by three main factors: the content of Si in the host glass; the pH of the fluids; the cations in the glass and in the fluids. These secondary minerals formed in environment where the glass has a high alkali composition; in particular chabazite and phillipsite are favored in K and Na-rich environments. Analyses on the BLT glass composition show that its composition is tephritic-phonolitic to phono-tephritic. This chemistry is suitable for the formation of these zeolites (Fig. 5.8).

As observed before, the distribution of K-chabazite and phillipsite aggregates is not homogeneous in the deposits. It has been observed that phillipsite crystals are mainly concentrated in the juvenile clasts; instead, K-chabazites are uniform in the deposits (ash matrix and pumices). Therefore there is a relationship between the kind of zeolite and where it was formed. In fact the phillipsite has a temperature formation range wider than chabazite and probably it is concentrated in the juvenile clasts because they have a major capacity to retail heat. Instead K-chabazite, with a lower range temperature formation is uniformly distributed in the deposits.

Timing

In the deposits of the “Ciampate del Dia-

volo" site the zeolitization process is relatively short. According to the dating obtained with $^{40}Ar/^{39}Ar$ method, the entire process, from its beginning the deposition of the following unit, lasted at most about 3000-4000 years. This is very similar to the time interval obtained with isotopic data by Capaldi et al. (1971) for the Neapolitan Yellow Tuff. They affirm that the zeolitization process in these deposits lasted 4000-5000 years, which is comparable with our data.

The passage of the hominids occurred over a surface that was relatively cold. The time for the cooling of a pyroclastic flow varies from deposit to deposit, depending on the thickness, the composition, the emplacement temperature and the homogeneity of the sediments. The Foresta site in particular shows some peculiar features that permit to better characterize the duration of the zeolitization. Here the surface is particular because it is steeply sloping, in opposition to all the other units, showing mud-crack structures and a superficial creep (Fig. 5.9). This is a very important characteristic because it involves the presence of a hydrographic network working between the deposition of the trampled unit (LS7) and the overlaying one (LS8). This hydrographic network is the cause of the high slope and the patterns of the surface. This slope represents a fossil record permitted by the rapidity of the lithification process.

Fig. 5.9 - **A**. The sloping surface of the "Ciampate del Diavolo" site; **B**. Mud cracks on the sloping surface

Deposit characteristics

The characteristics of the deposits are an essential element for the development of the zeolitization process because they represent the environment where the zeolite formed. The properties depend on the vesciculation, fragmentation, transport, sorting and water interaction. Besides, also some physical characteristics of the deposits, such as thickness, porosity, permeability and grain-size are decisive factors because they directly control the fluids' circulation in the units. Major thickness restrains the dispersion of

the heat in the deposits, favoring the ongoing zeolitization process (de' Gennaro et al., 2000). But thickness is not the only important element because, for example, there are zeolites both in thick and in thin deposits (de' Gennaro et al., 1999). Also the weight of the units is a key characteristic for the zeolitization, because it influences the porosity of the rocks and, as a consequence, the circulation of the fluids.

Grain-size is another key-factor, because it is proportional to the mean dimension of volcanic glass shards and influences their alteration rate. Heiken and Wolhetz (1985) found that there is a relationship between the amount of fine ash and the degree of alteration. Finer particles are more alterable than the bigger ones, but they do not permit the easy circulation of the fluids.

The BLT deposits until the LS7 trampled unit (LS1-LS7) are thick on average 20-25 m and they are poorly sorted with a coarse ash matrix. This is a peculiar characteristic for the circulation of the fluids: the course matrix increases the permeability of the deposit, permitting the passage of the zeolitizing fluids. In this way it increases the probability of the formation of zeolites and the lithification of the deposits.

Eruptive and depositional conditions

The parameters previously mentioned are related directly or indirectly to the kinds of eruptions that determined the BLT pyroclastic deposits. Literature includes numerous works concerning the typical characteristics which favor the post-depositional zeolitization: they agree on the fact that the conditions especially depend on the relation between magmatic constraints and the interaction water-magma during the eruptive event. The latter condition is however not visible during BLT eruptive cycle. (Hall, 1998; Bear et al., 2009)

The factors influencing zeolite formation, such as temperature, water content, glass chemistry and deposits' characteristic, are also related to the conditions in the conduit and to the way pyroclasts are deposited (de' Gennaro et al., 1999).

BLT has been subdivided into 8 units representing different eruptive phases. Not all the units are zeolitized: only few of them are characterized by an irregular zeolitization (LS3-LS7). Not lithified units are very friable and they do not present cavities. These cavities are common in the lithified units because they follow the dissolution of the pumices. The differential post-depositional history of these BLT deposits probably was influenced by a different exposure to meteoric events. It could be related to a climatic change or to an unusual event but we do not have evidences.

In these units no signs of magma-water interaction, typical for the formation of zeolites, can be observed. Therefore the hypothesis of a phreato-magmatic eruption as the origin of the BLT deposits can be excluded. Another restriction connected with the eruptive dynamics for the formation of zeolites is the capacity of the pyroclastic flow of trapping volatiles from the surface during the flowage (de' Gennaro et al., 1999; Cappelletti et al., 2003). In fact volatiles and heat are usually lost to the atmosphere during the transport, especially for the fallout deposits. Instead, during the pyroclastic flow phase volatiles are incorporated inside the flow and the heat is dispersed more slowly. So the tephra layers don't show zeolitization whereas in the pyro-

clastic flow units zeolites are present. Moreover, the tephra layer are clast-supported and the amount of fine ash is very low, therefore the reaction for the formation of zeolites is not possible: it needs fine vitric material to begin the post-depositional alteration, in opposition with the pyroclastic flow deposits.

5.3 CONCLUSIONS

On the basis of these considerations on the stratigraphy characteristics of the BLT units, it can be affirmed that the zeolitization in volcanic sediments is favored in wet and slightly warm deposits of pyroclastic flow nature. The deposits could be wet for several reasons, but the most probable reason in the case of the "Ciampate del Diavolo" site is a meteoric event occurred immediately after the emplacement of the LS7 unit. The magmatic eruptions rarely show high zeolitization, because the emplacement temperature is too high and the amount of water is too low. Therefore the external water was involved after the emplacement. The involvement of water after the emplacement has gradually lowered the temperature of the deposits, allowing humans to walk over the sloping and plastic surface. Then, zeolitization process completed its action, permitting the lithification of the surface with the record of the footprints and the characteristic inclination and creep.

Chapter 6

Dating of the footprints

6.1 Introduction

An important problem of the research was to understand when the human footprints were impressed. This was important under several points of view.

The first reason is an anthropological reason. During the period of the emplacement of the whole BLT deposits (385-325 ka, Luhr & Giannetti, 1987) in Europe lived a direct relative of *Homo erectus*, the *Homo heildebergensis*. Skeletal remains of this species of *Homo* were found at Heidelberg (Baden-Württemberg, Germany) and at Atapuerca (Spain). From these skeletons, researchers deduced that the specimens were very tall individuals (170-180 cm high) and that they had a powerful build. But all the footprints of the "Ciampate del Diavolo" site indicate that all the individuals were tall about 150-155 cm (Mietto et al., 2003). Dating are so necessary to understand if the footprints could be exactly imputable to *Homo heildebergensis* or to another "individual" not documented by anthropologists until now Fig. 6.1).

Another question is to determine since the

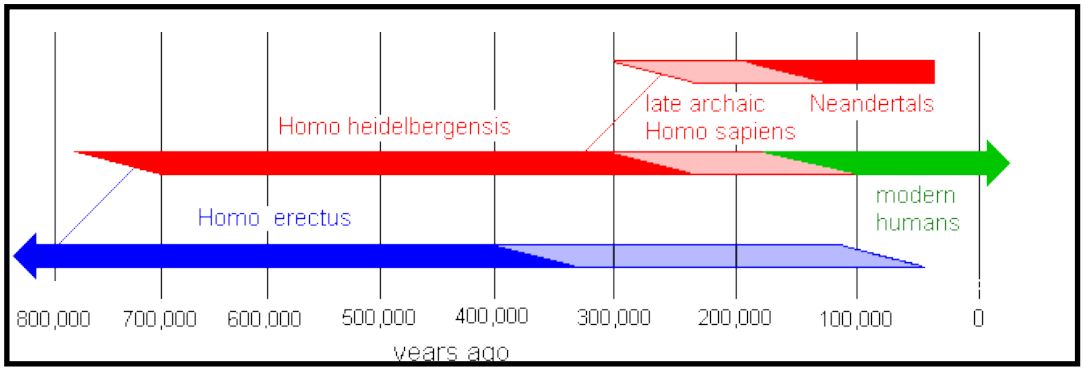

Fig. 6.1 - Modern human family tree (http://anthro.palomar.edu/homo2/mod_homo_1.htm)

"Ciampate del Diavolo" site is cropping out. This fact is very important to understand also the evolution of the site after the emplacement of the following LS7 unit over the trampling surface.

6.2 $^{40}Ar/^{39}Ar$ DATING

Theorical bases

$^{40}Ar/^{39}Ar$ method is used to date K-rich minerals with an age from 2000 years to 4 Ga. The sample is irradiated by a neutron beam coming from a reactor and with the energy useful to cause the expulsion of a proton with the substitution of a neutron.

The transformation is:

$^{39}K \rightarrow {}^{39}Ar$

where the amount of ^{39}Ar depends on the amount of ^{39}K present in the system.

The benefit of this method is that ^{40}Ar and ^{39}Art are both gas isotopes: the ^{40}Ar is the stable isotope instead ^{39}Ar is the decay products of K.

This system can give some problems because the irradiation of the beam can produce other interfering reactions such as $^{40}Ca \rightarrow {}^{39}Ar$, that can be corrected. Besides the dating are related to very carefully calibrated standard.

K is a very mobile element, as well. So alteration can modify the age of the rock. This can be solved with the Step-heating method. The sample is warmed till 500°C and the further warmed following steps of 50-100°C. Argon gets out from the sample for diffusion and then for each step the isotopic composition of the sample has to be analyzed, deducing an apparent age.

If the sample is not altered, the apparent age should be the same of the measured isotopic age. This age is a plateau-age.

The system is applied to K-rich materials, in particular to minerals in order to have a compositionally homogeneity for the analyses. The used minerals are plagioclase in basaltic rocks, alkaline-feldspar, biotite and muscovite for more evolved rocks.

Previous Data

Mietto et al. (2003) inferred the age of the footprints using the age of the BLT eruptive cycle. It was dated by Luhr & Giannetti (1987) using $^{40}K/^{39}Ar$ method and they obtained 385 ± 23 ka. These results were performed on phenocrysts of biotite and matrix glass separated directly by pumices of BLT rocks. Using these data Mietto et al. (2003) affirm that the "Ciampate del Diavolo" footprints are the oldest human footprints in the world.

Very recently Scaillet et al. (2008) updated the age at 345 ± 6 ka. They collected the samples directly near the trampled surface. This datum is very significant but incomplete. First of all, the localization of the sample was not indicated and not placed in a stratigraphy of the "Ciampate del Diavolo" site. Also the sloping of the surface was not considered by Scaillet et al. (2008), and this plays an essential role on the meaning of the dating. Then, only the trampled unit (LS7) was dated. So it was possible that the following unit (LS8) was settled also after a lot of time, belittling the ichnological importance of the site. New dating were so performed in order to complete the former data.

Method

For a more accurate data of the trampling event, a detailed $^{40}Ar/^{39}Ar$ dating was carried out on samples collected directly from the trampled (LS7) and the upper unit (LS8).

The dating of the pyroclastic units is difficult because of the nature of the deposits made by ash, pumice, lithic fragments and crystals, and also by the widespread alteration of the deposits. About 10 kg for each unit were sampled and crushed by technicians of the laboratory of Berkeley Geochronology Center to extract single crystals of primary-looking (automorphic) sanidine embedded in a brownish ash matrix. The leucite crystals were avoided because they are mostly altered in analcime. Secondary zeolites (K-chabazite and phillipsite) are present in small cavities and in the lithic fragments, but could be avoided during single grain sampling. Grains selected are typically 0.5mm to 2 mm in size, with well-preserved crystal faces, and were handpicked from the coarse crushed fraction. With a binocular microscope, 75% of a total of N=80 selected crystals were discarded because of their alteration. Grains were irradiated along with the flux monitor TCR sanidine (Renne et al., 1998) and individually analyzed with the $^{40}Ar/^{39}Ar$ dating laser probe.

Results

$^{40}Ar/^{39}Ar$ age analysis was performed at the Berkeley Geochronology Center with collaboration of Prof. Paul Renne using facilities and procedures similar to those described in Karner & Renne (1998).

The results for the "Ciampate del Diavolo" site are:

Sample	*Age (ka)*	*1σ (ka)*	*Crystals number*
LS7	349	3	13
LS7	350	3	13

On the basis of the standard deviation (1σ) it can be inferred that these two dating are absolutely indistinguishable. So it is possible to affirm that the eruptive event deposited LS8, occurred at most after 3.24 ka the emplacement of the LS7 trampled unit, fixing also the timing for the trampling and the lithification of the surface.

The value of 3.24 ka was obtained considering A and B as LS7 and LS8 age:

$A \pm \sigma_A$	$B \pm \sigma_B$
$\Delta t = A - B$	$\sigma_{\Delta t} = (\sigma_A^2 + \sigma_B^2)^{1/2}$
$\Delta t = 349\text{-}350$	$\sigma_{\Delta t} = (3^2 + 3^2)^{1/2} = 4.24$
$\Delta t = -1 \pm 4.24$	Max Δt = **3,24 ka**

We dated also another site with footprints (Carangi site) whose characteristics are very similar to the main ichnological site:

Sample	*Age (ka)*	*1σ (ka)*	*Crystals number*
Carangi	348	2	15

The obtained results are essential in this research because they give an additional value to the discovery. Two important consequences derive from these data. First of all they testify that the footprints belong to individuals living in the area during the Middle Pleistocene. Furthermore this dating is very useful to set the time span between the deposition of a unit and the following, fixing also the duration of the lithification process.

6.3 LICHENOMETRIC DATING AND ARCHIVES RESEARCHES

At this point is necessary to understand the post-lithification and post-eruption evolution of the site. Nowadays the footprints are on a visible and outcropping surface. If the trampled unit was covered with the following

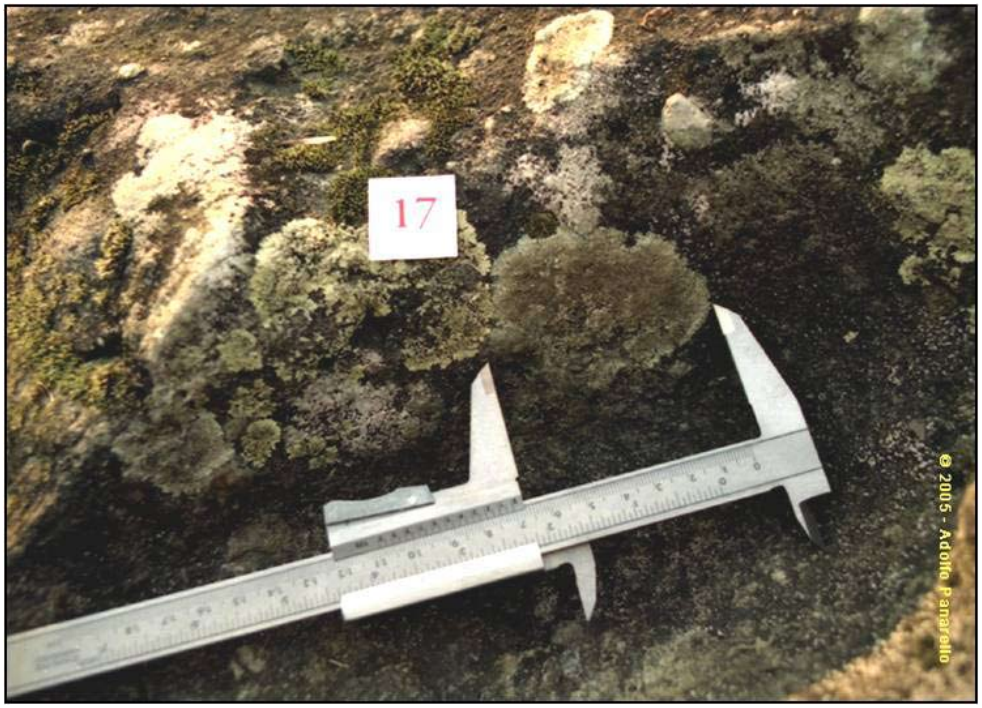

Fig. 6.2 - Lichens on the trampled surface (Courtesy of Adolfo Panarello)

unit (LS8) during BLT eruption cycle, the problem is to understand why and when this not lithified unit was removed. Thus it was necessary to find a methodology able to express the time of this exposure. This methodology used is the lichenometry and it is based on the dimension of the lichens.

The lichenometry is a particular method that uses the dimension of the thallus of the lichens to calculate the time of their formation. There are few types of lichens (for example *Aspicilia cinerea*) with a regular growth under stable micro-climatic condition. So the growth rate of these lichens could be a point of reference for calculating the age of the lichens on the trampled surface (Fig. 6.2). The *Aspicilia cinerea* lichens are very common on volcanic deposits and usually they are the first organism colonizing a volcanic surface.

In order to obtain a good result the calibration of the method was necessary. In this way the growing rate for year of the thallus was calculated. It is well-know that in the newly exposed surface the lichens are the first colonizing organisms. The ratio between the diameter of the bigger thallus measured on the surface and the growing rate is a good approximation of the time of exposure of the surface. The smaller thalluses belong to younger lichens or to lichens with a lower growing rate, so they had been excluded by the analysis.

This system was calibrated using lichens from old buildings and stone-quarries near the "Ciampate del Diavolo" site. Stone-quarries are made of the same material of the ichnological surface (BLT lithified rocks). Otherwise microclimate exposure and elevation is the same (Fig. 6.3). Several measures were taken in order to have more precise results.

The calculated growing rate of the lichens formed on the buildings is about 0.74 mm/yr. Measuring the thallus dimensions of the lichens in the "Ciampate del Diavolo" site maximum values were around 170-190 mm. So the calculated age of the exposure of the trampled surface was about 230-260 years

Fig. 6.3 - Lichens on the surface of an old building (Courtesy of Adolfo Panarello)

(pers. comm. Adolfo Panarello). Analyzing the surface in the whole, the dimensions of the thallus vary widely, indicating different time of formation of the lichens. This evidence is due to the inhomogeneous exposure of the unit itself. The parts of the surface where there are the footprints present younger lichens because the hollows were more difficultly cleared by incoherent sediments.

Historical archives researches prove that the site was unknown until 1754 (pers. comm. Marco De Angelis). Then during the late XVII-early XIX period exceptionally abundant meteoric precipitation was testified by numerous complaints about the destruction of streets and bridges. In particular, the area of the "Ciampate del Diavolo" was characterized by landslides, as reported in the archives of Tora e Piccilli municipality. After these events probably the trampled surface was exposed to the air and the locals began to think about the origin of the particular structures. When they finally knew them as human footprints, thay began to call them "Ciampate del Diavolo". Thus this term was used to indicate the area of the footprints (Fig. 6.4).

Fig. 6.4 - Sign at the beginning of the Foresta pathway

Chapter 7

Conclusions

The BLT deposits are the result of a series of sub-Plinian events, with collapses of the eruptive columns. These phases determined the deposition of several units in the Roccamonfina volcanic area with similar sedimentologic characteristics. The eruptive columns occurred in not highly energetic pulses which induced the emplacement of eight pyroclastic units. The units are composed by two sub-units which correspond to the fall phase of the eruptions for the former and of the flow phase for the latter.

The composition of the BLT rocks belongs to HK series (the first magmatic series of the volcano history). Studying the composition of these rocks it is possible to model the magmatic chamber as an inverted compositionally zoned magma chamber with magma compositions becoming progressively more basic as the eruption evolved. Thus this evolution represents the progressive emptying of a compositionally stratified magma chamber. In detail, however, the eruptive cycle is more complex, because brown, ochre, and white facies deposits, expressions of local characteristics of the emplacement, are interbedded among themselves especially in the upper part of the BLT stratigraphy.

Between the emplacement of one unit and the following one stasis periods occurred. These periods appear to be not long because no soils were formed. During the stasis period between the LS7 and the LS8 unit hominids walked over the pyroclastic surface, leaving their traces and a quick lithification process took place. Immediately after the end of LS7 unit deposition, abundant meteoric precipitations occurred, producing valleys and hills morphology. Thus the surface was soaked in fluids, which permitted the impression of the traces (Fig. 7.1). Then the lithification process cemented the LS7 unit and the ones below (LS3-LS7), permitting the conservation of the footprints, also after the deposition of the following LS8 not

lithified unit.

The lithification in this volcanic environment is the zeolitization. This process needs particular environmental conditions for its developing. The temperature was not high, because it permitted the passage of the hominids. Magmatic eruptions rarely show highly zeolitization, because the original emplacement temperature is too high and the earliest amount of water is too low. But the BLT sediments were involved in abundant meteoric precipitation after the emplacement, lowering the temperature of the deposits and allowing the humans to walk over the sloping and plastic surface. The amount of water is important also because it determined the circulation of the zeolitizing fluids.

The fluids percolated through the units dissolving the instable components of the pyroclastic deposits. Thus their composition directly depends on the composition of the instable volcanic shards, in this case alkaline. From the alkaline fluids precipitated zeolites aggregates, stable at low temperature and in alkaline environments: K-chabazite and phillipsite. The minerals created a rigid framework among the particles of the deposits, permitting the lithification of the surface with the record of the footprints and the characteristic inclination and creep.

To understand how long this process was and thus when the human footprints were impressed, $^{40}Ar/^{39}Ar$ dating were carried out. The obtained age is about 349 ± 3 ka for the trampled unit and 350 ± 3 ka for the following unit. Thus, on the basis of the standard deviation (1σ), these two dating are absolutely indistinguishable. The eruptive event deposited LS8, occurred at most after about 3 ka the emplacement of the LS7 trampled unit. So both the timing for the trampling and the lithification of the surface must have occurred within about 3 ka. During this period in Europe lived the *Homo*

Fig. 7.1 - Part of the trackway A (courtesy of Adolfo Panarello)

	Site Name	Country	Date	Substrate	Surface (flat/inclined)
1	Laetoli	Tanzania	3700 ka	Volcanic	Flat
2	Ilret	Kenya	1530-1510 ka	Volcanic	Flat
3	Koobi Fora	Kenya	1600-1500 ka	Volcanic	Flat
4	Roccamonfina	Italy	435 ± 6 ka	Volcanic	Inclined
5	Terra Amata	France	400-300 ka		Flat
6	Nahoon	South Africa	127 ka		Inclined
7	Langebaan	South Africa	117 ka		Inclined
8	Vartop Cave	Romania	62 ka		Flat
9	Theopetra Cave	Greece	45 ka		
10	Valsequillo	Mexico	40 ka	Volcanic	Flat
11	Lascaux	France			Flat
12	Niaux	France			Flat
13	Chauvet Cave	France	30-20 ka		
14	Peche Merle	France			
15	Fontanet	France			Flat
16	Ariege	France			
17	Willandra	Australia	23-19 ka		Flat
18	Lhasa region	Tibet	20 ka		
19	Ojo Guarena	Spain	15.6 ka		
20	Jeju Island	South Korea	15 ka		Flat
21	La Olla	Argentina	7000		
22	Monte Hermoso	Argentina	7000		
23	Acahualinca	Nicaragua	5945	Volcanic	Flat
24	Uskmouth	U.K.	6250-5720 BP		Flat
25	Formby	U.K.	5500 BP		Flat
26	Oro Grande site	California	5070		
27	Nola	Italy	3780	Volcanic	Flat
28	Chester	U.K.	900-700		
29	Gunma Prefecture	Japan	1280-400 A.D.		
30	Sunde Site	New Zealand	1400 A.D.		
31	Hawaii Volcanoes National Park	Hawaii	1790 A.D.	Volcanic	Flat

Tab. 7.1 - Worls ichnological sites

heildebergensis, a direct relative of *Homo erectus*. The footprints of the "Ciampate del Diavolo" site are thus confirmed to be the oldest human ichnological site in Europe and also one of the oldest in the world (Tab. 7.1).

Similar results were acquired also for another ichnological site with human footprints few kilometers far away from Foresta, the Carangi site. For these deposits the obtained age was 348 ± 2 ka, comparable to those of the main site of Foresta.

To complete the knowledge of the post-lithification and post-eruption evolution of the Foresta site, the lichenometry was used. This methodology permitted to express the time of the exposure of the trampled surface, using the dimension of the lichens, the first organism colonizing a volcanic origin surface. After the calibration of the method, the dimension of the thallus of the lichens permits to calculate the time of their formation and so the exposure of the surface. The result was about 230-260 years. Historical archives researches on the origin of the "Ciampate del Diavolo" place name prove that the site was unknown until 1754. Exceptionally abundant meteoric precipitation during the late seventeenth-early nineteenth period caused the destruction of streets and bridges near Foresta and probably the removal of the covering of the trampled surface.

During the Middle Pleistocene the Roccamonfina volcanic district, in spite of its activity, was an area inhabited by individuals belonging to *Homo heildebergensis* or coeval unknown species. The association

of coincidences which determined the exceptional formation and preservation of the footprints occurs not only in the Foresta site but covers a wider area, qualifying the Roccamonfina area as unique in the human heritage.

Appendix

A. Grain-size data

B. Geochemical data

A. Grain-size data

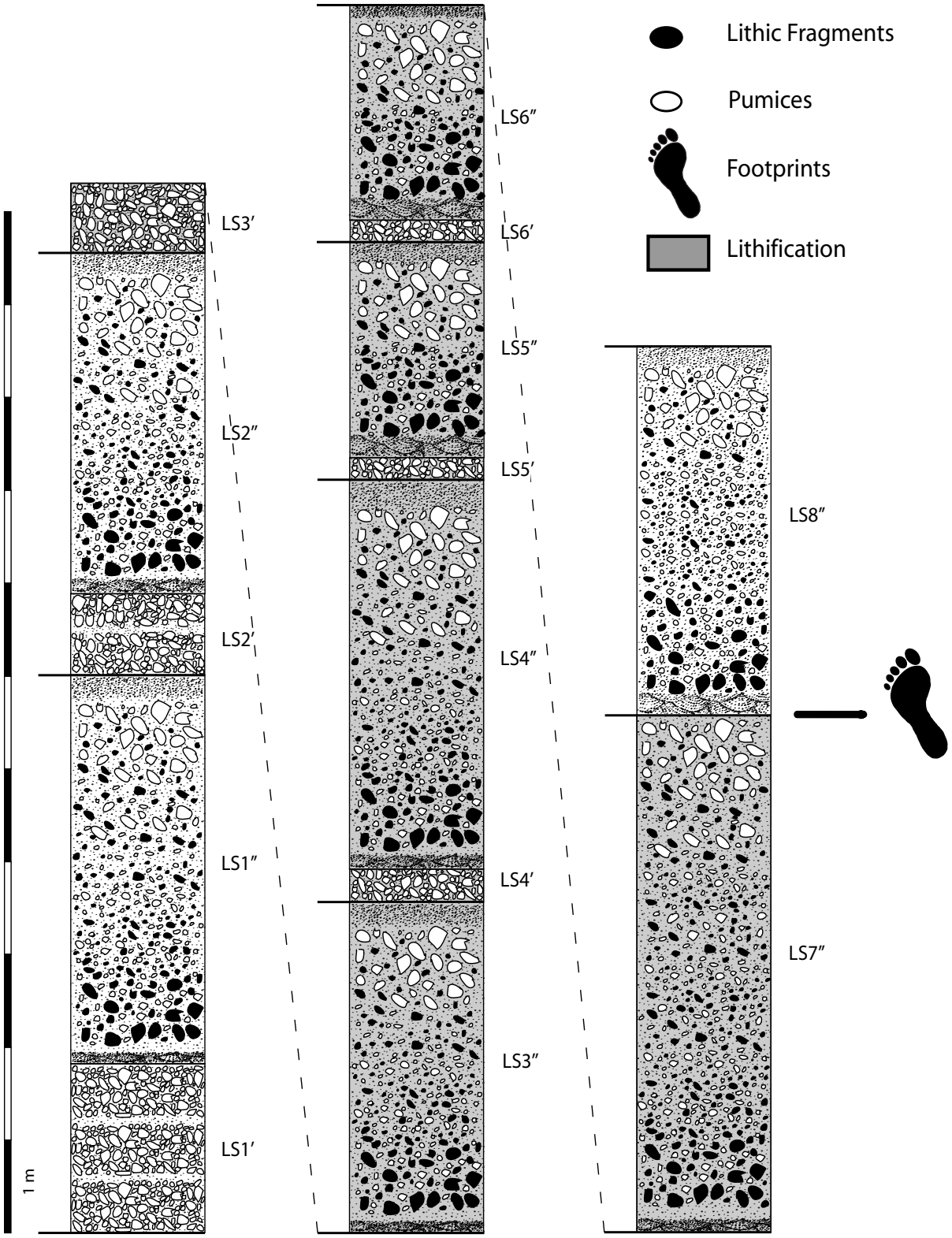

Fig A.1 - BLT stratigraphy. LS labels the sub-units.

1. Granulometric distributions

Here the grain size distribution for each sub-unit are represented.

LS1'

JUVENILES		
Aperture (mm)	Φ	Class Weight retained (g or %)
> 256	-8	0
256-181	-7,5	0,2
181-128	-7	0,6
128-90.5	-6,5	3,1
90.5-64	-6	2,1
64-45.3	-5,5	5,7
45.3-32	-5	4,6
32-22.6	-4,5	3,7
22.6-16	-4	3,2
16-11.3	-3,5	8,7
11.3-8	-3	12,1
8-5.66	-2,5	13,3
5.66-4	-2	12,1
4-2.8	-1,5	10,9
2.8-2	-1	8,2
2-1.4	-0,5	3,5
1.4-1	0	2,6
1-0.710	0,5	2,6
0.710-0.5	1	1,7
0.5-0.355	1,5	0,8
0.355-0.250	2	0,1
0.250-0.180	2,5	0,1
0.180-0.125	3	0,1
0.125-0.090	3,5	0
0.090-0.063	4	0
0.063-0.045	4,5	0
0.045-0.031	5	0
<0.031	5,5	0
		100

CRYSTALS		
Aperture (mm)	Φ	Class Weight retained (g or %)
> 256	-8	0
256-181	-7,5	0
181-128	-7	0
128-90.5	-6,5	0
90.5-64	-6	0
64-45.3	-5,5	0,2
45.3-32	-5	0,3
32-22.6	-4,5	2,1
22.6-16	-4	2,2
16-11.3	-3,5	3,1
11.3-8	-3	2,5
8-5.66	-2,5	12,7
5.66-4	-2	12,9
4-2.8	-1,5	14
2.8-2	-1	13,9
2-1.4	-0,5	14,2
1.4-1	0	13,2
1-0.710	0,5	6,7
0.710-0.5	1	1,9
0.5-0.355	1,5	0,1
0.355-0.250	2	0
0.250-0.180	2,5	0
0.180-0.125	3	0
0.125-0.090	3,5	0
0.090-0.063	4	0
0.063-0.045	4,5	0
0.045-0.031	5	0
<0.031	5,5	0
		100

LITHIC FRAGMENTS		
Aperture (mm)	Φ	Class Weight retained (g or %)
> 256	-8	0
256-181	-7,5	0
181-128	-7	0
128-90.5	-6,5	0
90.5-64	-6	0,7
64-45.3	-5,5	2,4
45.3-32	-5	5,1
32-22.6	-4,5	5,9
22.6-16	-4	6,9
16-11.3	-3,5	9,1
11.3-8	-3	10,6
8-5.66	-2,5	11,5
5.66-4	-2	9,7
4-2.8	-1,5	7,5
2.8-2	-1	7,1
2-1.4	-0,5	7
1.4-1	0	8,1
1-0.710	0,5	2,1
0.710-0.5	1	2,2
0.5-0.355	1,5	1,7
0.355-0.250	2	1,2
0.250-0.180	2,5	0,5
0.180-0.125	3	0,5
0.125-0.090	3,5	0,1
0.090-0.063	4	0,1
0.063-0.045	4,5	0
0.045-0.031	5	0
<0.031	5,5	0
		100

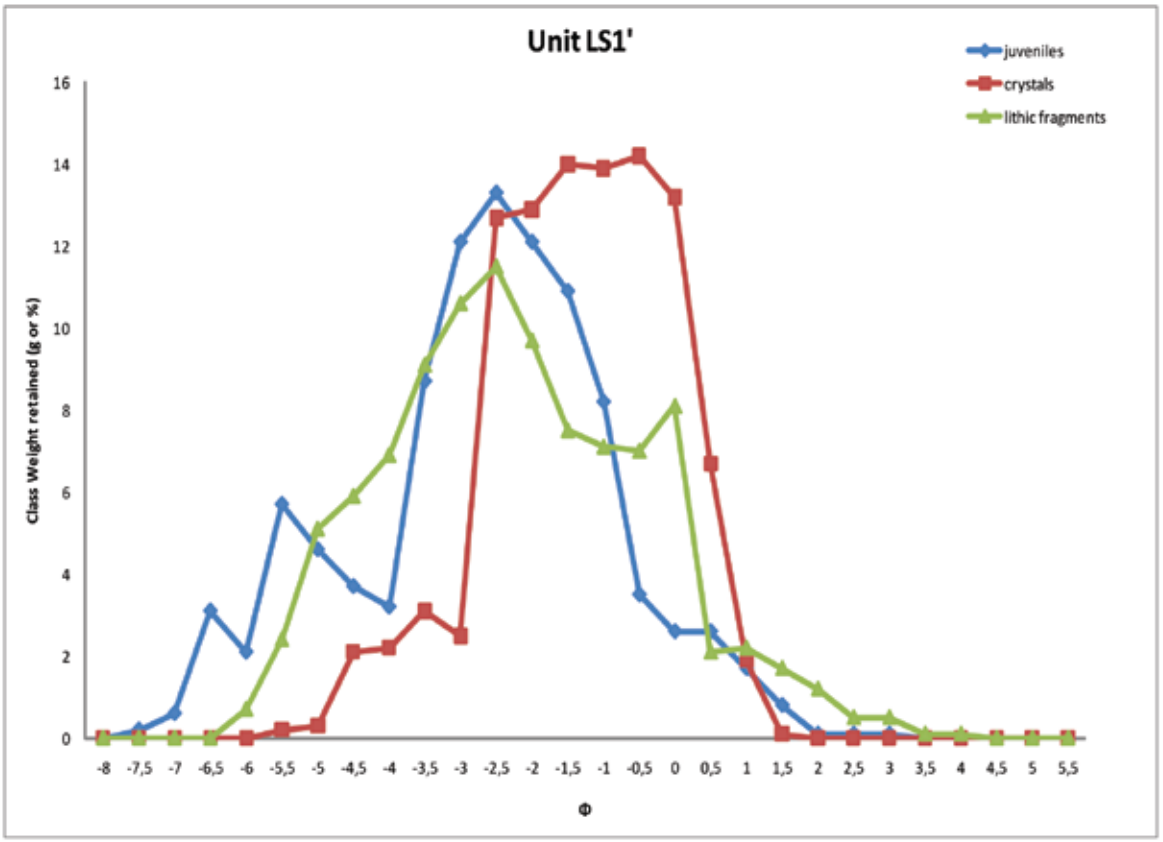

LS1”

JUVENILES		
Aperture (mm)	Φ	Class Weight retained (g or %)
> 256	-8	0
256-181	-7,5	0
181-128	-7	0
128-90.5	-6,5	0
90.5-64	-6	0
64-45.3	-5,5	0
45.3-32	-5	1,8
32-22.6	-4,5	1,5
22.6-16	-4	3,2
16-11.3	-3,5	8,7
11.3-8	-3	13,4
8-5.66	-2,5	16,1
5.66-4	-2	17,3
4-2.8	-1,5	13,7
2.8-2	-1	8,2
2-1.4	-0,5	7,4
1.4-1	0	5,2
1-0.710	0,5	3,2
0.710-0.5	1	0,3
0.5-0.355	1,5	0
0.355-0.250	2	0
0.250-0.180	2,5	0
0.180-0.125	3	0
0.125-0.090	3,5	0
0.090-0.063	4	0
0.063-0.045	4,5	0
0.045-0.031	5	0
<0.031	5,5	0
		100

CRYSTALS		
Aperture (mm)	Φ	Class Weight retained (g or %)
> 256	-8	0
256-181	-7,5	0
181-128	-7	0
128-90.5	-6,5	0
90.5-64	-6	0
64-45.3	-5,5	0
45.3-32	-5	0
32-22.6	-4,5	0
22.6-16	-4	0
16-11.3	-3,5	0
11.3-8	-3	0
8-5.66	-2,5	0,2
5.66-4	-2	0,3
4-2.8	-1,5	2,1
2.8-2	-1	2,2
2-1.4	-0,5	3,1
1.4-1	0	2,5
1-0.710	0,5	12,7
0.710-0.5	1	13,9
0.5-0.355	1,5	14,2
0.355-0.250	2	14,8
0.250-0.180	2,5	14,2
0.180-0.125	3	12,3
0.125-0.090	3,5	5,4
0.090-0.063	4	2,1
0.063-0.045	4,5	0
0.045-0.031	5	0
<0.031	5,5	0
		100

LITHIC FRAGMENTS		
Aperture (mm)	Φ	Class Weight retained (g or %)
> 256	-8	0
256-181	-7,5	0
181-128	-7	0
128-90.5	-6,5	0
90.5-64	-6	0
64-45.3	-5,5	0
45.3-32	-5	0
32-22.6	-4,5	0,7
22.6-16	-4	1,1
16-11.3	-3,5	1,8
11.3-8	-3	2,3
8-5.66	-2,5	2,5
5.66-4	-2	1,7
4-2.8	-1,5	1,1
2.8-2	-1	1,2
2-1.4	-0,5	4,5
1.4-1	0	8,3
1-0.710	0,5	5,4
0.710-0.5	1	6,7
0.5-0.355	1,5	12,6
0.355-0.250	2	4,2
0.250-0.180	2,5	8,2
0.180-0.125	3	13,3
0.125-0.090	3,5	14,5
0.090-0.063	4	6,1
0.063-0.045	4,5	2,6
0.045-0.031	5	1,2
<0.031	5,5	0
		100

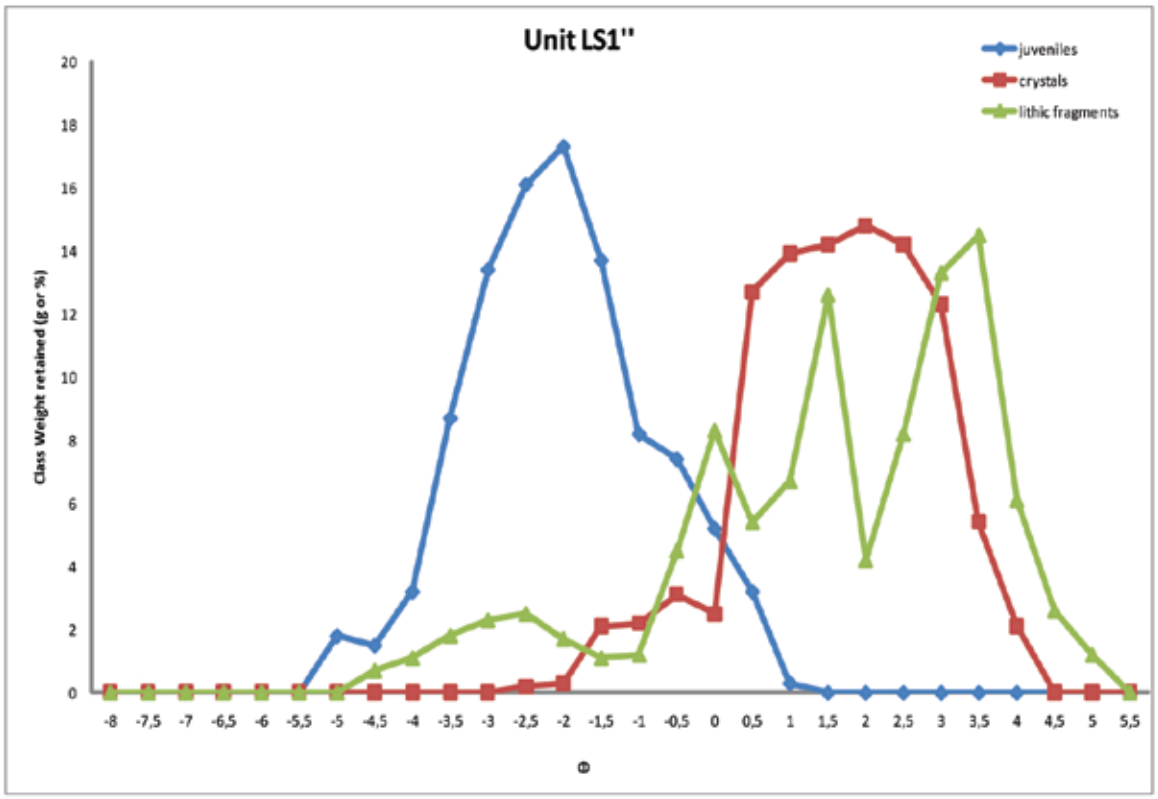

LS2'

JUVENILES		
Aperture (mm)	Φ	Class Weight retained (g or %)
> 256	-8	0
256-181	-7,5	0
181-128	-7	0
128-90.5	-6,5	0,6
90.5-64	-6	0,9
64-45.3	-5,5	1,2
45.3-32	-5	1,2
32-22.6	-4,5	2,3
22.6-16	-4	2,5
16-11.3	-3,5	6,5
11.3-8	-3	10,5
8-5.66	-2,5	11,9
5.66-4	-2	11,7
4-2.8	-1,5	12,3
2.8-2	-1	11,1
2-1.4	-0,5	8,8
1.4-1	0	8,9
1-0.710	0,5	6,4
0.710-0.5	1	2,1
0.5-0.355	1,5	0,6
0.355-0.250	2	0,3
0.250-0.180	2,5	0,2
0.180-0.125	3	0
0.125-0.090	3,5	0
0.090-0.063	4	0
0.063-0.045	4,5	0
0.045-0.031	5	0
<0.031	5,5	0
		100

CRYSTALS		
Aperture (mm)	Φ	Class Weight retained (g or %)
> 256	-8	0
256-181	-7,5	0
181-128	-7	0,2
128-90.5	-6,5	0,3
90.5-64	-6	1,5
64-45.3	-5,5	1,9
45.3-32	-5	2
32-22.6	-4,5	2,9
22.6-16	-4	3,1
16-11.3	-3,5	4,1
11.3-8	-3	5,5
8-5.66	-2,5	6,8
5.66-4	-2	12,3
4-2.8	-1,5	15,6
2.8-2	-1	13,5
2-1.4	-0,5	9,3
1.4-1	0	8,2
1-0.710	0,5	5,1
0.710-0.5	1	3,7
0.5-0.355	1,5	1,7
0.355-0.250	2	1,2
0.250-0.180	2,5	0,7
0.180-0.125	3	0,3
0.125-0.090	3,5	0,1
0.090-0.063	4	0
0.063-0.045	4,5	0
0.045-0.031	5	0
<0.031	5,5	0
		100

LITHIC FRAGMENTS		
Aperture (mm)	Φ	Class Weight retained (g or %)
> 256	-8	0
256-181	-7,5	0
181-128	-7	0
128-90.5	-6,5	0
90.5-64	-6	0
64-45.3	-5,5	0
45.3-32	-5	0
32-22.6	-4,5	0,7
22.6-16	-4	1,1
16-11.3	-3,5	1,8
11.3-8	-3	2,3
8-5.66	-2,5	2,5
5.66-4	-2	1,7
4-2.8	-1,5	1,1
2.8-2	-1	1,2
2-1.4	-0,5	3,5
1.4-1	0	7,1
1-0.710	0,5	5,4
0.710-0.5	1	6,7
0.5-0.355	1,5	11,6
0.355-0.250	2	9,7
0.250-0.180	2,5	8,2
0.180-0.125	3	12
0.125-0.090	3,5	13,5
0.090-0.063	4	6,1
0.063-0.045	4,5	2,6
0.045-0.031	5	1,2
<0.031	5,5	0
		100

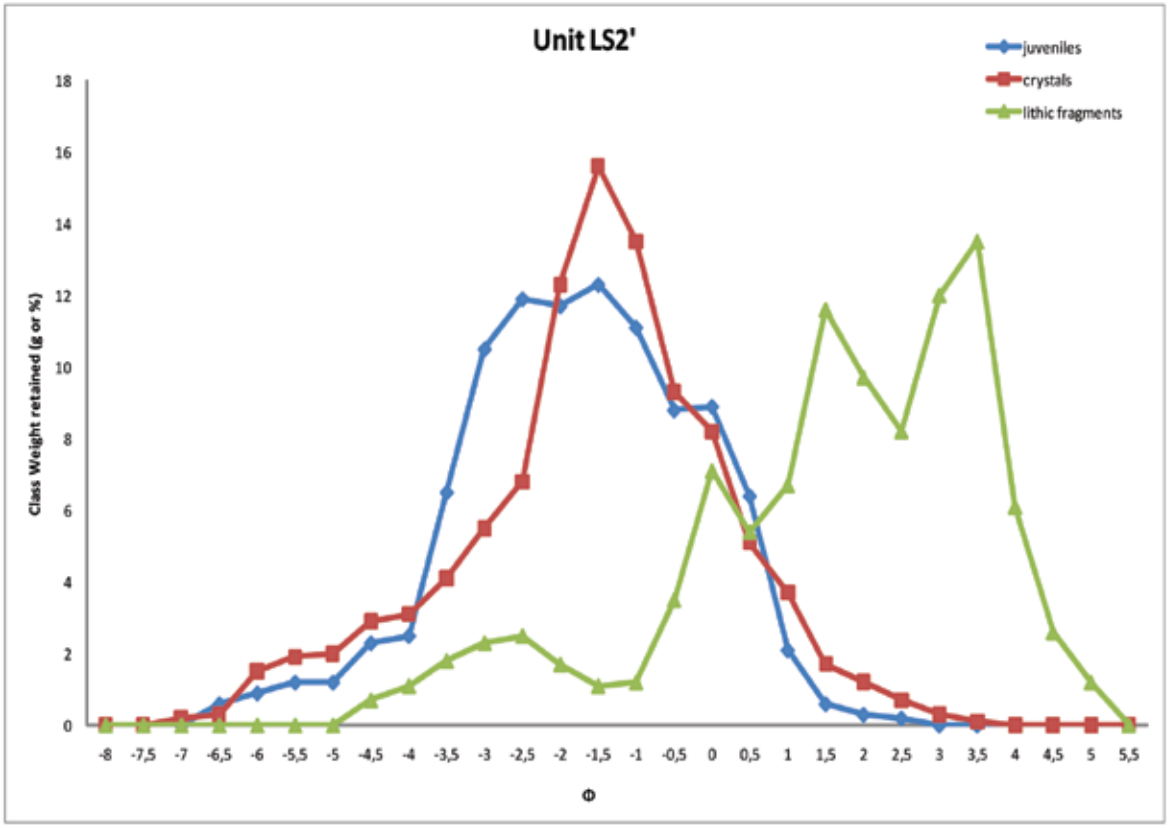

LS2”

JUVENILES		
Aperture (mm)	Φ	Class Weight retained (g or %)
> 256	-8	0
256-181	-7,5	0
181-128	-7	0
128-90.5	-6,5	0
90.5-64	-6	0
64-45.3	-5,5	0
45.3-32	-5	0
32-22.6	-4,5	0
22.6-16	-4	0,3
16-11.3	-3,5	0,9
11.3-8	-3	2,3
8-5.66	-2,5	4,1
5.66-4	-2	4,6
4-2.8	-1,5	3,9
2.8-2	-1	2,9
2-1.4	-0,5	8,1
1.4-1	0	9,4
1-0.710	0,5	12,8
0.710-0.5	1	14,6
0.5-0.355	1,5	9,9
0.355-0.250	2	13,9
0.250-0.180	2,5	8,6
0.180-0.125	3	2,8
0.125-0.090	3,5	0,9
0.090-0.063	4	0
0.063-0.045	4,5	0
0.045-0.031	5	0
<0.031	5,5	0
		100

CRYSTALS		
Aperture (mm)	Φ	Class Weight retained (g or %)
> 256	-8	0
256-181	-7,5	0
181-128	-7	0
128-90.5	-6,5	0
90.5-64	-6	0
64-45.3	-5,5	0
45.3-32	-5	0
32-22.6	-4,5	0
22.6-16	-4	0
16-11.3	-3,5	0
11.3-8	-3	0
8-5.66	-2,5	0
5.66-4	-2	0
4-2.8	-1,5	1,9
2.8-2	-1	2,2
2-1.4	-0,5	4,2
1.4-1	0	3,1
1-0.710	0,5	5,1
0.710-0.5	1	13,4
0.5-0.355	1,5	25,4
0.355-0.250	2	16,8
0.250-0.180	2,5	12,1
0.180-0.125	3	5,8
0.125-0.090	3,5	6,7
0.090-0.063	4	3,3
0.063-0.045	4,5	0
0.045-0.031	5	0
<0.031	5,5	0
		100

LITHIC FRAGMENTS		
Aperture (mm)	Φ	Class Weight retained (g or %)
> 256	-8	0
256-181	-7,5	0
181-128	-7	0
128-90.5	-6,5	0
90.5-64	-6	0
64-45.3	-5,5	0
45.3-32	-5	0
32-22.6	-4,5	0,3
22.6-16	-4	1
16-11.3	-3,5	0,9
11.3-8	-3	2,1
8-5.66	-2,5	3,9
5.66-4	-2	2,7
4-2.8	-1,5	3,9
2.8-2	-1	5,1
2-1.4	-0,5	8,4
1.4-1	0	7,2
1-0.710	0,5	18,8
0.710-0.5	1	14,2
0.5-0.355	1,5	15,7
0.355-0.250	2	7,4
0.250-0.180	2,5	5,6
0.180-0.125	3	2,1
0.125-0.090	3,5	0,7
0.090-0.063	4	0
0.063-0.045	4,5	0
0.045-0.031	5	0
<0.031	5,5	0
		100

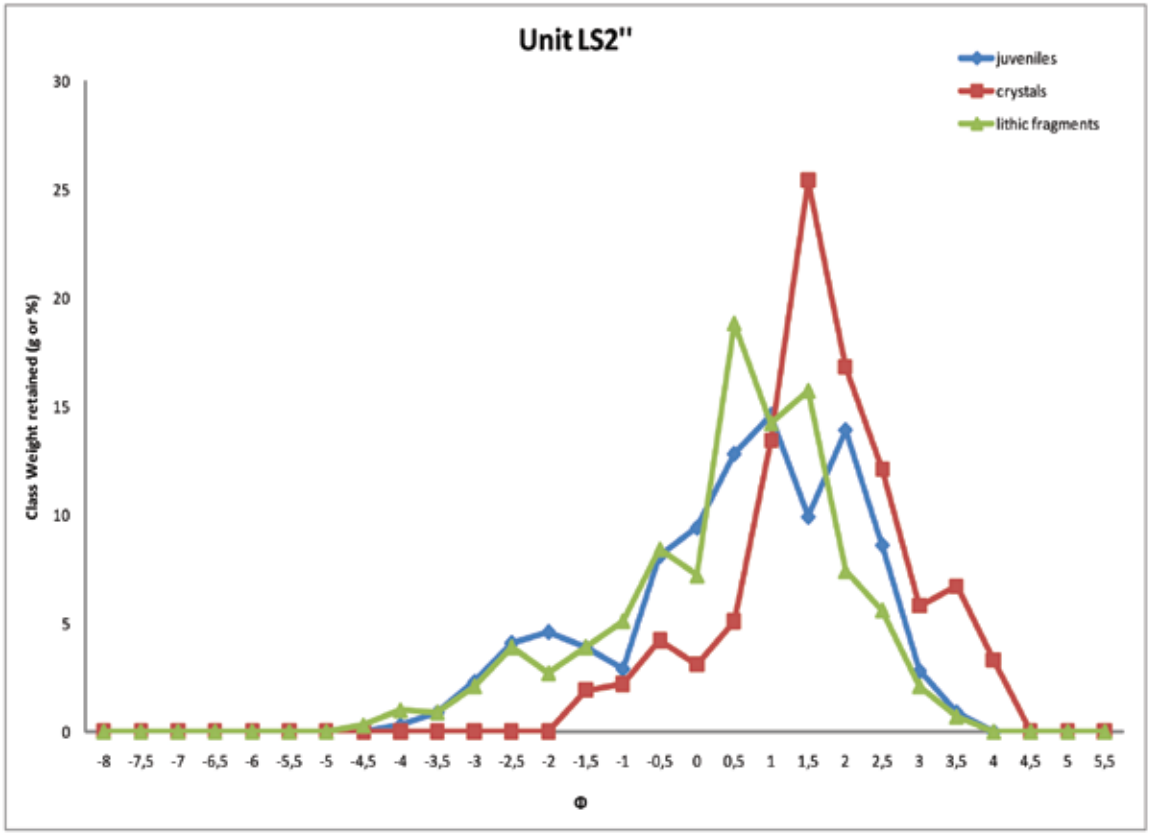

LS3'

JUVENILES		
Aperture (mm)	Φ	Class Weight retained (g or %)
> 256	-8	0
256-181	-7,5	0
181-128	-7	0
128-90.5	-6,5	0
90.5-64	-6	0
64-45.3	-5,5	0,2
45.3-32	-5	1,3
32-22.6	-4,5	1,5
22.6-16	-4	2,9
16-11.3	-3,5	2,8
11.3-8	-3	5,6
8-5.66	-2,5	7,8
5.66-4	-2	8,1
4-2.8	-1,5	10,9
2.8-2	-1	13,6
2-1.4	-0,5	11,9
1.4-1	0	10,5
1-0.710	0,5	7,7
0.710-0.5	1	5,9
0.5-0.355	1,5	3,6
0.355-0.250	2	2,5
0.250-0.180	2,5	1,2
0.180-0.125	3	1,1
0.125-0.090	3,5	0,9
0.090-0.063	4	0
0.063-0.045	4,5	0
0.045-0.031	5	0
<0.031	5,5	0
		100

CRYSTALS		
Aperture (mm)	Φ	Class Weight retained (g or %)
> 256	-8	0
256-181	-7,5	0
181-128	-7	0
128-90.5	-6,5	0
90.5-64	-6	0
64-45.3	-5,5	0
45.3-32	-5	0
32-22.6	-4,5	0,7
22.6-16	-4	1,1
16-11.3	-3,5	1,8
11.3-8	-3	1,6
8-5.66	-2,5	3,3
5.66-4	-2	5,4
4-2.8	-1,5	6,8
2.8-2	-1	7,2
2-1.4	-0,5	8,6
1.4-1	0	9,2
1-0.710	0,5	12,4
0.710-0.5	1	15,2
0.5-0.355	1,5	10,2
0.355-0.250	2	8,2
0.250-0.180	2,5	4,2
0.180-0.125	3	2,5
0.125-0.090	3,5	1,1
0.090-0.063	4	0,5
0.063-0.045	4,5	0
0.045-0.031	5	0
<0.031	5,5	0
		100

LITHIC FRAGMENTS		
Aperture (mm)	Φ	Class Weight retained (g or %)
> 256	-8	0
256-181	-7,5	0
181-128	-7	0
128-90.5	-6,5	0
90.5-64	-6	0
64-45.3	-5,5	0
45.3-32	-5	0
32-22.6	-4,5	0,7
22.6-16	-4	1,1
16-11.3	-3,5	1,8
11.3-8	-3	2,3
8-5.66	-2,5	2,5
5.66-4	-2	1,7
4-2.8	-1,5	1,1
2.8-2	-1	1,6
2-1.4	-0,5	4,1
1.4-1	0	6,3
1-0.710	0,5	4,8
0.710-0.5	1	5,7
0.5-0.355	1,5	9,8
0.355-0.250	2	10,6
0.250-0.180	2,5	11,1
0.180-0.125	3	11,4
0.125-0.090	3,5	13,5
0.090-0.063	4	6,1
0.063-0.045	4,5	2,6
0.045-0.031	5	1,2
<0.031	5,5	0
		100

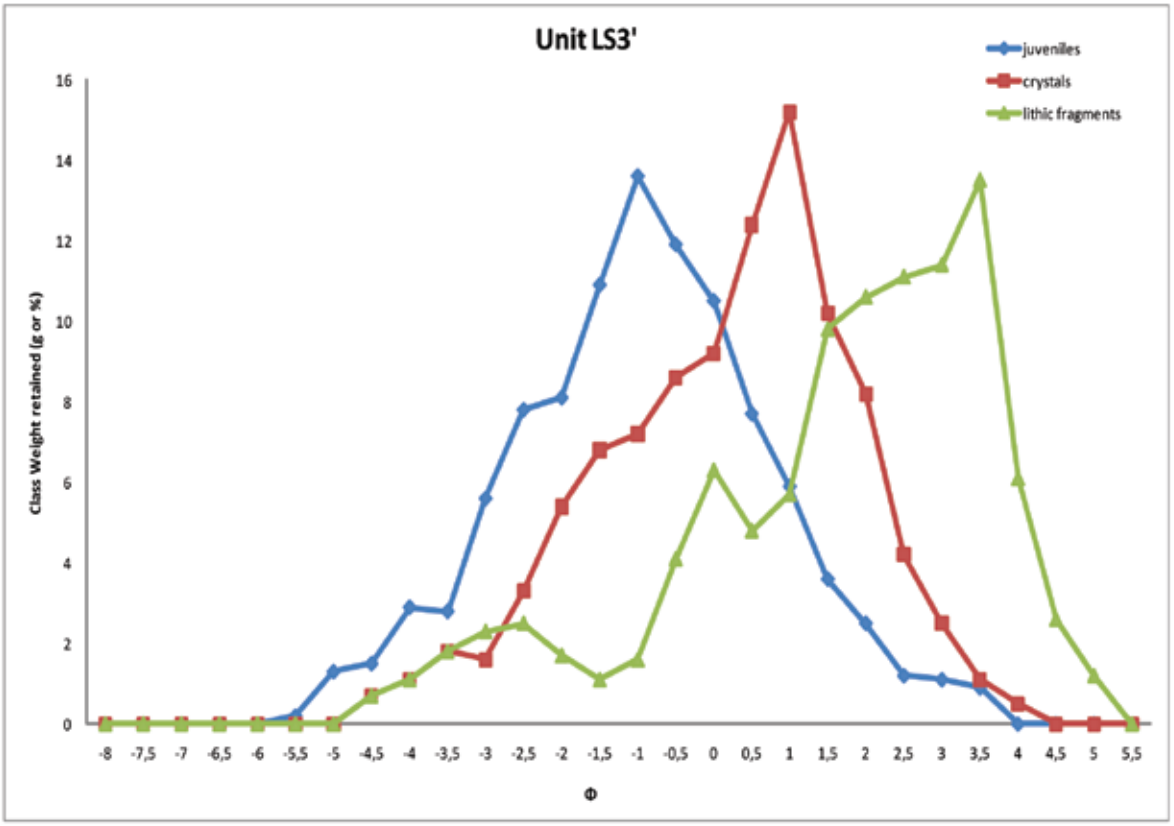

LS3”

JUVENILES		
Aperture (mm)	Φ	Class Weight retained (g or %)
> 256	-8	0
256-181	-7,5	0
181-128	-7	0
128-90.5	-6,5	0
90.5-64	-6	0
64-45.3	-5,5	0
45.3-32	-5	0
32-22.6	-4,5	0,3
22.6-16	-4	0,4
16-11.3	-3,5	1,1
11.3-8	-3	1,9
8-5.66	-2,5	1,5
5.66-4	-2	2,9
4-2.8	-1,5	4,8
2.8-2	-1	3,9
2-1.4	-0,5	6,3
1.4-1	0	16,1
1-0.710	0,5	11,3
0.710-0.5	1	10,5
0.5-0.355	1,5	18,8
0.355-0.250	2	7,9
0.250-0.180	2,5	7,4
0.180-0.125	3	1,6
0.125-0.090	3,5	2,7
0.090-0.063	4	0,6
0.063-0.045	4,5	0
0.045-0.031	5	0
<0.031	5,5	0
		100

CRYSTALS		
Aperture (mm)	Φ	Class Weight retained (g or %)
> 256	-8	0
256-181	-7,5	0
181-128	-7	0
128-90.5	-6,5	0
90.5-64	-6	0
64-45.3	-5,5	0
45.3-32	-5	0
32-22.6	-4,5	0
22.6-16	-4	0
16-11.3	-3,5	0
11.3-8	-3	0
8-5.66	-2,5	0,1
5.66-4	-2	0,1
4-2.8	-1,5	0,3
2.8-2	-1	0,5
2-1.4	-0,5	0,4
1.4-1	0	3,1
1-0.710	0,5	9,8
0.710-0.5	1	12,5
0.5-0.355	1,5	14,6
0.355-0.250	2	6,8
0.250-0.180	2,5	5,7
0.180-0.125	3	8,9
0.125-0.090	3,5	9,4
0.090-0.063	4	9,7
0.063-0.045	4,5	8,6
0.045-0.031	5	4,9
<0.031	5,5	4,6
		100

LITHIC FRAGMENTS		
Aperture (mm)	Φ	Class Weight retained (g or %)
> 256	-8	0
256-181	-7,5	0
181-128	-7	0
128-90.5	-6,5	0
90.5-64	-6	0
64-45.3	-5,5	0
45.3-32	-5	0
32-22.6	-4,5	0,2
22.6-16	-4	0,6
16-11.3	-3,5	2,4
11.3-8	-3	3,9
8-5.66	-2,5	3,3
5.66-4	-2	3,8
4-2.8	-1,5	3,1
2.8-2	-1	7,9
2-1.4	-0,5	14,6
1.4-1	0	12,9
1-0.710	0,5	15,2
0.710-0.5	1	10,4
0.5-0.355	1,5	7,1
0.355-0.250	2	6,6
0.250-0.180	2,5	5,3
0.180-0.125	3	1,8
0.125-0.090	3,5	0,6
0.090-0.063	4	0,3
0.063-0.045	4,5	0
0.045-0.031	5	0
<0.031	5,5	0
		100

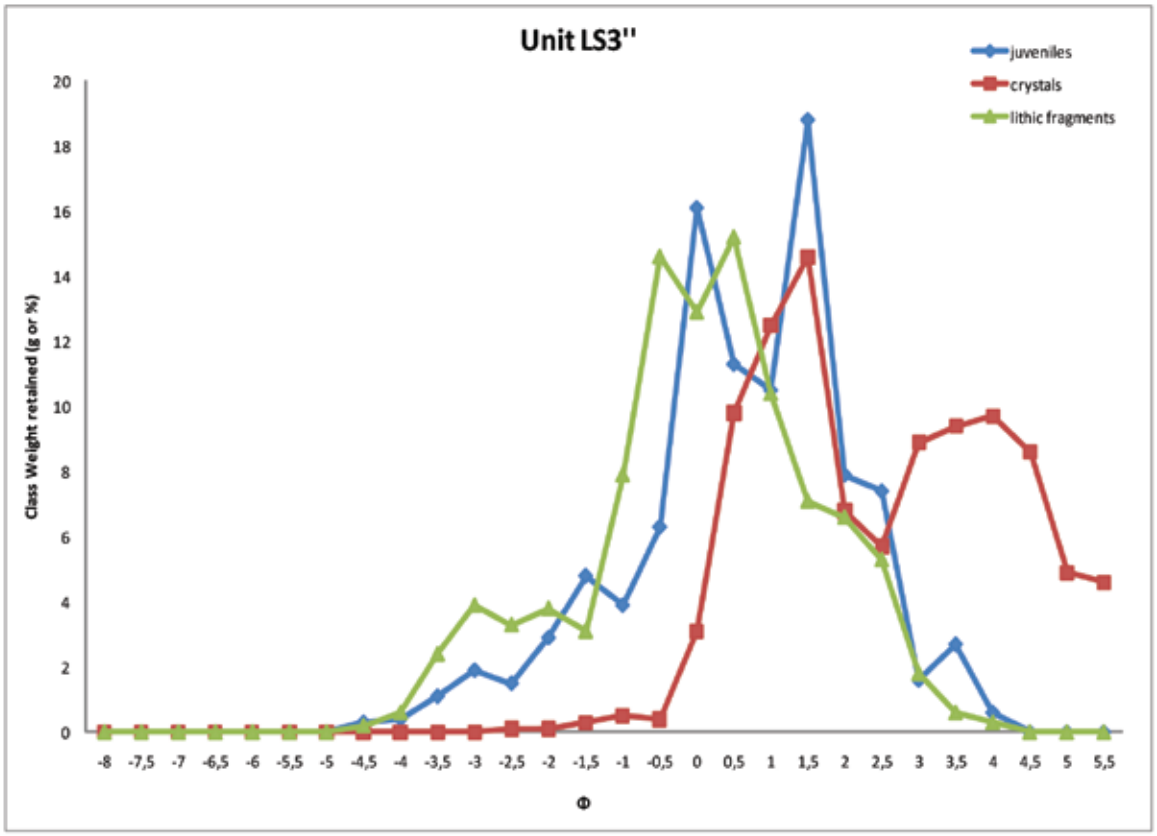

LS4'

JUVENILES		
Aperture (mm)	Φ	Class Weight retained (g or %)
> 256	-8	0
256-181	-7,5	0
181-128	-7	0
128-90.5	-6,5	0
90.5-64	-6	0
64-45.3	-5,5	0,3
45.3-32	-5	0,5
32-22.6	-4,5	1,2
22.6-16	-4	1,1
16-11.3	-3,5	1,7
11.3-8	-3	1,3
8-5.66	-2,5	2,2
5.66-4	-2	3,7
4-2.8	-1,5	4,8
2.8-2	-1	4,9
2-1.4	-0,5	7,3
1.4-1	0	10,9
1-0.710	0,5	12,5
0.710-0.5	1	13,7
0.5-0.355	1,5	14,4
0.355-0.250	2	8,4
0.250-0.180	2,5	5,8
0.180-0.125	3	2,7
0.125-0.090	3,5	1,7
0.090-0.063	4	0,6
0.063-0.045	4,5	0
0.045-0.031	5	0
<0.031	5,5	0,3
		100

CRYSTALS		
Aperture (mm)	Φ	Class Weight retained (g or %)
> 256	-8	0
256-181	-7,5	0
181-128	-7	0
128-90.5	-6,5	0
90.5-64	-6	0
64-45.3	-5,5	0
45.3-32	-5	0
32-22.6	-4,5	0
22.6-16	-4	0,1
16-11.3	-3,5	0,6
11.3-8	-3	0,8
8-5.66	-2,5	0,8
5.66-4	-2	1,3
4-2.8	-1,5	1,6
2.8-2	-1	2
2-1.4	-0,5	2,1
1.4-1	0	2,1
1-0.710	0,5	10,3
0.710-0.5	1	18,6
0.5-0.355	1,5	21,5
0.355-0.250	2	15,1
0.250-0.180	2,5	9,9
0.180-0.125	3	5,7
0.125-0.090	3,5	3,9
0.090-0.063	4	3,3
0.063-0.045	4,5	0,3
0.045-0.031	5	0
<0.031	5,5	0
		100

LITHIC FRAGMENTS		
Aperture (mm)	Φ	Class Weight retained (g or %)
> 256	-8	0
256-181	-7,5	0
181-128	-7	0
128-90.5	-6,5	0
90.5-64	-6	0
64-45.3	-5,5	0
45.3-32	-5	0
32-22.6	-4,5	0,6
22.6-16	-4	1,3
16-11.3	-3,5	1,1
11.3-8	-3	1,4
8-5.66	-2,5	1,9
5.66-4	-2	1,2
4-2.8	-1,5	2,1
2.8-2	-1	7,7
2-1.4	-0,5	11,4
1.4-1	0	11,9
1-0.710	0,5	11,1
0.710-0.5	1	12,3
0.5-0.355	1,5	15,5
0.355-0.250	2	8,7
0.250-0.180	2,5	4,9
0.180-0.125	3	2,7
0.125-0.090	3,5	2
0.090-0.063	4	1,3
0.063-0.045	4,5	0,9
0.045-0.031	5	0
<0.031	5,5	0
		100

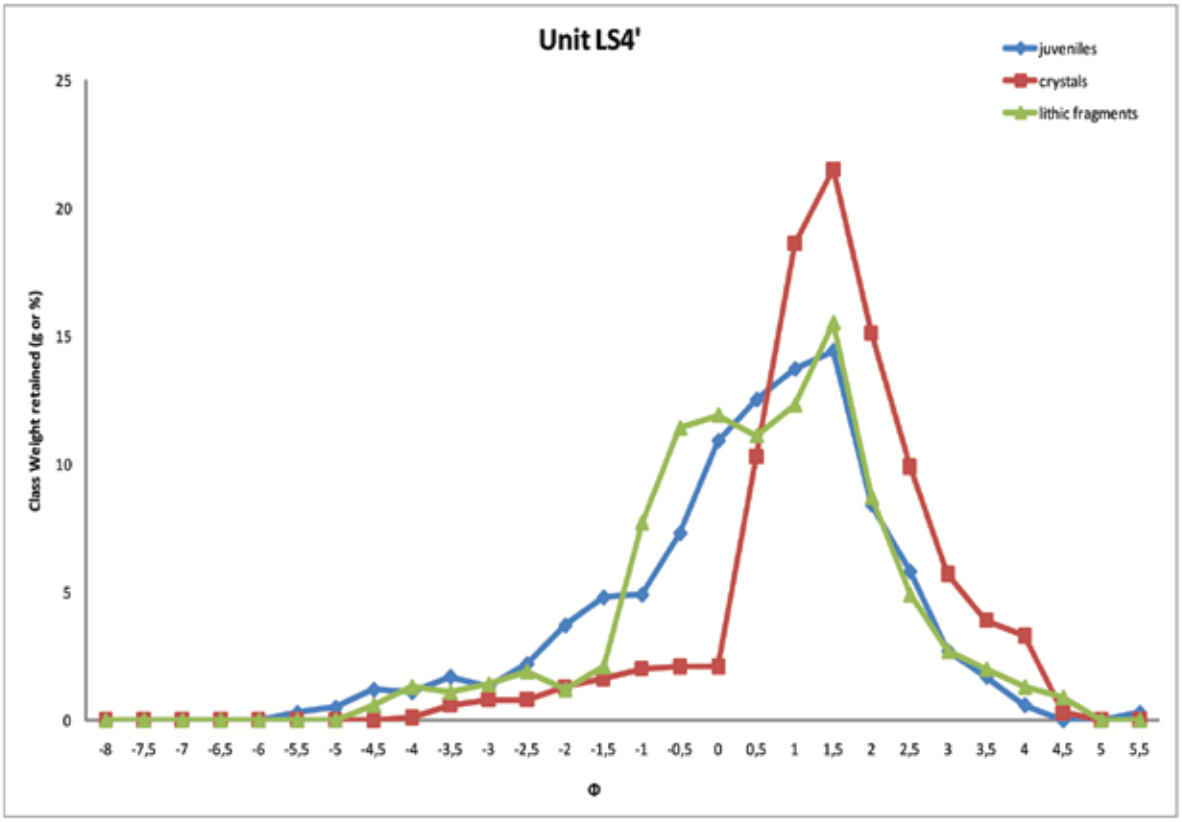

LS4”

JUVENILES		
Aperture (mm)	Φ	Class Weight retained (g or %)
> 256	-8	0
256-181	-7,5	0
181-128	-7	0
128-90.5	-6,5	0
90.5-64	-6	0
64-45.3	-5,5	0
45.3-32	-5	0
32-22.6	-4,5	0,5
22.6-16	-4	0,9
16-11.3	-3,5	0,9
11.3-8	-3	1,3
8-5.66	-2,5	2,1
5.66-4	-2	3,1
4-2.8	-1,5	2,3
2.8-2	-1	2
2-1.4	-0,5	8,3
1.4-1	0	11,8
1-0.710	0,5	11,2
0.710-0.5	1	17,5
0.5-0.355	1,5	20,6
0.355-0.250	2	7,8
0.250-0.180	2,5	5,9
0.180-0.125	3	2,3
0.125-0.090	3,5	0,7
0.090-0.063	4	0,3
0.063-0.045	4,5	0,1
0.045-0.031	5	0,1
<0.031	5,5	0,3
		100

CRYSTALS		
Aperture (mm)	Φ	Class Weight retained (g or %)
> 256	-8	0
256-181	-7,5	0
181-128	-7	0
128-90.5	-6,5	0
90.5-64	-6	0
64-45.3	-5,5	0
45.3-32	-5	0
32-22.6	-4,5	0
22.6-16	-4	0
16-11.3	-3,5	0
11.3-8	-3	0
8-5.66	-2,5	0
5.66-4	-2	0,1
4-2.8	-1,5	0,9
2.8-2	-1	0,8
2-1.4	-0,5	1,1
1.4-1	0	2,1
1-0.710	0,5	3,8
0.710-0.5	1	12,1
0.5-0.355	1,5	26
0.355-0.250	2	22,4
0.250-0.180	2,5	13,7
0.180-0.125	3	6,7
0.125-0.090	3,5	3,9
0.090-0.063	4	3,1
0.063-0.045	4,5	1,8
0.045-0.031	5	0,6
<0.031	5,5	0,9
		100

LITHIC FRAGMENTS		
Aperture (mm)	Φ	Class Weight retained (g or %)
> 256	-8	0
256-181	-7,5	0
181-128	-7	0
128-90.5	-6,5	0
90.5-64	-6	0
64-45.3	-5,5	0
45.3-32	-5	0
32-22.6	-4,5	0,6
22.6-16	-4	1,3
16-11.3	-3,5	2,1
11.3-8	-3	1,4
8-5.66	-2,5	1,9
5.66-4	-2	1,2
4-2.8	-1,5	3,1
2.8-2	-1	5,7
2-1.4	-0,5	11,4
1.4-1	0	13,3
1-0.710	0,5	9,6
0.710-0.5	1	16,5
0.5-0.355	1,5	11,2
0.355-0.250	2	4,8
0.250-0.180	2,5	5,9
0.180-0.125	3	2,9
0.125-0.090	3,5	3,2
0.090-0.063	4	1,9
0.063-0.045	4,5	1,2
0.045-0.031	5	0,6
<0.031	5,5	0,2
		100

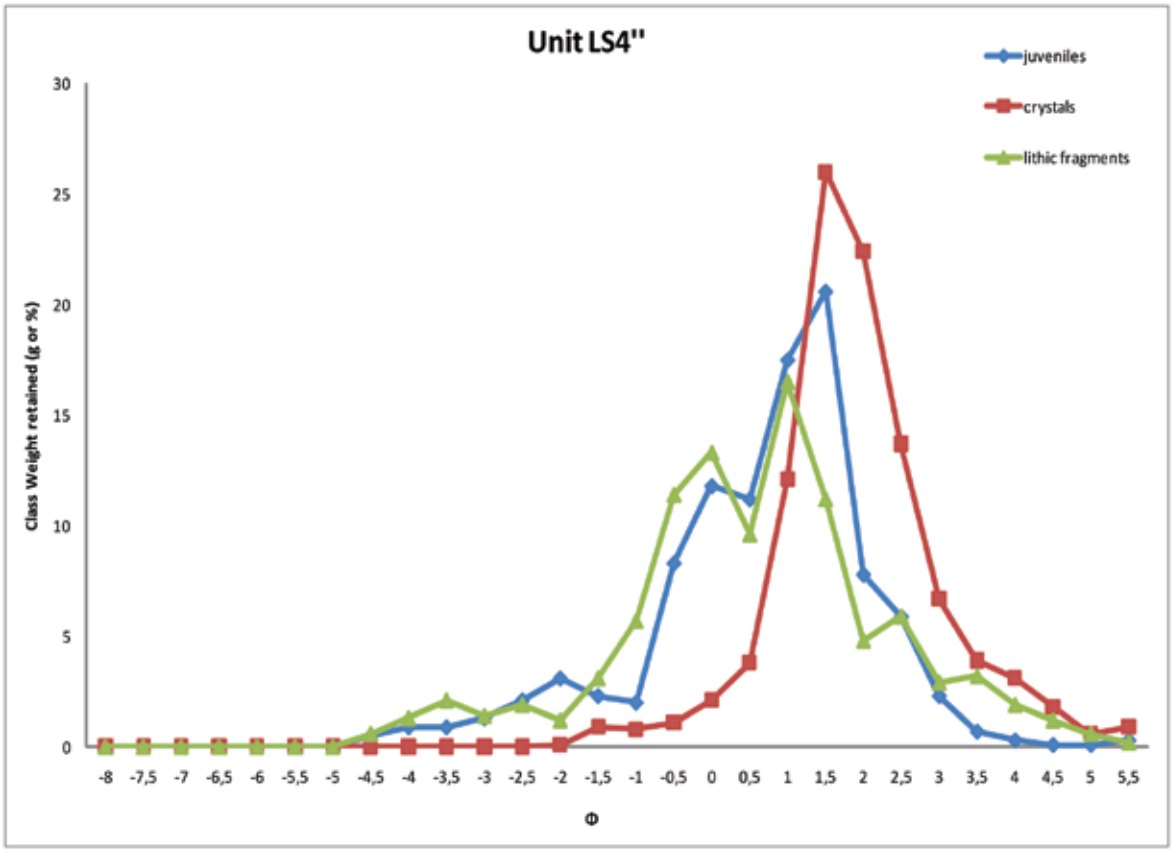

LS5'

JUVENILES		
Aperture (mm)	Φ	Class Weight retained (g or %)
> 256	-8	0
256-181	-7,5	0
181-128	-7	0
128-90.5	-6,5	0
90.5-64	-6	0
64-45.3	-5,5	0
45.3-32	-5	0,1
32-22.6	-4,5	1,1
22.6-16	-4	1,1
16-11.3	-3,5	1,3
11.3-8	-3	1,8
8-5.66	-2,5	2,1
5.66-4	-2	3,5
4-2.8	-1,5	4,3
2.8-2	-1	7,3
2-1.4	-0,5	13,5
1.4-1	0	10,8
1-0.710	0,5	15,3
0.710-0.5	1	12,8
0.5-0.355	1,5	9,9
0.355-0.250	2	8,1
0.250-0.180	2,5	4,2
0.180-0.125	3	1,7
0.125-0.090	3,5	0,8
0.090-0.063	4	0,3
0.063-0.045	4,5	0
0.045-0.031	5	0
<0.031	5,5	0
		100

CRYSTALS		
Aperture (mm)	Φ	Class Weight retained (g or %)
> 256	-8	0
256-181	-7,5	0
181-128	-7	0
128-90.5	-6,5	0
90.5-64	-6	0
64-45.3	-5,5	0
45.3-32	-5	0
32-22.6	-4,5	0
22.6-16	-4	0
16-11.3	-3,5	0
11.3-8	-3	0
8-5.66	-2,5	0,1
5.66-4	-2	1,4
4-2.8	-1,5	3,2
2.8-2	-1	4,2
2-1.4	-0,5	6,5
1.4-1	0	7,7
1-0.710	0,5	10,5
0.710-0.5	1	15,6
0.5-0.355	1,5	18,4
0.355-0.250	2	9,6
0.250-0.180	2,5	8,9
0.180-0.125	3	4,7
0.125-0.090	3,5	2,7
0.090-0.063	4	1,9
0.063-0.045	4,5	2,3
0.045-0.031	5	1,4
<0.031	5,5	0,9
		100

LITHIC FRAGMENTS		
Aperture (mm)	Φ	Class Weight retained (g or %)
> 256	-8	0
256-181	-7,5	0
181-128	-7	0
128-90.5	-6,5	0
90.5-64	-6	0
64-45.3	-5,5	0
45.3-32	-5	0
32-22.6	-4,5	0
22.6-16	-4	0,1
16-11.3	-3,5	0,9
11.3-8	-3	1,6
8-5.66	-2,5	2,3
5.66-4	-2	2,5
4-2.8	-1,5	2
2.8-2	-1	3,2
2-1.4	-0,5	4,2
1.4-1	0	7,1
1-0.710	0,5	9,3
0.710-0.5	1	15,4
0.5-0.355	1,5	16,3
0.355-0.250	2	16,2
0.250-0.180	2,5	7,5
0.180-0.125	3	3,6
0.125-0.090	3,5	2,5
0.090-0.063	4	2,7
0.063-0.045	4,5	1,5
0.045-0.031	5	1,1
<0.031	5,5	0
		100

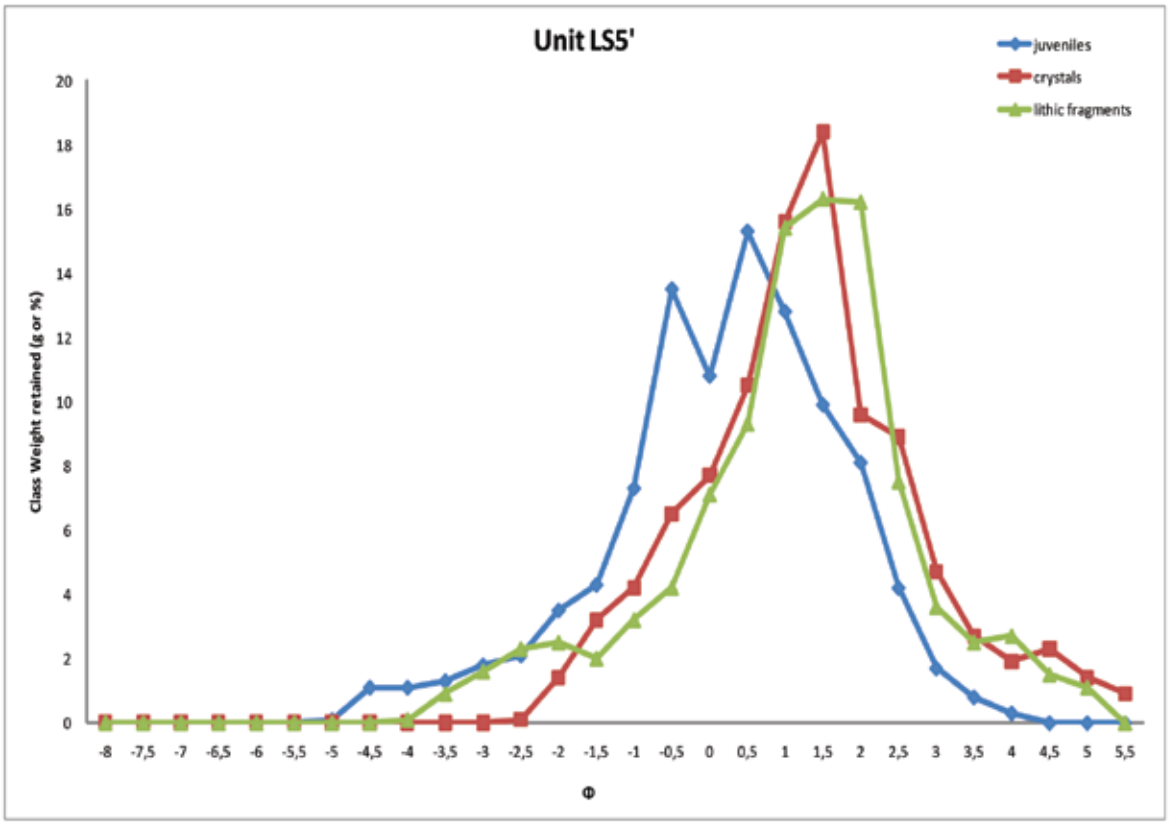

LS5”

JUVENILES		
Aperture (mm)	Φ	Class Weight retained (g or %)
> 256	-8	0
256-181	-7,5	0
181-128	-7	0
128-90.5	-6,5	0
90.5-64	-6	0
64-45.3	-5,5	0
45.3-32	-5	0,1
32-22.6	-4,5	0,4
22.6-16	-4	0,4
16-11.3	-3,5	1,3
11.3-8	-3	1,8
8-5.66	-2,5	2,1
5.66-4	-2	2,2
4-2.8	-1,5	2
2.8-2	-1	5,6
2-1.4	-0,5	9,4
1.4-1	0	5,6
1-0.710	0,5	14,8
0.710-0.5	1	11,5
0.5-0.355	1,5	18,6
0.355-0.250	2	11,7
0.250-0.180	2,5	5,2
0.180-0.125	3	2,9
0.125-0.090	3,5	1,8
0.090-0.063	4	0,5
0.063-0.045	4,5	0,5
0.045-0.031	5	0,3
<0.031	5,5	1,3
		100

CRYSTALS		
Aperture (mm)	Φ	Class Weight retained (g or %)
> 256	-8	0
256-181	-7,5	0
181-128	-7	0
128-90.5	-6,5	0
90.5-64	-6	0
64-45.3	-5,5	0
45.3-32	-5	0
32-22.6	-4,5	0
22.6-16	-4	0
16-11.3	-3,5	0
11.3-8	-3	0
8-5.66	-2,5	0,1
5.66-4	-2	0,1
4-2.8	-1,5	0,3
2.8-2	-1	1
2-1.4	-0,5	2,9
1.4-1	0	4
1-0.710	0,5	3,8
0.710-0.5	1	15,8
0.5-0.355	1,5	25,1
0.355-0.250	2	18,3
0.250-0.180	2,5	10,5
0.180-0.125	3	6,9
0.125-0.090	3,5	2,7
0.090-0.063	4	1,9
0.063-0.045	4,5	2,1
0.045-0.031	5	2,3
<0.031	5,5	2,2
		100

LITHIC FRAGMENTS		
Aperture (mm)	Φ	Class Weight retained (g or %)
> 256	-8	0
256-181	-7,5	0
181-128	-7	0
128-90.5	-6,5	0
90.5-64	-6	0
64-45.3	-5,5	0
45.3-32	-5	0
32-22.6	-4,5	0,1
22.6-16	-4	0,9
16-11.3	-3,5	1,6
11.3-8	-3	2,5
8-5.66	-2,5	2,5
5.66-4	-2	2
4-2.8	-1,5	2,1
2.8-2	-1	4,2
2-1.4	-0,5	5,1
1.4-1	0	9,3
1-0.710	0,5	18,8
0.710-0.5	1	17,3
0.5-0.355	1,5	15,2
0.355-0.250	2	6,2
0.250-0.180	2,5	3,6
0.180-0.125	3	2,5
0.125-0.090	3,5	2,7
0.090-0.063	4	1,4
0.063-0.045	4,5	1,1
0.045-0.031	5	0,9
<0.031	5,5	0
		100

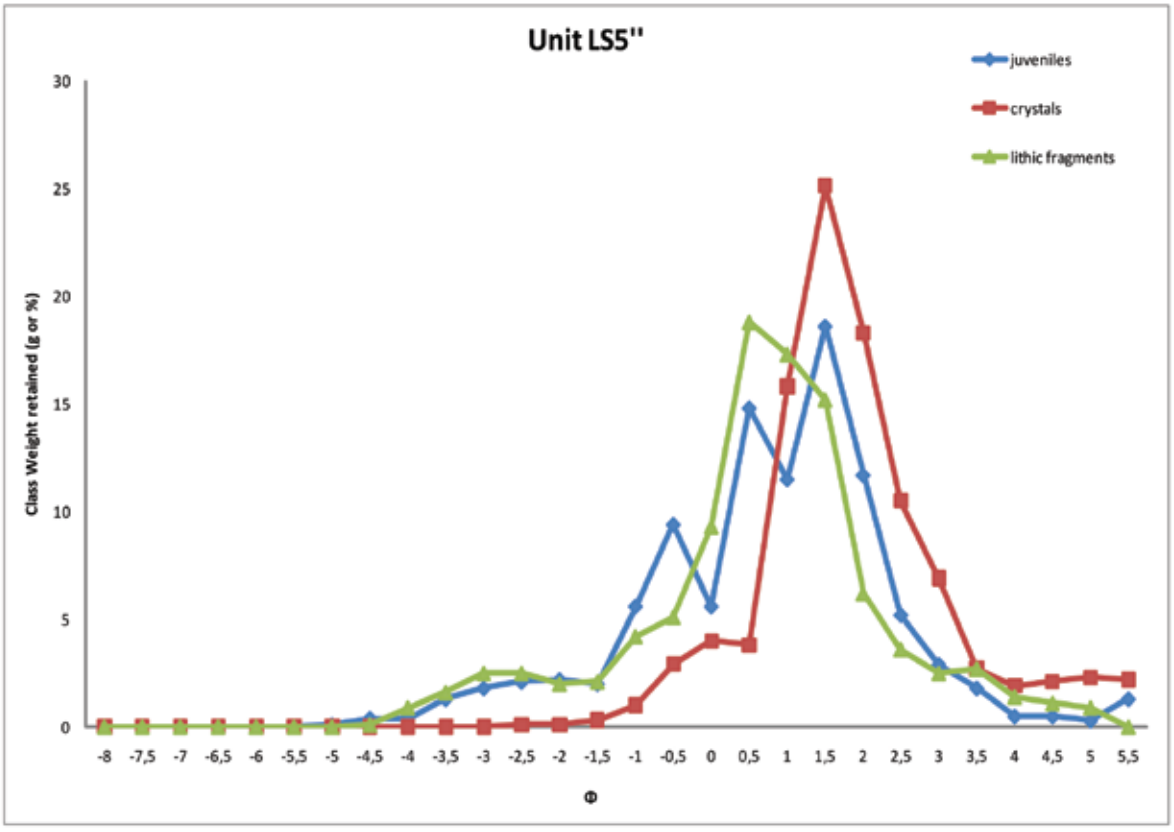

LS6'

JUVENILES		
Aperture (mm)	Φ	Class Weight retained (g or %)
> 256	-8	0
256-181	-7,5	0
181-128	-7	0
128-90.5	-6,5	0
90.5-64	-6	0
64-45.3	-5,5	0
45.3-32	-5	0
32-22.6	-4,5	0,7
22.6-16	-4	1,2
16-11.3	-3,5	2,2
11.3-8	-3	2,9
8-5.66	-2,5	4,1
5.66-4	-2	6,6
4-2.8	-1,5	7
2.8-2	-1	8,2
2-1.4	-0,5	8
1.4-1	0	11,3
1-0.710	0,5	15,1
0.710-0.5	1	16,9
0.5-0.355	1,5	10,1
0.355-0.250	2	3,1
0.250-0.180	2,5	2,1
0.180-0.125	3	0,4
0.125-0.090	3,5	0,1
0.090-0.063	4	0
0.063-0.045	4,5	0
0.045-0.031	5	0
<0.031	5,5	0
		100

CRYSTALS		
Aperture (mm)	Φ	Class Weight retained (g or %)
> 256	-8	0
256-181	-7,5	0
181-128	-7	0
128-90.5	-6,5	0
90.5-64	-6	0
64-45.3	-5,5	0
45.3-32	-5	0
32-22.6	-4,5	0
22.6-16	-4	0
16-11.3	-3,5	0,2
11.3-8	-3	0,5
8-5.66	-2,5	0,5
5.66-4	-2	1,2
4-2.8	-1,5	2,1
2.8-2	-1	2,2
2-1.4	-0,5	3,1
1.4-1	0	5,7
1-0.710	0,5	9,3
0.710-0.5	1	12,1
0.5-0.355	1,5	12,9
0.355-0.250	2	11,4
0.250-0.180	2,5	12,2
0.180-0.125	3	12,9
0.125-0.090	3,5	10,3
0.090-0.063	4	2,5
0.063-0.045	4,5	0,9
0.045-0.031	5	0
<0.031	5,5	0
		100

LITHIC FRAGMENTS		
Aperture (mm)	Φ	Class Weight retained (g or %)
> 256	-8	0
256-181	-7,5	0
181-128	-7	0
128-90.5	-6,5	0
90.5-64	-6	0
64-45.3	-5,5	0
45.3-32	-5	0
32-22.6	-4,5	0,7
22.6-16	-4	1,1
16-11.3	-3,5	1,8
11.3-8	-3	2,3
8-5.66	-2,5	2,5
5.66-4	-2	1,7
4-2.8	-1,5	1,1
2.8-2	-1	1,2
2-1.4	-0,5	4,5
1.4-1	0	8,8
1-0.710	0,5	6,4
0.710-0.5	1	7,7
0.5-0.355	1,5	12,6
0.355-0.250	2	10,5
0.250-0.180	2,5	10,2
0.180-0.125	3	12,3
0.125-0.090	3,5	11
0.090-0.063	4	2,5
0.063-0.045	4,5	1,1
0.045-0.031	5	0
<0.031	5,5	0
		100

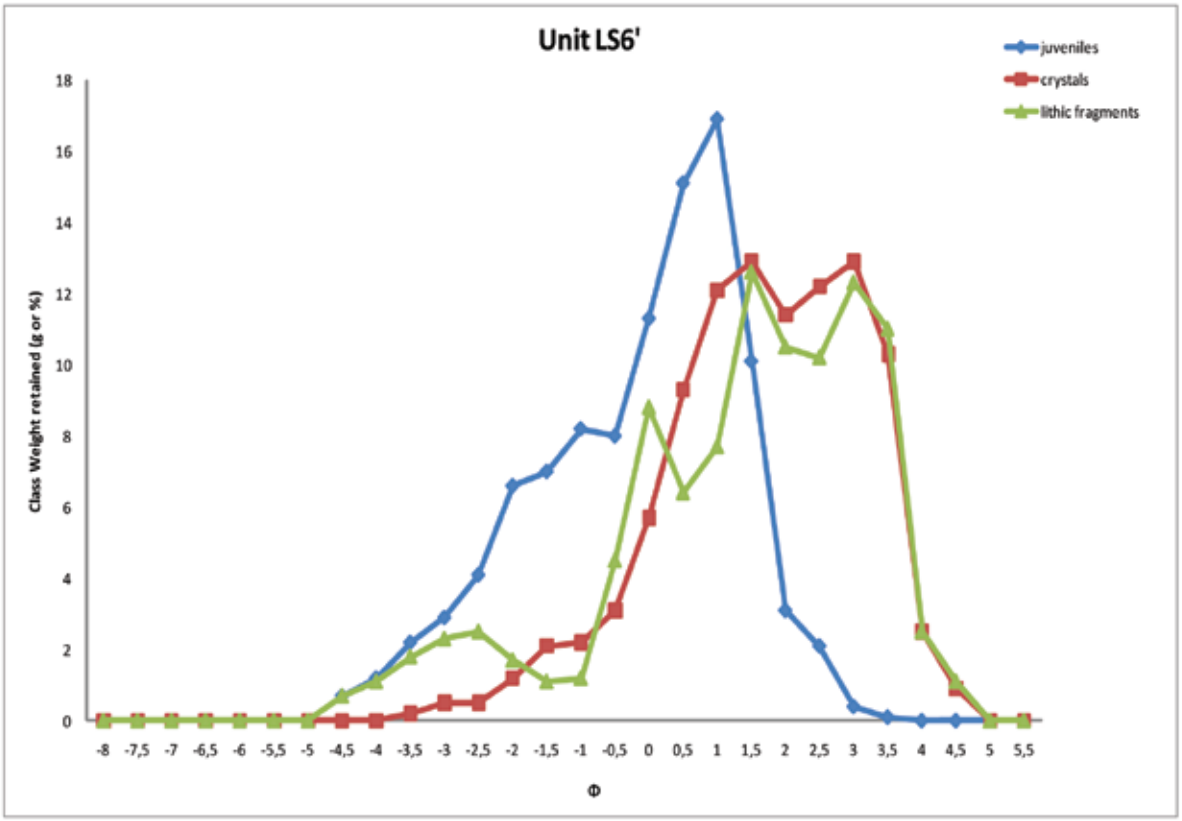

LS6”

JUVENILES		
Aperture (mm)	Φ	Class Weight retained (g or %)
> 256	-8	0
256-181	-7,5	0
181-128	-7	0
128-90.5	-6,5	0
90.5-64	-6	0
64-45.3	-5,5	0
45.3-32	-5	1,8
32-22.6	-4,5	3,1
22.6-16	-4	4,3
16-11.3	-3,5	8,7
11.3-8	-3	13,4
8-5.66	-2,5	11,9
5.66-4	-2	15,3
4-2.8	-1,5	10,6
2.8-2	-1	8,2
2-1.4	-0,5	10,4
1.4-1	0	7,1
1-0.710	0,5	3,2
0.710-0.5	1	0,3
0.5-0.355	1,5	0,8
0.355-0.250	2	0,9
0.250-0.180	2,5	0
0.180-0.125	3	0
0.125-0.090	3,5	0
0.090-0.063	4	0
0.063-0.045	4,5	0
0.045-0.031	5	0
<0.031	5,5	0
		100

CRYSTALS		
Aperture (mm)	Φ	Class Weight retained (g or %)
> 256	-8	0
256-181	-7,5	0
181-128	-7	0
128-90.5	-6,5	0
90.5-64	-6	0
64-45.3	-5,5	0
45.3-32	-5	0
32-22.6	-4,5	0
22.6-16	-4	0
16-11.3	-3,5	0
11.3-8	-3	0
8-5.66	-2,5	1,2
5.66-4	-2	0,3
4-2.8	-1,5	2,8
2.8-2	-1	2,8
2-1.4	-0,5	3,5
1.4-1	0	4,8
1-0.710	0,5	8,1
0.710-0.5	1	12,1
0.5-0.355	1,5	15,3
0.355-0.250	2	13,4
0.250-0.180	2,5	13,9
0.180-0.125	3	12,3
0.125-0.090	3,5	7,4
0.090-0.063	4	2,1
0.063-0.045	4,5	0
0.045-0.031	5	0
<0.031	5,5	0
		100

LITHIC FRAGMENTS		
Aperture (mm)	Φ	Class Weight retained (g or %)
> 256	-8	0
256-181	-7,5	0
181-128	-7	0
128-90.5	-6,5	0
90.5-64	-6	0
64-45.3	-5,5	0
45.3-32	-5	0
32-22.6	-4,5	1,7
22.6-16	-4	2,1
16-11.3	-3,5	1,8
11.3-8	-3	2,3
8-5.66	-2,5	2,5
5.66-4	-2	2,7
4-2.8	-1,5	2,1
2.8-2	-1	1,2
2-1.4	-0,5	4,5
1.4-1	0	8,3
1-0.710	0,5	5,4
0.710-0.5	1	6,7
0.5-0.355	1,5	10,8
0.355-0.250	2	6,8
0.250-0.180	2,5	8,5
0.180-0.125	3	10,5
0.125-0.090	3,5	12,2
0.090-0.063	4	6,1
0.063-0.045	4,5	2,6
0.045-0.031	5	1,2
<0.031	5,5	0
		100

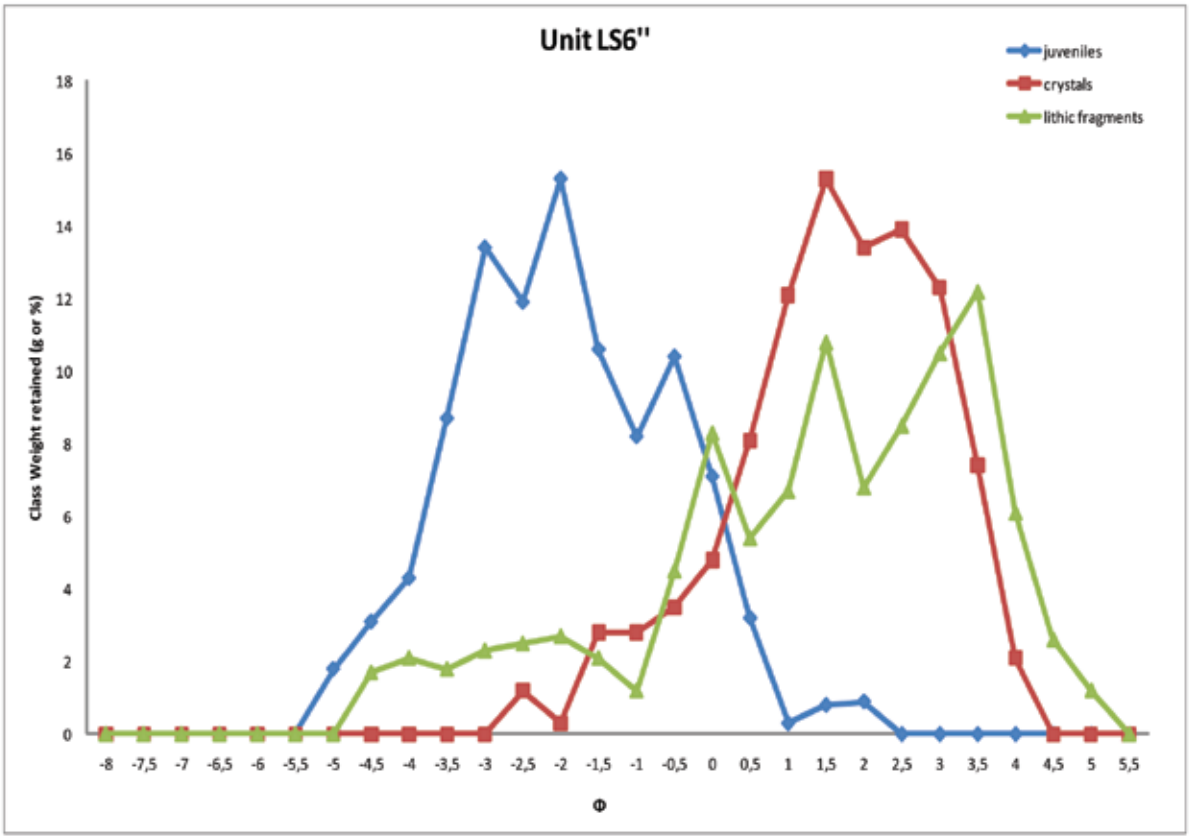

LS7”

JUVENILES		
Aperture (mm)	Φ	Class Weight retained (g or %)
> 256	-8	0
256-181	-7,5	0
181-128	-7	0
128-90.5	-6,5	0
90.5-64	-6	0
64-45.3	-5,5	0
45.3-32	-5	0
32-22.6	-4,5	2,1
22.6-16	-4	4,7
16-11.3	-3,5	8,7
11.3-8	-3	13,4
8-5.66	-2,5	15,5
5.66-4	-2	12,6
4-2.8	-1,5	10,3
2.8-2	-1	10,2
2-1.4	-0,5	10,6
1.4-1	0	8,1
1-0.710	0,5	2
0.710-0.5	1	1,1
0.5-0.355	1,5	0,5
0.355-0.250	2	0,1
0.250-0.180	2,5	0,1
0.180-0.125	3	0
0.125-0.090	3,5	0
0.090-0.063	4	0
0.063-0.045	4,5	0
0.045-0.031	5	0
<0.031	5,5	0
		100

CRYSTALS		
Aperture (mm)	Φ	Class Weight retained (g or %)
> 256	-8	0
256-181	-7,5	0
181-128	-7	0
128-90.5	-6,5	0
90.5-64	-6	0
64-45.3	-5,5	0
45.3-32	-5	0
32-22.6	-4,5	0
22.6-16	-4	0
16-11.3	-3,5	0
11.3-8	-3	0
8-5.66	-2,5	0,1
5.66-4	-2	0,1
4-2.8	-1,5	2,7
2.8-2	-1	2,1
2-1.4	-0,5	3,5
1.4-1	0	6,7
1-0.710	0,5	12,1
0.710-0.5	1	14,2
0.5-0.355	1,5	14,9
0.355-0.250	2	15,5
0.250-0.180	2,5	10,1
0.180-0.125	3	9,3
0.125-0.090	3,5	6,7
0.090-0.063	4	2
0.063-0.045	4,5	0
0.045-0.031	5	0
<0.031	5,5	0
		100

LITHIC FRAGMENTS		
Aperture (mm)	Φ	Class Weight retained (g or %)
> 256	-8	0
256-181	-7,5	0
181-128	-7	0
128-90.5	-6,5	0
90.5-64	-6	0
64-45.3	-5,5	0
45.3-32	-5	0
32-22.6	-4,5	0,7
22.6-16	-4	1,1
16-11.3	-3,5	1,8
11.3-8	-3	2,3
8-5.66	-2,5	2,5
5.66-4	-2	1,7
4-2.8	-1,5	1,1
2.8-2	-1	1,2
2-1.4	-0,5	4,5
1.4-1	0	8,3
1-0.710	0,5	7,4
0.710-0.5	1	8,5
0.5-0.355	1,5	12,6
0.355-0.250	2	10,5
0.250-0.180	2,5	11,1
0.180-0.125	3	12,2
0.125-0.090	3,5	10,4
0.090-0.063	4	2,1
0.063-0.045	4,5	0
0.045-0.031	5	0
<0.031	5,5	0
		100

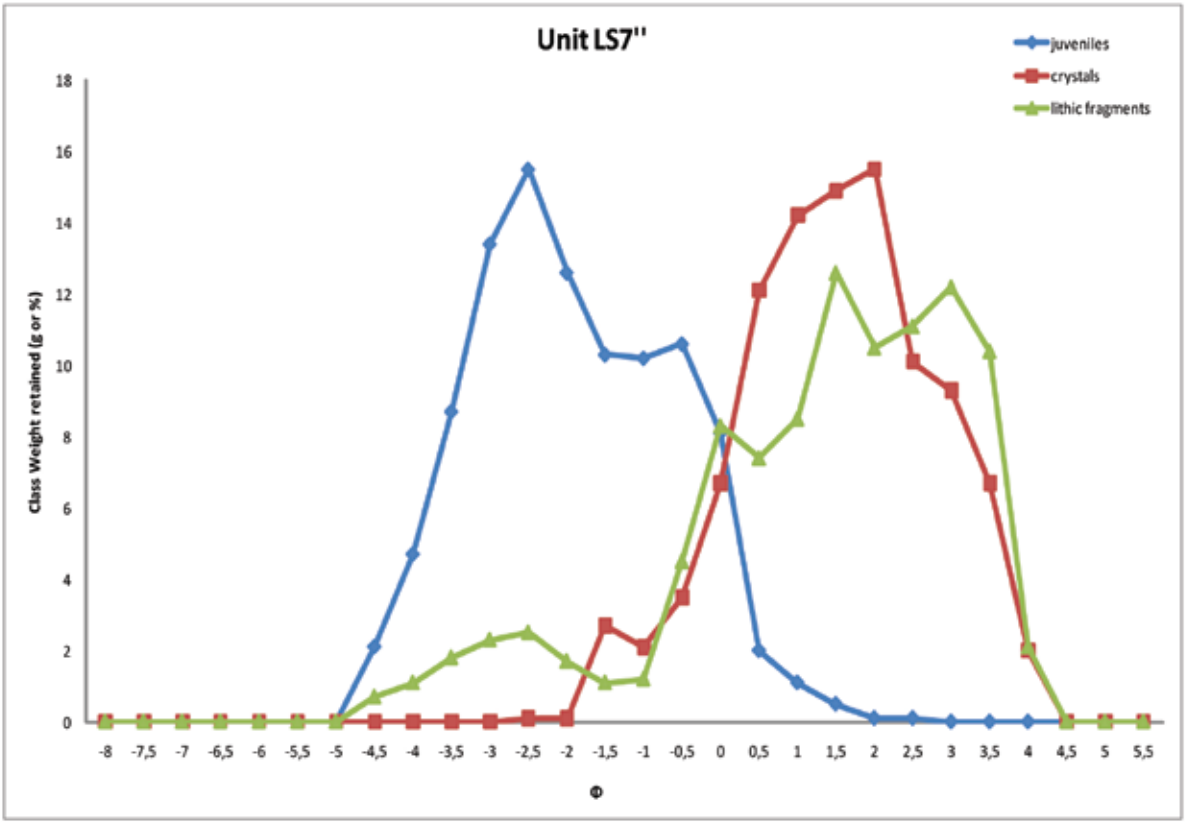

LS8”

JUVENILES		
Aperture (mm)	Φ	Class Weight retained (g or %)
> 256	-8,0	0,0
256-181	-7,5	0,0
181-128	-7,0	0,0
128-90.5	-6,5	0,0
90.5-64	-6,0	0,0
64-45.3	-5,5	0,0
45.3-32	-5,0	0,0
32-22.6	-4,5	0,3
22.6-16	-4,0	0,4
16-11.3	-3,5	1,7
11.3-8	-3,0	5,8
8-5.66	-2,5	8,3
5.66-4	-2,0	10,7
4-2.8	-1,5	10,6
2.8-2	-1,0	12,8
2-1.4	-0,5	12,3
1.4-1	0,0	10,4
1-0.710	0,5	9,5
0.710-0.5	1,0	10,1
0.5-0.355	1,5	4,1
0.355-0.250	2,0	1,4
0.250-0.180	2,5	1,1
0.180-0.125	3,0	0,5
0.125-0.090	3,5	0,0
0.090-0.063	4,0	0,0
0.063-0.045	4,5	0,0
0.045-0.031	5,0	0,0
<0.031	5,5	0,0
		100,0

CRYSTALS		
Aperture (mm)	Φ	Class Weight retained (g or %)
> 256	-8,0	0,0
256-181	-7,5	0,0
181-128	-7,0	0,0
128-90.5	-6,5	0,0
90.5-64	-6,0	0,0
64-45.3	-5,5	0,0
45.3-32	-5,0	0,0
32-22.6	-4,5	0,0
22.6-16	-4,0	0,0
16-11.3	-3,5	0,0
11.3-8	-3,0	0,1
8-5.66	-2,5	0,2
5.66-4	-2,0	0,3
4-2.8	-1,5	2,1
2.8-2	-1,0	3,0
2-1.4	-0,5	4,1
1.4-1	0,0	6,8
1-0.710	0,5	9,1
0.710-0.5	1,0	11,9
0.5-0.355	1,5	12,5
0.355-0.250	2,0	13,8
0.250-0.180	2,5	12,5
0.180-0.125	3,0	13,6
0.125-0.090	3,5	6,8
0.090-0.063	4,0	2,6
0.063-0.045	4,5	0,5
0.045-0.031	5,0	0,1
<0.031	5,5	0,0
		100,0

LITHIC FRAGMENTS		
Aperture (mm)	Φ	Class Weight retained (g or %)
> 256	-8,0	0,0
256-181	-7,5	0,0
181-128	-7,0	0,0
128-90.5	-6,5	0,0
90.5-64	-6,0	0,0
64-45.3	-5,5	0,0
45.3-32	-5,0	0,0
32-22.6	-4,5	0,7
22.6-16	-4,0	1,1
16-11.3	-3,5	1,8
11.3-8	-3,0	2,3
8-5.66	-2,5	2,5
5.66-4	-2,0	1,7
4-2.8	-1,5	1,1
2.8-2	-1,0	1,2
2-1.4	-0,5	4,5
1.4-1	0,0	8,3
1-0.710	0,5	5,4
0.710-0.5	1,0	6,7
0.5-0.355	1,5	12,6
0.355-0.250	2,0	4,2
0.250-0.180	2,5	8,2
0.180-0.125	3,0	13,3
0.125-0.090	3,5	14,5
0.090-0.063	4,0	6,1
0.063-0.045	4,5	2,6
0.045-0.031	5,0	1,2
<0.031	5,5	0,0
		100,0

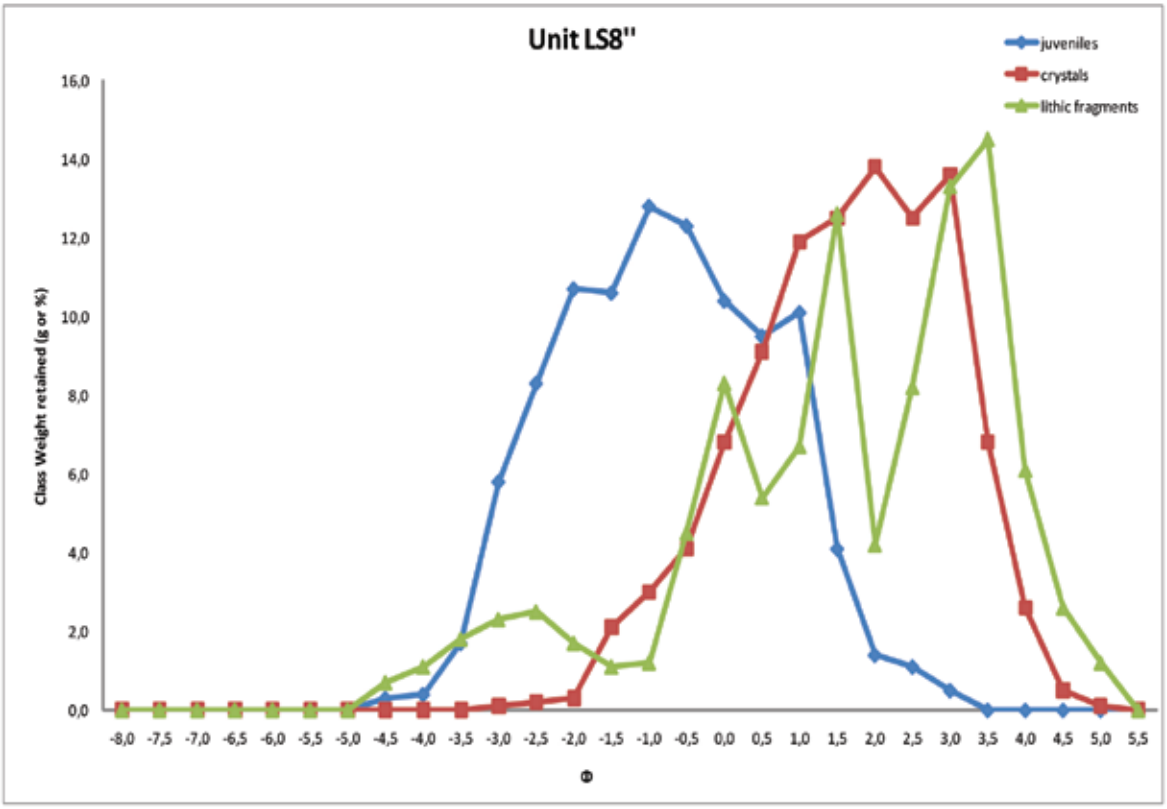

2. Cumulative percentage curves

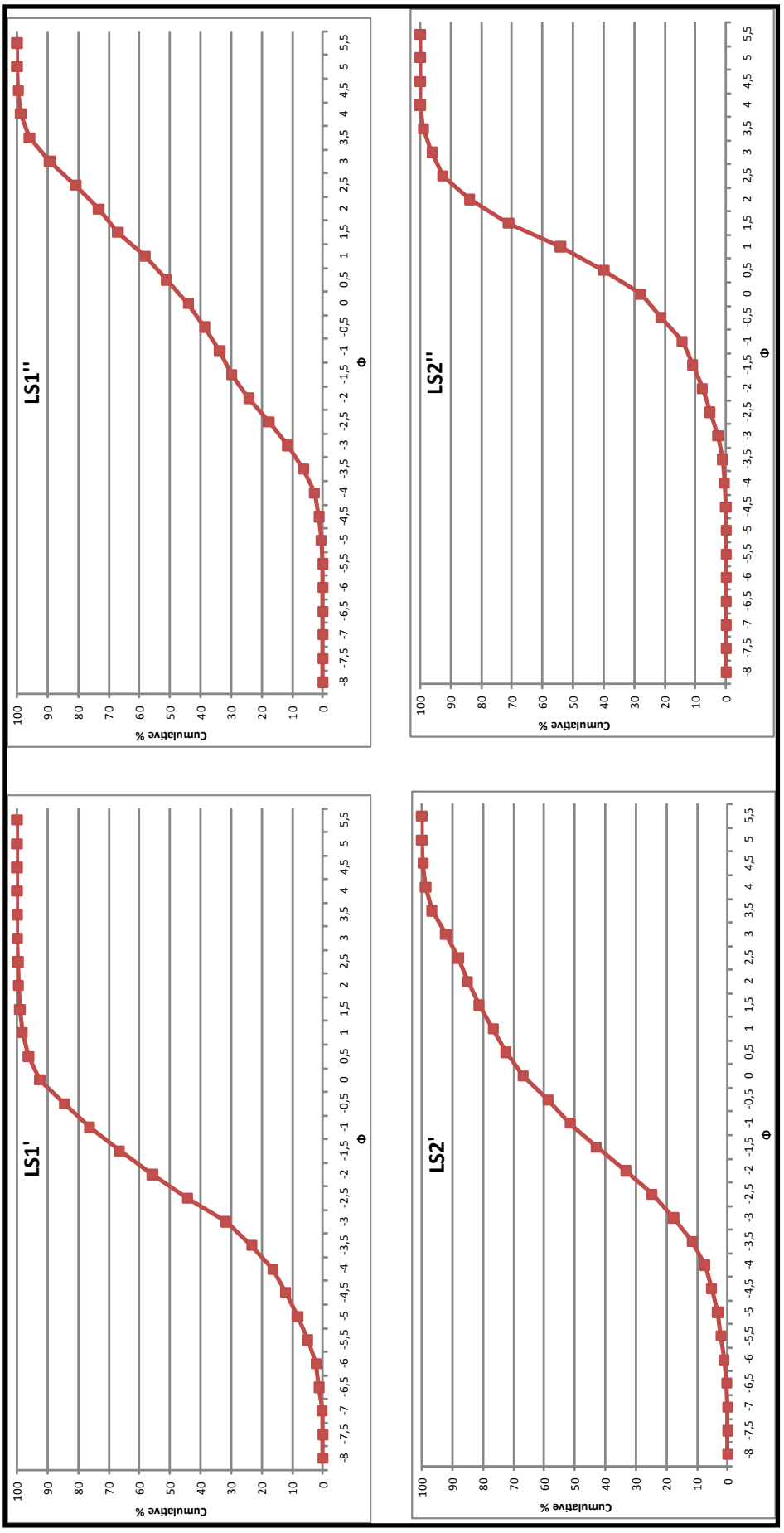

Fig A.2 - Cumulative curves for LS1 and LS2 units

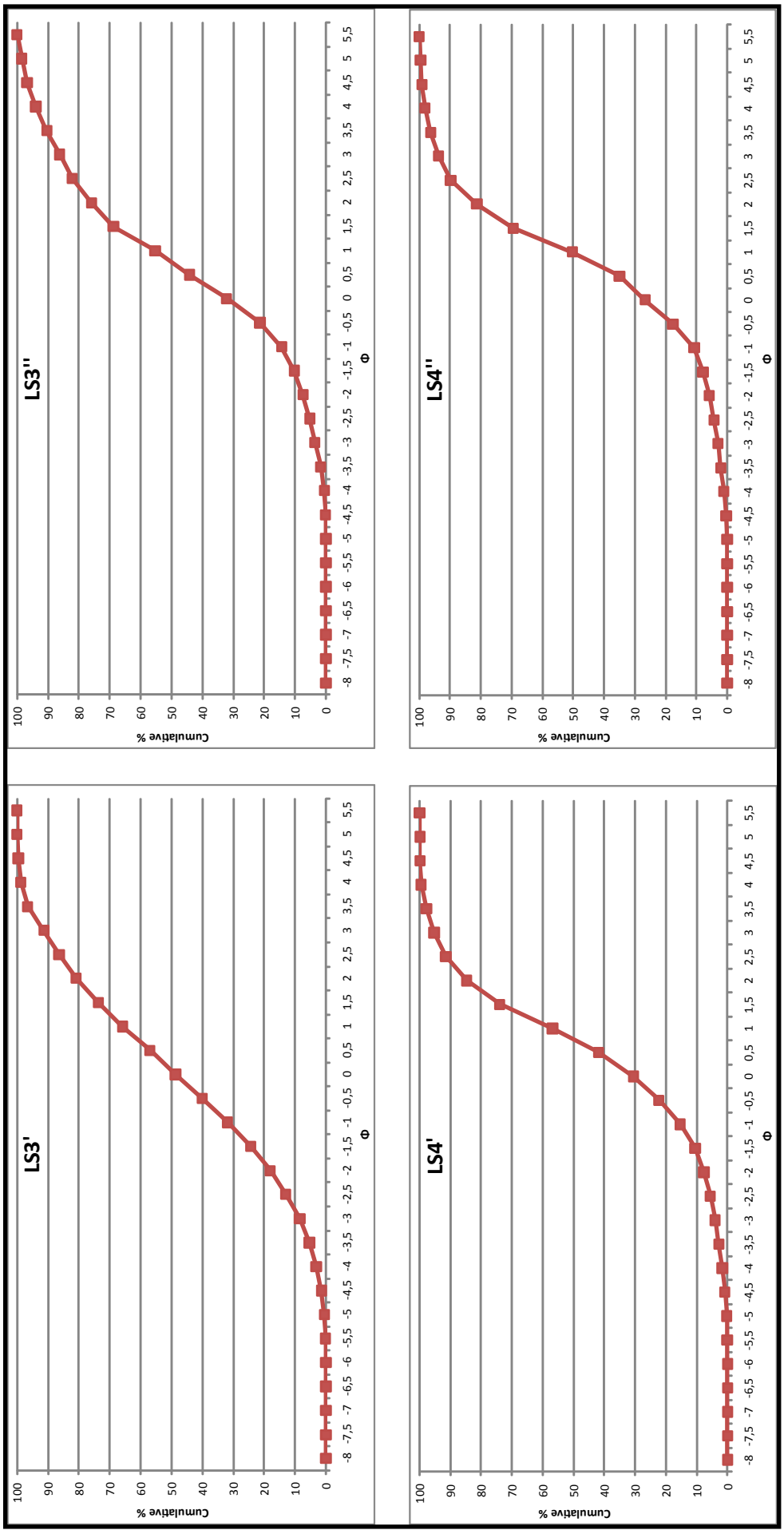

Fig A.3 - Cumulative curves for LS3 and LS4 units

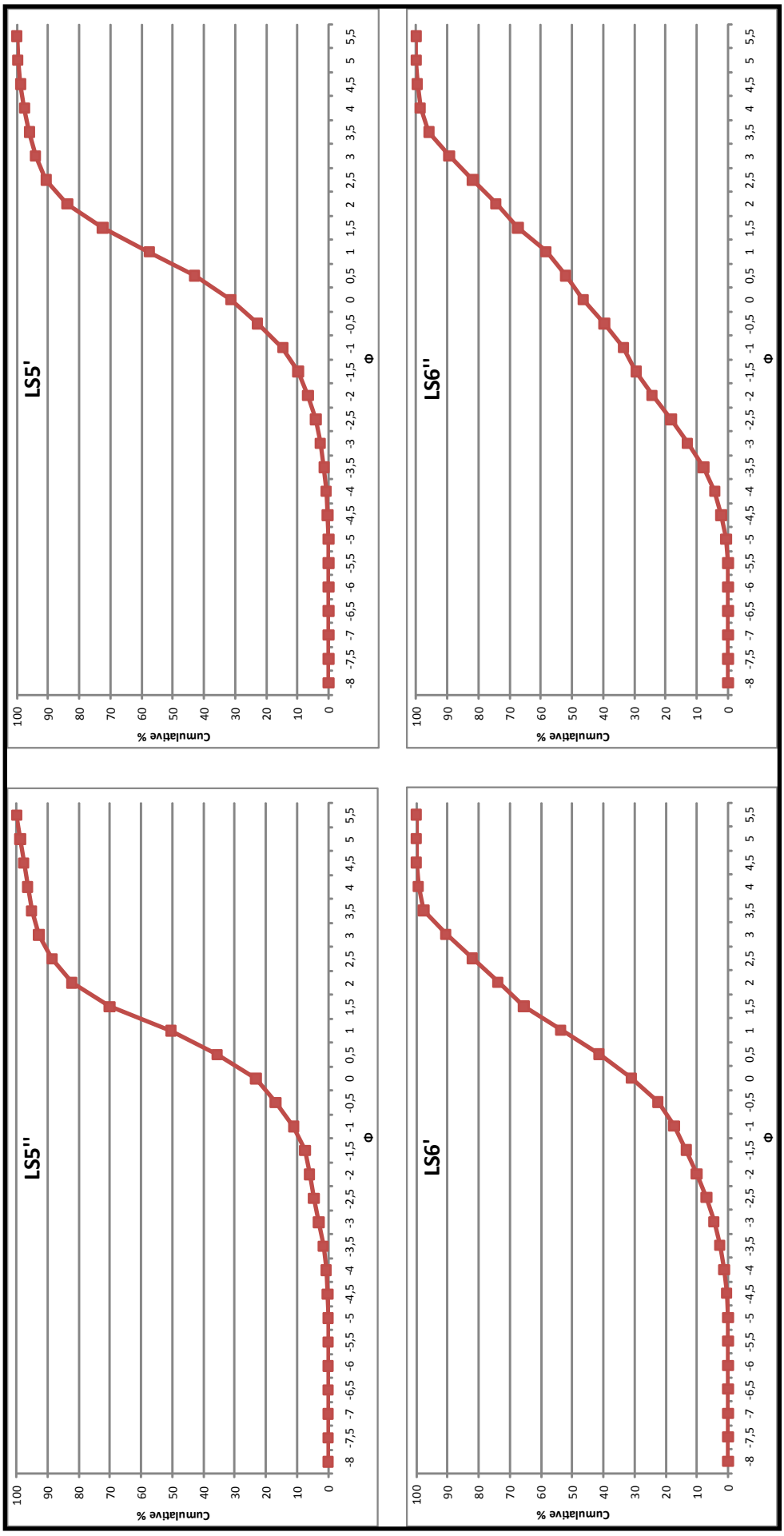

Fig A.4 - Cumulative curves for LS5 and LS6 units

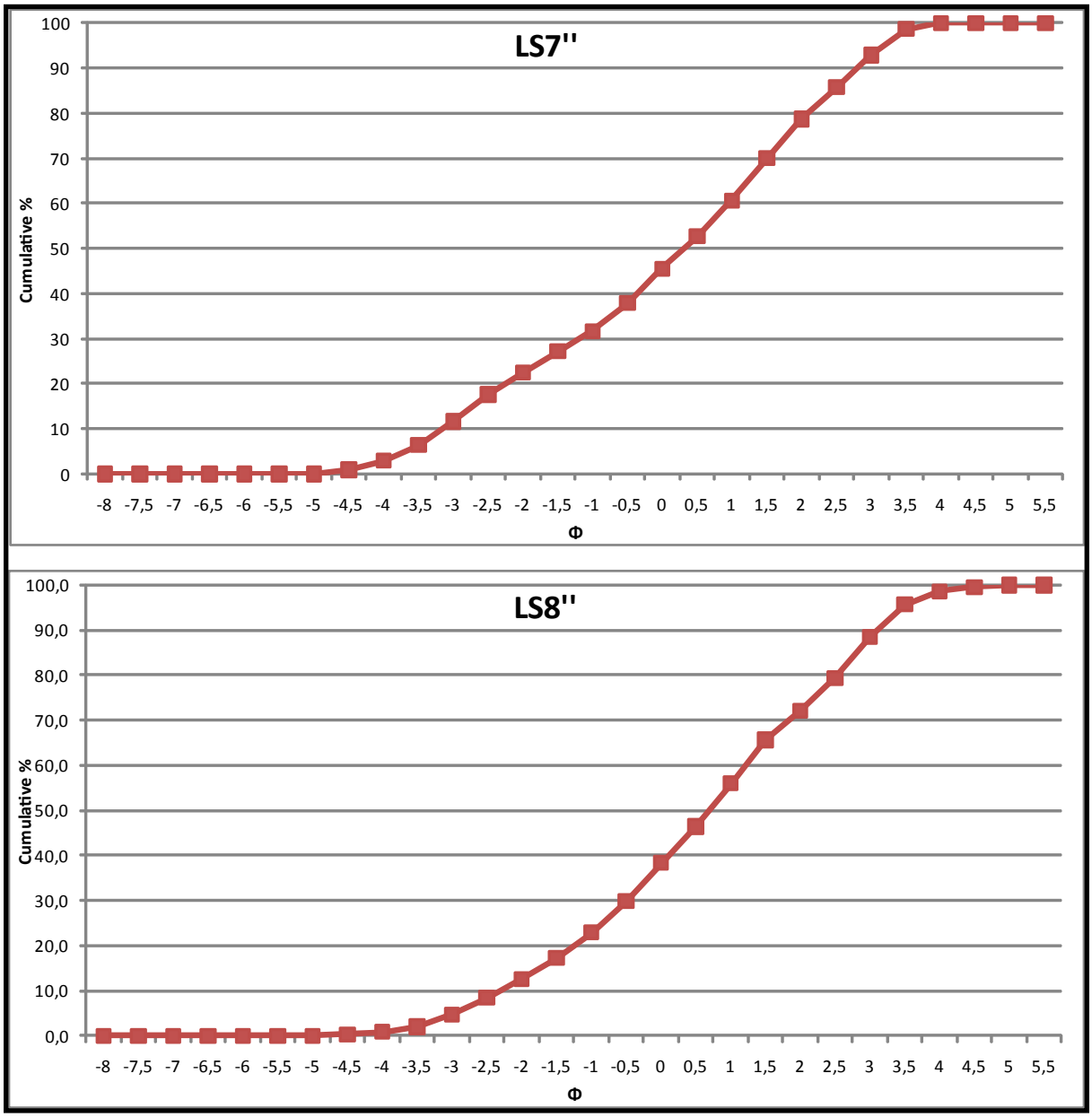

Fig A.5 - Cumulative curves for LS7'' and LS8'' sub-units

Φ	Juveniles		Crystals		Lithic fragments	
	%	cumulative %	%	cumulative %	%	cumulative %
-8	0	0	0	0	0	0
-7,5	0,2	0,2	0	0	0	0
-7	0,6	0,8	0	0	0	0
-6,5	3,1	3,9	0	0	0	0
-6	2,1	6	0	0	0,7	0,7
-5,5	5,7	11,7	0,2	0,2	2,4	3,1
-5	4,6	16,3	0,3	0,5	5,1	8,2
-4,5	3,7	20	2,1	2,6	5,9	14,1
-4	3,2	23,2	2,2	4,8	6,9	21
-3,5	8,7	31,9	3,1	7,9	9,1	30,1
-3	12,1	44	2,5	10,4	10,6	40,7
-2,5	13,3	57,3	12,7	23,1	11,5	52,2
-2	12,1	69,4	12,9	36	9,7	61,9
-1,5	10,9	80,3	14	50	7,5	69,4
-1	8,2	88,5	13,9	63,9	7,1	76,5
-0,5	3,5	92	14,2	78,1	7	83,5
0	2,6	94,6	13,2	91,3	8,1	91,6
0,5	2,6	97,2	6,7	98	2,1	93,7
1	1,7	98,9	1,9	99,9	2,2	95,9
1,5	0,8	99,7	0,1	100	1,7	97,6
2	0,1	99,8	0	100	1,2	98,8
2,5	0,1	99,9	0	100	0,5	99,3
3	0,1	100	0	100	0,5	99,8
3,5	0	100	0	100	0,1	99,9
4	0	100	0	100	0,1	100
4,5	0	100	0	100	0	100
5	0	100	0	100	0	100
5,5	0	100	0	100	0	100

	Φ5	Φ16	Φ25	Φ50	Φ75	Φ84	Φ95	Skewness	Graphic kurtosis
juveniles	-6,238	-5,033	-3,897	-2,774	-1,743	-1,274	0,077	-0,092	1,202
crystals	-3,968	-2,780	-2,426	-1,500	-0,609	-0,277	0,276	-0,087	0,957
lithic fragments	-5,314	-4,362	-3,780	-2,596	-1,106	-0,469	0,795	0,077	0,936

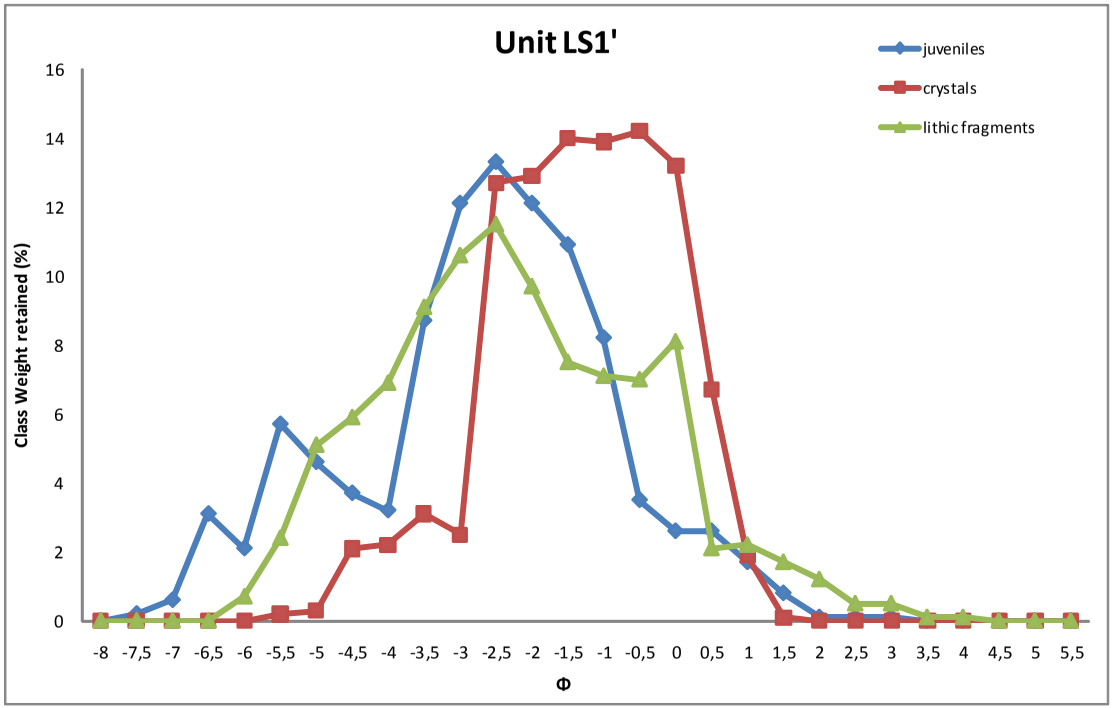

Φ	Juveniles		Crystals		Lithic fragments	
	%	cumulative %	%	cumulative %	%	cumulative %
-8	0	0	0	0	0	0
-7,5	0	0	0	0	0	0
-7	0	0	0	0	0	0
-6,5	0	0	0	0	0	0
-6	0	0	0	0	0	0
-5,5	0	0	0	0	0	0
-5	1,8	1,8	0	0	0	0
-4,5	1,5	3,3	0	0	0,7	0,7
-4	3,2	6,5	0	0	1,1	1,8
-3,5	8,7	15,2	0	0	1,8	3,6
-3	13,4	28,6	0	0	2,3	5,9
-2,5	16,1	44,7	0,2	0,2	2,5	8,4
-2	17,3	62	0,3	0,5	1,7	10,1
-1,5	13,7	75,7	2,1	2,6	1,1	11,2
-1	8,2	83,9	2,2	4,8	1,2	12,4
-0,5	7,4	91,3	3,1	7,9	4,5	16,9
0	5,2	96,5	2,5	10,4	8,3	25,2
0,5	3,2	99,7	12,7	23,1	5,4	30,6
1	0,3	100	13,9	37	6,7	37,3
1,5	0	100	14,2	51,2	12,6	49,9
2	0	100	14,8	66	4,2	54,1
2,5	0	100	14,2	80,2	8,2	62,3
3	0	100	12,3	92,5	13,3	75,6
3,5	0	100	5,4	97,9	14,5	90,1
4	0	100	2,1	100	6,1	96,2
4,5	0	100	0	100	2,6	98,8
5	0	100	0	100	1,2	100
5,5	0	100	0	100	0	100

	Φ5	Φ16	Φ25	Φ50	Φ75	Φ84	Φ95	Skewness	Graphic kurtosis
juveniles	-4,234	-3,470	-3,134	-2,347	-1,526	-0,993	-0,144	0,058	1,042
crystals	-0,968	0,220	0,568	1,458	2,317	2,654	3,231	-0,087	0,984
lithic fragments	-3,196	-0,600	-0,012	1,512	2,977	3,290	3,902	-0,201	0,973

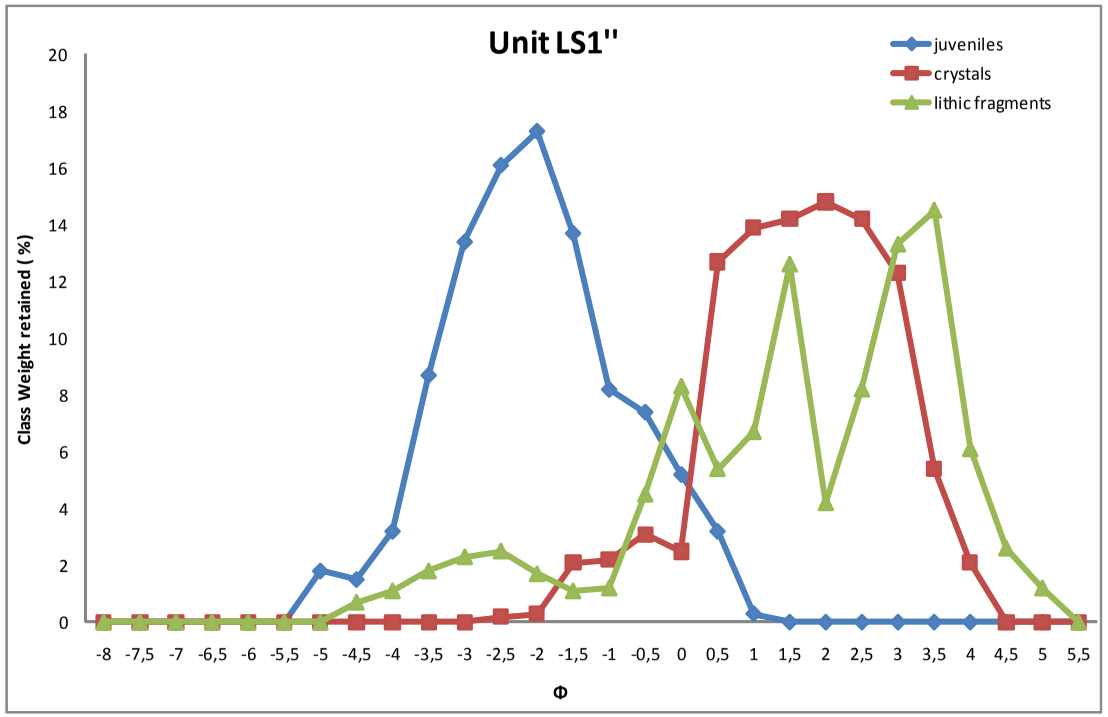

Φ	Juveniles		Crystals		Lithic fragments	
	%	cumulative %	%	cumulative %	%	cumulative %
-8	0	0	0	0	0	0
-7,5	0	0	0	0	0	0
-7	0	0	0,2	0,2	0	0
-6,5	0,6	0,6	0,3	0,5	0	0
-6	0,9	1,5	1,5	2	0	0
-5,5	1,2	2,7	1,9	3,9	0	0
-5	1,2	3,9	2	5,9	0	0
-4,5	2,3	6,2	2,9	8,8	0,7	0,7
-4	2,5	8,7	3,1	11,9	1,1	1,8
-3,5	6,5	15,2	4,1	16	1,8	3,6
-3	10,5	25,7	5,5	21,5	2,3	5,9
-2,5	11,9	37,6	6,8	28,3	2,5	8,4
-2	11,7	49,3	12,3	40,6	1,7	10,1
-1,5	12,3	61,6	15,6	56,2	1,1	11,2
-1	11,1	72,7	13,5	69,7	1,2	12,4
-0,5	8,8	81,5	9,3	79	3,5	15,9
0	8,9	90,4	8,2	87,2	7,1	23
0,5	6,4	96,8	5,1	92,3	5,4	28,4
1	2,1	98,9	3,7	96	6,7	35,1
1,5	0,6	99,5	1,7	97,7	11,6	46,7
2	0,3	99,8	1,2	98,9	9,7	56,4
2,5	0,2	100	0,7	99,6	8,2	64,6
3	0	100	0,3	99,9	12	76,6
3,5	0	100	0,1	100	13,5	90,1
4	0	100	0	100	6,1	96,2
4,5	0	100	0	100	2,6	98,8
5	0	100	0	100	1,2	100
5,5	0	100	0	100	0	100

	Φ5	Φ16	Φ25	Φ50	Φ75	Φ84	Φ95	Skewness	Graphic kurtosis
juveniles	-4,761	-3,462	-3,033	-1,972	-0,869	-0,360	0,359	-0,035	0,970
crystals	-5,225	-3,500	-2,743	-1,699	-0,715	-0,195	0,865	-0,101	1,231
lithic fragments	-3,196	-0,493	0,185	1,670	2,933	3,274	3,902	-0,251	1,058

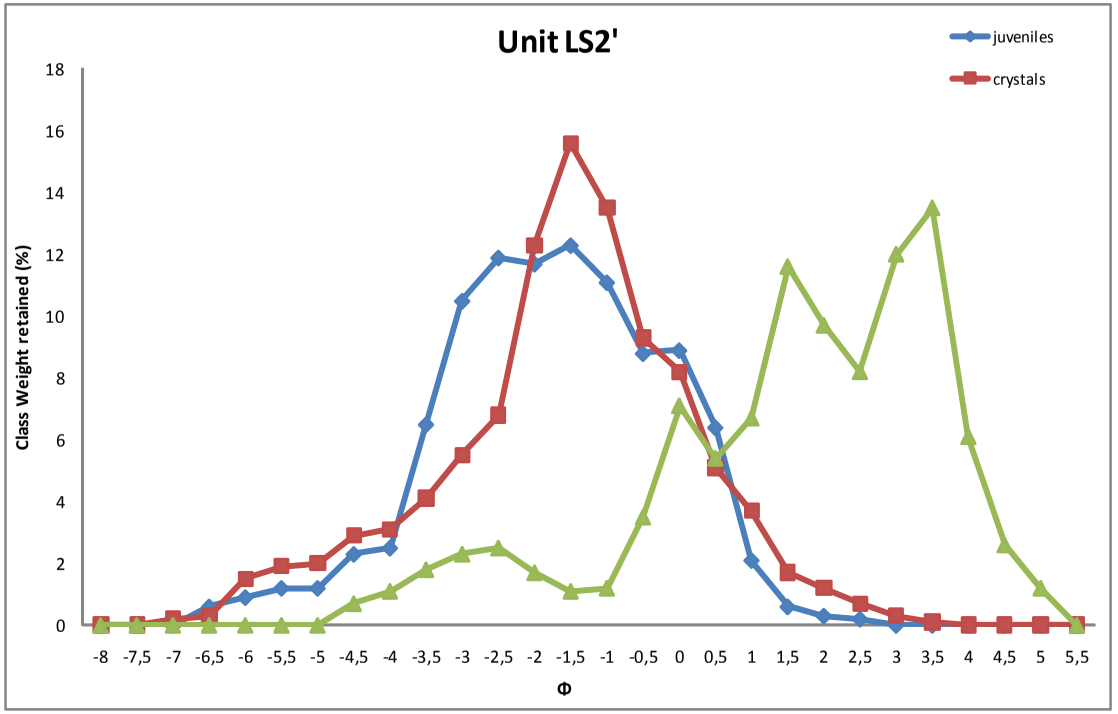

Φ	Juveniles		Crystals		Lithic fragments	
	%	cumulative %	%	cumulative %	%	cumulative %
-8	0	0	0	0	0	0
-7,5	0	0	0	0	0	0
-7	0	0	0	0	0	0
-6,5	0	0	0	0	0	0
-6	0	0	0	0	0	0
-5,5	0	0	0	0	0	0
-5	0	0	0	0	0	0
-4,5	0	0	0	0	0,3	0,3
-4	0,3	0,3	0	0	1	1,3
-3,5	0,9	1,2	0	0	0,9	2,2
-3	2,3	3,5	0	0	2,1	4,3
-2,5	4,1	7,6	0	0	3,9	8,2
-2	4,6	12,2	0	0	2,7	10,9
-1,5	3,9	16,1	1,9	1,9	3,9	14,8
-1	2,9	19	2,2	4,1	5,1	19,9
-0,5	8,1	27,1	4,2	8,3	8,4	28,3
0	9,4	36,5	3,1	11,4	7,2	35,5
0,5	12,8	49,3	5,1	16,5	18,8	54,3
1	14,6	63,9	13,4	29,9	14,2	68,5
1,5	9,9	73,8	25,4	55,3	15,7	84,2
2	13,9	87,7	16,8	72,1	7,4	91,6
2,5	8,6	96,3	12,1	84,2	5,6	97,2
3	2,8	99,1	5,8	90	2,1	99,3
3,5	0,9	100	6,7	96,7	0,7	100
4	0	100	3,3	100	0	100
4,5	0	100	0	100	0	100
5	0	100	0	100	0	100
5,5	0	100	0	100	0	100

	Φ5	Φ16	Φ25	Φ50	Φ75	Φ84	Φ95	Skewness	Graphic kurtosis
juveniles	-2,817	-1,513	-0,630	0,524	1,543	1,867	2,424	-0,208	0,989
crystals	-0,893	0,451	0,817	1,396	2,120	2,492	3,373	0,011	1,342
lithic fragments	-2,910	-1,382	-0,696	0,386	1,207	1,494	2,304	-0,210	1,123

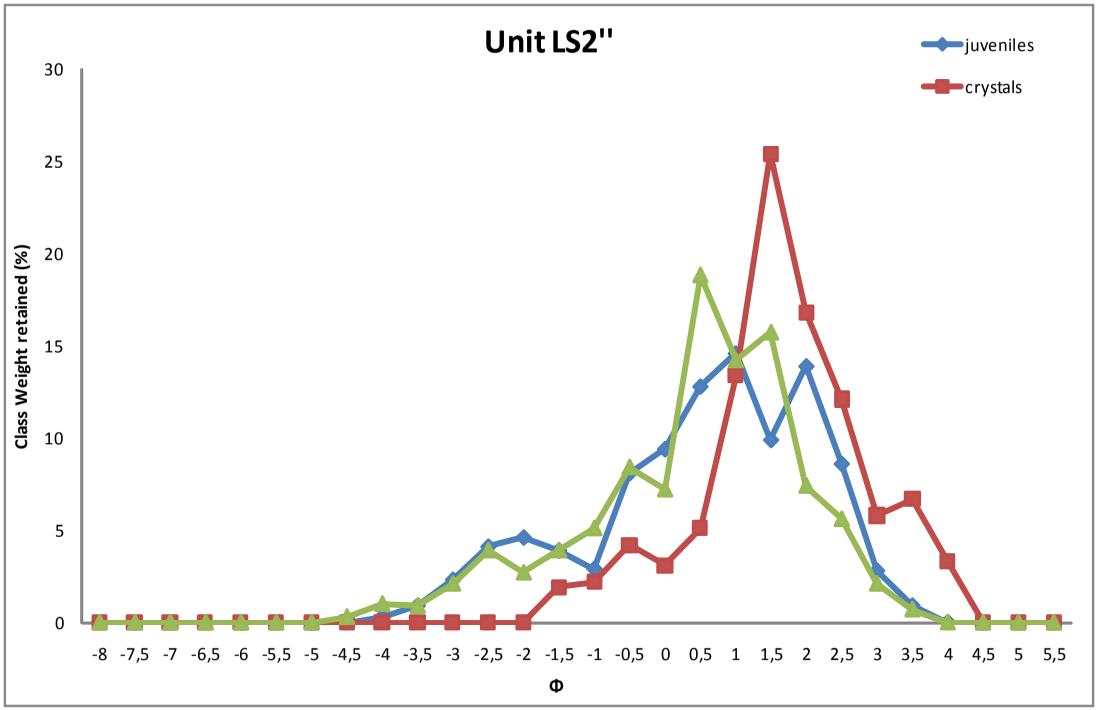

Φ	Juveniles		Crystals		Lithic fragments	
	%	cumulative %	%	cumulative %	%	cumulative %
-8	0	0	0	0	0	0
-7,5	0	0	0	0	0	0
-7	0	0	0	0	0	0
-6,5	0	0	0	0	0	0
-6	0	0	0	0	0	0
-5,5	0,2	0,2	0	0	0	0
-5	1,3	1,5	0	0	0	0
-4,5	1,5	3	0,7	0,7	0,7	0,7
-4	2,9	5,9	1,1	1,8	1,1	1,8
-3,5	2,8	8,7	1,8	3,6	1,8	3,6
-3	5,6	14,3	1,6	5,2	2,3	5,9
-2,5	7,8	22,1	3,3	8,5	2,5	8,4
-2	8,1	30,2	5,4	13,9	1,7	10,1
-1,5	10,9	41,1	6,8	20,7	1,1	11,2
-1	13,6	54,7	7,2	27,9	1,6	12,8
-0,5	11,9	66,6	8,6	36,5	4,1	16,9
0	10,5	77,1	9,2	45,7	6,3	23,2
0,5	7,7	84,8	12,4	58,1	4,8	28
1	5,9	90,7	15,2	73,3	5,7	33,7
1,5	3,6	94,3	10,2	83,5	9,8	43,5
2	2,5	96,8	8,2	91,7	10,6	54,1
2,5	1,2	98	4,2	95,9	11,1	65,2
3	1,1	99,1	2,5	98,4	11,4	76,6
3,5	0,9	100	1,1	99,5	13,5	90,1
4	0	100	0,5	100	6,1	96,2
4,5	0	100	0	100	2,6	98,8
5	0	100	0	100	1,2	100
5,5	0	100	0	100	0	100

	Φ5	Φ16	Φ25	Φ50	Φ75	Φ84	Φ95	Skewness	Graphic kurtosis
juveniles	-4,155	-2,891	-2,321	-1,173	-0,100	0,448	1,640	-0,022	1,069
crystals	-3,063	-1,846	-1,184	0,173	1,083	1,530	2,393	-0,157	0,986
lithic fragments	-3,180	-0,610	0,188	1,807	2,930	3,274	3,902	-0,310	1,058

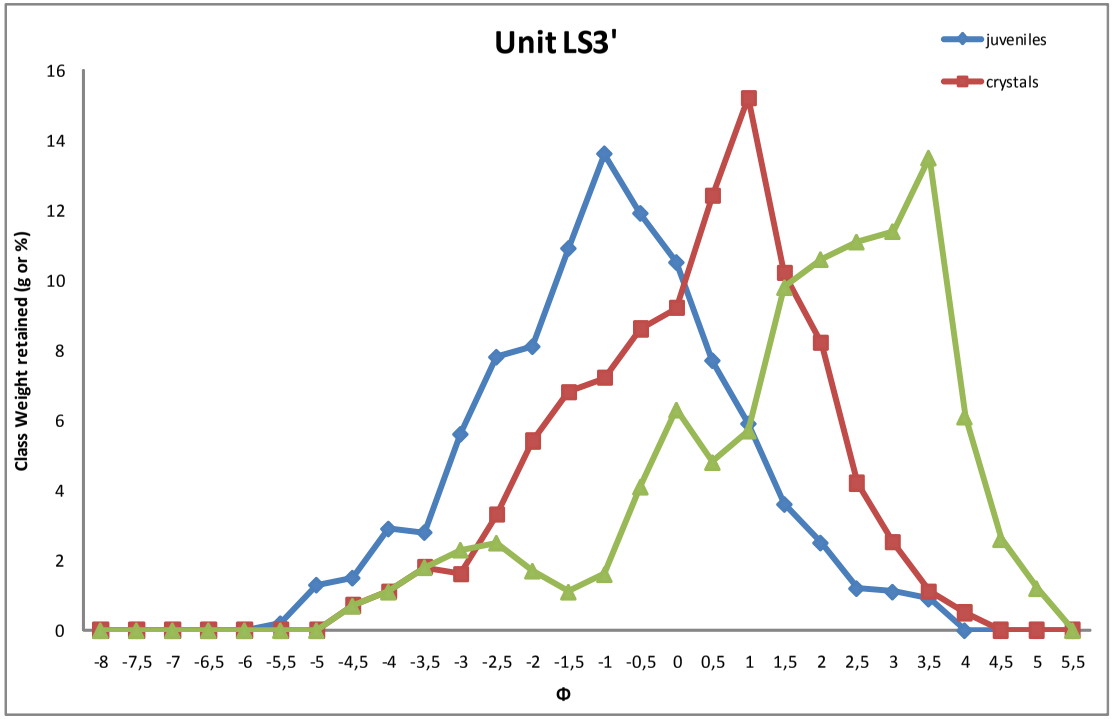

Φ	Juveniles		Crystals		Lithic fragments	
	%	cumulative %	%	cumulative %	%	cumulative %
-8	0	0	0	0	0	0
-7,5	0	0	0	0	0	0
-7	0	0	0	0	0	0
-6,5	0	0	0	0	0	0
-6	0	0	0	0	0	0
-5,5	0	0	0	0	0	0
-5	0	0	0	0	0	0
-4,5	0,3	0,3	0	0	0,2	0,2
-4	0,4	0,7	0	0	0,6	0,8
-3,5	1,1	1,8	0	0	2,4	3,2
-3	1,9	3,7	0	0	3,9	7,1
-2,5	1,5	5,2	0,1	0,1	3,3	10,4
-2	2,9	8,1	0,1	0,2	3,8	14,2
-1,5	4,8	12,9	0,3	0,5	3,1	17,3
-1	3,9	16,8	0,5	1	7,9	25,2
-0,5	6,3	23,1	0,4	1,4	14,6	39,8
0	16,1	39,2	3,1	4,5	12,9	52,7
0,5	11,3	50,5	9,8	14,3	15,2	67,9
1	10,5	61	12,5	26,8	10,4	78,3
1,5	18,8	79,8	14,6	41,4	7,1	85,4
2	7,9	87,7	6,8	48,2	6,6	92
2,5	7,4	95,1	5,7	53,9	5,3	97,3
3	1,6	96,7	8,9	62,8	1,8	99,1
3,5	2,7	99,4	9,4	72,2	0,6	99,7
4	0,6	100	9,7	81,9	0,3	100
4,5	0	100	8,6	90,5	0	100
5	0	100	4,9	95,4	0	100
5,5	0	100	4,6	100	0	100

	Φ5	Φ16	Φ25	Φ50	Φ75	Φ84	Φ95	Skewness	Graphic kurtosis
juveniles	-2,567	-1,103	-0,441	0,478	1,372	1,766	2,493	-0,139	1,144
crystals	0,026	0,568	0,928	2,158	3,644	4,122	4,959	0,130	0,744
lithic fragments	-3,269	-1,710	-1,013	-0,105	0,841	1,401	2,283	-0,080	1,227

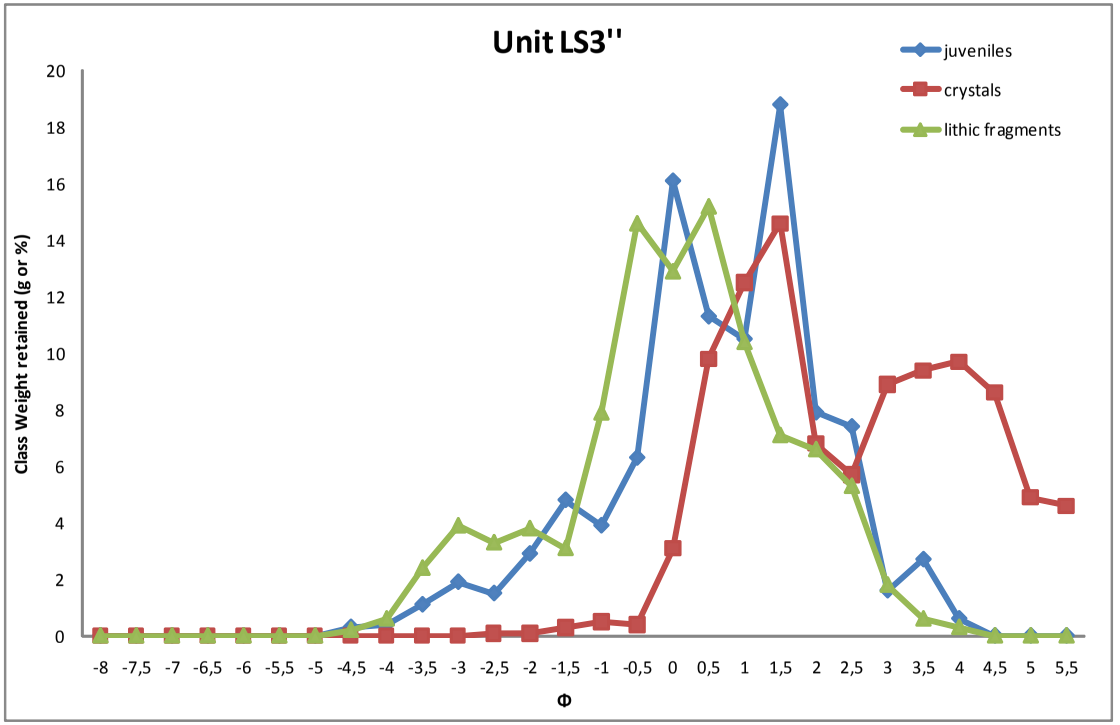

Φ	Juveniles		Crystals		Lithic fragments	
	%	cumulative %	%	cumulative %	%	cumulative %
-8	0	0	0	0	0	0
-7,5	0	0	0	0	0	0
-7	0	0	0	0	0	0
-6,5	0	0	0	0	0	0
-6	0	0	0	0	0	0
-5,5	0,3	0,3	0	0	0	0
-5	0,5	0,8	0	0	0	0
-4,5	1,2	2	0	0	0,6	0,6
-4	1,1	3,1	0,1	0,1	1,3	1,9
-3,5	1,7	4,8	0,6	0,7	1,1	3
-3	1,3	6,1	0,8	1,5	1,4	4,4
-2,5	2,2	8,3	0,8	2,3	1,9	6,3
-2	3,7	12	1,3	3,6	1,2	7,5
-1,5	4,8	16,8	1,6	5,2	2,1	9,6
-1	4,9	21,7	2	7,2	7,7	17,3
-0,5	7,3	29	2,1	9,3	11,4	28,7
0	10,9	39,9	2,1	11,4	11,9	40,6
0,5	12,5	52,4	10,3	21,7	11,1	51,7
1	13,7	66,1	18,6	40,3	12,3	64
1,5	14,4	80,5	21,5	61,8	15,5	79,5
2	8,4	88,9	15,1	76,9	8,7	88,2
2,5	5,8	94,7	9,9	86,8	4,9	93,1
3	2,7	97,4	5,7	92,5	2,7	95,8
3,5	1,7	99,1	3,9	96,4	2	97,8
4	0,6	99,7	3,3	99,7	1,3	99,1
4,5	0	99,7	0,3	100	0,9	100
5	0	99,7	0	100	0	100
5,5	0,3	100	0	100	0	100

	Φ5	Φ16	Φ25	Φ50	Φ75	Φ84	Φ95	Skewness	Graphic kurtosis
juveniles	-3,423	-1,583	-0,774	0,404	1,309	1,708	2,556	-0,210	1,176
crystals	-1,563	0,223	0,589	1,226	1,937	2,359	3,321	-0,037	1,484
lithic fragments	-2,842	-1,084	-0,662	0,423	1,355	1,759	2,852	-0,095	1,157

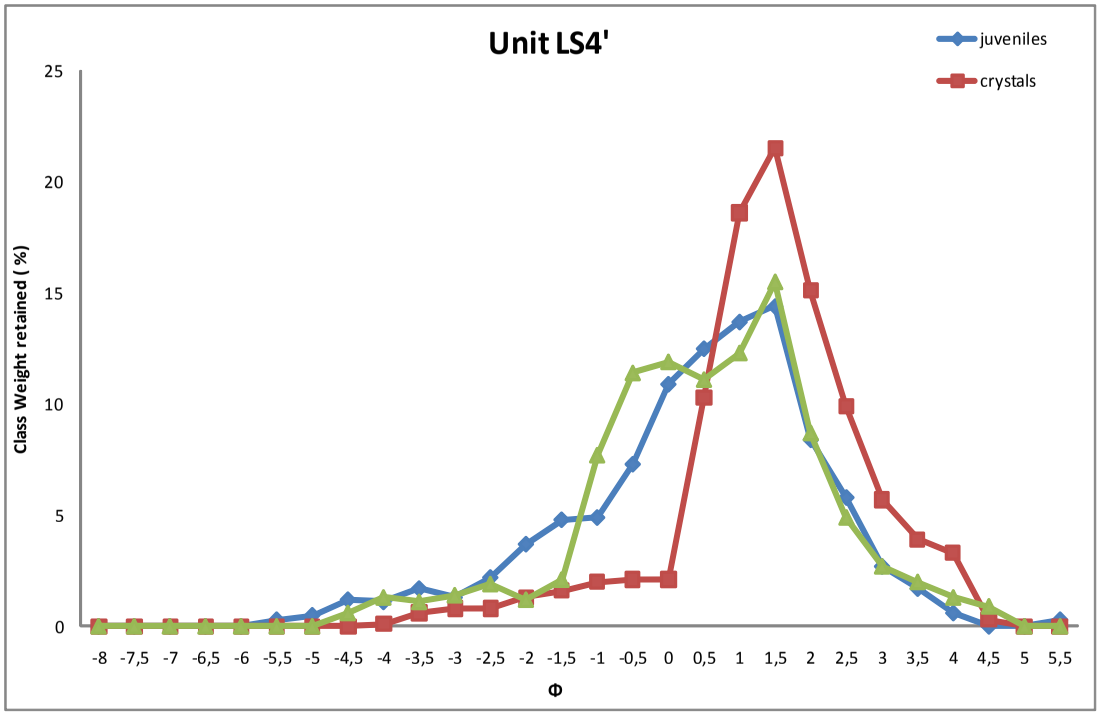

Φ	Juveniles		Crystals		Lithic fragments	
	%	cumulative %	%	cumulative %	%	cumulative %
-8	0	0	0	0	0	0
-7,5	0	0	0	0	0	0
-7	0	0	0	0	0	0
-6,5	0	0	0	0	0	0
-6	0	0	0	0	0	0
-5,5	0	0	0	0	0	0
-5	0	0	0	0	0	0
-4,5	0,5	0,5	0	0	0,6	0,6
-4	0,9	1,4	0	0	1,3	1,9
-3,5	0,9	2,3	0	0	2,1	4
-3	1,3	3,6	0	0	1,4	5,4
-2,5	2,1	5,7	0	0	1,9	7,3
-2	3,1	8,8	0,1	0,1	1,2	8,5
-1,5	2,3	11,1	0,9	1	3,1	11,6
-1	2	13,1	0,8	1,8	5,7	17,3
-0,5	8,3	21,4	1,1	2,9	11,4	28,7
0	11,8	33,2	2,1	5	13,3	42
0,5	11,2	44,4	3,8	8,8	9,6	51,6
1	17,5	61,9	12,1	20,9	16,5	68,1
1,5	20,6	82,5	26	46,9	11,2	79,3
2	7,8	90,3	22,4	69,3	4,8	84,1
2,5	5,9	96,2	13,7	83	5,9	90
3	2,3	98,5	6,7	89,7	2,9	92,9
3,5	0,7	99,2	3,9	93,6	3,2	96,1
4	0,3	99,5	3,1	96,7	1,9	98
4,5	0,1	99,6	1,8	98,5	1,2	99,2
5	0,1	99,7	0,6	99,1	0,6	99,8
5,5	0,3	100	0,9	100	0,2	100

	Φ5	Φ16	Φ25	Φ50	Φ75	Φ84	Φ95	Skewness	Graphic kurtosis
juveniles	-2,667	-0,825	-0,347	0,660	1,318	1,596	2,398	-0,241	1,246
crystals	0,000	0,798	1,079	1,569	2,208	2,575	3,726	0,198	1,352
lithic fragments	-3,143	-1,114	-0,662	0,417	1,308	1,990	3,328	-0,045	1,346

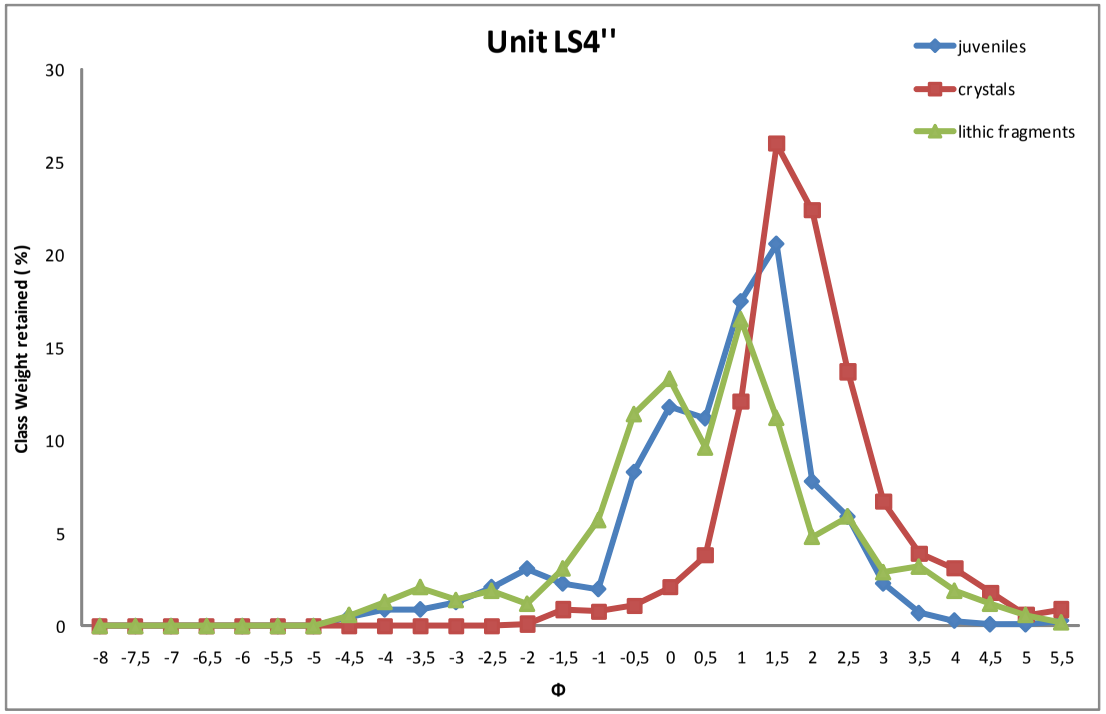

Φ	Juveniles		Crystals		Lithic fragments	
	%	cumulative %	%	cumulative %	%	cumulative %
-8	0	0	0	0	0	0
-7,5	0	0	0	0	0	0
-7	0	0	0	0	0	0
-6,5	0	0	0	0	0	0
-6	0	0	0	0	0	0
-5,5	0	0	0	0	0	0
-5	0,1	0,1	0	0	0	0
-4,5	1,1	1,2	0	0	0	0
-4	1,1	2,3	0	0	0,1	0,1
-3,5	1,3	3,6	0	0	0,9	1
-3	1,8	5,4	0	0	1,6	2,6
-2,5	2,1	7,5	0,1	0,1	2,3	4,9
-2	3,5	11	1,4	1,5	2,5	7,4
-1,5	4,3	15,3	3,2	4,7	2	9,4
-1	7,3	22,6	4,2	8,9	3,2	12,6
-0,5	13,5	36,1	6,5	15,4	4,2	16,8
0	10,8	46,9	7,7	23,1	7,1	23,9
0,5	15,3	62,2	10,5	33,6	9,3	33,2
1	12,8	75	15,6	49,2	15,4	48,6
1,5	9,9	84,9	18,4	67,6	16,3	64,9
2	8,1	93	9,6	77,2	16,2	81,1
2,5	4,2	97,2	8,9	86,1	7,5	88,6
3	1,7	98,9	4,7	90,8	3,6	92,2
3,5	0,8	99,7	2,7	93,5	2,5	94,7
4	0,3	100	1,9	95,4	2,7	97,4
4,5	0	100	2,3	97,7	1,5	98,9
5	0	100	1,4	99,1	1,1	100
5,5	0	100	0,9	100	0	100

	Φ5	Φ16	Φ25	Φ50	Φ75	Φ84	Φ95	Skewness	Graphic kurtosis
juveniles	-3,111	-1,452	-0,911	0,101	1,000	1,455	2,238	-0,123	1,147
crystals	-1,464	-0,461	0,090	1,022	1,885	2,382	3,895	0,018	1,224
lithic fragments	-2,480	-0,595	0,059	1,043	1,812	2,193	3,556	-0,156	1,411

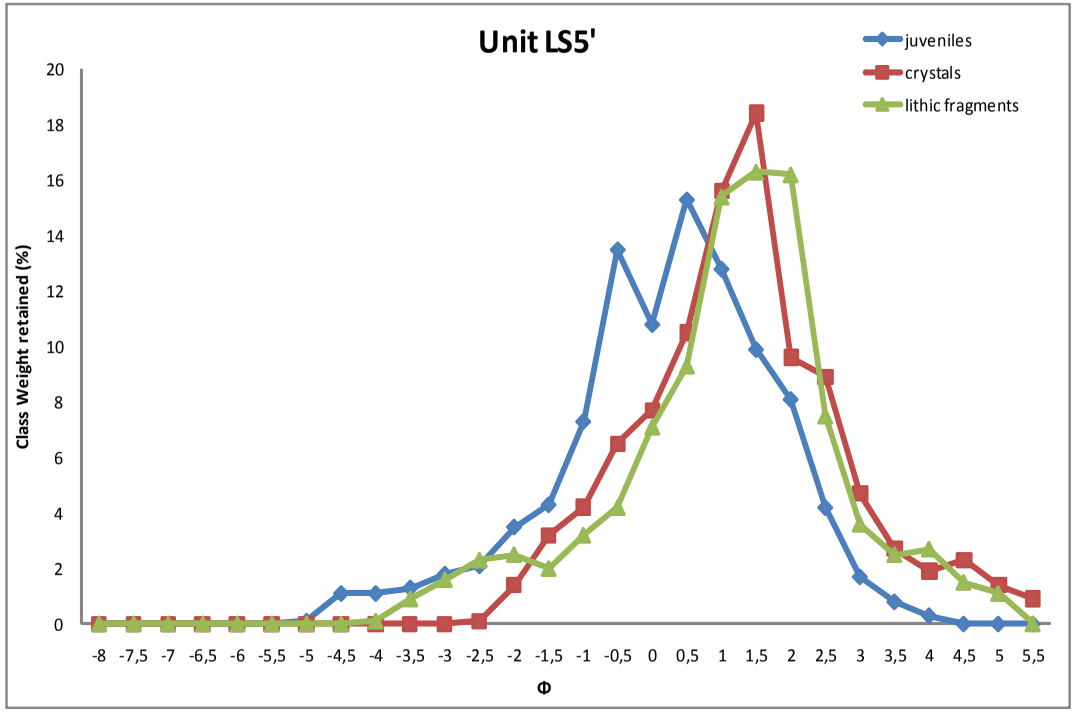

Φ	Juveniles		Crystals		Lithic fragments	
	%	cumulative %	%	cumulative %	%	cumulative %
-8	0	0	0	0	0	0
-7,5	0	0	0	0	0	0
-7	0	0	0	0	0	0
-6,5	0	0	0	0	0	0
-6	0	0	0	0	0	0
-5,5	0	0	0	0	0	0
-5	0,1	0,1	0	0	0	0
-4,5	0,4	0,5	0	0	0,1	0,1
-4	0,4	0,9	0	0	0,9	1
-3,5	1,3	2,2	0	0	1,6	2,6
-3	1,8	4	0	0	2,5	5,1
-2,5	2,1	6,1	0,1	0,1	2,5	7,6
-2	2,2	8,3	0,1	0,2	2	9,6
-1,5	2	10,3	0,3	0,5	2,1	11,7
-1	5,6	15,9	1	1,5	4,2	15,9
-0,5	9,4	25,3	2,9	4,4	5,1	21
0	5,6	30,9	4	8,4	9,3	30,3
0,5	14,8	45,7	3,8	12,2	18,8	49,1
1	11,5	57,2	15,8	28	17,3	66,4
1,5	18,6	75,8	25,1	53,1	15,2	81,6
2	11,7	87,5	18,3	71,4	6,2	87,8
2,5	5,2	92,7	10,5	81,9	3,6	91,4
3	2,9	95,6	6,9	88,8	2,5	93,9
3,5	1,8	97,4	2,7	91,5	2,7	96,6
4	0,5	97,9	1,9	93,4	1,4	98
4,5	0,5	98,4	2,1	95,5	1,1	99,1
5	0,3	98,7	2,3	97,8	0,9	100
5,5	1,3	100	2,2	100	0	100

	Φ5	Φ16	Φ25	Φ50	Φ75	Φ84	Φ95	Skewness	Graphic kurtosis
juveniles	-2,762	-0,995	-0,516	0,687	1,478	1,850	2,897	-0,177	1,163
crystals	-0,425	0,620	0,905	1,438	2,171	2,652	4,381	0,253	1,555
lithic fragments	-3,020	-0,990	-0,285	0,526	1,283	1,694	3,204	-0,117	1,627

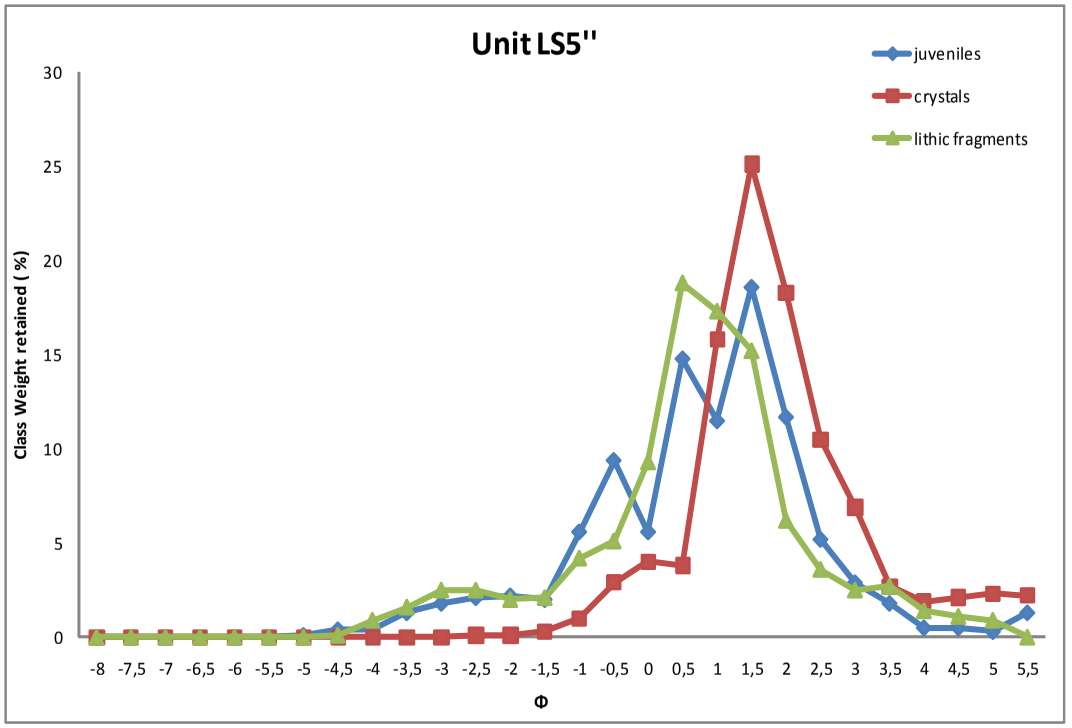

Φ	Juveniles		Crystals		Lithic fragments	
	%	cumulative %	%	cumulative %	%	cumulative %
-8	0	0	0	0	0	0
-7,5	0	0	0	0	0	0
-7	0	0	0	0	0	0
-6,5	0	0	0	0	0	0
-6	0	0	0	0	0	0
-5,5	0	0	0	0	0	0
-5	0	0	0	0	0	0
-4,5	0,7	0,7	0	0	0,7	0,7
-4	1,2	1,9	0	0	1,1	1,8
-3,5	2,2	4,1	0,2	0,2	1,8	3,6
-3	2,9	7	0,5	0,7	2,3	5,9
-2,5	4,1	11,1	0,5	1,2	2,5	8,4
-2	6,6	17,7	1,2	2,4	1,7	10,1
-1,5	7	24,7	2,1	4,5	1,1	11,2
-1	8,2	32,9	2,2	6,7	1,2	12,4
-0,5	8	40,9	3,1	9,8	4,5	16,9
0	11,3	52,2	5,7	15,5	8,8	25,7
0,5	15,1	67,3	9,3	24,8	6,4	32,1
1	16,9	84,2	12,1	36,9	7,7	39,8
1,5	10,1	94,3	12,9	49,8	12,6	52,4
2	3,1	97,4	11,4	61,2	10,5	62,9
2,5	2,1	99,5	12,2	73,4	10,2	73,1
3	0,4	99,9	12,9	86,3	12,3	85,4
3,5	0,1	100	10,3	96,6	11	96,4
4	0	100	2,5	99,1	2,5	98,9
4,5	0	100	0,9	100	1,1	100
5	0	100	0	100	0	100
5,5	0	100	0	100	0	100

	Φ5	Φ16	Φ25	Φ50	Φ75	Φ84	Φ95	Skewness	Graphic kurtosis
juveniles	-3,345	-2,129	-1,482	-0,097	0,728	0,994	1,613	-0,245	0,920
crystals	-1,386	0,027	0,508	1,509	2,562	2,911	3,422	-0,116	0,960
lithic fragments	-3,196	-0,600	-0,040	1,405	2,577	2,943	3,436	-0,250	1,039

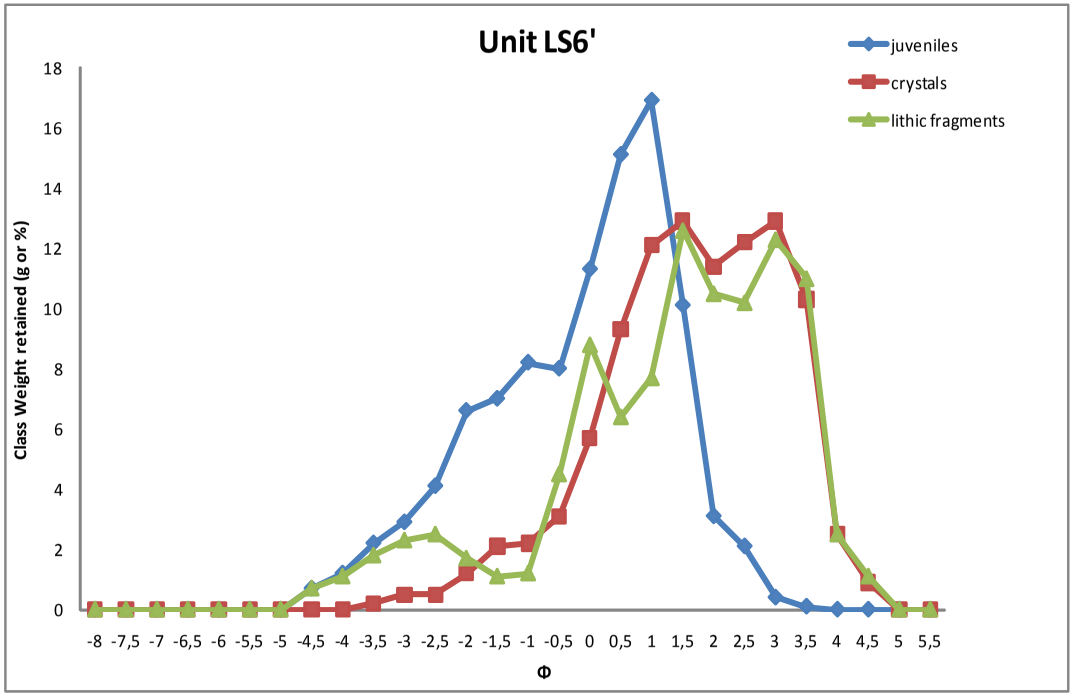

Φ	juveniles		crystals		lithic fragments	
	%	cumulative %	%	cumulative %	%	cumulative %
-8	0	0	0	0	0	0
-7,5	0	0	0	0	0	0
-7	0	0	0	0	0	0
-6,5	0	0	0	0	0	0
-6	0	0	0	0	0	0
-5,5	0	0	0	0	0	0
-5	1,8	1,8	0	0	0	0
-4,5	3,1	4,9	0	0	1,7	1,7
-4	4,3	9,2	0	0	2,1	3,8
-3,5	8,7	17,9	0	0	1,8	5,6
-3	13,4	31,3	0	0	2,3	7,9
-2,5	11,9	43,2	1,2	1,2	2,5	10,4
-2	15,3	58,5	0,3	1,5	2,7	13,1
-1,5	10,6	69,1	2,8	4,3	2,1	15,2
-1	8,2	77,3	2,8	7,1	1,2	16,4
-0,5	10,4	87,7	3,5	10,6	4,5	20,9
0	7,1	94,8	4,8	15,4	8,3	29,2
0,5	3,2	98	8,1	23,5	5,4	34,6
1	0,3	98,3	12,1	35,6	6,7	41,3
1,5	0,8	99,1	15,3	50,9	10,8	52,1
2	0,9	100	13,4	64,3	6,8	58,9
2,5	0	100	13,9	78,2	8,5	67,4
3	0	100	12,3	90,5	10,5	77,9
3,5	0	100	7,4	97,9	12,2	90,1
4	0	100	2,1	100	6,1	96,2
4,5	0	100	0	100	2,6	98,8
5	0	100	0	100	1,2	100
5,5	0	100	0	100	0	100

	Φ5	Φ16	Φ25	Φ50	Φ75	Φ84	Φ95	Skewness	Graphic kurtosis
juveniles	-4,488	-3,609	-3,235	-2,278	-1,140	-0,678	0,031	0,031	0,884
crystals	-1,375	0,037	0,562	1,471	2,385	2,736	3,304	-0,140	1,052
lithic fragments	-3,667	-1,167	-0,253	1,403	2,862	3,250	3,902	-0,235	0,996

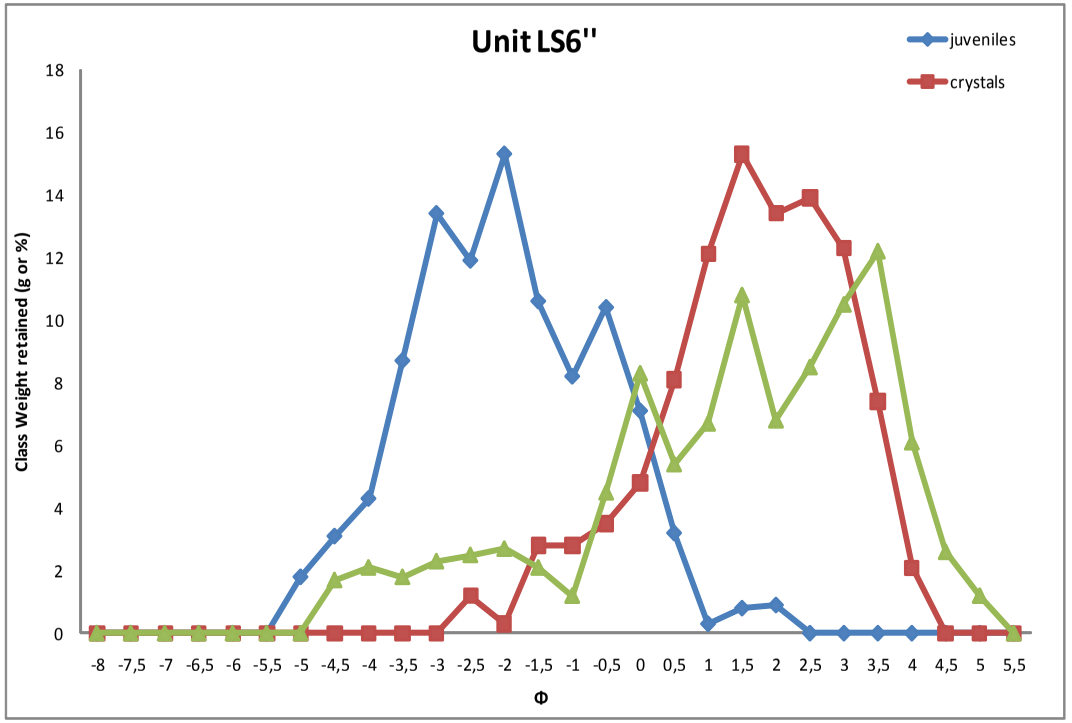

Φ	Juveniles		Crystals		Lithic fragments	
	%	cumulative %	%	cumulative %	%	cumulative %
-8	0	0	0	0	0	0
-7,5	0	0	0	0	0	0
-7	0	0	0	0	0	0
-6,5	0	0	0	0	0	0
-6	0	0	0	0	0	0
-5,5	0	0	0	0	0	0
-5	0	0	0	0	0	0
-4,5	2,1	2,1	0	0	0,7	0,7
-4	4,7	6,8	0	0	1,1	1,8
-3,5	8,7	15,5	0	0	1,8	3,6
-3	13,4	28,9	0	0	2,3	5,9
-2,5	15,5	44,4	0,1	0,1	2,5	8,4
-2	12,6	57	0,1	0,2	1,7	10,1
-1,5	10,3	67,3	2,7	2,9	1,1	11,2
-1	10,2	77,5	2,1	5	1,2	12,4
-0,5	10,6	88,1	3,5	8,5	4,5	16,9
0	8,1	96,2	6,7	15,2	8,3	25,2
0,5	2	98,2	12,1	27,3	7,4	32,6
1	1,1	99,3	14,2	41,5	8,5	41,1
1,5	0,5	99,8	14,9	56,4	12,6	53,7
2	0,1	99,9	15,5	71,9	10,5	64,2
2,5	0,1	100	10,1	82	11,1	75,3
3	0	100	9,3	91,3	12,2	87,5
3,5	0	100	6,7	98	10,4	97,9
4	0	100	2	100	2,1	100
4,5	0	100	0	100	0	100
5	0	100	0	100	0	100
5,5	0	100	0	100	0	100

	Φ5	Φ16	Φ25	Φ50	Φ75	Φ84	Φ95	Skewness	Graphic kurtosis
juveniles	-4,191	-3,481	-3,146	-2,278	-1,123	-0,693	-0,074	0,066	0,834
crystals	-1,000	0,033	0,405	1,285	2,153	2,608	3,276	-0,021	1,002
lithic fragments	-3,196	-0,600	-0,012	1,353	2,486	2,857	3,361	-0,249	1,075

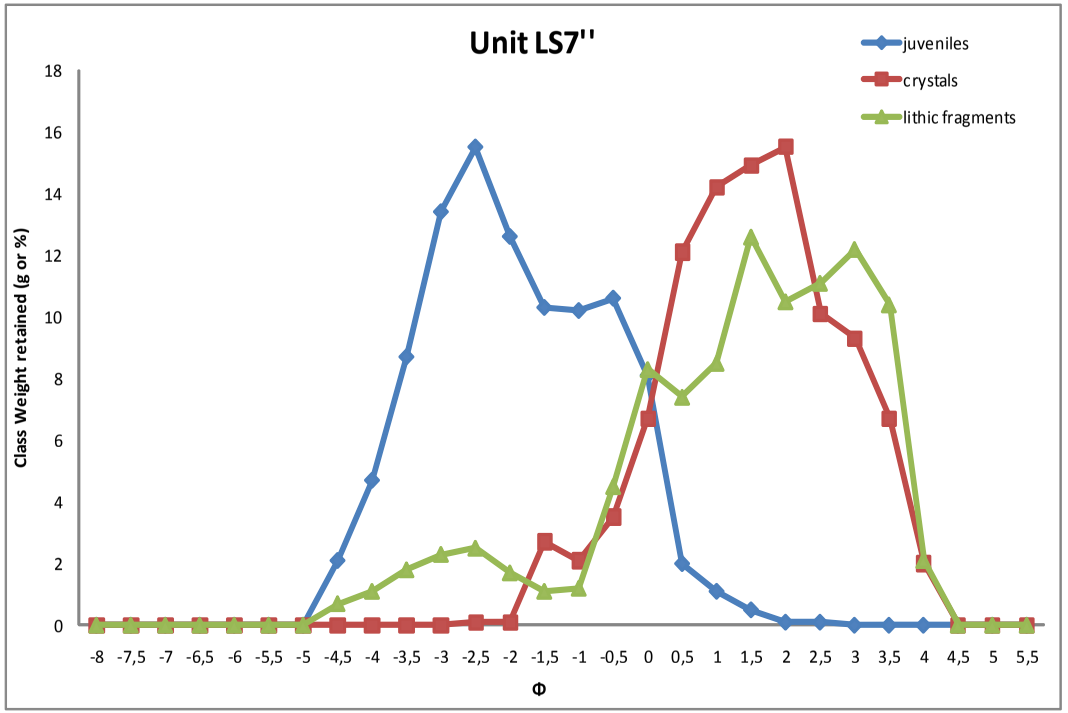

Φ	Juveniles		Crystals		Lithic fragments	
	%	cumulative %	%	cumulative %	%	cumulative %
-8	0,0	0	0,0	0	0,0	0
-7,5	0,0	0	0,0	0	0,0	0
-7	0,0	0	0,0	0	0,0	0
-6,5	0,0	0	0,0	0	0,0	0
-6	0,0	0	0,0	0	0,0	0
-5,5	0,0	0	0,0	0	0,0	0
-5	0,0	0	0,0	0	0,0	0
-4,5	0,3	0,3	0,0	0	0,7	0,7
-4	0,4	0,7	0,0	0	1,1	1,8
-3,5	1,7	2,4	0,0	0	1,8	3,6
-3	5,8	8,2	0,1	0,1	2,3	5,9
-2,5	8,3	16,5	0,2	0,3	2,5	8,4
-2	10,7	27,2	0,3	0,6	1,7	10,1
-1,5	10,6	37,8	2,1	2,7	1,1	11,2
-1	12,8	50,6	3,0	5,7	1,2	12,4
-0,5	12,3	62,9	4,1	9,8	4,5	16,9
0	10,4	73,3	6,8	16,6	8,3	25,2
0,5	9,5	82,8	9,1	25,7	5,4	30,6
1	10,1	92,9	11,9	37,6	6,7	37,3
1,5	4,1	97	12,5	50,1	12,6	49,9
2	1,4	98,4	13,8	63,9	4,2	54,1
2,5	1,1	99,5	12,5	76,4	8,2	62,3
3	0,5	100	13,6	90	13,3	75,6
3,5	0,0	100	6,8	96,8	14,5	90,1
4	0,0	100	2,6	99,4	6,1	96,2
4,5	0,0	100	0,5	99,9	2,6	98,8
5	0,0	100	0,1	100	1,2	100
5,5	0,0	100	0,0	100	0,0	100

	Φ5	Φ16	Φ25	Φ50	Φ75	Φ84	Φ95	Skewness	Graphic kurtosis
juveniles	-3,276	-2,530	-2,103	-1,023	0,089	0,559	1,256	0,010	0,847
crystals	-1,117	-0,044	0,462	1,496	2,444	2,779	3,368	-0,127	0,927
lithic fragments	-3,196	-0,600	-0,012	1,512	2,977	3,290	3,902	-0,201	0,973

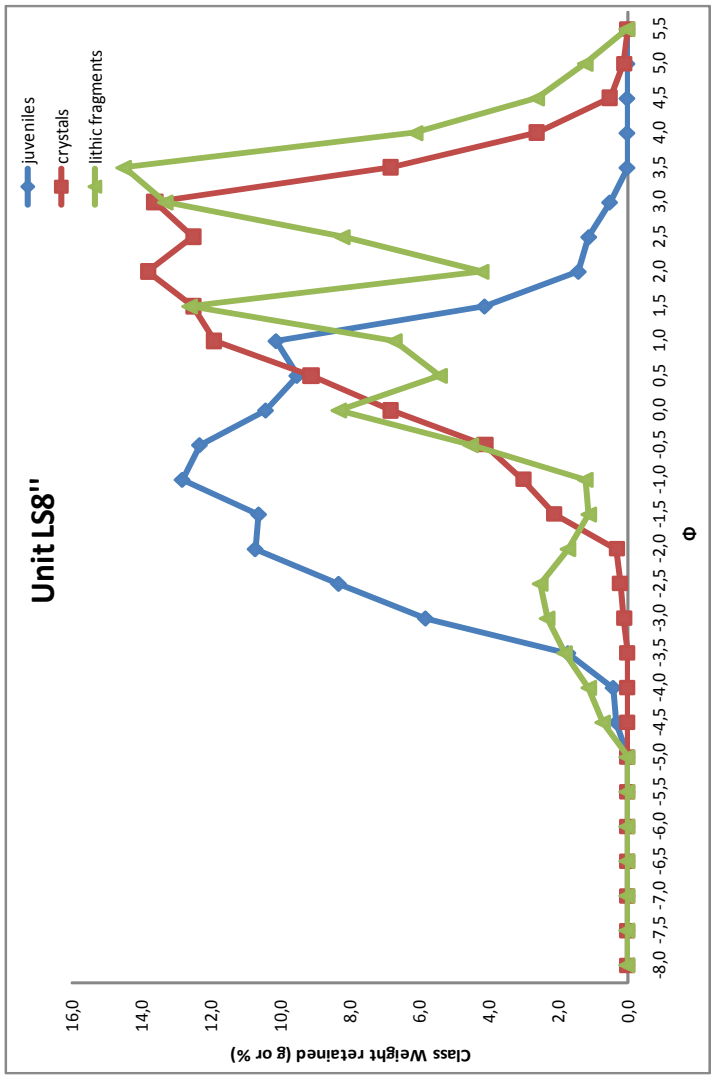

B. Geochemical data

	SiO2	Al2O3	Fe2O3	MgO	Cao	Na2O	K2O	TiO2	P2O5	MnO	Cr2O3	Ni (ppm)	Sc (ppm)	LOI (%)
LS1	49,31	17,88	5,90	2,43	7,03	2,04	3,47	0,60	0,22	0,15	0,006	<20	11,00	10,40
LS2	49,49	17,80	5,33	2,60	7,41	1,36	5,31	0,62	0,23	0,10	0,007	<20	13,00	9,30
LS3	47,91	22,04	7,78	1,87	4,31	1,20	4,51	0,67	0,21	0,12	0,016	<20	9,00	8,80
LS4	50,55	20,12	5,96	2,01	4,94	2,36	4,55	0,60	0,20	0,11	0,006	<20	9,00	8,20
LS5a	49,34	19,04	6,89	2,24	5,62	1,46	4,43	0,61	0,23	0,21	0,006	<20	10,00	9,20
LS6a	49,75	18,30	5,75	2,28	6,75	1,90	5,25	0,57	0,20	0,13	0,004	<20	10,00	8,70
LS6b	49,73	18,07	5,68	2,35	6,74	1,55	5,35	0,58	0,21	0,13	0,006	<20	10,00	9,10
LS7a	50,38	18,99	5,90	2,18	6,56	1,93	4,96	0,61	0,22	0,11	0,004	<20	9,00	7,70
LS8a	50,40	18,84	5,85	2,21	6,60	1,93	5,01	0,62	0,22	0,11	0,007	<20	10,00	7,70
LS5b	50,83	19,09	6,12	2,42	6,40	2,04	4,64	0,64	0,22	0,10	0,005	<20	11,00	6,90
LS7b	50,64	18,80	6,04	2,43	6,69	2,06	4,54	0,63	0,22	0,10	0,005	<20	11,00	7,30
LS6c	50,00	20,64	6,63	2,45	5,24	1,95	4,09	0,67	0,27	0,12	0,005	<20	12,00	7,50
LS7c	48,82	20,57	8,14	2,09	4,46	1,63	4,03	0,65	0,25	0,11	0,006	<20	11,00	8,80
LS8b	49,30	18,48	5,89	2,35	6,79	1,60	5,42	0,60	0,22	0,19	0,005	<20	10,00	8,70

Tab. B.1 - Geochemical composition of the BLT deposits. Major elements

	Ba (ppm)	Be (ppm)	Co (ppm)	Cs (ppm)	Ga (ppm)	Hf (ppm)	Nb (ppm)	Rb (ppm)	Sn (ppm)	Sr (ppm)	Ta (ppm)	Th (ppm)	U (ppm)	V (ppm)
LS1	761,00	6,00	14,20	33,90	18,10	6,10	20,70	741,40	3,00	3078,00	1,00	35,30	5,40	144,00
LS2	766,00	5,00	15,60	22,20	16,70	5,70	19,00	379,10	3,00	1618,00	1,00	32,30	9,70	162,00
LS3	1183,00	8,00	12,50	70,80	21,10	7,80	28,30	491,80	3,00	2028,00	1,50	44,70	8,00	165,00
LS4	806,00	8,00	10,80	50,00	19,70	7,10	24,40	574,20	3,00	1479,00	1,30	41,60	7,50	135,00
LS5a	1019,00	9,00	14,80	128,70	19,30	6,90	22,30	530,20	3,00	3462,00	1,20	39,50	7,80	139,00
LS6a	731,00	7,00	12,60	38,50	16,80	6,50	21,20	476,00	3,00	1661,00	1,10	37,30	8,10	144,00
LS6b	767,00	7,00	13,50	38,00	17,20	6,20	21,20	522,10	3,00	2007,00	1,10	37,40	8,40	143,00
LS7a	812,00	7,00	13,40	37,10	17,90	6,80	21,00	602,60	3,00	1956,00	1,20	39,00	7,50	134,00
LS8a	835,00	7,00	13,50	39,50	17,00	6,70	21,00	636,60	3,00	2165,00	1,10	37,50	7,50	141,00
LS5b	865,00	7,00	13,70	49,10	18,40	6,70	21,00	696,90	3,00	2466,00	1,10	36,90	7,30	147,00
LS7b	847,00	8,00	14,40	51,00	17,90	6,90	20,70	687,10	3,00	2398,00	1,10	40,00	7,60	143,00
LS6c	863,00	9,00	14,00	134,80	18,40	7,50	23,20	429,60	3,00	1429,00	1,20	46,10	11,80	156,00
LS7c	737,00	8,00	12,70	55,40	19,00	7,80	23,80	292,10	3,00	1290,00	1,20	45,20	13,10	152,00
LS8b	707,00	7,00	13,50	30,60	16,80	6,20	20,50	351,40	3,00	1487,00	1,20	35,90	7,60	208,00

Tab. B.2 - Geochemical composition of the BLT deposits. Minor elements and REE

	W (ppm)	Zr (ppm)	Y (ppm)	La (ppm)	Ce (ppm)	Pr (ppm)	Nd (ppm	Sm (ppm)	Eu (ppm)	Gd (ppm)	Tb (ppm)	Dy (ppm)	Ho (ppm)	Er (ppm)
LS1	3,00	278,00	32,60	89,70	179,20	20,22	73,00	12,18	2,41	9,02	1,21	5,70	1,01	2,92
LS2	2,20	245,10	33,60	84,10	170,50	19,83	72,90	12,41	2,50	9,33	1,25	5,94	1,02	2,86
LS3	6,80	343,70	36,20	120,40	212,20	25,76	92,50	14,46	2,76	10,49	1,39	6,82	1,16	3,12
LS4	7,00	297,20	33,50	96,30	192,10	0,88	74,30	12,61	2,48	9,08	1,24	6,02	1,04	3,01
LS5a	6,00	299,50	45,40	167,90	182,80	31,47	110,30	16,81	3,12	12,41	1,65	7,81	1,36	3,79
LS6a	3,50	284,20	32,10	91,10	173,90	20,09	72,50	11,90	2,39	8,89	1,19	5,70	0,99	2,81
LS6b	3,20	280,90	30,10	92,90	176,70	21,13	74,10	11,82	2,35	8,76	1,19	5,70	0,99	2,71
LS7a	3,80	282,50	31,90	92,80	181,40	10,12	73,20	12,07	2,45	9,03	1,20	5,94	1,04	2,93
LS8a	3,80	286,60	31,00	91,20	178,50	20,00	73,50	12,07	2,44	9,18	1,20	5,89	1,00	2,86
LS5b	4,20	297,30	32,80	99,00	180,80	20,86	76,40	12,42	2,52	9,39	1,26	5,98	1,06	2,92
LS7b	4,20	298,70	32,80	98,70	181,50	20,94	77,30	12,57	2,53	9,39	1,26	6,26	1,06	2,95
LS6c	6,90	334,60	35,50	98,70	198,20	21,27	79,60	12,97	2,63	9,97	1,29	6,42	1,11	3,29
LS7c	8,60	340,20	33,30	98,70	188,60	21,00	76,30	12,45	2,48	9,21	1,24	6,15	1,03	3,01
LS8b	4,60	297,20	28,60	87,10	167,50	18,54	69,10	11,53	2,34	8,53	1,12	5,59	0,93	2,69

Tab. B.3 - Geochemical composition of the BLT deposits. Minor elements and REE

	Tm (ppm)	Yb (ppm)	Lu (ppm)	TOT/C %	TOT/S %	Mo (ppm)	Cu (ppm)	Pb (ppm)	Zn (ppm)	Ni (ppm)
LS1	0,45	2,66	0,41	0,05	0,03	0,40	23,00	37,10	59,00	8,50
LS2	0,43	2,64	0,38	0,03	<0,02	0,30	22,90	28,20	51,00	9,30
LS3	0,51	3,06	0,45	0,12	0,04	1,00	28,50	49,40	97,00	9,90
LS4	0,45	2,74	0,41	0,08	<0,02	1,20	28,00	45,10	85,00	14,60
LS5a	0,58	3,55	0,49	0,06	0,03	0,60	21,60	35,80	63,00	22,90
LS6a	0,42	2,58	0,38	0,04	<0,02	0,30	21,90	33,70	59,00	8,10
LS6b	0,41	2,60	0,38	0,13	0,02	0,40	20,70	33,30	59,00	8,80
LS7a	0,44	2,69	0,40	0,10	<0,02	0,40	19,40	32,30	59,00	7,40
LS8a	0,44	2,65	0,39	0,10	<0,02	0,30	20,60	29,30	58,00	7,80
LS5b	0,44	2,74	0,40	0,07	<0,02	0,30	20,30	28,70	56,00	7,40
LS7b	0,43	2,69	0,39	0,15	<0,02	0,30	22,30	30,10	60,00	7,70
LS6c	0,49	3,02	0,44	0,15	0,04	0,40	18,30	34,80	59,00	10,90
LS7c	0,44	2,77	0,40	0,13	0,06	0,50	24,30	34,00	58,00	8,80
LS8b	0,38	2,44	0,36	0,12	0,05	0,50	38,50	33,00	63,00	11,90

Tab. B.4 - Geochemical composition of the BLT deposits. Minor elements and REE

	As (ppm)	Cd (ppm)	Sb (ppm)	Bi (ppm)	Ag (ppm)	Au (ppm)	Hg (ppm)	Tl (ppm)	Se (ppm)
LS1	4,30	0,20	0,20	0,60	<0,1	<0,5	0,01	2,00	<0,5
LS2	3,60	<0,1	0,10	0,50	<0,1	0,60	<0,01	1,60	<0,5
LS3	7,40	0,20	0,40	1,20	0,10	13,50	0,06	2,60	<0,5
LS4	7,60	0,20	0,20	0,60	<0,1	15,90	0,09	1,80	<0,5
LS5a	5,70	0,20	0,10	0,60	<0,1	2,60	0,01	4,60	<0,5
LS6a	5,60	<0,1	0,30	0,60	<0,1	<0,5	<0,01	1,40	<0,5
LS6b	5,50	0,10	0,30	0,60	<0,1	<0,5	<0,01	2,00	<0,5
LS7a	3,90	0,20	0,20	0,60	<0,1	<0,5	<0,01	2,20	<0,5
LS8a	4,40	<0,1	0,20	0,50	<0,1	<0,5	<0,01	2,10	<0,5
LS5b	4,30	<0,1	0,20	0,50	<0,1	<0,5	0,01	2,20	<0,5
LS7b	4,20	0,10	0,20	0,50	<0,1	<0,5	0,01	2,70	<0,5
LS6c	14,70	<0,1	0,10	0,60	<0,1	<0,5	0,03	2,00	<0,5
LS7c	19,30	<0,1	0,10	0,70	<0,1	<0,5	0,04	0,80	<0,5
LS8b	5,40	0,20	0,30	0,60	<0,1	5,70	0,02	4,80	<0,5

Tab. B.5 - Geochemical composition of the BLT deposits. Minor elements and REE

References

Aldhouse Green, S. H. R., Whittle, A. W. R., Allen, J. R. L., Casaldine, A. E., Culver, S. J., Day, M. H., Lundquist, J., & Upton, D. (1995). Prehistoric human footprints from the Severn estuary at Uskmouth and Magor Paill, Gwent Wales. *Archaeologia Cambrensis*, 141:14-55.

Aleksiev, B., Djourova, E. & Milakovska-Vergilova, Z. (1997). Geology of the Oligocene zeolitic rocks in NE Rhodopes, Bulgaria: A review and new data. In: Kirov, G., Filizova, L. & Petrov, O. (Eds.). *Natural Zeolites*, Sofia'95, 249-262.

Alexander, R.M. (1984). Stride lengths and speed for adults, children, and fossil hominids. *Am. J. Phys. Anthropol*., 63: 23-27.

Altaner, S.P. & Grim, R.E. (1990). Mineralogy, chemistry and diagenesis of tuffs in the Sucker Creek Formation (Miocene), eastern Oregon. *Clays and Clay Minerals*, 38: 561-572.

Appleton, J. D. (1972). Petrogenesis of potassium-rich lavas from the Roccamonfina volcano, Roman Region, Italy. *J. Petrol.*, 13: 425-456

Avanzini, M., De Angelis, M., Mietto, P., Panarello, A., & Rolandi, G. (2004). Pleistocene human footprints preserved on a zeolite-rich pyroclastic flow (Roccamonfina, Italy). *32nd International Geological Congress*, Florence Italy, 598.

Avanzini, M., Mietto, P., De Angelis, M., Panarello, A., & Rolandi, G. (2008). The Devil's Trails: Middle Pleistocene human footprints preserved in a volcanoclastic deposit of southern

Italy. *Ichnos*, 15(3/4):179-189.

Aveleyra Arroyo de Anda, L. (1950). Prehistoria de Mexico. Ediciones Mexicanas, *S. A. Mexico City*, Mexico, 167.

Bahn, P. G. & Vertut, J. (1988). Images of the Ice Age. *Facts on File*, New York, 240 pp.

Ballini, A., Barberi, F., Laurenzi, M. A., Mezzetti, F., Oddone, M. & Villa, I. M. (1990). Chrono-Stratigraphy of Roccamonfina volcanic complex. *Symp. Ischia (Abstract)*.

Ballini, A., Barberi, F., Laurenzi, M. A., Mezzetti, F. & Villa, I. M. (1989). Nuovi dati sulla stratigrafia del vulcano di Roccamonfina. *Boll. Gnv.,* 2: 533-556.

Banks, N. G., & Hoblitt, R. P. (1981). The 1980 eruptions of Mount St. Helens, Washington: summary of temperature studies of 1980 deposits. *U.S. Geological Survey, Professional Paper*, 1250: 295-313.

Bayon, C. & Politis, G. (1998). Las huellas del pasado. Las huellas humanas prehistóricas en la costa Pampeana. *Ciencia Hoy*, 8:48.
Retrieved from www.ciencia-hoy.retina.ar/hoy48/huella01.htm.

Bear, A. N., Giordano, G., Giampaolo, C. & Cas R. A. F. (2009). Volcanological constraints on the post-emplacement zeolitisation of ignimbrites and geoarchaeological implications for Etruscan tomb construction (6th–3rd century B.C) in the Tufo Rosso a Scorie Nere, Vico Caldera, Central Italy. *J. Volcan. Geoth. Res*., 183: 183-200.

Bergomi, C., Catenacci, C., Cestari, G., Manfredini, M. & Manganeli, V. (1969). Note illustrative alla carta geologica d'Italia alla scala 1:100.000, foglio 171: Gaeta e vulcano di Roccamonfina. *Servizio geologico d'Italia.*

Bice, D. C. (1979). Tephra correlation and the age of human footprints near Managua, Nicaragua. *Geological Society of America*, Abstracts, 11(7): 388.

Bornstein, M. N. & Bornstein, H. G. (1976). The pace of life. *Nature,* 259: 557-558.

Brauer, A., Wulf, S., Mangili, C. & Moscariello, A. (2007). Tephrochronological dating of varved interglacial lake deposits from Pianico-Sellere (Southern Alps, Italy) to around 400 ka. *Journal of Quaternary Science,* 22: 85-96.

Brinton, D. G. (1887). On an ancient human footprint from Nicaragua. *Proceedings of the*

American Philosophical Society, 437-444.

Bryan, A. L. (1973). New light on ancient Nicaraguan footprints. *Archaeology*, 26:146-147.

Capaldi, G., Civetta, L. & Gasparini, P. (1971). Fraction of the U^{238} decay series in the zeolitization of volcanic ashes. *Gechim Cosmochim Acta,* 35: 1067-1072.

Cappelletti, P., Cerri, G., Colella, A., de'Gennaro, M., Langella, A., Perrotta A. & Scarpati, C. (2003). Post-eruptive processes in the Campanian ignimbrite. *Mineral. Petrol.,*79: 79-97.

Cappelletti, P., Rolandi, G. & de'Gennaro, M. (2006). Zeolitization processes in Roccamonfina ignimbrite (Southern Italy): a help in recording fossil human tracks?. In: R.S. Bowman, R. S. & Delap S. E., Eds., *Zeolite '06, 7th International Conference on the Occurrence, Properties, and Utilization of Natural Zeolites, Socorro, New Mexico USA, 16-21 July 2006*.

Capuano, P., Continisio, R. & Gasparini, P. (1992). Structural setting of a typical alkali-potassic volcano: Roccamonfina, Southern Italy. *J. Volcanol. Geoth. Res.,* 53: 355-369.

Chamberlain, A. T., Sellars, W., Murphy, P., & Goddard, A. (1997). The archaeology of Rawthey Cave, Sedbergh, Cumbria. *Archaeology North*, 14:11-20.

Charteris, J., Wall, J. C. & Nottrodt, J. W. (1981). Functional reconstruction of gait from the Pliocene hominid footprints at Laetoli, Northern Tanzania. *Nature*, 290: 496-498.

Chiapella, V. G. (1952). Orsi e uomini preistorici nella grotta della 'Strega', (Genova). *Rivista del Comune (Genova)*, XXIX, 4: 22-29.

Chiesa, S., Cornette, Y, Gillot, P. Y. & Vezzoli, L. (1985). New interpretation of Roccamonfina volcanic history. IAVCEI 1985 Scientific Assembly, *Potassic Volcanism*, Ist. Volc. Catania Publ., Mount Etna Volcano, Giardini-Naxos (Italy).

Chiesa, S., Floris, B., Gillot, P. Y., Prosperi, L. & Vezzoli L. (1995). Il Vulcano di Roccamonfina. In: ENEA Editor, *Lazio Meridionale*, 128-150.

Chipera, S. J. & Apps, J. A. (2001). Geochemical stability of natural zeolites. In: Bish, D., Ming, D. (Eds.), *Natural Zeolites: Occurrence, Properties, Applications*. Mineral. Soc. Amer., Reviews in Mineralogy, 45: 117-161.

Cole, P. D., Guest, J. E. & Duncan, A. M. (1993). The emplacement of intermediate volume ignimbrite: a case study from Roccamonfina volcano, Southern Italy. *Bull. Volcanol*., 55: 467-480

Cole, P. D., Guest, J. E., Duncan, A. M., Chester, D. K. & Bianchi, R. (1992). Post-collapse volcanic history of calderas on a composite volcano: an example from Roccamonfina, Southern Italy. *Bull. Volcanol., 54: 253-266.*

Conticelli, S., Marchionni, S., Rosa, D., Giordano, G., Boari, E. & Avanzinelli, R. (2009). Shoshonite and sub-alkaline magmas from an Ultrapotassic Volcano: Sr-Nd-Pb isotope data on the Roccamonfina volcanic rocks, Roman Magmatic Province, Southern Italy. *Contrib. Mineral. Petrol.,* 157: 41-63.

Cowell, R. W., Milles, A. & Roberts, G. (1993). Prehistoric footprints on Formby Point Beach, Merseyside. In Middleton, R. (compiler), *NorthWestWetlands Survey Report*, 43-48.

Cox, K. G., Hawkesworth, C. J., O'Nions, R. K. & Appleton J. D. (1976). Isotopic evidence for the derivation of some Roman Region volcanics from anomalously enriched mantle. *Contrib Mineral Petrol*, 56:173-180.

de' Gennaro, M., Adabbo, M. & Langella, A. (1995). Hypothesis on the genesis of zeolites in some european volcaniclastic deposits. In *Natural Zeolites '93,* D.W. Ming and EA. Mumpton, Eds., Brockport, New York, 51-67.

de' Gennaro, M., Cappelletti, P., Langella, A., Perrotta, A. & Scarpati, C. (2000). Genesis of zeolites in the Neapolitan Yellow Tuff: geological, volcanological and mineralogical evidence. *Contrib. Mineral. Petrol.,* 139: 17-35.

de' Gennaro, M. & Colella, C. (1991). The critical role of temperature in the natural zeolitization of volcanic glass. *Neues Jahrbuch Fiir Mineralogie-Monatshefte,* 8: 355-362.

De' Gennaro, M. & Franco, E. (1976). La K-Cabasite di alcuni tufi del Vesuvio. *Rend. Acc. Naz. Lincei*, 60: 490-497.

de' Gennaro, M. & Langella, A. (1996). Italian zeolitized rocks of technological interest. *Mineralium Deposita,* 31: 452-472.

de' Gennaro, M., Langella, A., Cappelletti, P. & Colella, C. (1999). Hydrothermal conversion of trachytic glass to zeolite. *Clays and clays minerals*, 3: 348-357.

De Lumley, H. (1966). Les fouilles de Terra Amata a Nice. Premiers resultats. *Bulletin of the Museum of Anthropology and Prehistory of Monaco*, 13: 29-51.

De Rita, D. & Giordano, G. (1996). Volcanological and structural evolution of Roccamonfina volcano southern Italy and structural origin. *Volcano Instability on the Earth and other planets. Geol. Soc. Spec. Publ.,* 100: 209-224.

De Rita, D., Giordano, G. & Milli, S. (1997). Forestepping-backstepping pattern of volcaniclastic successions: Roccamonfina volcano, Italy. *J. Volcan. Geoth. Res*., 78: 267-288.

Di Girolamo, P. (1968). Rilevamento petrografico nel settore SW (Sessa Aurunca) del volcano di Roccamonfina. *Rend. Acc. Sci. Fis. Mat. Napoli*; 4, 35: 675-722.

Dillehay, T. (1999). Monte Verde under fire. Archeology
(online features: http://archaeology.org/online/features/clovis.html).

Di Vito, M. A., Zanella, E., Gurioli, L., Lanza, R., Sulpizio, R., Bishop, J., Tema, E., Boenzi, G. & Laforgia, E. (2009). The Afragola settlement near Vesuvius, Italy: The destruction and abandonment of a Bronze Age village revealed by archaeology, volcanology and rock-magnetism. *EPSL*, 277: 408-421

Flint, E. (1883). Report of the Peabody Museum (not seen: cited in Lockley et al., 2008).

Folk, R. L. (1966). A review of grain-size parameters. *Sedimentology,* 6: 73-93.

Fornaseri, M. & Penta, A. (1960). Elementi alcalini minori negli analcimi e loro compartamento nel processo di analcimizzazione della leucite. *Periodico Mineralogia*, 29: 85-101.

Garcia, M. A. (1999). La piste de pas humains de la grotte Chauvet `a Vallon-Pont d'Arc. *International Newsletter on Rock Art*, 24:1-4.

Garcia, M. A. (2001). Les empreintes et les traces humaines et animals. In Clottes, J. (ed.), *La grotte chauvet: l'art des origines*. Threshold, Sevil, Paris, 34-43.

Garcia Hernandez, J. E., Notario del Pino, J. S., Gonzalez Martin, M. M., Hernan Reguera, F., & Rodriguez Losada, J. A. (1993). Zeolites in pyroclastic deposits in southeastern Tenerife (Canary Islands). *Clays and Clay Minerals*, 41: 521-526.

Ghiara, M. R., Biasco, A., Franco, E., Petti, C., & Stanzione, D. (1991). A geochemical and

mineralogical study on the reaction of natural phonolitic–tephritic glass with deionized water in a closed system. in Colella, C., eds., *Atti 1o Convegno Nazionale di Scienza e Tecnologia delle Zeoliti*. L'Aquila, 26-27 September 1991, 83-90.

Ghiara, M. R. & Lirer L. (1977). Mineralogy and geochemistry of the "low potassium" series of the Roccamonfina volcanic suite (Campania, South Italy). *Bull Volcanol,* 41: 39-56.

Giampaolo, C., Lo Mastro, S., De Rita, D. & Giordano, G. (2006). Lateral and vertical zeolite grade variations in the Tufo Lionato ignimbrite unit (Colli Albani, Roma, central Italy). In: Bowman, R.S., Delop, S.E. (Eds.), *Zeolite '06'-7th International Conference on the Occurrence, Properties and Utilisation of Natural Zeolites*, Socorro, New Mexico, USA.

Giannetti, B. (1964). Contributo alla conoscenza de1 vulcano di Roccamonfina. Nota I: Le ultime manifestazioni eruttive della caldera. *Boll. Soc. Geol. Ital*., 83 (3): 87-133.

Giannetti, B. (1970). Contributo alla conoscenza delle lave leucitiche e delle piroclastiti della cinta calderica di Roccamonfina e petrochimica del complesso vulcanico. *Mem. Soc. Geol. Ital*., 9: 497-556.

Giannetti, B. (1974). Nuove ricerche petrografiche e petrogenetiche sulle lave fonolitiche della caldera vulcanica di Roccamonfina. *Atti Soc. Toscana Sci. Nat. Pisa, Mem*., 81: 253-306.

Giannetti, B. (1979). The geology of Roccamonfina caldera (Campanian Province, Italy). *Giornale Geologia ser 2*, 43: 187-206.

Giannetti, B. (1982). Cumulate inclusions from K-rich magmas, Roccamonfina volcano, Italy. *EPSL*, 57: 313-335

Giannetti, B. (1996). The geology of the Yellow Trachytic Tuff, Roccamonfina volcano, Italy. *J. Volcan. Geoth. Res*., 71: 53-72.

Giannetti, B. (1998). Geology of proximal, small volume tachyte–trachyandesite pyroclastic flows and associated surge deposits, Roccamonfina volcano, Italy. *J. Volcan. Geoth. Res*., 80: 113-136.

Giannetti, B. (2001). Origin of the calderas and evolution of Roccamonfina volcano (Roman region, Italy). *J. Volcan. Geoth. Res*., 106: 301-319.

Giannetti, B. & De Casa, G. (2000). Stratigraphy, chronology, and sedimentology of ignimbrites from the white trachytic tuff, Roccamonfina Volcano, Italy. *J. Volcan. Geoth. Res*.,

96: 243-295.

Giannetti, B. & Francaviglia, V. (1994). New geological, structural and petrological evidence concerning the White Trachytic Tuff, Roccamonfina volcano Italy. *Preliminary note. Boll. Serv. Geol. Ital*., 111: 179-198.

Giannetti, B. & Luhr J. F. (1983). The White Trachytic tuff of Roccamonfina Volcano (Roman Region, Italy). *Contrib. Mineral. Petrol*, 84: 235-252.

Giordano, G., De Benedetti, A., Diana, A., Diano, G., Gaudioso, F., Marasco, F., Miceli, M., Mollo, S., Cas, R. A. F. & Funiciello, R. (1996). The Colli Albani mafic caldera (Roma, Italy): Stratigraphy, structure and petrology. *J. Volcan. Geoth. Res*., 155: 49-80.

Gonzalez, S., Huddart, D., Bennett, M. R., & Gonzalez-Huesca, A. (2006). Human footprints in Central Mexico older than 40,000 years. *Quaternary Science Reviews*, 25: 201-222.

Gore, R. (1997). The dawn of humans. Tracking the first of our kind. *National Geographic Magazine*, 192: 92-99.

Gottardi, G. (1989). The genesis of zeolites. *Eur J Mineral,* 1: 479-487.

Grieve, D. W. & Gear, R. J. (1966). The relationship between length of stride, step, frequency, time of swing and speed of walking for children and adults. *Ergonomics*, 5: 379-399.

Hall, A. (1998) Zeolitization of volcaniclastic sediments: the role of temperature and pH. J. *Sedim. Res.*, 68(5): 739-745.

Harada, T. & Noto, T. (1984). Volcanic calamity season. *Bulletin of the Gunma Prefectural Museum of History*, 5:1-21.

Harrington, S. P. M. (1999). Human footprints at Chauvet Cave. *Archaeology*, 52(5). Retrieved from www.archaeology.org/9909/newsbriefs/chauvet.html.

Hawkesworth, C. J. & Vollmer, R. (1979). Crustal contamination versus enriched mantle: $^{143}Nd/^{144}Nd$ and $^{87}Sr/^{86}Sr$ evidence from the Italian volcanic. *Contrib. Mineral. Petrol*., 69: 151-165.

Hay, R. L. (1963). Zeolitic weathering in Olduvai Gorge, Tanganyika. *Geological Society of America, Bulletin*, 74: 1281-1286.

HAY, R. L. & LEAKEY, M. D. (1982). The fossil footprints of Laetoli. *Scientific American*, 246: 50-57.

HEIKEN, G. & WOHLETZ, K. H. (1985). Volcanic Ash. Univ. California Press, Berkeley, pp. 246.

HILDRETH, E. C. (1983). The computation of the velocity field. *M. I. T. A. I. Memo*, 734.

HILDRETH, W. (1979). The Bishop Tuff: Evidence for the origin of compositional zonation in silicic magma chambers. *Geol. Soc. Am. Spec. Paper*., 180: 43-75.

HILDRETH, W. (1981). Gradients in silicic magma chambers: Implications for lithospheric magmatism. *J. Geophys. Res*., 86, BI1: 10153-10192.

HUDDART, D., BENNETT, M. R., GONZALEZ, S., & VELAY, X. (2008). Analysis and preservation of Pleistocene human and animal footprints: An example from Toluquilla, Valsequillo basin (Central Mexico). *Ichnos*, 15(3/4): 232-245.

INMAN, D. L. (1952). Measures for describing the size distribution of sediments. *J.Sedim. Petrol.,* 22: 125-145.

INMAN, D. L. (1953). Areal and seasonal variations in beach and near-shore sediments at La Jolla, California. *Beach Erosion Board Tech, Memo,* No. 39.

JAGGAR, T. A. (1921). Fossil human footprints in Kau Desert. *Hawaiian Volcano Observ. Monthly Bull.*, 9: 114-118.

KARNER, D. B. & RENNE, P. R. (1998). $^{40}Ar/^{39}Ar$ geochronology of Roman volcanic province tephra in the Tiber River valley: age calibration of Middle Pleistocene sea-level changes. *Bulletin Geological Society of America*, 110: 740-747.

KIM, S. K., KIM, K. S., PARK, S. I., & SHIN, M. K. (2004). (Eds). International Symposium on Quaternary Footprints of Hominids and other Vertebrates. 175 pp. Jeju, Korea, Oct 9-11.

KIM, J. Y., LOCKLEY, M. G., KIM, S. K., & MATTHEWS, N. (2008). Hominid ichnotaxonomy: An exploration of a neglected discipline. *Ichnos*, 15(3/4): 126-139

KRUMBEIN, W. C. (1983). Size frequency distribution of sediments and the normal phi curve. *J. Sediment. Petrol*., 8: 84-90.

Leakey, M. D. & Harris, J. M. (1987). Laetoli: A Pliocene site in northern Tanzania. Clarendon Press, Oxford, 561 pp.

Leakey, M. D. & Hay, R. L. (1979). Pliocene footprints in the Laetoli beds at Laetoli, northern Tanzania. *Nature*, 278: 317-319.

Les Bas, M. J., Le Maitre, R. W. Strekeisen, A. & Zanettin, B. (1986). A chemical classification of volcanic rocks based and the total alkali-silica diagram. *Journal of Petrology* 27: 745-750.

Lockley, M. G. (1999). The eternal trail: A tracker looks at evolution. Perseus Books, Reading, PA, 334 pp.

Lockley, M. G. & Meyer, C. A. (2000). Dinosaur tracks and other fossil footprints of Europe. Columbia University Press, New York, 323 pp.

Lockley, M. G. Roberts, G. & Kim, J. Y. (2008). In the Footprints of Our Ancestors: An Overview of the Hominid Track Record. *Ichnos*, 15:106-125.

Luhr, J. F. & Giannetti, B. (1987). The Brown Leucitic Tuff of Roccamonfina volcano (Roman Region, Italy). *Contrib. Miner. Petrol.*, 95, 420-436.

Marantos, I., Markopoulos, T. & Christidis, G. E. (2007). Zeolitic alteration in the Tertiary Feres volcano-sedimentary basin, Thrace, NE Greece. *Mineralogical Magazine*, 71(3): 327-345.

Marra, F., Taddeucci, J., Freda, C., Marzocchi, W. & Scarlato, P. (2004). Eruption recurrence interval of the Alban Hills and coupling with other volcanic districts of the Tyrrhenian margin of Italy: possible tectonic influence and implications for volcanic hazard. *Tectonics*, 23: TC4013.

Mastrolorenzo, G., Petrone, P., Pappalardo, L., & Sheridan, M. F. (2006). The Avellino 3780-yr-B.P. catastrophe as a worst case scenario for a future eruption at Vesuvius. *Proceedings of the National Academy of Sciences*, 103: 4366-4370.

Meldrum, D. J. (2006). Sasquatch: Legend meets science. Tom Doherty Associates Book, New York, 297 pp.

Mietto, P., Avanzini, M., & Rolandi, G. (2003). Human footprints in a Pleistocene volcanic

ash. *Nature*, 422: 133.

MISKOVSKI, J. C. (1967). Les paleosols Mindel-Riss et Riss-Wurm de Terra Amata. Etude sédimentologique, Académie Science Paris, 264: 2361-2363.

NEWHALL, C. G. & SELF, S. (1982). The Volcanic Explosivity Index (VEI), An Estimate of Explosive Magnitude for Historical Volcanism, *J. Geophys. Res.*, 87(C2): 1231-1238.

NICHOL, R. (1982). Fossilized human footprints in Rangitoto ash on Motutapu Island. *Geological Society of New Zealand Newsletter*, 51: 11-13.

ORDOÑEZ, E. (1945). Las huellas de pisadas humanas en Rincòn de Guadalupe, Amanalco de becerra, Estado de Mexico. Manuscript "en Miméografo." Biblioteca del Instituto de Geologìa, Mexico, D. F.

PALES, L. (1954). Les empreintes de pieds humains de la "Tana della Basura" (Toriano). *Rivista di Studi Liguri*, 20: 5-12.

PALES, L. (1960). Les empreintes de pieds humains de la "Grotta della Basura" (Toriano). *Revue des études ligures*, 26: 25-90.

PALES, L. (1976). Les empreintes de pieds Humains dans les cavernes. *Archives de l'Institut de Paléontologie Humaine*, 36: 1-166.

PALOMBO, M. R. & MUSSI, M. (2006). Large mammal guilds at the time of the first human colonization: The case of the Italian Pleistocene record. *Quaternary International*, 149: 94-103.

PASSAGLIA, E. & VEZZALINI. G. (1985). Crystal chemistry of diagenetic zeolites in volcaniclastic deposits of Italy. *Contrib. Mineral. Petrol*., 90: 190-198.

PECCERILLO, A. (2005). Plio-Quaternary Volcanism in Italy, Springer-Verlag, 365 pp.

PECCERILLO, A., POLI, G. & TOLOMEO, L. (1984). Genesis, evolution and tectonics of K-rich volcanics from the Alban Hills (Roman Comagmatic Region) as inferred from trace element geochemistry. *Contrib. Miner. Petrol.*, 86: 230-240.

PEREZ-TORRADO, F. J., MARTI, J., QUERALT, I. & MANGAS, J. (1995). Alteration processes of the Roque Nublo ignimbrites (Gran Canaria, Canary Islands). *J. Volcan. Geoth. Res*., 65: 191-204.

Radicati di brozolo, F., Di Girolamo, P., Turi, B. & Oddone, M. (1988). $^{40}Ar/^{39}Ar$ and K/Ar dating of K-rich rocks from Roccamonfina volcano, Roman comagmatic region, Italy. *Geochimica et Cosmochimica Acta,* 52: 1435-1441.

Rector, C. H. (1979). 5,000-year-old footprints on the Mojave River, California, USA. *Antiquity*, 54:149-150.

Rector, C. H. (1983). Appendix B. Ancient human and animal trackway. *In* Rector, C. H., Swenson, J. D., and Wilke, P. J. (Eds.), *Archaeological Studies at Oro Grande, Mohave Desert, California*. San Bernardino County Museum Association, Redlands, CA, pp. 161-168.

Rector, C. H. (1999). Human and animal trackway at Oro Grande. *San Bernardino County Museum Association Quarterly*, 46: 53-55.

Renne, P. R., Feinberg, J. M., Waters, M. R., Arroyo-Cabrales, J., Ochoa-Castillo, P., Perez-Campa, M., & Knight, K. B. (2005). Age of Mexican ash with alleged 'footprints.' *Nature*, 438: E7–E8.

Renne, P. R., Swisher C. C., Deino, A. L., Karner, D. B., Owens, T. L., & DePaolo, D .L. (1998). Intercalibration of Standards, Absolute Ages and Uncertainties in 40Ar/39Ar Dating. *Chemical Geology*, 145: 117-152.

Riehle, J. R., Miller, T. F. & Bailey, R. A. (1995). Cooling, degassing and compaction of rhyolitic ash-flow tuffs: computational model. *Bull. Volcan.*, 57: 319-336.

Roberts, D. (2008). Last interglacial hominid and associated vertebrate fossil trackways in coastal eolianites, South Africa. *Ichnos*, 15(3/4):190-207.

Roberts, D. & Berger, L. R. (1997). Last interglacial (c. 117 Kr) human footprints from South Africa. *South African Journal of Science*, 93: 349-350.

Roberts, G., Gonzalez, S., & Huddart, D. (1996). Intertidal Holocene footprints and their archaeological significance. *Antiquity*, 70: 647-51.

Rodrìguez-de la Rosa, R. A., Aguillòn-Martìnez, M. C., Lòpez-Espinoza, J., & Eberth, D. A. (2004). The fossil record of vertebrate tracks in Mexico. *Ichnos*, 11:27-38.

Rouchon, V., Gillot, P. Y., Quidelleur, X., Chiesa, S. & Floris B. (2008). Temporal evolution of the Roccamonfina volcanic complex (Pleistocene), Central Italy. *J. Volcan. Geoth.*

Res., 177: 500-514.

Scaillet, S., Vita-Scaillet, G. & Guillou, H. (2008). Oldest human footprints dated by Ar/Ar. *EPSL*, 275: 320-325.

Schmincke, H. U., Kutterolf, S., Pérez, W., Rausch, J., Freundt, A. & Strauch, W. (2009). Walking through volcanic mud: the 2100 year-old Acahualinca footprints (Nicaragua) I: Stratigraphy, lithology, volcanology and age of the Acahualinca section. *Bull Volcanol*, 71: 479-493.

Serri, G., Innocenti, F., Manetti, P., Tonarini, S. & Ferrara, G. (1991). Il magmatismo neogenico-Quaternario dell'area tosco-laziale-umbra. In *Studi preliminari all'acquisizione dati del profilo CROP03 Punta-Ala- Gabice*. Studi Geologic Camerti, volume speciale 1991/1.

Sheppard, R. A. (1991). Zeolitic diagenesis of tuffs in the Miocene Chalk Hills Formation, western Snake River Plain, Idaho. *U.S. Geological Survey, Bulletin*, 1963, 27.

Smith, R. L. (1979). Ash-flow magmatism. *Geol. Soc. Am. Spec. Pap.*, 180: 5-27.

Smith, R. L. & Bailey, R. A. (1965). The Bandelier Tuff: a study of ash-flow eruption cycles from zoned magma chambers. *Bull. Volcanol.*, 29: 83-104.

Sparks, R. S. J., Self, S. & Walker, G. P. L. (1973). The products of ignimbrite eruptions. *Geology,* 1: 115-118.

Suwa, G. (1984). Could *Australopithecus afarensis* have made the hominid tracks at Laetoli?. *Journal of Physical Anthropology*, 963: 224-225.

Swanson, D. A. & Christiansen, R. L. (1973). Tragic base surge in 1790 at Kilauea volcano. *Geology*, 1: 83-86.

Swanson, D. A. & Rausch, J. (2008). Human Footprints in Relation to the 1790 Eruption of Kilauea. Abstract in AGU (San Francisco, USA)

Tedesco, C. (1964). Main lines of the history of Roccamonfina Volcano. *Bull. Volcanol.*, 28:119-141.

Tuttle, R. H., Webb, D., Weidi, E., & Baksh, M. (1990). Further progress on the Laetoli trails. *Journal of Archeological Science*, 17: 347-362.

VOLLMER, R. & HAWKESWORTH, C. J. (1980) Lead isotopic composition of the potassic rocks from Roccamonfina (South Italy). *EPSL*, 47: 91-101.

WALKER, G. P. L. (1971). Grainsize characteristics of pyroclastic deposits. J Geol 79: 696-714.

WALKER, G. P. L. (1973). Explosive volcanic eruptions - a new classification scheme. *Geol. Rundsch*., 62: 431-446.

WALKER, G. P. L. (1983). Ignimbrite types and ignimbrite problems. J. Volcan. Geoth. Res., 17: 65-88.

WATTS, M. D. (1987). Geothermal exploration of Roccamonfina volcano, Italy. *Geothermics* 16: 527–528.

WENTWORTH, C. K. (1922). A scale of grade and class terms for clastic sediments. *Journal of Geology*, 30: 377-392.

WHITE, T. D. (1980). Evolutionary implications of Pliocene hominid footprints. *Science*, 208: 175-176.

WHITE, T. D. & SUWA, G. (1987). Hominid footprints at Laetoli; facts and interpretations. American Journal of Physical Anthropology, 72: 485-514.

WILLIAMS, H. (1952). Geological observations on the ancient human footprints near Managua. *Contributions to American Anthropology and History*, 52: 1-31.

ZHANG, D. D. & LI, S. H. (2002). Optical dating of Tibetan human hand and footprints: An implication for the paleoenvironment of the last glaciation of the Tibetan Plateau. *Geophysical Research Letters*, 29: 161-163.

ZHANG, D. D., LI., S. H., HE, Q. E., & LI, B. S. (2003). Human settlement of the last glaciation on the Tibetan plateau. *Current Science*, 84: 701-704.